A Mobile Wireless Channel State Recognition Algorithm:

Introduction, Definition, and Verfication: Sensing for Cognitive Environmental Awareness

By

Kenneth Dewayne Brown

Submitted to the graduate degree program in Electrical Engineering and Computer Science and the
Graduate Faculty of the University of Kansas
in partial fulfillment of the requirements for the degree of
Doctor of Philosophy

Committee members

Dr. Glenn Prescott, Chairperson

Dr. Chris Allen

Dr. Victor Frost

Dr. Rick Hale

Dr. Gary Minden

Date defended: _____

The Dissertation Committee for Kenneth Dewayne Brown certifies
that this is the approved version of the following dissertation :

A Mobile Wireless Channel State Recognition Algorithm:

Dr. Glenn Prescott, Chairperson

Date approved: _____

Abstract

This research includes mobile wireless systems limited by time and frequency dispersive channels. A blind mobile wireless channel (MWC) state recognition (CSR) algorithm that detects hidden coherent nonselective and noncoherent selective processes is verified. Because the algorithm is blind, it releases capacity based on current channel state that traditionally is fixed and reserved for channel gain estimation and distortion mitigation. The CSR algorithm enables cognitive communication system control including signal processing, resource allocation/deallocation, or distortion mitigation selections based on channel coherence states.

MWC coherent and noncoherent states, ergodicity, stationarity, uncorrelated scattering, and Markov processes are assumed for each time block. Furthermore, a hidden Markov model (HMM) is utilized to represent the statistical relationships between hidden dispersive processes and observed receive waveform processes. First-order and second-order statistical extracted features support state hard decisions which are combined in order to increase the accuracy of channel state estimates.

This research effort has architected, designed, and verified a blind statistical feature recognition algorithm capable of detecting coherent nonselective, single time selective, single frequency selective, or dual selective noncoherent states. A MWC coherence state model (CSM) was designed to represent these hidden dispersive processes. Extracted statistical features are input into a parallel set of trained HMMs that compute state sequence conditional likelihoods. Hard state decisions are combined to produce a single most likely channel state estimate for each time block. To verify the CSR algorithm performance, combinations of hidden state sequences are applied to the CSR

algorithm and verified against input hidden state sequences. State sequence recognition accuracy sensitivity was found to be above 99% while specificity was determined to be above 98% averaged across all features, states, and sequences.

While these results establish the feasibility of a MWC blind CSR algorithm, optimal configuration requires future research to further improve performance including: 1) characterizing the range of input signal configurations, 2) waveform feature block size reduction, 3) HMM parameter tracking, 4) HMM computational complexity and latency reduction, 5) feature soft decision combining, 6) recursive implementation, 7) interfacing with state based mobile wireless communication control processes, and 8) extension to wired or wireless waveform recognition.

This work is dedicated to those that dare to dream, possess an insatiable appetite for learning, and a tenacious will to achieve.

Acknowledgements

I am compelled to thank my God, my advocate Jesus, and the Holy Spirit for their faithful presence and answered prayers. My partner in life, Julie for her endless patience and support. My children, for repeated understanding. My advisor, Dr. Prescott for his willingness to invest in an old dog, guidance, and encouragement. The University of Kansas Faculty for accomodating a nontraditional graduate student. My employer, the Applied Physics Laboratory, for investing in staff education. Without the support of these, my achievement would not have been possible.

Contents

List of Figures

List of Tables

List of Acronyms

AP Adaptive Processing

AWGN Additive White Gaussian Noise

BER Bit Error Rate

CFR Channel Frequency Response

CIR Channel Impulse Response

CSF Channel Scattering Function

CSE Channel State Estimate

CSE Channel State Estimates

CSM Channel State Model

CSR Channel State Recognition

CPA Cognitive Processing Architecture

CP Cognitive Processing

BWM Coherence Bandwidth Magnitude

BWP Coherence Bandwidth Phase

BWc Coherence Bandwidth

TcM Coherence Time Magnitude

TcP Coherence Time Phase

Tc Coherence Time

CEM Complex Envelope Magnitude

CEP Complex Envelope Phase

CVT CSR Verification Testbed

DSM Delay Spread Magnitude

DSP Delay Spread Phase

DS Delay Spread

DPM Doppler Spread Magnitude

DPP Doppler Spread Phase

DP Doppler Spread

EM Expectation Maximum

FE Feature Extraction

FE Feature Extraction

FSE Feature State Estimate

4WDP Four Wave Diffuse Power

FSCM Finite State Channel Model

FNTN Frequency Nonselective and Time Nonselective

FNTS Frequency Nonselective and Time Selective

FSTN Frequency Selective and Time Nonselective

FSTS Frequency Selective and Time Selective

FS Frequency Selective

HDE Hard Decision Estimate

HMM Hidden Markov Model

IFI Interfrequency Interference

ISI Intersymbol Interference

KF Kalman Filter

ML Maximum Likelihood

MWC Mobile Wireless Channel

MIMO Multiple Input Multiple Output

PSD Power Spectral Density

PDF Probability Density Function

POC Proof of Concept

ROL Rank Order Likelihood

RX Receiver

RFD Relative Frequency Distribution

RMS Root Mean Square

ROT Rules of Thumb

SNR Signal to Noise Ratio

SISO Single Input Single Output

SWAP Size, Weight, and Power

SDE State Decision Estimate

SDV State Decision Vector

SD State Decision

SLE State Likelihood Estimate

SLP State Likelihood Parameter

SLP State Likelihood Parameter

SLV State Likelihood Vector

SL State Likelihood

SML State Maximum Likelihood

SWG State Waveform Generator

TS Time Selective

TXR Transceiver

TP True Positive

TWDP Two Wave Diffuse Power

WFV Waveform Feature Vector

WSR Waveform State Recognition

WSS Wide Sense Stationary

Chapter 1

Introduction

The scope of this research is the communication system shown in Figure 1.1 with a transmitter and receiver connected through a mobile wireless channel (MWC). It is assumed that in addition to mobile frequency dispersion, multipath time dispersion occurs based on geometry and terrain reflections (i.e. ground, water, mountains, and buildings); both capable of producing significant fading and distortion effects upon the received waveform characteristics.

These systems are stressed by operations across diverse terrain, propagation conditions, fast moving platforms, and size, weight, and power (SWAP) disadvantaged terminals. It is assumed that environmentally aware cognitive and adaptive processes are required to maintain optimum performance across these broad operational environments.

This research has created a coherence state model (CSM) and a new channel state recognition (CSR) algorithm to ease the fading and distortion challenges. The result combines multiple receive waveform statistical features into a channel coherence state estimate using statistical feature recognition methods. The CSR algorithm provides detection of channel coherent nonselective and noncoherent selective states rather than channel transfer function gain; thus increasing communication processing environmental awareness beyond conventional channel state estimation methods. This new environmental awareness enables state based communication system control processes that select appropriate signal processing methods when current channel state is favorable, disable

those for which the current channel state is unfavorable, and applying appropriate mitigation methods when the current channel state is debilitating. The CSR algorithm enables environmentally responsive resource allocations such as capacity, power, and spectral efficiency.

This research contribution provides background, assumptions, and introduces the CSR algorithm in Chapter 1. Chapter 2 develops a preliminary CSR algorithm utilized to establish hidden Markov model (HMM) statistical feature recognition feasibility, while Chapter 3 describes enhancements including expanded waveform feature extraction, parallel feature recognition, and diversity decision combining. Chapter 4 includes algorithm verification testing, and Chapter 5 presents conclusions, lessons learned, and future steps.

1.1 Background

1.1.1 Mobile Wireless Communication

The mobile wireless communication system shown in Figure 1.1 provides simplex transfers between a mobile source and destination applications through a single input single output (SISO) physical layer link. A duplex link between two transceivers can be constructed from a pair of forward and reverse simplex SISO links.

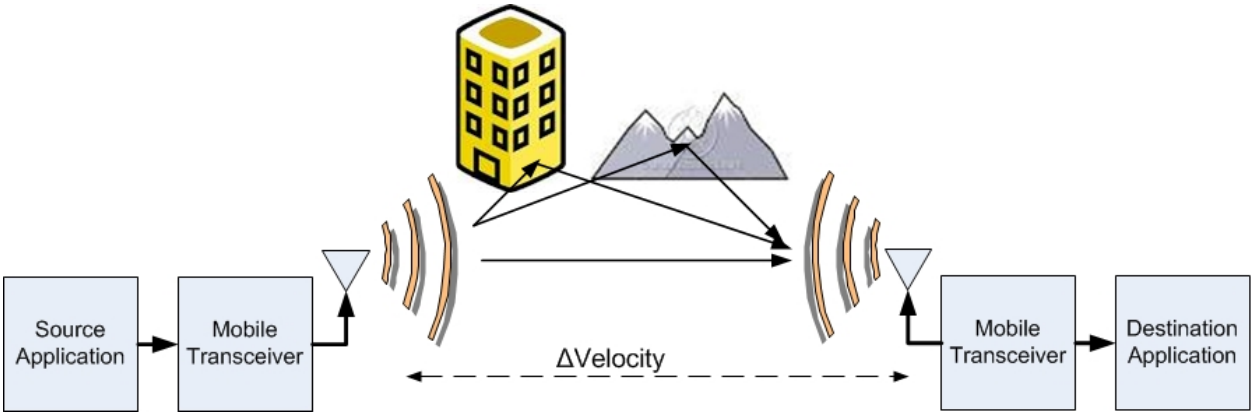

Figure 1.1: Mobile Wireless Communication System

1.1.2 Mobile Wireless Channel

The MWC architecture shown in Figure 1.2, comprises source and destination applications, transmit, mobile wireless fading, noise, interference, and receiver processes. It is assumed that the MWC output includes 4 specular plus diffuse components that result from locally reflected waves from surrounding surfaces. Refer to Appendix Section A.3 for background on this spectral model. This model can represent Ricean or Rayleigh amplitude distributions with the configuration of a gain parameter. It can also be configured to represent mobile Doppler frequency dispersion. With these capabilities, it can represent a broad range of discrete waveform, power, bandwidth, noise, large scale loss, and small-scale fading cases.

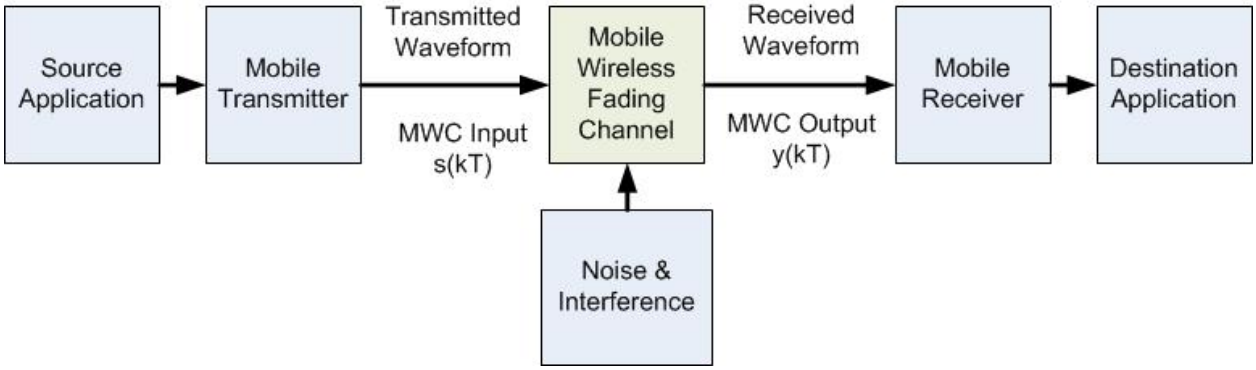

Figure 1.2: Mobile Wireless Channel Architecture

1.1.3 MWC Time Domain Features

The MWC passband input is assumed to be a real continuous time waveform described by equation (1.1),

$$s_{pb}(t) = Re\left\{c(t)e^{j\omega_o t}\right\}, \tag{1.1}$$

where $c(t)$ is the continuous time waveform magnitude. If this waveform is discrete time sampled, the discrete time passband waveform results as defined by equation (2.3),

$$s_{pbk}(kT) = Re\left\{c(kT)e^{j\omega_o kT}\right\}, \tag{1.2}$$

where k is the sample index and $0 < k < \infty$. The MWC passband output is assumed to be a real continuous time waveform defined by equation (1.3)

$$y_{pb}\,(t) = Re\left\{z(t)e^{j\omega_o t}\right\}. \tag{1.3}$$

If this waveform is discrete time sampled, the discrete time waveform results as defined by equation (1.4)

$$y_{pbk}\,(kT) = Re\left\{z(kT)e^{j\omega_o kT}\right\}, \tag{1.4}$$

where $z(t)$ is the baseband complex envelope, and $e^{j\omega_o kT}$ describes a carrier at frequency ω_o .

The output baseband complex waveform $y_{bb}(t)$ with magnitude and phase components is defined by equation (1.5) and (1.6)

$$y_{bb}(t) = z(t) = x(t) + y(t) = \ |z(t)|\, e^{j\theta(t)} = \ \sqrt{x^2(t) + y^2(t)}e^{j\theta(t)}, \tag{1.5}$$

$$\theta(t) = \tan^{-1}\frac{y(t)}{x(t)}. \tag{1.6}$$

It is common to define the channel gain transfer function $h(t)$ which can be related to the input signal $s(t)$, the output signal $y(t)$, and Gaussian noise n(t) , with a convolution as defined in equation (1.7),

$$y_{pb}(t) = \left[s_{pb}(t) \otimes h_{pb}(t)\right] + n(t). \tag{1.7}$$

Here $n(t)$ is Gaussian white noise. Analyzing these functions at baseband conveniently drops references to the carrier as shown in equation (1.8),

$$y_{\tilde{bb}}(t) = \frac{1}{2}\left[s_{\tilde{bb}}(t) \otimes \tilde{h}_{bb}(t)\right] + \tilde{n}(t). \tag{1.8}$$

Application of Fourier transforms provides baseband and passband spectral versions of these waveforms as defined in equation (1.9) and (1.10) respectively,

$$Y_{pb}(f) = X_{pb}(f) H_{pb}(f) + N_{pb}(f), \tag{1.9}$$

$$\tilde{Y}_{bb}(f) = \frac{1}{2}\left[\tilde{X}_{bb}(f) \tilde{H_{bb}}(f) + \tilde{N}_{bb}(f)\right]. \tag{1.10}$$

For the time-varying channel case, frequency or time domain multiplication in equation 1.9 or 1.10 does not hold and therefore the expression in equation (1.11) must be utilized,

$$y_{\tilde{bb}}(t) = \frac{1}{2}\int_{-\infty}^{+\infty}\left[\{\tilde{X}_{bb}(f) \tilde{H_{bb}}(f,t) + \tilde{N}_{bb}(f)\} e^{(j2\pi ft)dt}.\right] \tag{1.11}$$

For equation (1.11) the frequency domain channel transfer function is time-variant, therefore, values of frequency and time are no longer valid transform pairs as they were in the time-invariant case. In contrast to blind channel estimation methods, these channel transfer functions (equation 1.7 through 1.10) require knowledge of both the input waveform as well as the output waveform in order to compute the channel gain function. Refer to Appendix Section A.1 for additional background on channel models.

1.1.4 MWC Challenges

Time-variant noncoherent selectivity and distortion are problematic MWC conditions. MWCs can transition between nondispersive, single time, single frequency, or dual dispersive states depending on dynamic environmental factors such as multipath and velocity. Time selectivity results

from moderate to severe frequency dispersion while frequency selectivity results from moderate to severe time dispersion. Moderate to full selectivity (when dispersion exceeds 10-20% of symbol period/rate) results in amplitude and phase distortion yielding irreducible error rate floors that cannot be mitigated with signal to noise (SNR) gain. Without alternative mitigation methods, these channels become severely handicapped. Mild selectivity (dispersion less than 10-20% of the symbol period) is less problematic, with reduced sensitivity to SNR gain.

Many advanced communication signal processing waveforms (e.g. MIMO, OFDM, WCDMA) depend upon accurate and timely channel state estimation. It is common for these methods to define channel state in terms of channel transfer function gain. These methods do not directly detect channel coherence or selectivity and require knowledge of both the transmit and receive waveform. These methods degrade when channels become time or dual selective and also are sensitive to latency between the receiver and the transmitter. For example, if these methods are designed for a particular channel state, and are exposed to a restricted channel state (i.e., a time domain equalizer applied in time selective conditions) the overall system performance degrades. Furthermore, if these resource intensive methods are misapplied under unfavorable channel conditions, suboptimum resource allocations result. For example, when static distortion guard bands designed for single dispersive conditions are applied in coherent or dual dispersive cases, inefficient resource allocation (capacity, bandwidth, or power) results in decreased communication system efficiency. Additionally, capacity is not maximized with overhead allocated for channel estimation when a channel is coherent or dual dispersive.

1.1.5 Cognitive Architectures

Cognitive processing (CP) builds on a foundation of adaptive processing (AP) as shown in Figure 1.3. These systems respond to internal and external conditions with autonomous adaptive methods. These cognitive processing architectures (CPA) are comprised of functions for environmental awareness, cognitive processing, self-awareness, in addition to AP functions. For example, CPAs are sensitive to external environmental conditions such as channel state, or location, as well as

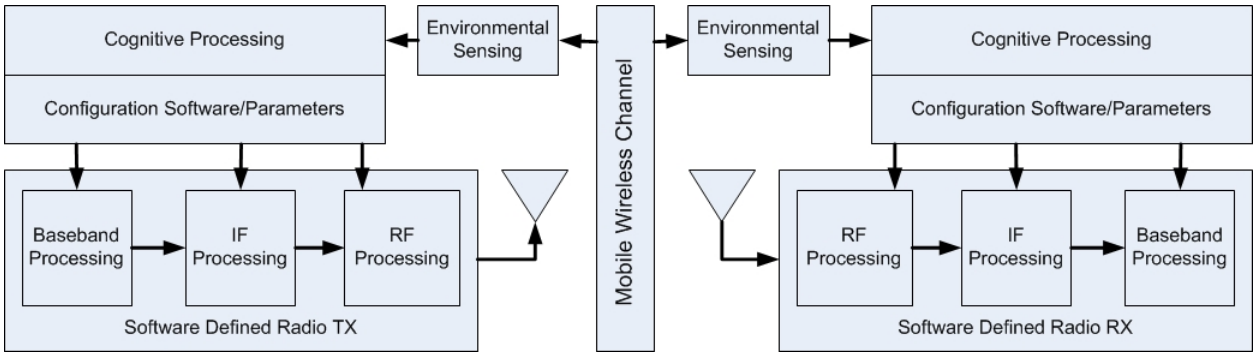

Figure 1.3: Cognitive Processing Architecture (CPA)

internal state such as power levels, health, and status conditions. This awareness provides input for policy-based decision engines that can provide selection of state based control, adaptive operational parameters, alternative signal processing methods, or adverse condition compensation.

1.1.6 Channel State Recognition (CSR) Algorithm

The CSR algorithm architecture is shown in Figure 1.4. The input is a sequence of MWC complex baseband samples that are observed at the receiver (RX) antenna and organized into blocks of 50k samples. This quantity of samples is conservatively long to establish statistical significance. The output is a sequence of channel CSM estimates, one for each input sample block. The CSR algorithm comprises functions for waveform feature extraction, feature state likelihood, and state decision estimation. It provides the local cognitive transceiver (TXR) environmental awareness of MWC coherent nonselective and noncoherent selective states, does not require knowledge of the channel input, and is insensitive to feedback latency.

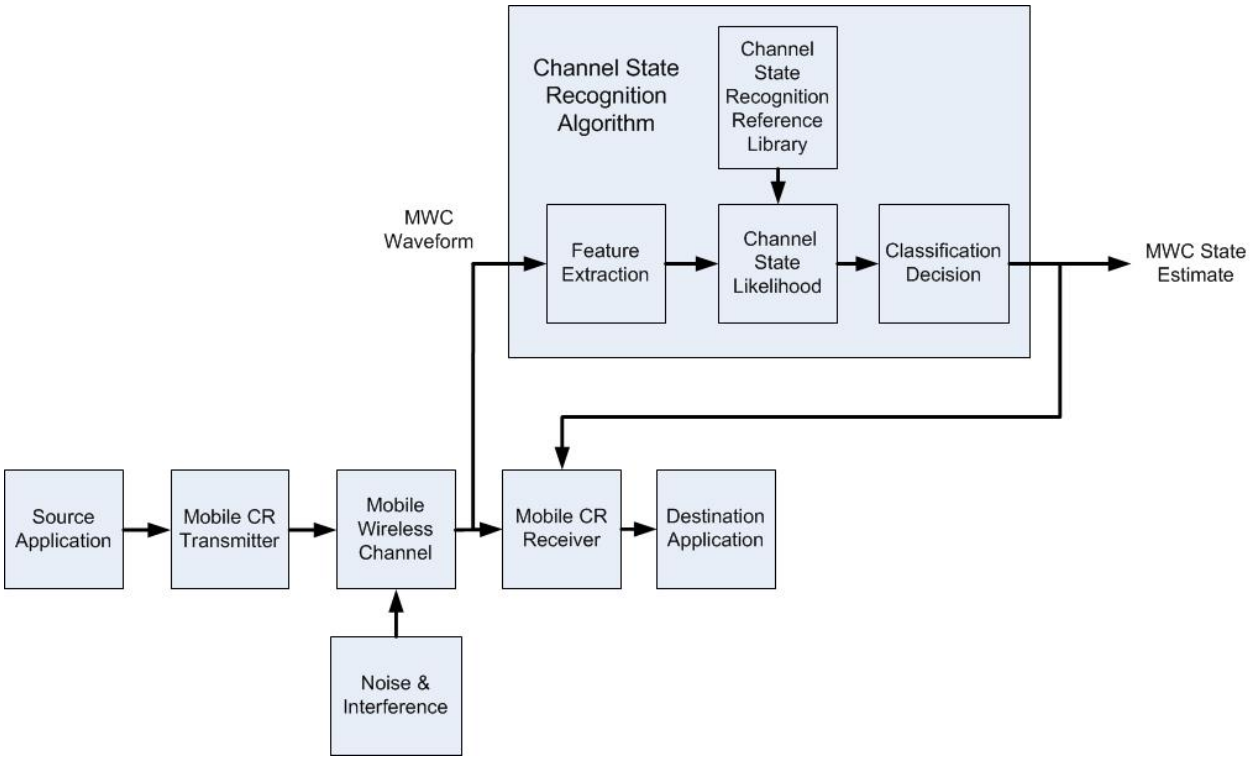

Figure 1.4: Channel State Recognition (CSR) Architecture

1.2 Assumptions

1.2.1 Coherence State Model

A MWC is noncoherent or selective if the magnitude varies as a function of time, frequency, or space. In contrast, a MWC is coherent if it does not change, or nearly constant, as a function of time, frequency, or space. According to Dr. Durgin, a published researcher in Virginia Tech's Mobile & Portable Radio Research Group, the "fundamental concept in channel modeling is classifying the three possible channel dependencies of time, frequency, and space as either coherent or selective"[2]. The CSM and the CSR algorithm are motivated to achieve Durgin's idea with an accurate blind process. Refer to Appendix Section A.7 for additional background on the CSM.

1.2.2 Channel Time Coherence and Selectivity

A channel is time coherent if the unmodulated complex envelope does not change in a period of interest, typically this is the symbol period. This condition is defined by equation (1.12)

$$\left|\tilde{h}(t)\right| \approx V_o \; for \; |t - t_o| \leq \frac{T_c}{2}, \tag{1.12}$$

where V_o is some constant voltage, T_c is the coherence period, or equivalently the coherence time, and t_o is some arbitrary time. The coherence time is defined as the largest value for which equation (1.12) is true and is the time period over which the channel is considered to be static [2]. During the coherence time sample magnitudes would be highly correlated [3].

The primary reason for loss of time coherence is relative velocity between the transmitter and the receiver, or mobile scatters in the propagation environment. If resulting frequency dispersion is much less than the symbol rate, then coherence time is much larger than the symbol period; the channel is considered coherent, or time-flat. As frequency dispersion exceeds 10-20% of the symbol rate, then interfrequency interference (IFI) becomes increasingly problematic. In this case energy is displaced from one frequency to another resulting in signal distortion. As frequency dispersion approaches the symbol rate, the channel becomes fully time selective.

Given that coherence time is related to time correlation and to Doppler spread through an inverse Fourier transform, an approximation for envelope unit autocovariance is defined in equation (1.13)[2]

$$\rho_{\mathrm{R}}(\mathrm{t}) \approx \mathrm{e}^{\left(\frac{-23}{2\pi^2}\sigma_\omega^2 \mathrm{t}^2\right)}. \tag{1.13}$$

Here σ_ω is the RMS Doppler spread; this expression provides a close approximation when t is small since the error of this expression remains small until the complex envelope becomes uncorrelated.

If coherence time is defined as when the correlation decays to a value of e^{-1}, a definition of

coherence time is provided by equation (1.14),

$$\mathrm{T_c} = \frac{2\pi}{\sqrt{46}\sigma_\omega} = \frac{1.08}{\sigma_\omega}. \tag{1.14}$$

A common wireless engineering approximation [3] to coherence time characterized by a frequency correlation of approximately .5 is defined by equation (1.15),

$$T_c \approx \frac{2\pi}{5\sigma_\omega}. \tag{1.15}$$

Refer to Appendix Section A.5 for additional background material.

1.2.3 Channel Frequency Coherence and Selectivity

Frequency coherence exists if the magnitude of the envelope does not change over a frequency band of interest, typically this is the symbol rate. This condition is defined by equation (1.16)

$$\left|\tilde{h}(f)\right| \approx V_o \;\; for \; |f_c - f| \leq \frac{B_c}{2}. \tag{1.16}$$

where $\mathrm{V_o}$ is some constant amplitude, $\mathrm{B_c}$ is the coherence bandwidth, and $\mathrm{f_c}$ is the carrier frequency. The largest value of $\mathrm{B_c}$ for which equation (1.16) is true is called the coherence bandwidth and is the range of frequencies over which the channel is static [2]. Two received frequencies within the coherence bandwidth would be correlated [3].

Loss of frequency coherence in a MWC is primarily due to time dispersion from multipath propagation. If time dispersion is much less than the symbol period, then the coherence bandwidth is much greater than the symbol rate; the channel is coherent and defined as a frequency-flat channel. As time dispersion exceeds 10-20% of the symbol period, intersymbol interference (ISI) becomes increasingly problematic. In this case, waveform energy is displaced in time into adjacent symbol periods resulting in waveform distortion. As time dispersion approaches or exceeds the symbol period then full intersymbol interference results.

Given that the coherence bandwidth is related to frequency correlation and to delay spread through a Fourier transform, an approximation for magnitude unit autocovariance is defined by equation (1.17),

$$\rho_{\mathrm{R}}(\mathrm{f}) \approx \mathrm{e}^{\left(-46\sigma_{\tau}^{2}\mathrm{f}^{2}\right)}, \tag{1.17}$$

where σ_τ is the RMS delay spread. The unit autocovariance has been normalized and is an important tool for estimating how a waveform tends to change with respect to itself when it has a nonzero mean.

If coherence bandwidth is defined as when the correlation decays to a value of e^{-1}, a definition of coherence bandwidth is provided by equation (1.18),

$$\mathrm{B_c} = \frac{1}{\sqrt{46}\sigma_\tau} = \frac{1}{6.78\sigma_\tau} \approx \frac{1}{5\sigma_\tau}. \tag{1.18}$$

A common wireless engineering approximation [3] is to estimate the coherence bandwidth characterized when the time correlation is approximately .5 is defined by equation (1.19),

$$B_c \approx \frac{1}{5\sigma_\tau}. \tag{1.19}$$

Refer to Appendix Section A.5 for additional background material.

1.2.4 RMS Delay Spread and Doppler Spread

The waveform power spectral density (PSD) bandwidth as inversely related to time correlation or dispersion, therefore, the PSD bandwidth is an indicator for time correlation. The RMS delay spread can be estimated by equation (1.20),

$$\sigma_\tau^2 = \overline{\tau^2} - (\bar{\tau})^2, \textit{ where } \overline{\tau^n} = \frac{\int_{-\infty}^{+\infty} \tau^n S_{\tilde{h}}(\tau)\, d\tau}{\int_{-\infty}^{+\infty} S_{\tilde{h}}(\tau)\, d\tau}, \tag{1.20}$$

and the RMS Doppler spread can be estimated by equation (1.21)

$$\sigma_{\omega}^2 = \overline{\omega^2} - (\bar{\omega})^2, \; where \; \overline{\omega^n} = \frac{\int_{-\infty}^{+\infty} \omega^n S_{\tilde{h}}(\omega)\, d\omega}{\int_{-\infty}^{+\infty} S_{\tilde{h}}(\omega)\, d\omega}. \tag{1.21}$$

Refer to Appendix Section A.5 for additional background material.

1.2.5 Channel Ergodicity

In this work, ergodic conditions are assumed such that time statistics are equivalent to ensemble statistics given heterogeneous scattering of homogeneous plane waves in the local area of the receiver. Ergodicity is a necessary assumption for channel observability in order that the channel output at the receiver can be modeled as a sum of received waveforms. In this model the MWC output is a sum of specular and diffuse components as defined in Section A.3 of the Appendix.

1.2.6 Channel Stationarity and Waveform Scattering

Stationarity is an important attribute to characterize a stochastic process; there are several different types of stationarity which are discussed in Section A.2 of the Appendix. For this work, first order stationarity is assumed such that first order statistical parameters are constant for the period of interest. Additionally, wide sense stationarity (WSS) is assumed such that second order statistical parameters such as autocorrelation and covariance are stable and represent the waveform in the local area of the receiver.

When a waveform is WSS, then spectral components must be uncorrelated as defined by equation (1.22),

$$C_{\tilde{H}}(\omega_1, \omega_2) = 2\pi S_{\tilde{h}}(\omega_1)\, \delta(\omega_1 - \omega_2), \tag{1.22}$$

which evaluates to zero whenever $\omega_1 \neq \omega_2$.

1.2.7 Channel Finite State Markov Processes

Beginning with Shannon in the 1950s, continuing with Gilbert and Elliott at Bell Labs in the 1960s [4], and through the maturation of 2G wireless systems in the 1980s, finite state Markov chains (FSMC) have been utilized to model flat and time varying channels [5, 6, 7]. FSMC transition probabilities are independent of time and they embody the Markov property which is known as the first order assumption. The first order assumption means that the transition to the current state is primarily influenced only by the previous state. FSMC assume a finite set of states and a sequence of states typically defined as a set of nonoverlapping quantized amplitude, power, or SNR. Considerable research has proven the accuracy of modeling Rayleigh amplitude distributions. Investigations into higher order Markov models reach a point of diminishing return after the first order model (complexity increases rapidly after the first order). While FSMC provide foundational state based system models, they cannot express how states relate to independent outputs. The ability to relate system states to independent outputs is what HMM provide such that observable stochastic processes can be related to internal system state processes.

1.2.8 Channel Hidden Markov Model

MWC internal processes such as coherence and selectivity can be related to observable processes such as a receive waveform as shown in Figure 1.5. These relationships can be expressed with a dual statistical system formulated with a HMM.

Refer to Rabiner [1, 8]and Durbin [9] for an introduction to HMMs. When a system's internal states are not observable, a representative FSMC can be embedded in a HMM, where the unobservable or hidden states are represented as an internal statistical process and the output is related as a secondary output statistical process. HMMs can operate in a generative mode, whereby dwelling in a single internal hidden state, time-invariant output statistics are observed on the output. However, when the HMM transitions from the initial hidden state to another hidden state, the output statistics change based on a different output probability distribution. Unique output probability dis-

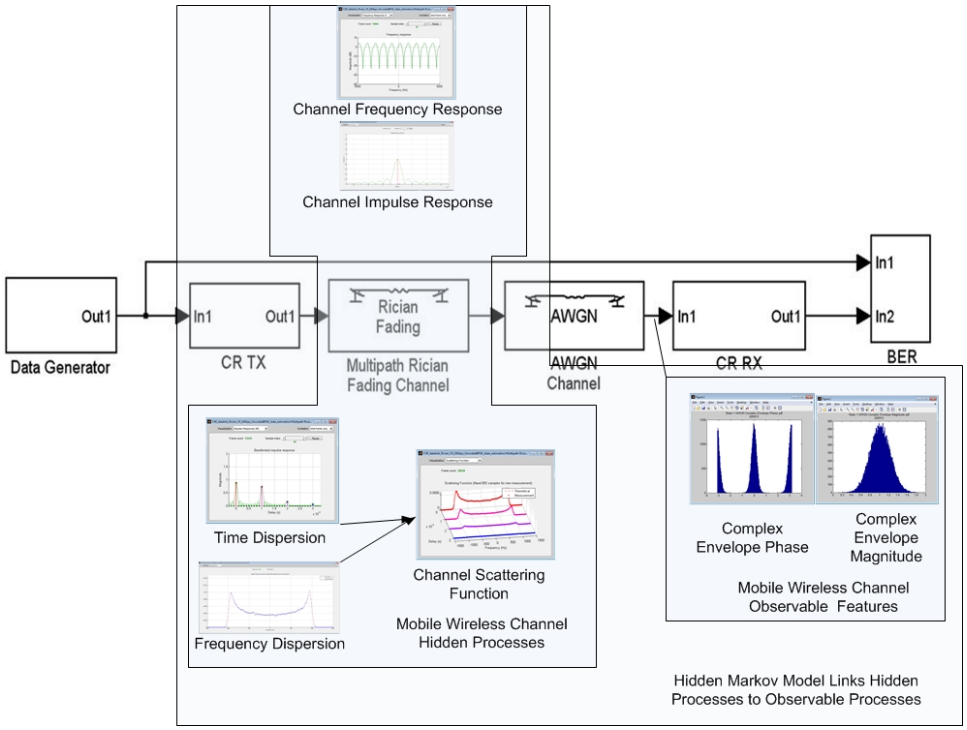

Figure 1.5: HMM System Architecture

tributions relate each hidden state to the output. Thus observed time-variant output behavior can be related to the hidden state sequence. A transition probability matrix governs transitions among the unobservable internal hidden states and an output probability matrix relates each hidden state to the output. An initial probability matrix defines which state is most likely to occur at initialization. When the HMM is operating in the training mode, off-line input training sequences are input to estimate the transition and output probability matrices. These HMM parameters provide memory for the HMM which is utilized in one of the two operational modes where input sequences are evaluated against the HMM memory parameters or the hidden state sequences are decoded. Either the Viterbi or Baum-Welch forward/backward algorithms serve to estimate the HMM parameters. Once the HMM has been trained, it can operate in an evaluation mode where given an input data sequence, the probability that the input sequence matches the trained model is estimated with a dynamic programming forward pass algorithm. A trained HMM can also operate in a decode mode based on the maximum likelihood (ML) Viterbi algorithm where given an input sequence, an optimum (ML is an optimum approach) hidden state sequence is estimated. HMMs have also

been successfully utilized for decades in mature structured pattern recognition applications such as automatic speech, image, facial, hand writing, gait, biological sequence, waveform, and network traffic recognition systems. HMMs have known limitations such as: 1) complexity, 2) extensive training requiring significant amounts of relevant data, 3) convergence rate, and 4) accuracy.

1.2.9 Waveform First-order Statistical Features

An important first-order tool for characterizing MWC processes is the probability density function (PDF). An approach for computing a complex envelope magnitude (CEM) PDF is equation (1.23) that defines specular and diffuse waveform components;

$$\mathrm{f_R}(\rho) = \rho \int_0^\infty J_o(v\rho) e^{\left(\frac{-v^2 P_{diff}}{4}\right)} \left[\prod_{i=1}^{N} J_o(V_i v)\right] v dv, \tag{1.23}$$

for $\mathrm{R} = \left|\tilde{V}_{\mathrm{diff}} + \sum_{\mathrm{i}=1}^{\mathrm{N}} \mathrm{V_i} e^{(\mathrm{j}\Phi_\mathrm{i})}\right|$ and $\mathrm{E}\left\{\left|\tilde{V}_{\mathrm{diff}}\right|^2\right\} = \mathrm{P_{diff}}$, which is valid for $\rho \geq 0$. Additional details can be found in Section A.4 of the Appendix.

Six closed form PDFs cases are defined in the Appendix for: 1) single wave, 2) two wave, 3) three wave, 4) Rayleigh, 5) Ricean, and 6) two wave plus diffuse power (TWDP) [2]. The single wave case is trivial; generated by integration of the second specular term of equation (1.23) with $\mathrm{N} = 1$ and the diffuse term $\mathrm{P_{diff}} = 0$. The two wave case is common, well researched, and is generated by integration of the second specular term of equation (1.23) with $\mathrm{N} = 2$ and diffuse term $\mathrm{P_{diff}} = 0$. While case three is more complicated, it provides insight into differences in behavior between the specular and nonspecular components and is generated with the specular term $\mathrm{N} = 3$ and diffuse term $\mathrm{P_{diff}} = 0$. The central limit theorem begins to dominate the PDF in the three wave case; additional nonspecular components move the PDF toward a Gaussian distribution and results approach the Rayleigh case.

In this work, these claims underlie assumptions for MWC simulations which are based on 4 specular components in addition to diffuse components (4WDP). With this configuration, observations

of received waveform pdfs are expected to approach Gaussian distributions. A Rayleigh PDF distribution is derived in Section A.4.1 of the Appendix. For the CSR algorithm, a more general Ricean distribution is assumed and the first order PDF is estimated with a histogram method.

1.2.10 Waveform Second-order Statistical Features

A common second order statistical feature for characterizing stochastic MWC behavior is the autocorrelation function. A definition for the autocorrelation function $C_{\tilde{h}}(t_1, t_2)$ of a time-varying stochastic baseband channel $\tilde{h}(t)$ is described by equation (1.24)

$$C_{\tilde{h}}(t_1, t_2) \doteq E\left\{\tilde{h}(t_1)\tilde{h}^*(t_2)\right\}. \tag{1.24}$$

The autocorrelation function characterizes how the waveform compares to itself by averaging the products of all samples in the random process at two different times, t_1 and t_2.

A Fourier transform applied to a baseband time-varying channel transfer function gain results in a frequency-varying process $\tilde{H}(\omega)$. A frequency domain autocorrelation $C_{\tilde{H}}(\omega_1, \omega_2)$ is defined by equation (1.25),

$$C_{\tilde{H}}(\omega_1, \omega_2) = E\left\{\tilde{H}(\omega_1)\tilde{H}^*(\omega_2)\right\}, \tag{1.25}$$

for characterizing correlation between frequency components ω_1 and ω_2. The frequency domain autocorrelation can be related to the PSD by equation (1.26),

$$C_{\tilde{H}}(\omega_1, \omega_2) = 2\pi S_{\tilde{h}}(\omega_1)\,\delta(\omega_1 - \omega_2), \tag{1.26}$$

where the function $S_{\tilde{h}}(\omega_1)$ is known as the PSD and it describes how the spectral power is distributed in the frequency domain.

The unit autocovariance $\rho_{\tilde{h}}(t)$ of a time-varying stochastic process may be computed by subtracting the mean value from the autocorrelation and normalizing the result. The autocorrelation $C_{\tilde{h}}(t)$ in turn is calculated from the PSD $S_{\tilde{h}}(\omega)$ by performing an inverse Fourier transform. These

relationships are shown in equation (1.27)

$$S_{\tilde{h}}(\omega) \rightarrow C_{\tilde{h}}(t) \rightarrow \rho_{\tilde{h}}(t). \tag{1.27}$$

A similar set of relationships can be developed for the spectrum of received envelope as defined in equation (1.28)

$$S_R(\omega) \rightarrow C_R(t) \rightarrow \rho_R(t), \tag{1.28}$$

given that the envelope and complex baseband channels are related by equation (1.29),

$$R(t) = \left|\tilde{h}(t)\right|. \tag{1.29}$$

1.2.11 Channel State Waveform Generation and CSR Algorithm Testbed

MWC System Behavioral Simulation The MWC behavioral model shown in Figure 1.6 enables investigation of primary parameters of coherent and selective channel state waveforms. This behavioral model was formulated in SIMULINK with a MATLAB foundation; it serves as a MWC CSM waveform generator. The waveform generator provides input to the CSR algorithm testbed shown in Figure 1.7. In this testbed several major parameters can be controlled to support analytical methods for the CSR algorithm. For example, parametric investigation of data format, rate, encoding, modulation, power, noise, fading, demodulation, and decoding effects on quality of service can be investigated. To verify the CSR algorithm, several different CSM state sequences were generated and provided as input to the algorithm as shown in 1.7. The output state estimates were evaluated against the input sequence for accuracy in terms of sensitivity and specificity.

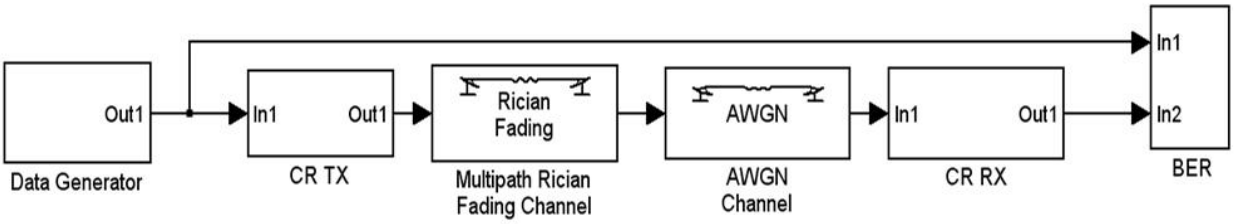

Figure 1.6: MWC Waveform Generator

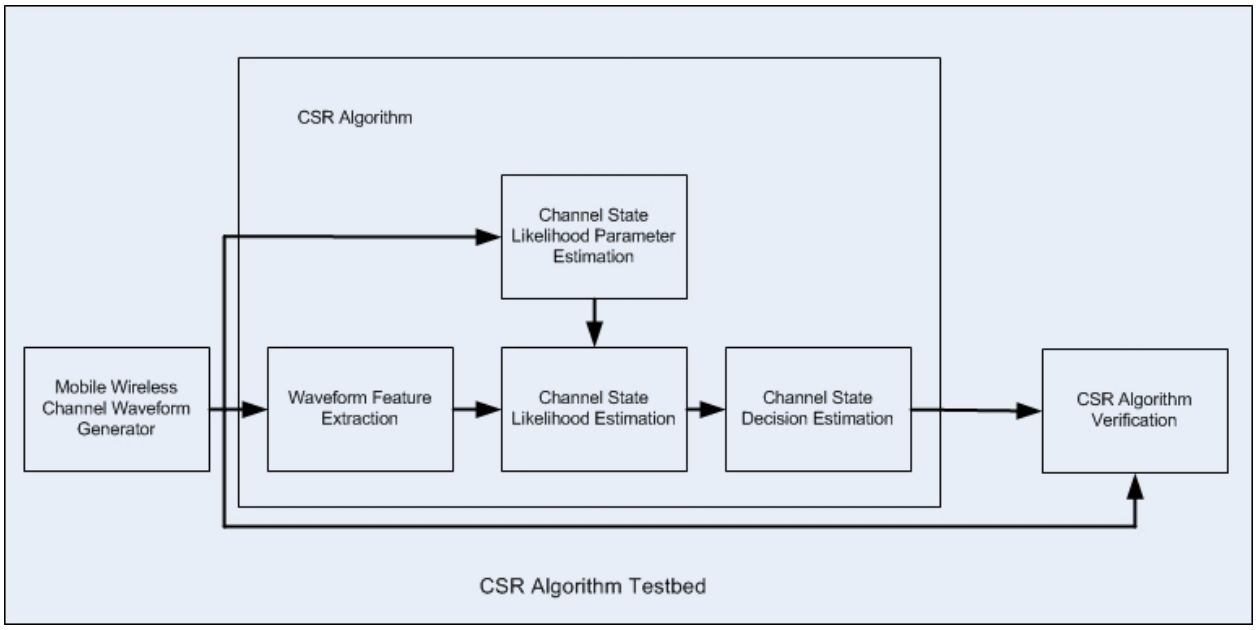

Figure 1.7: CSR Algorithm Testbed

1.3 Research Contribution

1.3.1 Existing State of Art

Channel State Model Literature Review

A more detailed discussion of a mobile wireless channel state modeling is located in A.7, a summary of this material is provided here. Several historical accounts of the evolution of finite state channel models (FSCM) are provided in the literature originating in the 1960s. Several different approaches based on Markov processes have various state definitions from simple on-off error models to more sophisticated SNR, or dwell-time states. More complex higher order models have been found to approach representative Rayleigh and Ricean distributions, error memory problems, and other accurate approaches, however, complexity limits these modeling applications. Several approaches have been reported based on state-based approaches for modeling multiple input multiple output (MIMO) channels. State space approaches with Kalman filtering (KF) have been demonstrated for dynamic tracking of channel parameters. Several state definitions were described in the literature that is summarized in Table 1.1. After this literature review, the CSM defined in this work, is determined to be a unique channel state system description. While some of these models describe MWC behavior, they do not model coherence or selectivity as hidden states. Examples of signal processing recognition systems have been developed over the past 4-5 decades for speech, facial, silhouette, handwriting, and target recognition among others. However, the CSR algorithm is one of the first applications of channel state recognition HMMs to recognizing MWC hidden coherence and selective state recognition.

Channel State Estimation Literature Review

A more detailed discussion of a CSR literature review is located in A.8, and a summary of this material is provided here. Common assumptions were discovered including: 1) stationarity for a fixed time period, 2) channel state defined by transfer function gain, 3) specific waveform or

Table 1.1: Published Mobile Wireless Channel State Definitions

Channel Definition	Reference
CIR or FIR Coefficients	[10, 11]
Bit Error Rate Statistics	[12, 13]
Block Error Rate Statistics	[14, 15]
Quantized Signal Strength	[4, 16, 17, 18, 19]
Quantized SNR	[20, 21, 22, 23, 5, 24, 25, 26, 27]
Partitioned Statistical Distributions	[28, 29, 30]
Fading Level	[30, 31, 32]
AWGN	Numerous-Refer toA.7
Log Normal Fading	Numerous-Refer toA.7
Rayleigh Distributoin	Numerous-Refer toA.7
Ricean Distribution	Numerous-Refer toA.7
Hybrid Distributions	Numerous-Refer toA.7
Cellular Systems	Numerous-Refer toA.7
Satellite Systems	Numerous-Refer toA.7
Personal Area Networks	Numerous-Refer toA.7
Indoor Propagation	Numerous-Refer toA.7
Large, Small Scale Fading	Numerous-Refer toA.7

specific communication channel fading type constraint, 4) critical processing dependence upon channel impulse response estimates at the transmitter, receiver, or both, 5) Channel impulse response tracking, 6) data assisted channel estimation processes, 7) blind and semi-blind channel state estimation approaches, 8) Gaussian distributed noise. A few articles are based on HMM methods and a few are based on cognitive, SDR, or neural network architectures. Only one article claimed distortion estimation. Performance advantages claimed include: 1) reduced computational complexity, 2) reduced overhead approaches, 3) shorten training sequences, 4) faster convergence, 5) global maximum convergence, or 6) reduced latency.

Most importantly, channel state estimation weaknesses emerge from this body of literature which are summarized in Table 1.2. The first three weaknesses are a primary focus for the CSR algorithm research, namely maintaining robust performance, optimizing resource allocations, or distortion mitigation despite dynamic MWC conditions. Secondary objectives include reducing overhead and feedback latency. Processing latency, computational complexity, and convergence will be topics for future work. The last two weaknesses are resolved by the CSR algorithm approach.

Table 1.2: Channel State Estimation Literature Search Weaknesses

1	Degraded communication performance is often assumed under very specific channel conditions. Claims by this body of literature are without exception limited to a single channel type such as: 1) flat time (invariant), 2) frequency selective, 3) low mobility (flat frequency), 4) fast fading (time selective). This set of constraints is particularly difficult to implement, given that MWC will not behave as a single channel type. When channel conditions become dynamic, the constraint is violated, and the claims fall apart.
2	Resource allocations (power efficiency, spectral efficiency, or capacity) are often based on optimal channel state or waveform configuration; when these conditions vary, suboptimum resource allocations result,
3	Distortion mitigation methods are often restricted to a single channel condition or waveform configuration; these methods depend upon accurate channel gain estimation, when these assumptions are violated, distortion mitigation degrades,
4	Overhead associated with channel impulse response estimation,
5	Processing and feedback latency,
6	Computational complexity,
7	Convergence to local maximum or weak convergence rates,
8	Offline operational processing,
9	Assumptions regarding availability of perfect and timely channel state estimates.

1.3.2 Research Questions

Several relevant and unanswered questions emerge from the weaknesses found in the the literature search on channel state and distortion estimation in the previous Section. In mobile wireless communication systems, channel state estimation methods are common and communication processing often critically depends upon accurate channel gain estimation. Most channel estimation methods define channel state as the gain of the channel transfer function. Additionally, it is common for these methods to be restricted to either coherent, or singly selective channel types, with very rare methods for dually selective channels. Furthermore, resource allocations are often fixed or based upon channel state defined in terms of time invariant impulse response. Again, distortion mitigation methods are common and restricted to either coherent, or singly selective channel conditions. When MWC conditions change, performance, resource allocations, and/or distortion mitigation methods degrade. Significant percentages of capacity (10-15%) is reserved for estimation of channel gain and distortion mitigation. Blind channel estimation methods exist to reduce overhead, but most of these methods are restricted to either coherent, or singly selective channel conditions. Data or tone assisted channel gain estimation in nonreciprocal links is common, but each of these methods requires latency for feedback from the receiver to the transmitter on a control channel. When the time period of the noncoherence decreases below the feedback latency, the channel state estimates become stale. This results in degraded system performance. Guiding research questions can be formulated and are summarized in Table 1.3.

1.3.3 Original Contribution

Coherence State Model

Table 1.3: Channel State Estimation Literature Research Questions

1	Fundamentally, is channel gain the only meaningful definition of channel state?
2	Can dispersion become a basis for channel state definitions such as coherent, singly selective, or dually selective?
3	Is there a control method whereby appropriate signal processing methods can be dynamically selected based on channel conditions other than channel transfer function gain?
4	Is there a technique to maintain communication processing performance when channels dynamically migrate between coherent, singly, or dually noncoherent?
5	Is there an approach that enables detection of channel selectivity and associated distortion?
6	Can signal processing methods be disabled when channel conditions are unfavorable?
7	Can expensive resource allocations such as power, spectrum, or bandwidth be controlled based on channel conditions other than channel impulse response?
8	Is there a means to minimize overhead associated with channel state estimation?
9	Is there a means to minimize feedback latency associated with channel state estimation?

An alternative channel state definition has been formulated based on hidden MWC dispersion processes. These MWC processes are important indicators of coherence and selectivity. The CSM shown in Figure 1.8 illustrates the designed coherent nonselective and noncoherent selective states. These states were chosen because they are relevant for signal processing environmental awareness.

Coherent State Definitions State 1 (AWGN = Additive White Gaussian Noise). In this state virtually no multipath effects and virtually no Doppler shift exist, tt represents coherent, nondispersive channel conditions.

State 2 (FN&TN = Time Non Selective and Frequency Non-selective). In this state multipath component delay and gain are minimal such that time dispersion is less than 10% of the symbol period, and velocity is minimal such that frequency dispersion is less than 10% of the symbol rate. In this state This state is represents very low relative velocities between the transmitter and the receiver; and perhaps multipath components are present, however, their delay and magnitudes are such that frequency non-selective and time non-selective channel conditions exist.

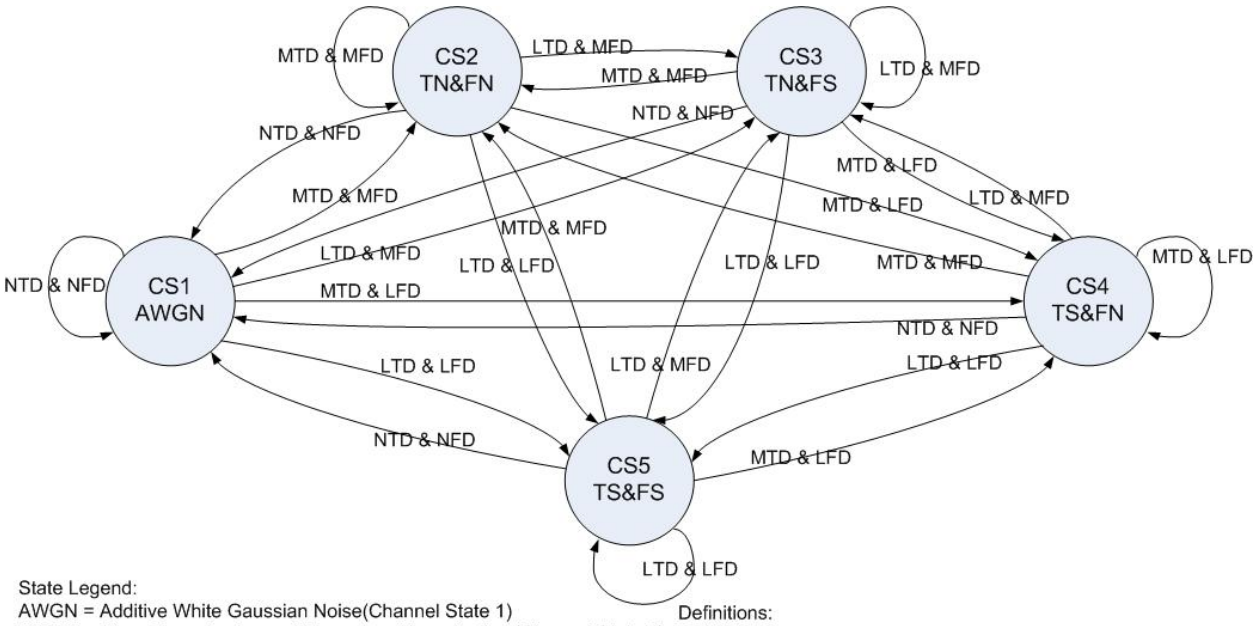

Figure 1.8: Mobile Wireless Channel Distortion State Model

Single Selective State Definitions

Single time selective (TS) or frequency selective (FS) dispersion cases also exist where either significant relative velocities or multipath effects lead to selective distortion independently in either the time or frequency domain. Selective distortion conditions are defined relative to the symbol rate. When time dispersion exceeds ~10-20% of the symbol period, frequency selectivity becomes increasingly problematic and once it approaches and exceeds the symbol period full intersymbol interference distortion produces frequency selective distortion. In a similar manner, when frequency dispersion exceeds ~10-20% of the symbol rate, interfrequency interference increases, and time selectivity becomes increasingly problematic. Once it approaches and exceeds the symbol rate, the MWC becomes fully time selective.

State 3 (FS&TN = Frequency Selective and Time Non-selective). In this state multipath delay and gain are large enough such that time dispersion exceeds 20% of the symbol period, however velocity is small enough that Doppler spread is less than 10% of the symbol rate. In this state, frequency selective and time non-selective channel conditions exist.

State 4 (FN&TS = Frequency Non-selective and Time Selective). In this state multipath delay and gain are small enough such that time dispersion is less than 10% of the symbol period, however velocity is large enough such that Doppler spread is greater than 20% of the symbol rate. In this state, frequency non-selective and time selective channel conditions exist.

Dual Selective State Definitions

Dual TS and FS dispersion is representative of MWC conditions when relative velocities between transmitter and receiver locations are large enough to cause time selective distortion and multipath components arrive with delays and magnitude sufficient to cause frequency selective distortion.

State 5 (FS&TS = Frequency Selective and Time Selective). In this state multipath delay and gain are large enough such that time dispersion is greater than 20% of the symbol period, and velocity

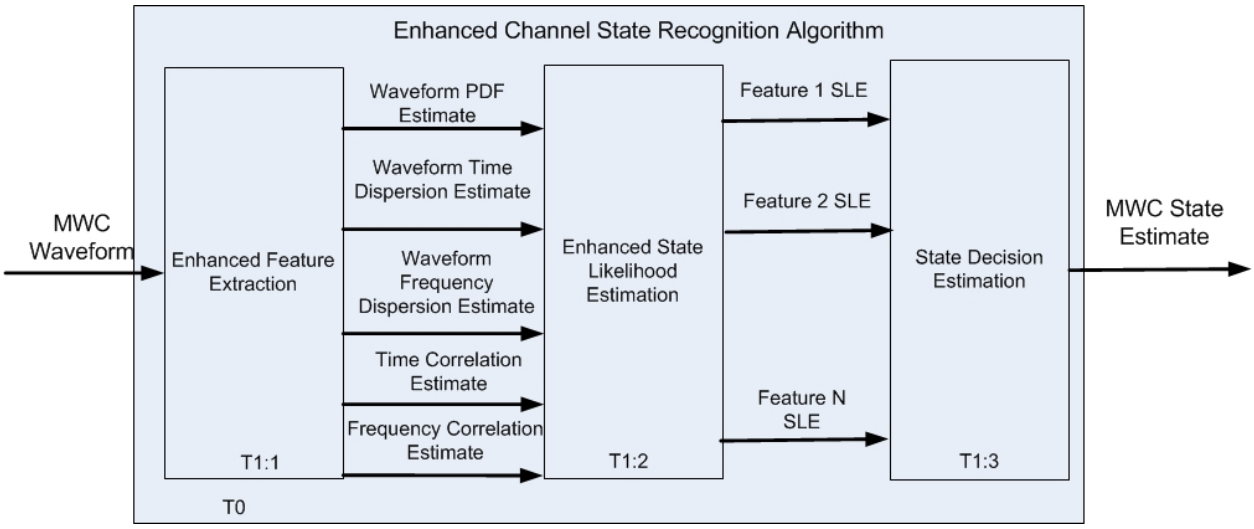

Figure 1.9: Enhanced CSR Algorithm Tier 1 System Model1.9

is large enough such that Doppler spread is greater than 20% of the symbol rate. In this state, frequency selective and time selective channel conditions exist.

CSM State Transitions

As shown in Figure 1.8, the CSM represents dynamic MWCs (changes in degrees of velocity or multipath producing variable frequency and time dispersion), by providing for transitions between the states. If MWC time-invariant conditions exist, the DSM settles into a single stable state.

CSR Algorithm Design and Verification

To investigate the feasibility of a blind coherence state awareness, a CSR algorithm shown in Figure 1.9 has been architected, designed, and verified. This channel state awareness algorithm is based on statistical feature recognition HMMs capable of detecting whether a mobile wireless channel is coherent, single time, single frequency, or dual selective. This algorithm also based upon hard state decision combining which significantly increases accuracy in terms of sensitivity and specificity performance. A CSR algorithm testbed as shown in Figure 1.10 was created.

A CSM state waveform generator was designed to create a set of waveforms whose statistics have been shaped by controlled Ricean channel impulse response configurations. These statistical re-

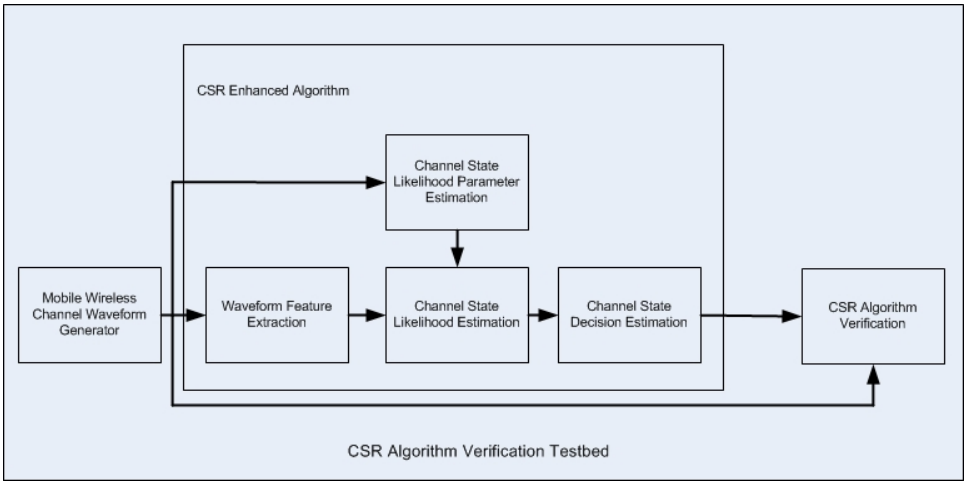

Figure 1.10: CSR Algorithm Testbed

lationships were utilized to establish HMM transition and output probability parameters. A set of statistical features were extracted from these channel dispersion state waveforms. First order amplitude probability distribution functions and second order autocorrelation functions in both the time and frequency domain were extracted from consecutive time blocks. These statistical features were input to a set of trained HMMs which for each feature computed a symbol sequence conditional likelihood estimate. These likelihood computations are proportional to the likelihood that the input sequence agrees with the training sequence. A value of 1 would signify perfect correlation between the input sequence and the training sequence while an estimate of 0 would signify perfect decorrelation between the input sequence and the training sequence. State hard decisions were computed for each feature in each time block. These hard decisions were based on a likelihood that exceeds 90% that the input sequence agrees with the training sequence. The hard decision were selected from a set of values {1, 2, 3, 4, 5} given that there are five states in the channel dispersive state model. In a given time block, the hard decisions were numerically summed to arrive at the most likely channel state decision. In this manner, the state that was most recognizable across all waveform features was weighted higher and selected as the output channel state estimate.

Table 1.4: CSR Algorithm Test State Sequences

Seqeunce ID	State Sequence
1	[1,2,3,4,5]
2	[2,3,4,5,1]
3	[3,4,5,1,2]
4	[4,5,1,2,3]
5	[5,1,2,3,4]

1.3.4 Impact

The CSR algorithm output is an estimate of channel coherent and selective states for each waveform sample block. Given this new channel state awareness, state based control processes can adapt signal processing methods as the MWC transitions between coherent and noncoherent states. Performance processes that are sensitive to channel conditions can be selected when channel characteristics are favorable or disabled when channel conditions are unfavorable. Resource consuming processes that consumed reserve capacity currently are not coherent state aware; they consume excess power, bandwidth, or capacity even when channel state offers positive margin or when conditions are unfavorable thus resulting in wasteful resource allocations. Distortion mitigation processing that are designed for a single channel characteristic, can be disabled when dynamic channel conditions change to a channel characteristic that is not favorable to the mitigation method. When the state based communication control process becomes sensitive to coherent, single time, frequency, or dual selective states, transitions between alternative resource efficient processing is enabled. This is an advantage because many existing signal processing methods, which are dependent upon accurate and timely channel transfer gain, degrade when MWC state becomes singly time selective or dual selective, rendering them ineffective. When the channel estimation methods degrade, the communication system performance is compromised. When these processes become sensitive to MWC coherent, time, frequency, and dual selective states, then dynamic performance, resource , and mitigation appropriate processing selections increase communication system resilience.

1.3.5 Significance

Environmental Impact A typical wireless network is composed of mobile switching centers, base station transceivers, and mobile devices. The core network power consumption is reported as relatively low and the power consumption of the mobile devices has been optimized, and on the order of a few Watts. However, the base station transceiver is documented as the largest power consumer in these networks. More than 60% of the base station power budget is consumed by radio equipment and amplifiers, while 11% is utilized by DC power systems, and 25% is required for equipment cooling. [33]. Published research in 2011 studied wireless network power consumption across the Italian nation; it combined power auditing data over a 1000 day period, from 95 base stations, and four wireless commercial carriers, with both second generation and third generation systems. The yearly average power consumption for a base station transceiver was determined to be 35,500 kWh/year [33]. As shown in Figure 1.11 the number of cell phone towers in the continental United States in 2012 was estimated to be 190000 [34]. Given these assumptions, a rough order of magnitude estimate of the total power consumption of the United States wireless network is 6.74 TWh/year. According to the U.S. Department of Energy, the total electric energy consumption of the United States power grid is estimated to be 3886.4 TWh/year [35]. For comparison, the U.S. wireless network consumes less than one percent, approximately .17%, of the total U.S. power consumption. Considering the environmental impact, the total U.S. annual carbon footprint is 5420 MTonnesCO2 [36], which is estimated to be 18% of the global total. Therefore, a rough order of magnitude estimate of the annual U.S wireless network carbon footprint is 9.4 MTonnes$CO_{2effective}$. Assuming $.16 per KWh, the cost to power the U.S. wireless network is approximately $1.078B. Clearly the U.S. wireless network consumes a small percentage of the electric power grid production and the global carbon footprint. However, it does incur a significant economic cost which is passed on to consumers.

As a relevant case study, consider the mobile WiMAX waveform standard [37] that was designed to provide broadband wireless service at up to 20 Mbps within 3 km diameter cells, with non-line-of-sight links and mobile speeds exceeding 60 mph. This waveform has many dynamic features

including: 1) a scalable bandwidth and data rate OFDM waveform, 2) adaptive modulation, 3) adaptive coding, 4) MIMO modes, 5) time division or frequency division duplexing modes, 6) OFDMA to enable multiple users to share the wireless service, 7) security, and 8) mobility support such as power control, delay tolerance, and channel estimation. The WiMAX waveform has allocated approximately 10% of available subcarriers as pilot channels in both UL and DL frame/subchannel configurations for channel gain estimation. It also has allocated another approximate 15% of subcarriers as frequency guard bands to mitigate the effects of frequency dispersive mobile environments. Furthermore, another 3% to 25% of time slots are allocated for cyclic-prefix time guard bands to mitigate time dispersive multipath conditions. Dynamic bandwidth, modulation, and coding rates are based upon closed loop, channel impulse response gain estimations. Periodic sounding signals are sent from the mobile station to the basestation on the uplink to estimate the channel impulse response under the assumption that the channel is reciprocol and time nonselective. The WiMAX waveform offers a relevant case study for demonstrating the potential significance of applying the CSR algorithm.

It is clear that a significant percentage of the WiMAX network capacity (10-15%) is consumed in overhead to mitigate time dispersive multipath and frequency dispersive mobile effects. Additionally, adaptive waveform features to maximize performance across dynamic link configurations depend upon accurate and timely channel gain estimation. When the mobile wireless channel is coherent, a minimum excess capacity is reserved for cyclic prefix time guard bands, and a minimum excess capacity is reserved for frequency guard bands. Additionally, when the channel becomes time variant, the adaptive performance features become compromised. In both these cases, power efficiency and spectral efficiency is degraded [38] resulting in reduced energy utilization efficiency.

The likelihood that pedestrian traffic would experience coherent channel conditions can roughly be estimated as CLE_p by the percentage of people that use the wireless system in non-urban environments vs. urban areas. This is estimated to be 21% in the continental United States [39]. The likelihood that mobile vehicle traffic would experience coherent conditions can roughly be estimated as CLE_v by the percentage of vehicles in non-urban areas verses urban areas of the con-

tinental United States. This is estimated to be 75% based on U.S. Census data [40]. The excess WiMAX capacity $\eta_{coherence}$ is estimated to be 4.8% by combining the excess WiMAX system capacity EC_{wimax} (overhead reserved for channel estimation and distortion mitigation) of 5%, the likelihood of pedestrian coherent conditions (21%), and likelihood of vehicular coherent conditions (75%) as defined in equation (1.30),

$$\eta_{coherence} = EC_{wimax} * CLE_p + EC_{wimax} * CLE_v. \tag{1.30}$$

As the market penetration of WiMAX continues to grow [41] a proportional percentage of the U.S annual wireless network power consumption will be consumed by the WiMax excess overhead without associated value. However, if the WiMAX waveform were coherent state aware, then this excess power consumption can be reduced in the following cases: 1) when coherent MWC conditions exist the guard bands can be reduced further and the channel estimation sounding period can be increased resulting in conversion of overhead to productive capacity, 2) when the MWC is singly time selective, cyclic prefix overhead can be increased while maintaining low frequency guard bands resulting in conversion of current overhead to productive capacity, 3) when the MWC is singly frequency selective, frequency guard bands can be increased while maintaining low cyclic prefix durations resulting in conversion of current overhead to productive capacity, and 4) when the MWC is dual selective, a case in which WiMAX is not effective, rather than pursue the current WiMAX waveform, alternative waveforms designed for fast fading conditions could be implemented.

It is implied that other mobile wireless waveform standards also rely upon excess capacity overhead for mitigation of time and frequency dispersion. It is also assumed that a significant percentage ~5% of the energy consumed by the continental United States wireless infrastructure is expended to support unnecessary overhead. Application of the channel coherence state model and the CSR algorithm would enable MWC awareness and wireless communications controls that would convert excess overhead to useful operational capacity when coherent states existed. The end result

Figure 1.11: Notional representation of cell phone tower distribution across United States

would therefore be increased energy benefit-cost ratios of the U.S. wireless network infrastructure. A benefit/cost ratio BC_{energy} can be formed such as defined in equation (1.31) which could be increased by approximately 5%.

$$BC_{energy} = \frac{systemcapacity(Mbps)}{annualenergyconsumption(TWh/year)} \tag{1.31}$$

A similar environmental benefit-cost ratio of the U.S. wireless network infrastructure could be formed as defined in equation (1.32),

$$BC_{environment} = \frac{systemcapacity(Mbps)}{annualcarbonfootprint(MTonnesCO_2/year)} \tag{1.32}$$

which could also be increased by approximately 5% with the application of the CSR algorithm.

Economic Impact As shown in Figure 1.12 the U.S. wireless data market revenues were forecasted to exceed $70B in 2012. As a case study, if the CSR algorithm is applied to the WiMax wireless network, the conversion of 4.8% of excess overhead capacity to operational capacity would positively impact revenues for wireless data services. Clearwater Inc. reported 11 million WiMAX subscribers with average of $11 per month revenue for a total of $1.4B in 2012 annual revenues [42]. Application of the CSR algorithm to the WiMAX waveform would convert excess overhead

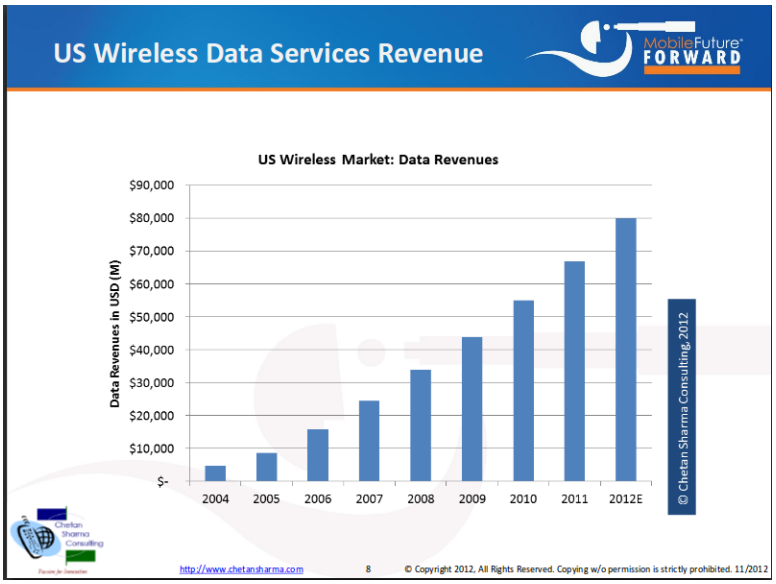

Figure 1.12: Economic Impact of Wireless Communications (Used with permission from Chetan Sharma)

to operational capacity, on the order of 4.8%; it would result in an increase of $62.72M in annual revenues.

1.4 Contribution Limits and Future Research

Limitations in the enhanced version of the CSR algorithm are noted in Table 1.5. Each is elaborated in the following paragraphs.

1.4.1 Input Waveform Configurations

The input waveforms utilized for testing of the CSR algorithm were created directly from the channel state training waveforms. This increased the likelihood that the statistical feature recognition would be successful. Generation and application of real waveforms that are representative of CSM states would be more stressful to the statistical feature recognition processes. Future work would investigate the sensitivity of the front end first order and second order statistical features that would enable discrimination of unobservable MWC state processes.

Table 1.5: Recommended Future Research

1	Input Waveform Configuration
2	Waveform Feature Block Size
3	HMM Parameter Tracking
4	HMM Computational Complexity
5	HMM Soft Decision Combining
6	Recursive Implementation
7	Cognitive Processing Integration
8	Extend CSM to Waveform State Model
9	Extend CSR to Waveform State Recognition

1.4.2 Waveform Feature Block Size

The input waveforms were partitioned into block sizes that are 10x the size of 3G/4G frames. For example, given a 1 Mbps bit rate, a 50 ms frame would be equivalent to 50K samples. This was an arbitrary choice in the original formulation of the CSR algorithm. Investigation into shorter block lengths would enable the extension of the CSR algorithm to MWCs with frame lengths on the order of 3G/4G frame sizes. For example, reducing the number of samples to 5K samples would be on the order of a 3G/4G frame size, while reduction further to 500 samples would extend the CSR algorithm to MWC with much shorter coherence times of .5 usec. These reduced frame size lengths would enable the CSR algorithm to be responsive to faster moving MWC conditions. Additionally the reduction in frame size would reduce complexity and computational intensity for the statistical feature recognition process.

1.4.3 HMM Parameter Error Tracking

HMM parameters are derived from offline training data. If the training data is representative of the input feature stream, then when waveforms with similar statistical features are applied, the sequence conditional probabilities will approach a value of 1. However, if the first order or second order statistical feature distributions become different, training data is no longer representative.

Kalman filters can be utilized to track measured covariance between the training data and the input waveform as an indicator that the training data is no longer representative. Given this error a snapshot of new data can be stored and utilized to train a new set of statistical features. Investigation into Kalman filters for tracking HMM parameter error to trigger new training data sets would enable the CSR to be adaptive to new MWC environments.

1.4.4 HMM Computation Complexity

HMM computation of sequence conditional probabilities is based on maximum likelihood algorithms which require $O(N^2T)$ computations for each feature where N is the number of states and T is the length of the time record. This is computationally intensive and makes HMMs expensive to implement. Investigation into equivalent recursive implementations of the maximum likelihood sequence conditional probability process would reduce the complexity of the CSR algorithm enabling scaling to larger state systems, and larger feature sets.

1.4.5 Feature Soft State Decison Combining

For the enhanced version of the CSR algorithm, multiple parallel waveform features are extracted. A sequence state conditional probability is computed for each input feature. The enhanced version of the CSR algorithm gnerates a hard state decision for each feature, then combines these parallel feature state decision into a single MWC state estimate for each time block. Further investigation into combining the parallel feature soft decision rather than hard decisions would improve the accuracy of each timeblock estimate.

1.4.6 Recursive Algorithm

The current version of the CSR algorithm works on batches of input data files. This architecture limits the current version to offline applications. Further investigation into recursive versions of

the CSR algorithm would enable online versions of the algorithm which would not be limited to batch processing.

1.4.7 Cognitive Processing Integration

The output channel state stream provides MWC environmental awareness regarding channel coherence and noncoherence states. These outputs can be input to communication state based control processes which could enable adapting between signal processing methods based on current channel coherence state. Investigation of a communication control system that integrates the CSR algorithm for environmental awareness would demonstrate increased performance robustness, resource efficiency and improved latency.

1.4.8 Waveform State Model

Investigation into extending the CSM to a waveform state model. This could provide the basis for waveform state recognition (WSR) algorithms.

1.4.9 Waveform State Recognition

Investigation into extending the CSR algorithm to waveform state recognition. Waveform state recognition could open approaches for wired or wireless waveform signature, modulation, coding, error, distortion recognition.

Chapter 2

Baseline CSR Algorithm

There are two versions of the CSR algorithm; the first is a baseline version utilized for proof-of-concept (POC) verification. It serves to prove that the CSM and CSR are feasible. A second enhanced version includes additional feature extraction methods, parallel state likelihood estimation, and hard decision combining, to improve state recognition accuracy sensitivity and specificity. This chapter analyzes the baseline CSR algorithm by defining architecture, system, data, and analytical models at four levels of detail.

2.1 Tier 0 Analysis

This Section will describe the baseline algorithm first and lowest level of detail. Subsequent subsections will embellish additional details.

2.1.1 Architecture

The CSR algorithm architecture shown in Figure 2.1 contributes environmental awareness to CPA by recognizing MWC hidden coherent nonselective and noncoherent selective states from the observable received waveform. The CSR algorithm relies upon state-based statistical feature recognition HMMs to produce blind MWC hidden state estimates (without the aid of online training

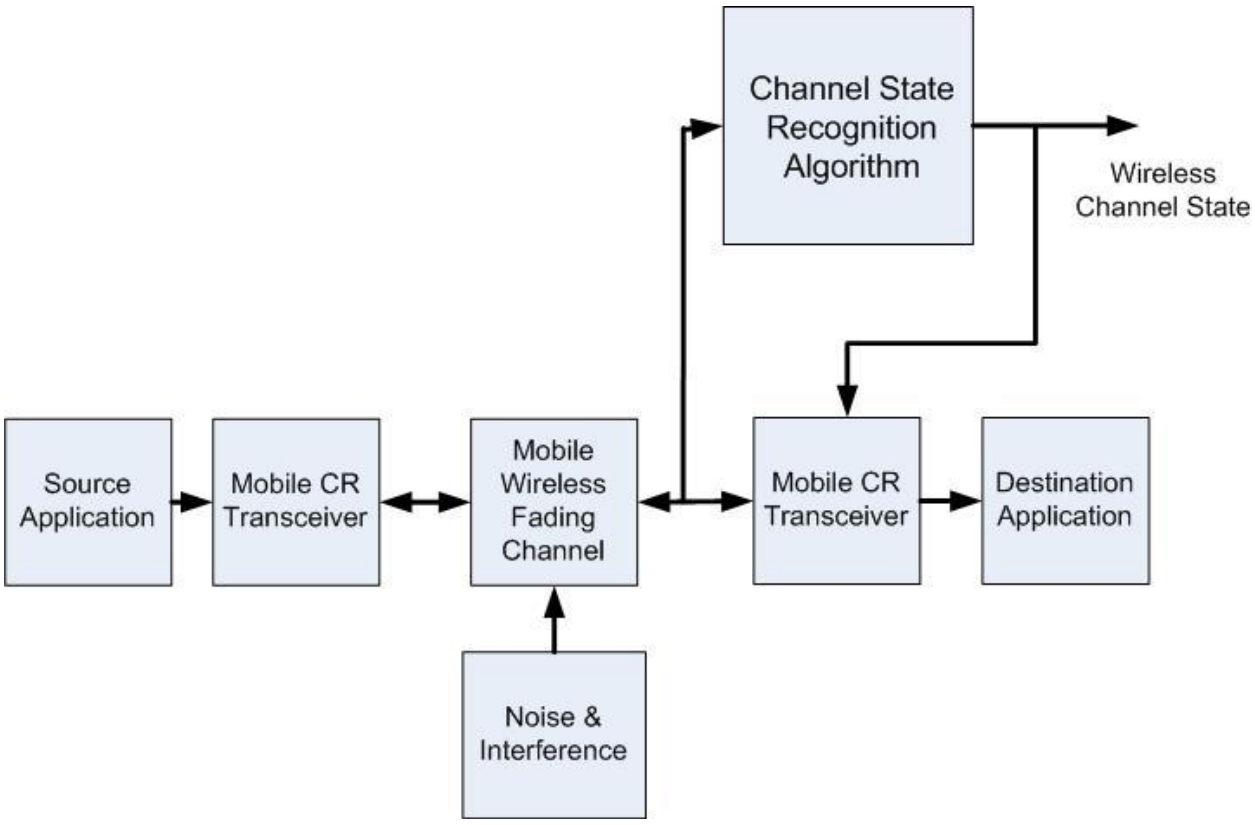

Figure 2.1: CSR Algorithm Architecture

sequences or pilot tones). Note that at present the CSR algorithm is an independent process which provides channel sensing that produces environmental awareness as an input to the mobile cognitive transceiver. The cognitive TXR and communication control processes are outside the scope of the CSR algorithm. In the future the CSR algorithm could be integrated directly into the cognitive TXR.

2.1.2 Data Model

Referring to Figure 2.2, the input can be described as a vector of complex waveform samples defined by equation (2.1)

$$WS_{mn} = \begin{bmatrix} WS_{11} & WS_{12} & \cdots & WS_{1N_{tot}} \\ WS_{21} & WS_{22} & \cdots & WS_{2N_{tot}} \end{bmatrix}, \tag{2.1}$$

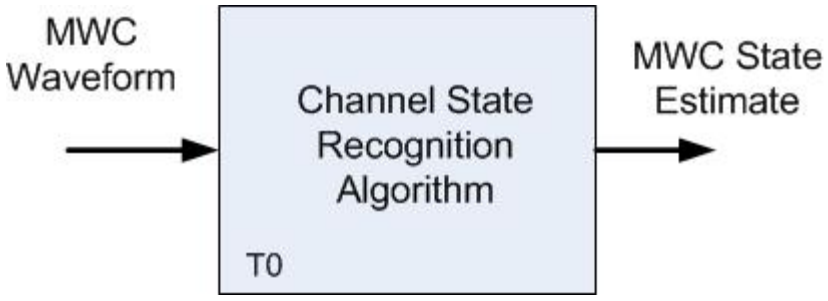

Figure 2.2: Tier 0 System Model

with each waveform sample defined as $WS_{mn} \in R$, *and* $WS_{min} < WS_{mn} < WS_{max}$.

The following parameter definitions apply:

Minimum waveform amplitude = WS_{min},

Maximum waveform amplitude = WS_{max},

R = Set of Real Numbers,

I/Q component index = m = $\begin{cases} 1 & for\ waveform\ symbol\ real\ component \\ 2 & for\ waveform\ symbol\ imaginary\ component \end{cases}$,

Waveform sample index = n = $\{0 \quad 1 \quad \cdots N_{tot}\}$,

Input waveform sample rate = $f_s > 2 * f_m$,

Input waveform maximum frequency component = f_m,

Input waveform sample period = $T_s = \frac{1}{f_s}$,

Total number of waveform samples = N_{tot},

Total observation period = $T_{tot} = N_{tot} * T_s$,

Total number of samples in a waveform block = N_{blk},

Total number of waveform blocks = $k_{blk} = \frac{N_{tot}}{N_{blk}}$,

Waveform block period = T_{blk},

Waveform block sample rate = $f_{blk} = \frac{1}{T_{blk}} = \frac{1}{N_{blk} \times T_s} = \frac{f_s}{N_{blk}}$,

Waveform block stream = $WB_k = \left[WB_1 \quad WB_2 \quad \cdots \quad WB_{k_{blk}} \right]$,

Waveform block index = k $= \left\{ 0 \quad 1 \quad k_{blk} \right\}$,

Waveform sample blocks = $BS_{ij} = \begin{bmatrix} BS_{11} & BS_{12} & \cdots & BS_{1N_{blk}} \\ BS_{21} & BS_{22} & \cdots & BS_{2N_{blk}} \end{bmatrix}$,

I/Q component index = i $= \begin{cases} 1 & for\ block\ symbol\ real\ component \\ 2 & for\ block\ symbol\ imaginary\ component \end{cases}$,

Block sample index = j $= \left\{ 0 \quad 1 \quad N_{blk} \right\}$.

Again referring to Figure 2.2, the output is a sequence of channel state estimates (CSE) defined by equation (2.2),

$$\widehat{CSE_k} = \left[\widehat{CSE_1} \quad \widehat{CSE_2} \quad \cdots \quad \widehat{CSE_{N_{cse}}} \right]. \tag{2.2}$$

The following parameter definitions apply:

$CSE_x \in N\ and\ 0 < CSE_x < N_{cs}$,

$N =\ Set\ of\ Natural\ Numbers$,

Total number of channel states = N_{cs},

Total number of channel state estimates = $N_{cse} = k_{blks} = \frac{N_{tot}}{N_{blk}}$,

Channel state estimate sample rate = $f_{cs} = f_{blk} =\ waveform\ block\ sample\ rate = \frac{f_s}{N_{blk}}$,

Total waveform samples in a block = N_{blk},

Waveform block index = k $= \left\{ 0, \quad 1, \ldots \quad k_{blk} \right\}$,

Channel state estimate period = $T_{cs} = \frac{1}{f_{blk}} = T_{blk}$.

2.1.3 Analytical Model

The analytical model defines a transfer function in equation (2.3) such that is possible to compute the output channel state estimate sequence on a floating point or a fixed point processor given the

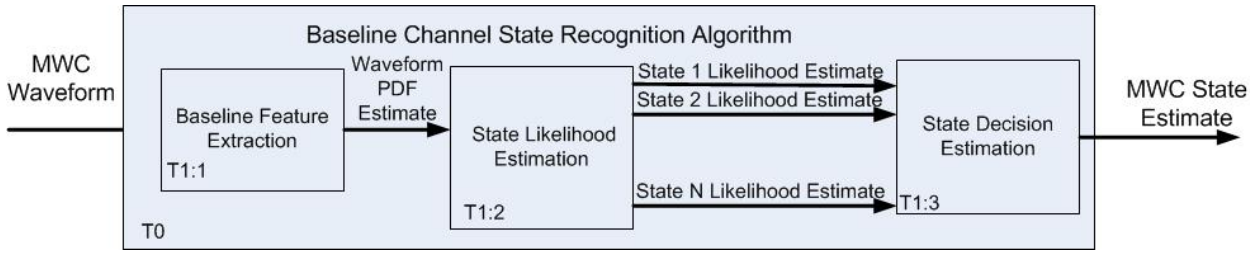

Figure 2.3: Tier 1 Architecture

input waveform sequence. The Tier 0 analytical process can be expressed as the product of the Tier 1 subprocesses where: 1) $CSR(\ldots)$ is a function defined in either the time or the frequency domain; 2) $f(\ldots)$is a function based on the feature extraction (FE) process; 3) $g(\ldots)$is a function based on the state likelihood (SL) process; and 4) $h(\ldots)$is a function based on the state decision (SD) process. Each of these functions will be defined in the Tier 1-3 analytical models to follow.

$$CSR_0(\ldots) = \frac{C\hat{S}E_k}{WS_{mn}} = f(FE) * g(SL) * h(SD). \tag{2.3}$$

2.2 Tier 1 Analysis

This Section will analyze the baseline algorithm second level of detail.

2.2.1 Architecture

The Tier 1 architecture shown in Figure 2.3 comprises three subprocesses: 1) feature extraction (T1:1), 2) state likelihood estimation (T1:2), and 3) state decision estimation (T1:3). The feature extraction (FE) process transforms the input envelope magnitude into a sequence of waveform feature vectors (WFV) via a histogram approximation method. The state likelihood estimation process transforms the WFV into a sequence of state likelihood estimate (SLE) vectors via a statistical feature recognition HMM. The state decision estimation (SDE) process transforms the SLE vector into a sequence of channel state estimates (CSE) with maximum likelihood sequence estimation methods. All these processes operate at the waveform block rate.

Figure 2.4: Feature Extraction System Model

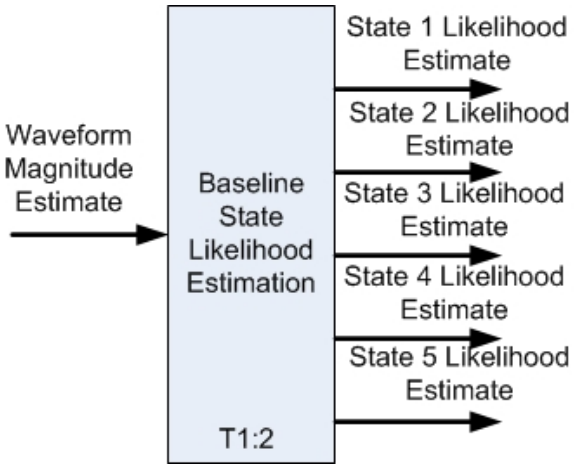

Figure 2.5: State Likelihood Estimate System Model

Waveform Feature Extraction

The FE process (T1:1) shown in Figure 2.4, provides a method for extracting the input waveform magnitude PDF.

State Likelihood Estimation

The state likelihood estimation process (T1:2) shown in Figure 2.5, produces a sequence of SLE which defines how well the input WFV compares to the state sequence memory of the trained HMM. The SLE contains a vector of likelihood estimates, one for each hidden state. Each SLE indicates how likely the input WFV agrees with each training hidden state sequence. For N hidden states, the SLE will contain N parameters. For example, if the waveform sample block is actually from state 1, then you would expect a high likelihood for the channel state 1 parameter and low likelihood for all other channel state parameters.

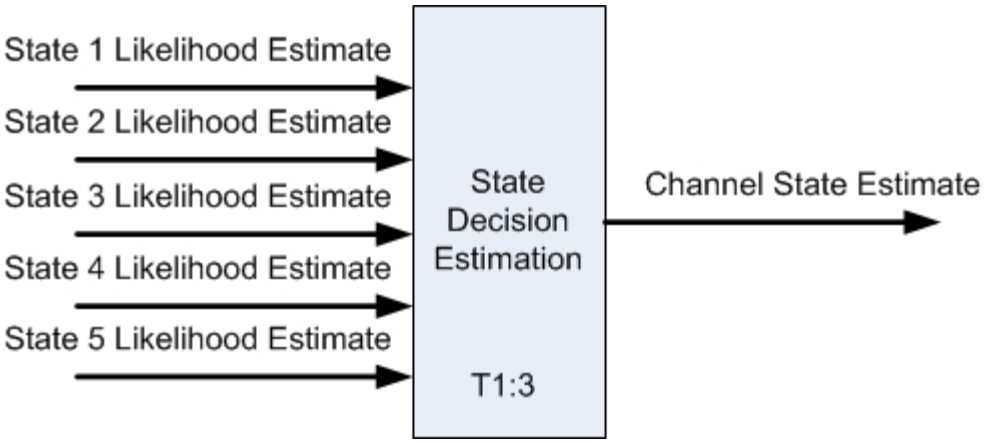

Figure 2.6: State Decision Estimation System Model

State Decision Estimation

The state decision estimation process (T1:3) shown in Figure 2.6, selects the most likely channel state. It evaluates each of the input SLE vectors and identifies the maximum likelihood state. The state decision estimation process includes methods for sorting and selecting the maximum likely state within each SLE vector.

2.2.2 Data Model

Feature Extraction

Referring to Figures 2.3 and 2.4, the output of the baseline FE process is a sequence of WFV each containing a complex envelope magnitude PDF estimate defined as equation (2.4)

$$WFV = \left[\widehat{CEM}_1\widehat{CEM}_2\ldots\widehat{CEM}_{k_{blk}}\right]. \tag{2.4}$$

The following parameter definitions apply:

Waveform block index = k,

Total number of waveform blocks = k_{blk},

Channel state estimation period = $T_{cs} = \frac{1}{f_{blk}} = T_{blk}$,

Complex envelope magnitude relative frequency = $\widehat{CEM}_j \in N$,

where $CEM_{minbin} < \widehat{CEM}_j < CEM_{maxbin}$,

CEM bin index = j,

Waveform block rate = f_{blk},

Waveform block period = T_{blk},

Symbol Period = T_s,

Input waveform sample rate = f_s,

Natural numbers = N,

CEM_{minbin} = Minimum bin index, and

CEM_{maxbin} = Maximum bin index.

State Likelihood Estimation

The output of the state likelihood estimation process is a state likelihood vector (SLV) comprising one SLE for each WFV. The SLV is defined by equation (2.5)

$$SLV = \left[\widehat{SLE_1} \quad \widehat{SLE_2} \quad \cdots \quad \widehat{SLE_{kblk}}\right]. \tag{2.5}$$

The following parameter definitions apply:

Waveform block index = k,

Total number of State Likelihood Estimates = $k_{blks} = N_{SLE}$,

Waveform block rate = f_{blk},

State Likelihood Estimates = $SLE_k = \left[\widehat{S1E} \quad \widehat{S2E} \quad \cdots \quad \widehat{SN_{cs}E}\right]$,

State Likelihood Estimate = $\widehat{SLE} \in R$ *and* $0 \leq \widehat{SLE} \leq 1$, and

Number of channel states = N_{CS}.

State Decision Estimation

The output of the state decision process is a state decision vector (SDV) that includes a sequence of SDE, one for each waveform block, defined by equation (2.6)

$$SDV = \left[SDE_1 \quad SDE_2 \quad \cdots \quad SDE_{N_{SD}}\right]. \tag{2.6}$$

The following parameter definitions apply:

Natural numbers = N,

State decision estimate = SDE = $SDE_k \in N, \;\; 1 \leq SDE_k \leq N_{CS}$,

State decision estimate index = k, $1 < k < N_{SD}$,

Number of possible channel states = N_{CS},

Total number of state decision estimates = $N_{SD} = k_{blk}$.

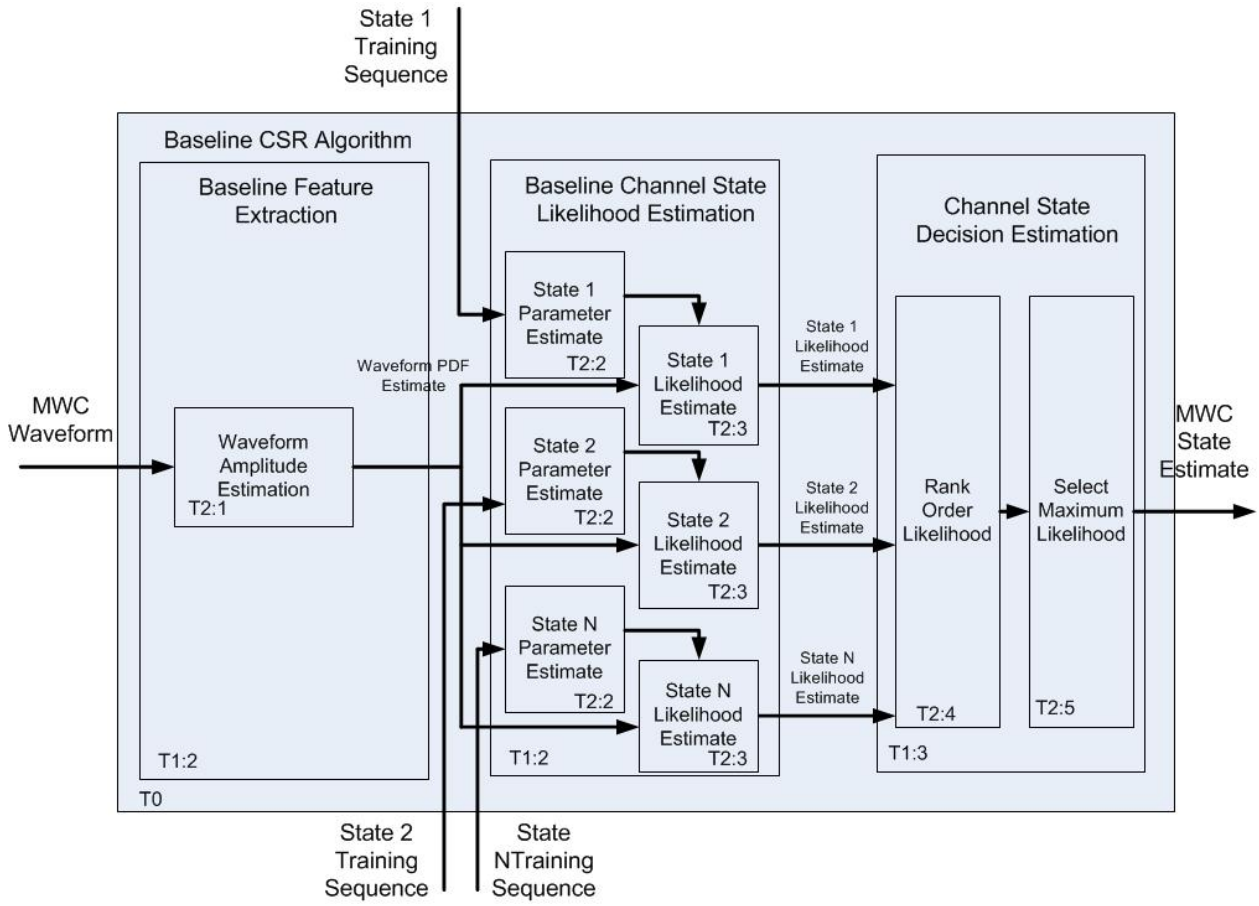

Figure 2.7: Tier 2 Architecture

2.3 Tier 2 Analysis

This Section will analyze the baseline algorithm third level of detail.

2.3.1 Architecture

The Tier 2 architecture, shown in Figure 2.7, comprises five subprocesses: 1) waveform PDF estimation (T2:1), 2) state likelihood parameter estimation (T2:2), 3) state likelihood estimation (T2:3), 4) likelihood rank order (T2:4), and 5) likelihood maximum selection (T2:5).

Waveform Magnitude Estimation

Referring to Figure 2.7, the CEM process (T2:1) shown in Figure 2.8, estimates the CEM PDF.

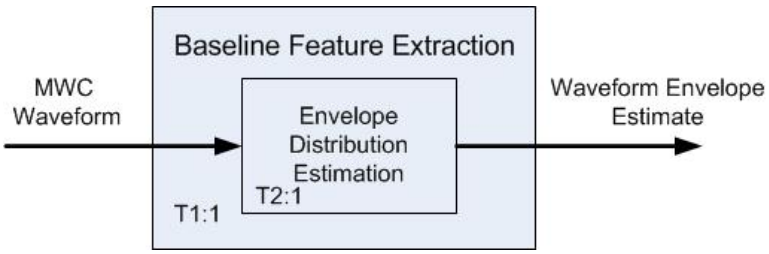

Figure 2.8: Complex Envelope Magnitude Distribution Estimation

State Likelihood Estimation

Referring to Figure 2.7, the feature state likelihood estimator (T1:2), shown in Figure 2.9, produces a SLE for each channel state. To implement the CSM, which has five defined coherent nonselective and noncoherent selective states, a trained HMM will generated five SLEs for each input waveform block. The baseline state likelihood estimator process includes two subprocesses: 1) state likelihood parameter (SLP) estimator, and 2) state likelihood estimator. An HMM requires a set of memory parameters estimated from an associated training sequence that has statistics similar to the operational waveform sequence. The output of the SLP estimation process includes an HMM state transition and output probability matrix which define how each hidden state is likely to transition to the next state and also how likely the output value is given the current hidden state. The SLP process relies upon a common dynamic programming algorithm, however the training sequence for each state is required to be unique. The output of the SLP estimator is a pair of transition and output probability matrices. These parameters formulate the HMM memory and are required by the HMM to implement a common ML sequence estimation algorithm applied to the operational sequence for state likelihood estimation. There are two inputs to the state likelihood estimation process: 1) state likelihood parameters, and 2) operational waveform sequences. The output is an estimate of the likelihood that the input sequence statistics match the statistics of the HMM training sequence.

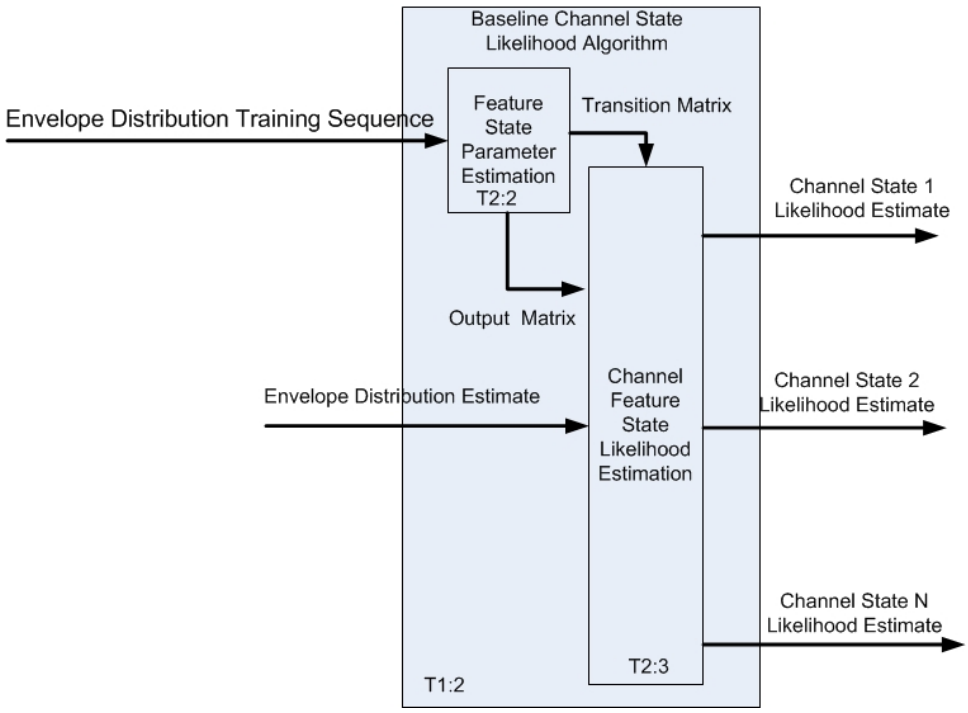

Figure 2.9: Channel Feature State Likelihood System Model

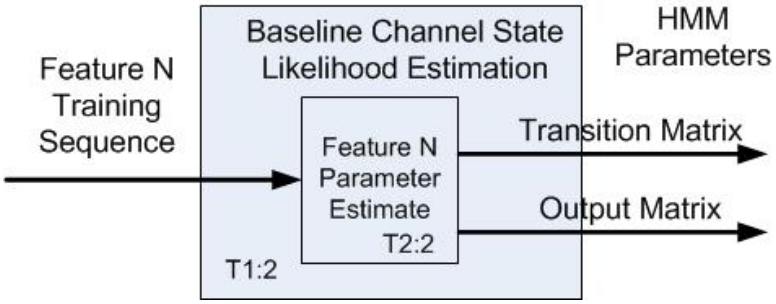

Figure 2.10: State Likelihood Parameter Estimation System Model

State Parameter Estimation

Referring to Figure 2.9, the SLP estimation process (T2:2) shown in Figure 2.10, estimates the state likelihood parameters for each HMM. The SLP estimation input is an offline sequence of training symbols that are statistically similar to the expected operational sequence.

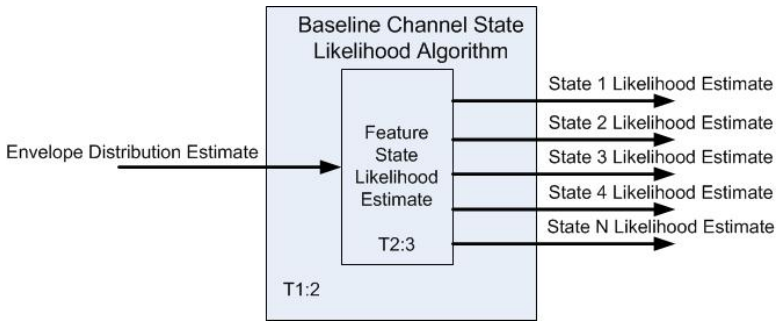

Figure 2.11: State Likelihood Estimation System Model

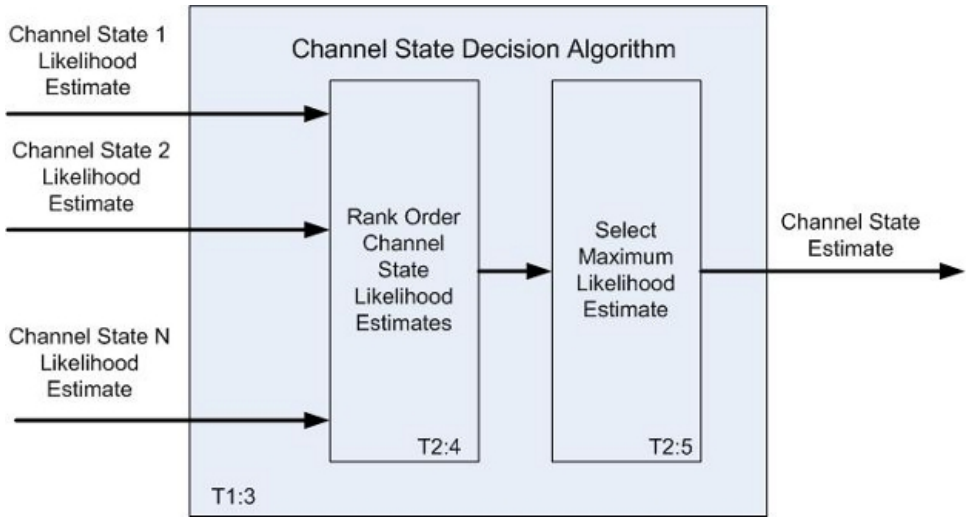

Figure 2.12: State Decision Estimation System Model

State Likelihood Estimation

Referring to Figure 2.9, the Tier 2 state likelihood estimation method (T2:3) shown in Figure 2.11, estimates the likelihood that the input sequence matches the trained HMM hidden state sequence.

State Decision Estimation

The Tier 2 state decision estimator (T1:3) process shown in Figure 2.12, comprises two subprocesses: 1) rank order state likelihood, and 2) select the maximum likelihood. Referring to Figure 2.12, the CSE is selected as the most likely state based on the largest SLE provided by the state likelihood estimator.

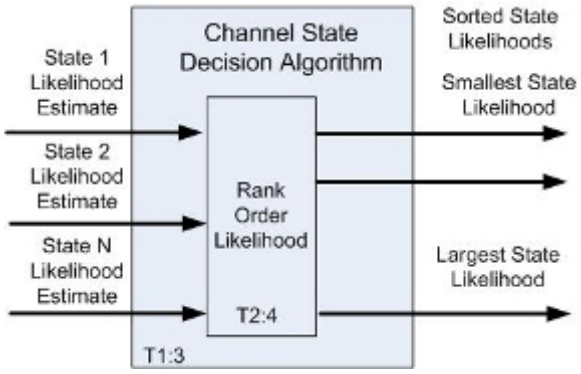

Figure 2.13: Likelihood Rank Order System Model

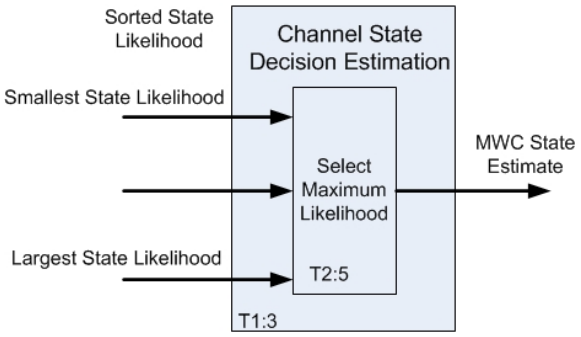

Figure 2.14: Likelihood Maximum Selection System Model

Likelihood Rank Order Referring to Figure 2.12 and Figure 2.13, the Tier 2 rank order likelihood method (T2:4) sorts the input state likelihood estimates into ascending order. The output of this function is a sequence of SLE that have been reorganized into ascending order.

Likelihood Maximum Selection System Model Referring to Figure 2.12 and Figure 2.14, the Tier 2 select maximum likelihood method (T2:5) selects the maximum SLE. The output of this function is a sequence of the most likely CSE.

2.3.2 Data Model

Waveform Magnitude PDF Feature Extraction

The CEM PDF estimation output is a sequence of CEM samples CEM_x quantized into a set of characters $C_x \in \begin{bmatrix} C_1 & C_{N_{char}} \end{bmatrix}$ where C_x is a member of the character alphabet, and N_{char} is the

number of characters in the alphabet, given $\widehat{A_j} \in R$, and $0 < \widehat{A_j} < A_{max}$. Each character in the alphabet is assigned a key index to each equally sized amplitude bins that partition the amplitude range between 0 and A_{max}. The bin index size = $\frac{A_{max}}{N_{char}}$ and bin index j is the bin number where $A_{j-1} < A_j < A_{j+1}$.

State Parameter Estimation

The output of the SLP estimation process is a set of HMM memory parameters defined by three matrices: 1) initial probability, 2) transition probability, and 3) output probability. The initial probability matrix defines the initial state probability occurring at $t_0 = 0$. The initial probability matrix is defined by equation (2.7),

$$P_i = \begin{bmatrix} 1 & 0 & 0 & 0 & 0 \end{bmatrix}, \tag{2.7}$$

where the baseline SLE process is assumed to be initialized in state 0. The transition probability matrix is defined by equation (2.8),

$$P_t = \begin{bmatrix} \alpha_{11} & \alpha_{12} & \alpha_{13} & \alpha_{14} & \alpha_{15} \\ \alpha_{21} & \alpha_{22} & \alpha_{23} & \alpha_{24} & \alpha_{25} \\ \alpha_{31} & \alpha_{32} & \alpha_{33} & \alpha_{34} & \alpha_{35} \\ \alpha_{41} & \alpha_{42} & \alpha_{43} & \alpha_{44} & \alpha_{45} \\ \alpha_{51} & \alpha_{52} & \alpha_{53} & \alpha_{54} & \alpha_{55} \end{bmatrix}, \tag{2.8}$$

describes the transition probabilities between the hidden states. The parameter α_{mn} determines the likelihood of a transition from state m to state n. The output probability matrix is defined by equation (2.9),

$$P_t = \begin{bmatrix} \varepsilon_{11} & \cdots & \varepsilon_{1N_{char}} \\ \vdots & \ddots & \vdots \\ \varepsilon_{N_{CS}1} & \cdots & \varepsilon_{N_{cs}N_{char}} \end{bmatrix}, \tag{2.9}$$

describes the probability of an observed output symbol given a particular state. The parameter ε_{xy} defines the probability that an observed output symbol C_y in an alphabet N_{char} given the current state of the system.

The following definitions apply:

$\varepsilon_{xy} \in R$, where R is the set of real numbers,

$y \in \left[1 \ldots \quad N_{char}\right]$, where N_{char} is the number of characters in the output alphabet,

$x \in \left[1 \quad \ldots N_{cs}\right]$, where N_{cs} is the number of channel states in the HMM,

$C_y \in \left[C_1 \ldots \quad C_{N_{char}}\right]$, where C_x is a character in the output symbol alphabet.

Rank Order Likelihood The output of the rank order likelihood (ROL) process is a SLV where each SLE element has been rank ordered in ascending order of magnitude as defined in equation (2.10),

$$\mathrm{SL}E_{\mathrm{k}} = \left[\widehat{\mathrm{S1E}} \quad \widehat{\mathrm{S2E}} \quad \cdots \quad \widehat{\mathrm{SN_{CS}E}}\right], \tag{2.10}$$

where $\widehat{\mathrm{S1E}} < \widehat{\mathrm{S2E}} < \cdots < \widehat{\mathrm{SN_{CS}}}$.

Select Maximum Likelihood Data Model The output of the select maximum likelihood (SML) process is a CSE which is the maximum SLE previously defined in the Tier 0 data model.

2.4 Tier 3 Analysis

This Section will analyze the baseline algorithm fourth level of detail.

2.4.1 Architecture

The Tier 3 architecture shown in Figure 2.15 comprises five methods: 1) complex envelope magnitude pdf extraction (T3:1), 2) Viterbi and Baum Welch likelihood model parameter estimation

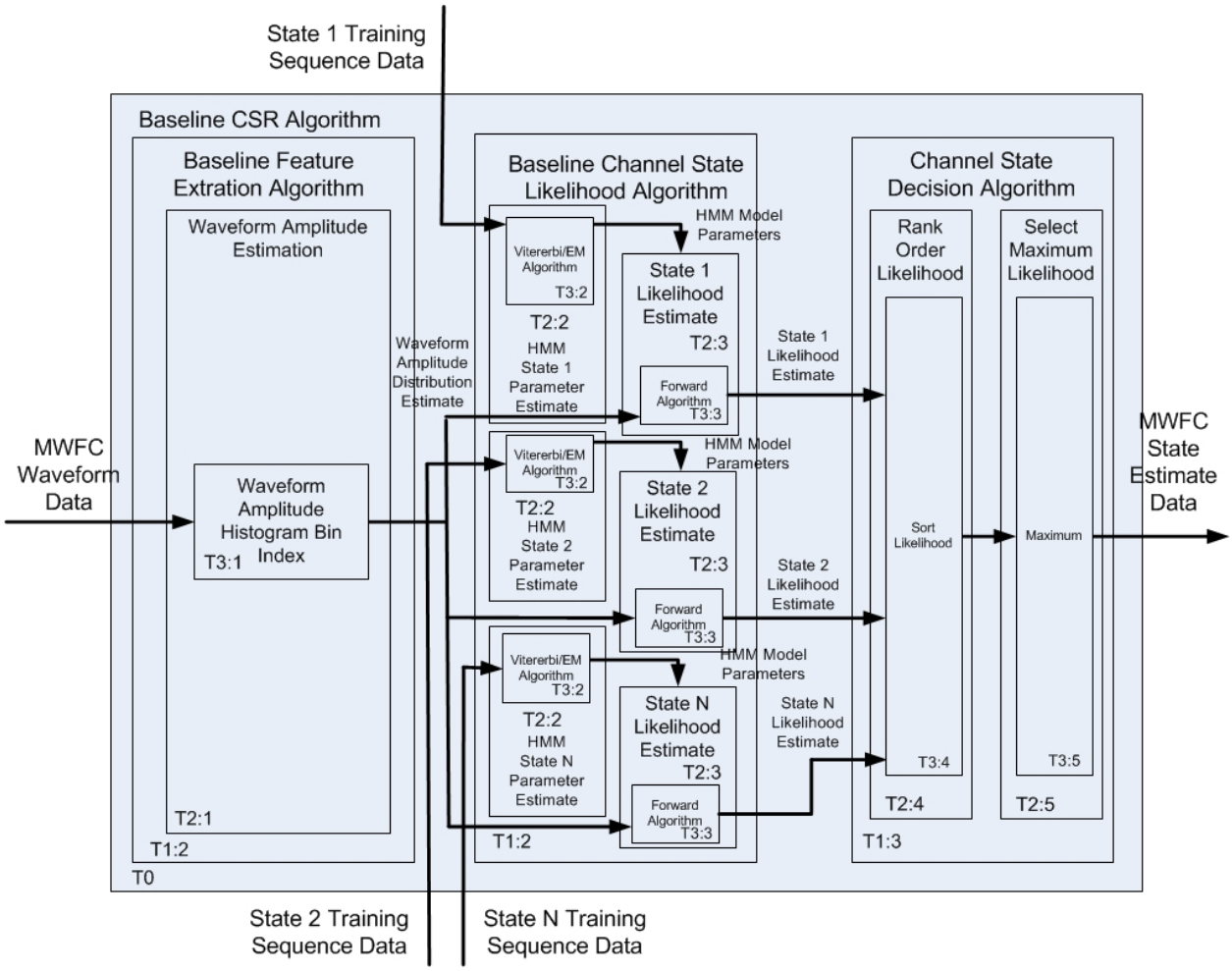

Figure 2.15: Tier 3 Architecture

(T3:2), 3) forward state likelihood estimation (T3:3), 4) rank order likelihood (T3:4), and 5) select maximum likelihood (T3:5).

Waveform Magnitude Distribution Estimation

Referring to Figure 2.15, the CEM PDF extraction method shown in Figure 2.16, estimates the MWC CEM distribution. This method implements a histogram algorithm by accumulating CEM relative frequency in each equally sized magnitude bins. The output of this method is a sequence of CEM distribution estimates; one for each input waveform block.

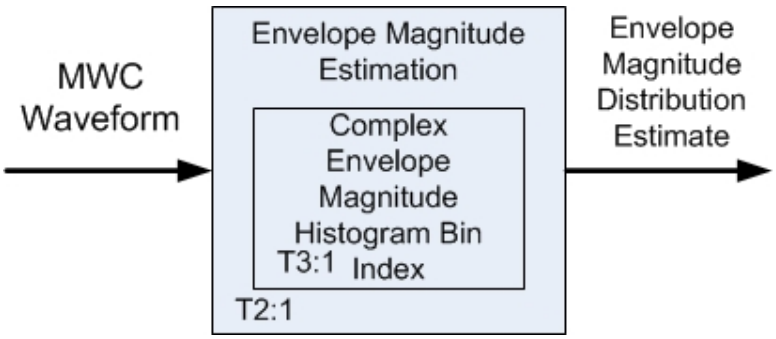

Figure 2.16: Complex Envelope Magnitude Distribution System Model

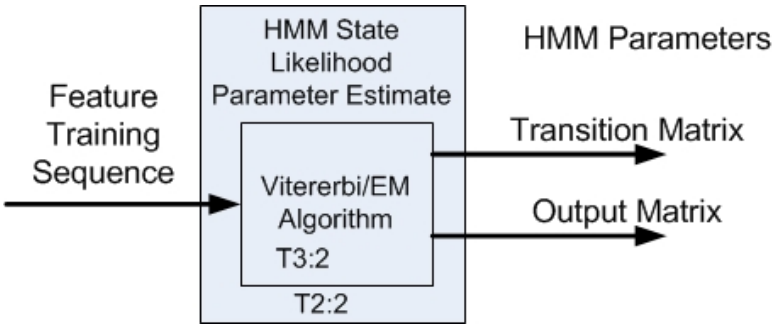

Figure 2.17: State Parameter Estimation System Model

State Parameter Estimation System

Referring to Figure 2.15, the SLP estimation (T3:2) system model shown in Figure 2.17, estimates the HMM state likelihood parameters. The SLP estimation output includes both a transition, and output probabilities that defines the state sequence memory for the feature recognition HMM. This method implements either or both the Viterbi and Expectation Maximum (EM) algorithm to produce the HMM parameters. The Viterbi algorithm is applied if the input state sequence is available in addition to the symbol sequence while the EM algorithm is applied if only the symbol sequence is available. Additionally the EM algorithm can be iteratively applied to the output of the Viterbi process to reduce the mean squared error of the parameter estimates.

State Likelihood Estimation

Referring to Figure 2.15, the state likelihood estimate system model (T3:3) shown in Figure 2.18, computes a SLE for each hidden state with the forward ML algorithm. The inputs to this method

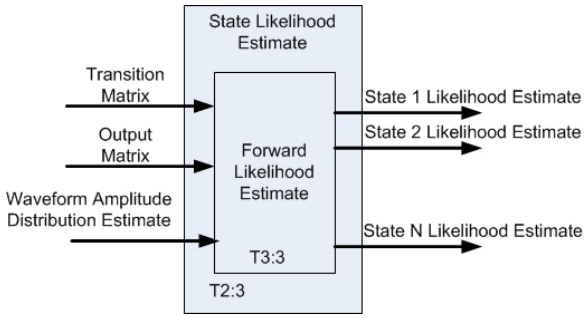

Figure 2.18: State Likelihood Estimation System Model

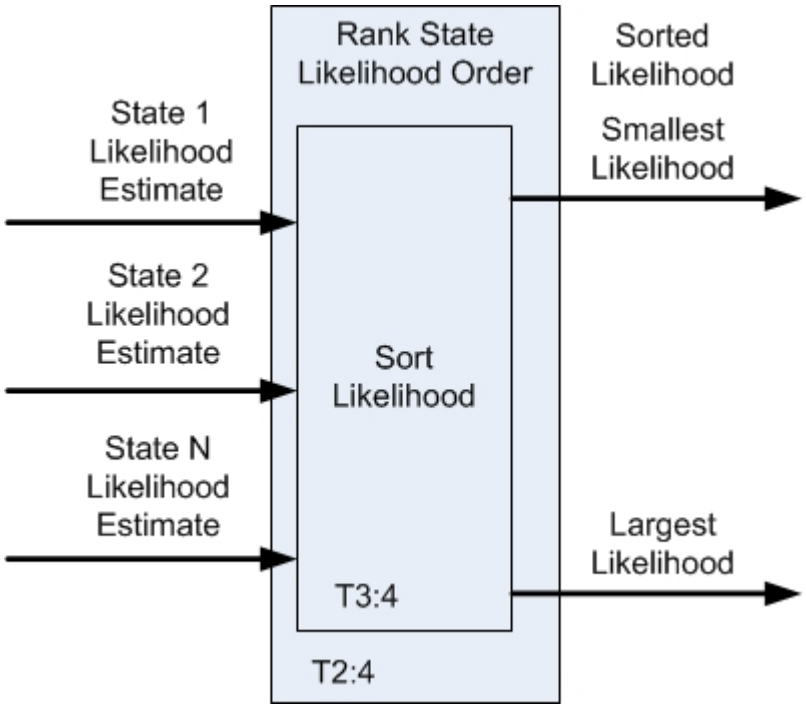

Figure 2.19: Likelihood Rank Order System Model

include: 1) transition probability matrix, 2) output probability matrix, and 3) operational WFV. The output of this function is a sequence of SLE.

Rank Order Likelihood Referring to Figure 2.15, the ROL method (T3:4) shown in Figure 2.19, sorts the input SLE into ascending order. The output of this method is a sequence of sorted SLE.

Select Maximum Likelihood Referring to Figure 2.15, the SML method (T3:5) shown in Figure 2.20, selects the maximum SLE.

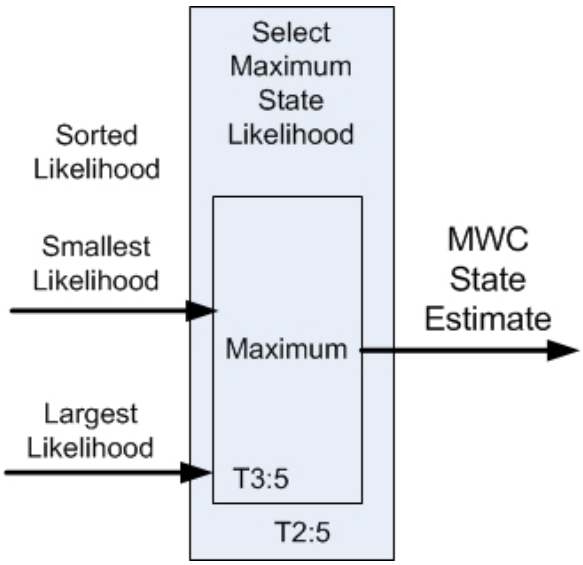

Figure 2.20: Select Maximum State Likelihood System Model

2.4.2 Analytical Model

The purpose of this mathematical model is to express the baseline CSR process behavior in terms of mathematical operators such that its transfer function can be implemented with a floating or fixed-point processor.

Waveform Feature Extraction

Given that the input is a MWC random process, first order statistics are useful for characterization and a histogram estimation algorithm will be utilized to estimate the CEM frequency distribution. The mathematical model for estimating the CEM distribution is shown in equations (2.11 - 2.13). The histogram can be defined by equation (2.11),

$$N = \sum_{i=1}^{j} N_{bin}. \tag{2.11}$$

Where N is the total number of observations, j is the total number of bins, and N_{bin} are the number of observed discrete complex envelope magnitude $|R(kT)|$ samples in each bin. The number of bins can be defined with a number of alternative approaches. For this CEM distribution, bin width

B_{width} is defined by equation (2.12),

$$B_{width} = \frac{R_{magmax} - R_{magpmin}}{k}. \tag{2.12}$$

Where k is an arbitrary number of bins chosen to produce a smooth and continuous distribution, R_{magmax} is the maximum CEM observation, and R_{magmin} is the minimum CEM observation. Next, distribute the CEM observations into each bin and accumulate the total number of observations (N_{bin}) in each bin. Finally, normalize the magnitude of each bin as defined in equation (2.13),

$$f = \frac{N_{bin}}{N}, \tag{2.13}$$

such that the total area under the curve is equal to one by dividing the total number of observations in each bin by the total number of observations such that the area of each bin approaches the percentile of observations in that bin. With these constraints, the histogram approaches an estimate of probability distribution. Given that a block of MWC random complex symbols are provided as input to this process, the output is an estimate of the waveform CEM distribution for each input block. The mean magnitude level can be estimated from the distribution with equation (2.14),

$$\hat{\mu} = \frac{1}{j}\sum_{i=1}^{j} f_i. \tag{2.14}$$

Furthermore, the variance of the received waveform complex envelope is estimated from the distribution with equation (2.15),

$$\widehat{\sigma^2} = \frac{1}{j}\sum_{i=1}^{j} (f_i - \hat{\mu})^2. \tag{2.15}$$

Refer to Appendix Section A.11.2 for additional background material.

State Likelihood Parameter Estimation

The discussion of HMMs will be based on widely cited introductory works by Durbin [9] and Rabiner [1]. Introduction to the difference between state sequences and symbol sequences is given by Rabiner [1]. For the MWC state recognition algorithm, states are defined by the CSM and hidden state sequences correspond to the presence of MWC coherent nonselective or noncoherent selective states. The observed symbol sequences correspond to the MWC received waveform symbols.

The 5 elements of an HMM [1] are defined as:

1. The number of hidden states in the model (N_s) . The states are defined as $S = \{S_1, S_2, \cdots S_{N_s}\}$ and the state probability at time $t = q_t$. For the CSR algorithm, the CSM defines 5 channel coherent and selective states, therefore, the number of HMM states is five.

2. The number of discrete observable symbols per state is M; the character alphabet size. The individual symbols are defined as $V = \{v_1, v_2, \cdots v_M\}$. For the CSR algorithm, waveform feature distributions are estimated with a resolution equal to k, the size of each histogram bin, and M has been fixed at 200.

3. State transition probability matrix $A = \{a_{ij}\}$, where $a_{ij} = P\left[q_{t+1} = S_j \middle| q_t = S_i\right]$, and $1 \leq i,\ j \leq N$.

4. Observed symbol probability distribution in state j is defined by $B = \{b_j(k)\}$ where $b_j(k)$ is defined by equation (2.16),

$$b_j(k) = P\left[v_k \ at \ \ t \middle| q_t = S_j\right], \tag{2.16}$$

where $1 \leq j \leq N_s$, and $1 \leq k \leq M$.

5. Initial state distribution $\pi_i = P[q_1 = S_i]$ where $1 \leq i \leq N_s$.

Given values for $N_s,\ M,\ A,\ B,\ and\ \pi$, a generative HMM is defined, and an observed output sequence $O = \{O_1, O_2, \cdots O_T\}$ where each observation O_t is one of the symbols from V, and T is the number of observations in the sequence [9].

The symbol sequence is assumed to be from a Markov process such that each state is dependent

only on the previous state $P(S_i = q_t | S_{i-1} = q_{t-1})$. The transitions are defined by the transition matrix which specifies the probability of starting in state S_i and ending in state S_j. Because the hidden states are not directly connected to the symbol sequence, the output matrix defines the conditional probability of the observed symbol given the current state.

HMM parameter estimation methods can be divided into two groups 1) parameter estimation when both the symbol sequence and an associated state sequence is known, and 2) parameter estimation when the symbol sequence is known but the associated state sequence is unknown [9].

For the first case, when the associated state sequence is known, a closed form of the ML algorithm is utilized. In this case, the number of times each particular state transition or a particular output occurs is enumerated in the training sequence. Each transition probability parameter can be computed based on number of observed transitions from state i to state j A_{ij} defined by equation (2.17),

$$a_{ij} = \frac{A_{ij}}{\sum_{j'} A_{ij'}}, \tag{2.17}$$

where the number of observed transitions is normalized by the sum of all transitions from state i. Each output probability parameter can be computed as the number of symbol observations b from state i $E_i(b)$ defined by equation (2.18),

$$e_i(b) = \frac{E_i(b)}{\sum_{b'} E_i(b')}, \tag{2.18}$$

where the the number of observed symbols is normalized by the sum of all observed symbols.

Maximum likelihood estimators are vulnerable to errors given overfitting when insufficient training data is available. Another problem is encountered if a state S_i is not observed in a training sequence resulting an indeterminant case when $\frac{0}{0}$ occurs. To avoid this case, pseudo-counts are added to the transition and output probability matrices as defined in equations (2.19) and (2.20),

$$A_{ij} = \text{number of transitions i to j in training data} + r_{ij}, \tag{2.19}$$

$$E_j(k) = \text{ occurances of the symbol from state k in training data} + r_j(k). \tag{2.20}$$

The pseudo counts r_{ij} and $r_j(k)$ reflect prior knowledge about the probability values[9].

In the second case, when state sequence information is unknown, parameters are estimated by one of two recursive approaches [9]. The first is the Baum-Welch EM algorithm and the second is the Viterbi algorithm. The Baum-Welch which is discussed in Rabiner's tutorial, will be provided in the paragraphs that follow. Following the Baum-Welch discussion, the Viterbi algorithm as described by Durbin [9] will be provided.

There is no known way to analytically solve for the HMM parameters which maximizes the probability of the observation sequence. Given any finite observation sequence as training data, there is no optimal way of estimating the HMM parameters. However, by choosing λ such that $P(O|\lambda)$ of the observed symbol sequence is locally maximized can be accomplished using iterative procedures such as the Baum-Welch method, or equivalently the EM method [43]. Rabiner [1] overviews the Baum-Welch algorithm which is presented below. Refer to Figure 2.21 and equation (2.21) for the computation of joint probability of being in state S_i at time t and being in state S_j at time t+1,

$$\zeta_t(i,j) = P\left(q_t = S_i, q_{t+1} = S_j \middle| O, \lambda\right). \tag{2.21}$$

Here $\zeta_t(i,j)$ can be defined in terms of forward $\alpha_t(i)$ and backward $\beta_{t+1}(j)$ variables as defined in equation (2.22),

$$\zeta_t(i,j) = \frac{\alpha_t(i)\, a_{ij} b_j(O_{t+1})\, \beta_{t+1}(j)}{P(O|\lambda)}, \tag{2.22}$$

and equation (2.23),

$$\zeta_t(i,j) = \frac{\alpha_t(i)\, a_{ij} b_j(O_{t+1})\, \beta_{t+1}(j)}{\sum_{i=1}^{N_s}\sum_{j=1}^{N_s} \alpha_t(i)\, a_{ij} b_j(O_{t+1})\, \beta_{t+1}(j)}. \tag{2.23}$$

The transition probability parameter computation is defined below in equations (2.24) to (2.28) while the output probability parameter computation is defined in equation (2.29).

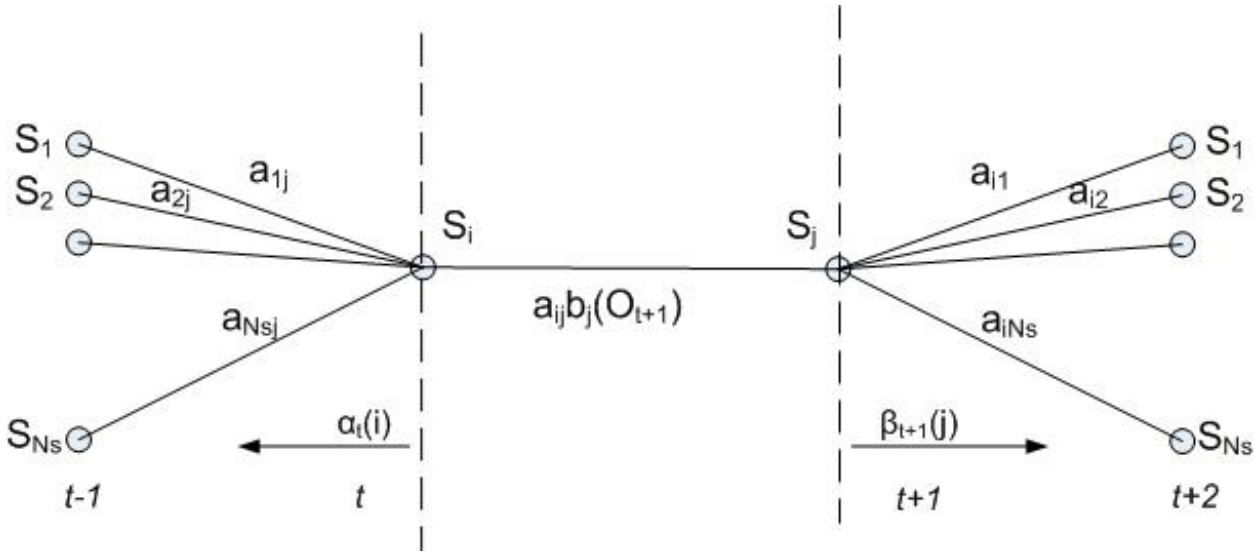

Figure 2.21: Joint Probability of State S_i at Time t and State S_j at Time t+1[1]

The probability of being in state S_i at time t, given the observation sequence and the model is $\gamma_t(i)$ defined by equation (2.24),

$$\gamma_t(i) = \sum_{j=1}^{N_s} \xi_t(i,j). \tag{2.24}$$

If $\gamma_t(i)$ is summed over the time index t, a quantity which can be interpreted as the expected number of times that state S_i is visited as defined in equation (2.25),

$$\sum_{t=1}^{T-1} \gamma_t(i) = \text{expected number of transitions from } S_i, \tag{2.25}$$

or equivalently, the expected number of transitions made from state S_i (if the time slot t = T is excluded).

Similarly, summation of $\zeta_t(i,j)$over t (from t = 1 to t = T-1) can be interpreted as the expected number of transitions from state S_i to state S_j as defined by equation (2.26),

$$\sum_{t=1}^{T-1} \xi_t(i,j) = \text{expected number of transitions from } S_i \text{ to } S_i\,. \tag{2.26}$$

The expected number of times in state S_i is defined by equation (2.27),

$$\widehat{\overline{\pi_i}} = \textit{expected frequency (number of times) in state } S_i \textit{ at time } (t=1) = \gamma_1(i). \tag{2.27}$$

The transition probabilities are defined by equation (2.28) and the output probabilities are defined by equation (2.29),

$$\widehat{\overline{a_{ij}}} = \frac{\textit{expected number of transitions from state } S_i \textit{ to } S_j}{\textit{expected number of transitions from state } S_i} = \frac{\sum_{t=1}^{T-1} \xi_t(i,j)}{\sum_{t=1}^{T-1} \gamma_i(i)}, \tag{2.28}$$

$$\widehat{\overline{b_j(k)}} = \frac{\textit{expected number of times in state } j \textit{ and observing symbol } v_k}{\textit{expected number of times in state } j} =$$

$$\frac{\sum_{t=1}^{T} \gamma_t(j) \textit{ subject to } O_t = v_k}{\sum_{t=1}^{T} \gamma_t(j)}. \tag{2.29}$$

The Baum Welch algorithm provides a method for iterative restimation of HMM parameters defined as follows. A set of equations for estimation of $\hat{\lambda} = \{\hat{\pi}, \hat{A}, \hat{B}\}$ is provided in equations (2.25) to (2.29). The initial HMM estimation is defined as λ which is utilized as the right hand sides of equations (2.28) to (2.29). The HMM reestimation defined as $\hat{\lambda}$ is utilized as the left hand sides of equations (2.28) to (2.29). It has been proven by Baum and Welch that either: 1) the initial model λ defines a critical point of the likelihood function in which case $\lambda = \hat{\lambda}$, or 2) λ is more likely than model $\hat{\lambda}$ in the sense that $P\left(O|\hat{\lambda}\right) > P(O|\lambda)$ (that is a new model has been found from which the sequence is more likely to have been produced). If the estimation is iterated, the probability of O being observed from the model can be improved until a point of diminishing return is reached. The final result is considered a ML estimate of the model. This forward backward algorithm suffers from convergence to local maximum, and given complex optimization surfaces with many local maxima, it is difficult to achieve global maximums.

The Baum Welch algorithm utilizes the forward variable and the reverse variable to estimate the HMM parameters. The forward variable $\alpha_t(i) = P(O_1 O_2 \cdots O_t, q_t = S_i|\lambda)$, is defined as the probability of the partial observation sequence, $O_1 O_2 \cdots O_t$ ending in state S_i at time t, given the model λ . An inductive solution for the forward variable is provided in equations (2.30) to (2.32). Initialization of the forward probability as the joint probability of state S_i and the initial observation O_1 is defined in equation (2.30),

$$\alpha_t(i) = \pi_i b_i(O_1),\ 1 \leq i \leq N_s. \tag{2.30}$$

Referring to Figure 2.23 and equation 2.31 for the computation of the partial observation forward probability. This equation defines how the state S_j can be reached at time *t+1* from the N_s possible states S_i, where $1 \leq i \leq N_s$ at time t. Since $\alpha_t(i)$ is the probability of the joint event that $O_1 O_2 \cdots O_t$ are observed, and the state at time t is S_i , the product $\alpha_t(i)a_{ij}$ is the probability of the joint event that $O_1 O_2 \cdots O_t$ are observed, and state S_j is reached at time t+1 via state S_i at time t. Summing this product over all the possible states S_i, where $1 \leq i \leq N_s$ at time t, results in the probability of S_j at time t+1 with all the previous partial observations. Given S_j is known, $\alpha_{t+1}(j)$ is obtained by accounting for observation O_{t+1} in state j by multiplying by the probability $b_j(O_{t+1})$. The computation in equation (2.31) is completed for all states j, where $1 \leq j \leq N_s$ for a given t, and iterated for $t = 1, 2, \cdots, T-1$,

$$\alpha_{t+1}(j) = \left[\sum_{i=1}^{N_s} \alpha_t(i)a_{ij}\right] b_j(O_{t+1}), 1 \leq t \leq T+1,\ 1 \leq j \leq N_s. \tag{2.31}$$

Termination provides the probability of the partial observed sequence, $O_1 O_2 \cdots O_t$, given the model λ, as defined in equation (2.32) which is the summation of the forward variables $\alpha_T(i)$,

$$P(O|\lambda) = \sum_{i=1}^{N_s} \alpha_T(i). \tag{2.32}$$

Computation of the forward variable requires on the order of N_s^2T computations.

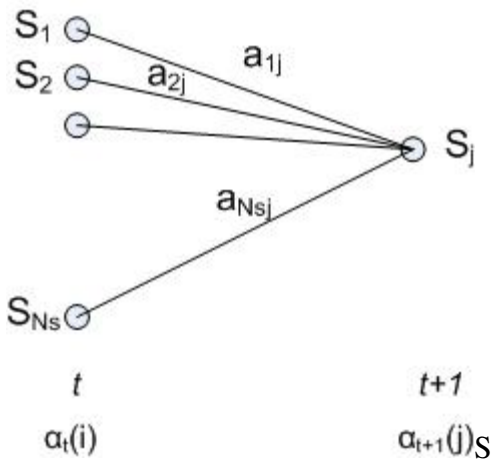

Figure 2.22: Computation of Partial Observation Forward Probability [1]

The backward variable is $\beta_t(i) = P(O_{t+1}O_{t+2}\cdots O_T, q_t = S_i|\lambda)$ which is the probability of the partial observation sequence from time t+1 to the end of the sequence, given state S_i at time t and the model λ. An inductive solution for the backward variable is provided in equations (2.33) to (2.34). Initialization of the reverse probability is arbitrarily set to 1 for all i as defined in equation (2.33),

$$\beta_T(i) = 1,\ 1 \leq i \leq N_s. \tag{2.33}$$

For computation of the reverse partial sequence observation, refer to Figure 2.23 and equation (2.34). It shows that in order to have been in state S_i at time t, and to account for: 1) the observation sequence from time t+1 backward, 2) all states S_j at time t+1, 3) transitions from S_i to S_j (the α_{ij} term), 4) the observation (O_{t+1}(the $b_j(O_{t+1})$ term), and 5) the remaining partial observation sequence from state j, the $\beta_{t+1}(j)$term must be defined as in equation (2.34),

$$\beta_t(i) = \sum_{j=1}^{N_s} a_{ij} b_j(O_{t+1})\beta_{t+1}(j), t = T-1, T-2, \cdots, 1, 1 \leq i \leq N_s. \tag{2.34}$$

Computation of the backward variable requires on the order of $N_s^2 T$ computations.

The second HMM parameter estimation method when the hidden state sequences are unknown

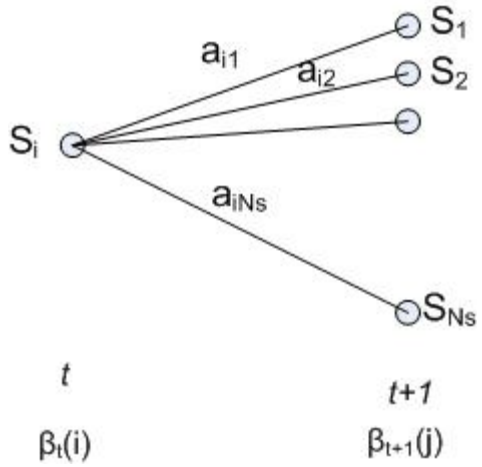

Figure 2.23: Computation of Partial Observation Reverse Joint Probability [1]

is provided by the Viterbi algorithm. Given a sequence of observed symbols, it is desirable to identify the underlying sequence of hidden states. The process of identifying the hidden state sequence associated with an observed symbol sequence is called decoding. The Viterbi dynamic programming algorithm is the most common algorithm utilized for decoding. There is more than one state sequence which could produce the same observed symbol sequence, however, they have different probabilities. The most probable path $S^* = \underset{q}{\operatorname{argmax}} P(x,q)$ can be identified recursively. Suppose the probability $q_k(i)$ of the most probable path ending in state k with observation I is known for all the states k. Then these probabilities can be calculated for the observation x_{i+1} as defined in the full Viterbi parameter estimation algorithm shown in equations (2.35) to (2.39). All sequences start in state 0 so the initial condition is that $q_0(0) = 1$. Maintaining reverse pointers, the actual state sequence can be found by backtracking from the end state to the beginning state.

Initialization $q_0(0) = 1, q_k(0) = 0 \; for \; k > 0$ begins with equation (2.35),

$$q_i(i+1) = e_i(x_{i+1}) \max_j \left(q_j(i) a_{ij} \right). \tag{2.35}$$

Recursion $(i = 1 \ldots\ldots L)$ continues with equation (2.36),

$$q_i(i) = e_j(x_i) = \max_k \left(q_k(i-1) a_{ij} \right). \tag{2.36}$$

Backward pointers are defined by equation (2.37),

$$ptr_i(i) = \underset{k}{\operatorname{argmax}} \left(q_k(i-1)\, a_{ij}\right). \tag{2.37}$$

Termination is defined by equation (2.38),

$$P(x, S^*) = \max_k \left(q_k(L)\, a_{k0}\right); S_L^* = \underset{k}{\operatorname{argmax}} \left(q_k(L)\, a_{k0}\right). \tag{2.38}$$

Traceback $i = L \ldots\ldots 1)$ is defined by equation (2.39),

$$S^*{}_{i-1} = ptr_i(S_i^*). \tag{2.39}$$

Note that a_{k0} is an assumed end state which can be dropped if the end state is never reached. The Viterbi algorithm results in the multiplication of many small numbers which can result in an underflow; this can be avoided if the computation is completed in log space. This is completed by $\log\left(q_j(i)\right)$ which transforms the multiplications to sums so that the numerical computations remain reasonable. The Viterbi algorithm performs less well than the Baum-Welch, however, it is widely utilized , and when the HMM is to be utilized for decoding state sequences then it is effective to estimate the model parameters with the Viterbi algorithm.

State Likelihood Estimation

The state likelihood estimation problem is: given the observational sequence $O = O_1, O_2, \cdots O_T$, and an HMM model λ, how to choose a corresponding state sequence $Q = q_1, q_2, \cdots, q_T$ which best matches the observed sequence[1]. If optimal is defined as choosing the individual states which will maximum the correct number of states decoded in the state sequence then $\gamma_t(i)$ can be defined as equation (2.40),

$$\gamma_t(i) = P(q_t = S_i | O, \lambda). \tag{2.40}$$

It is the probability of being in state S_i at time t, given the observation sequence O, and the model λ.

This probability is defined in equation (2.41),

$$\gamma_t(i) = \frac{\alpha_t(i)\,\beta_t(i)}{P(O|\lambda)} = \frac{\alpha_t(i)\,\beta_t(i)}{\sum_{i=1}^{N_s}\alpha_t(i)\,\beta_t(i)}, \tag{2.41}$$

as a function of the forward and backward variables provided in equations (2.30) to (2.31) and (2.33) to (2.34) respectively.

Equation (2.42),

$$q_t = \underset{1\le i\le N_s}{\operatorname{argmax}}\left[\gamma_t(i)\right],\ 1 \le t \le T, \tag{2.42}$$

defines the partial observation sequence $O_1, O_2, \cdots, O_t$ in state S_i at time t with $\alpha_t(i)$. The remainder of the sequence is defined by $\beta_t(i)$ given $O_{t+1}, O_{t+2}, \cdots, O_T$ and state S_i at time t. The normalization factor provides the condition that $\sum_{i=1}^{N_s}\gamma_t(i) = 1$. Choosing the largest $\gamma_t(i)$ enables a solution for the most likely state q_t at time t as defined in equation (2.42). Although this produces the most likely state at each time t, if the number of state transitions is zero, the criteria becomes undefined. An alternative is to define the optimum state sequence that maximizes $P(Q|O,\lambda)$ which is equivalent to maximizing $P(Q, O|\lambda)$. This result can be achieved with the dynamic programming Viterbi algorithm defined in equations (2.35) to equation (2.39). The Viterbi algorithm is similar to the forward variable computation except for substitution of a maximization step (2.38) for the summation step in equation (2.32).

Rank Order Likelihood

Given that the input is a sequence of MWC SLE, and the output is a permuted stream of rank ordered SLE, a data sorting algorithm will be utilized to implement this process. Several general purpose sorting algorithms have been invented which are described by Cormen et al. [44], Press et al. [45], and Estivill-Castro [46]. Like all algorithms, these algorithms are analyzed by running time which can be established by the number of program steps and number of iterations. Some

algorithms are more efficient for shorter input data structures while more advanced algorithms are more asymptotically efficient for large input data structures. Basic algorithm strategies are incremental while more advanced strategies are based on divide and conquer techniques. Some sorting algorithms execute without additional memory while others require substantial memory requirements. Examples of basic sorting algorithms are Insertionsort and Mergesort while examples of more advanced sorting algorithms include Heapsort and Quicksort.

Quicksort is a classical sorting algorithm with optimal upper bound of *O(n log n)* runtime with worst case runtime upper bound of *O(n2)* with an input array of *n* numbers. On average,Quicksort is more efficient than Heapsort, for long input record lengths by a factor of 1.5 to 2X. Therefore, Quicksort will be utilized for the CSR algorithm. Estivill-Castro [46] describe Quicksort as a popular divide and conquer algorithm with a guarantee that in place memory requirements will not exceed the log of the input array size. Standard Quicksort algorithms do the bulk of the work in the divide phase bisecting the input array successively until the primitive subarrays are smaller than a controlled length. After each bisection step, each resultant subarray is sorted in ascending order before the process is repeated. Variants on the standard Quicksort algorithm seek to avoid worst case performance through effective choices of the array partition point in rare special cases where multiple equal valued data keys are adjacent to the divide point.

Cormen [44] describes the Quicksort procedure as follows:

Divide: Rearrange and partition the array $A[a \cdots zzz]$ into two subarrays $A[a \cdots q-1]$

and $A[q+1 \cdots zzz]$such that each element of the first subarray is less than or equal to $A[q]$

and the elements of the second subarray are larger than $A[q]$.

Conquer: Sort the two subarrays by recursively calling Quicksort.

Combine: Because the subarrays are already sorted, when the subarrays are combined, the original subarray is sorted.

Maximum Likelihood Selection

Given that the input is a sequence of sorted SLE, and the output is the maximum SLE, a maximum selection algorithm will be utilized to implement this process. Therefore to select the maximum SLE requires access and extraction of either the first or the last element of the input array.

2.5 Conclusion

The baseline algorithm served as a proof of concept for the channel state model and the channel state recognition algorithm. Preliminary baseline verification test results provided in Chapter 4 indicate that the channel state model and the channel state recognition algorithm are feasible. While the verification results are not comprehensive, they suggested, that continued development of the CSR algorithm could produce significant results. Several enhancements are added to the CSR algorithm in the next Chapter and verification testing in Chapter 4 confirm improved performance results of the enhanced CSR algorithm.

This Page Intentionally Left Blank

Chapter 3

Enhanced CSR Algorithm

Building upon the baseline CSR algorithm described in the previous chapter, this chapter analyzes the enhanced CSR algorithm by defining architecture, system, data, and analytical models at four levels of detail.

3.1 Tier 0 Analysis

The Tier 0 system model is shown in Figure 3.1. Given that the Enhanced Tier 0 process first and lowest level of detail is the same as the baseline Tier 0 process, refer to Section 2.1.

3.2 Tier 1 Analysis

This Section will analyze the enhanced algorithm second level of detail.

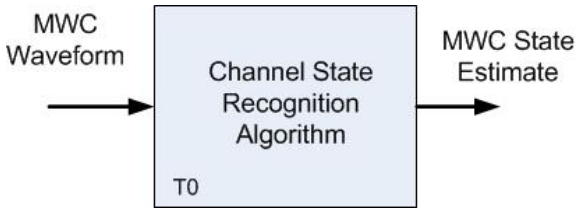

Figure 3.1: Tier 0 System Model

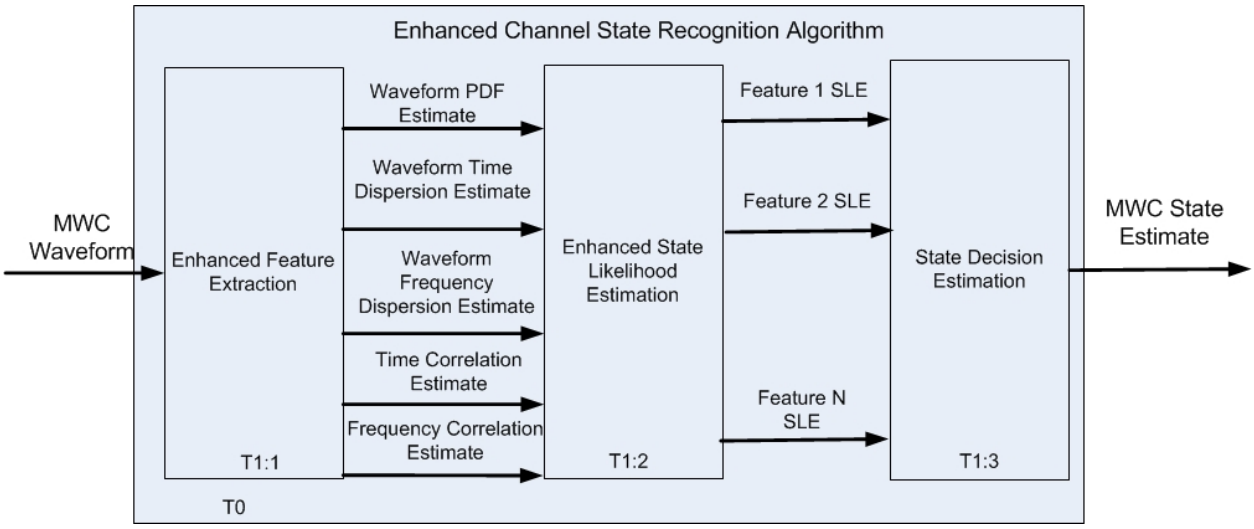

Figure 3.2: Tier 1Architecture

3.2.1 Architecture

Referring to Figure 3.2, the Tier 1 architecture comprises three subprocesses: 1) feature extraction (T1:1), 2) state likelihood estimation (T1:2), and 3) state decision estimation (T1:3). The FE process extracts multiple parallel waveform statistical features providing waveform feature diversity. The state likelihood estimation process produces parallel sequences of feature SLEs. The state decision estimation process produces sequences of state hard decision estimates (HDE) and combines them into a sequence of most likely CSE.

Waveform Feature Extraction

Referring to Figure 3.2, the FE system model (T1:1) shown in Figure 3.3, extracts a diverse set of waveform features. This FE process comprises five statistical feature extraction subprocesses: 1) complex envelope magnitude PDF, 2) time dispersion PDF, 3) frequency dispersion PDF, 4) time correlation PDF, and 5) frequency correlation PDF. These features were designed to support the coherence state model (CSM) and the CSR algorithm which defines MWC states in terms of coherent nonselective and noncoherent selective states. Time dispersion is a direct indicator of noncoherent frequency selectivity while frequency dispersion is a direct indicator of noncoherent

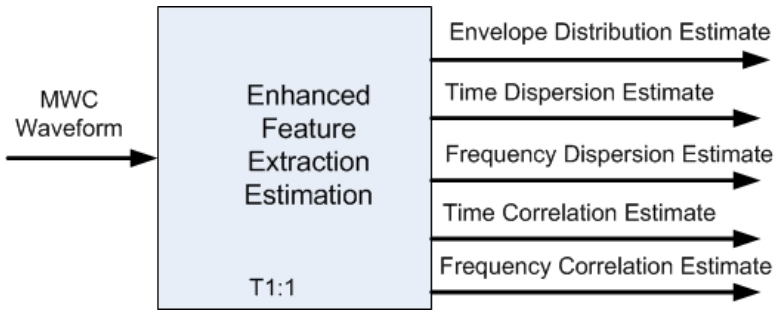

Figure 3.3: Feature Extraction System Model

time selectivity. Heuristic rules of thumb (ROT) suggest that if time dispersion is less than 10-20% of the symbol period, then ISI is minimal, and the MWC behaves as if it were nondispersive. As time dispersion approaches the symbol period duration, ISI distortion components increase such that SNR increases will not be effective at improving BER performance. Heuristic ROT also suggests that if frequency dispersion is less than 10-20% of the symbol rate, then IFI is minimal, and the MWC behaves as if it were nondispersive. However, as frequency dispersion approaches the symbol rate, IFI distortion components increase such that SNR increases become ineffective at improving BER performance.

It is common knowledge that MWC conditions can dynamically transition between coherent, single time selective, single frequency selective, or dual selective conditions. Referring to Figure 3.4, several notional CSR zones are defined to support discussion about communication power efficiency, CSM states, and waveform feature extraction processes. These zones are useful to demonstrate that with MWC state recognition, a broad range of cognitive adaptive state based communication processing decisions are enabled. These zones provide insight among performance, resource allocation, and distortion mitigation processing alternatives under dynamic MWC conditions. Four notional zones are defined: 1) coherent zone representative of AWGN conditions, 2) SNR mitigation processing zone with coherent minimally dispersive frequency flat or time flat conditions, 3) distortion mitigation processing zone with single time selective or single frequency selective conditions, and 4) dual selective conditions. These zones provide insight regarding adaptive communication performance, resource allocation, or distortion

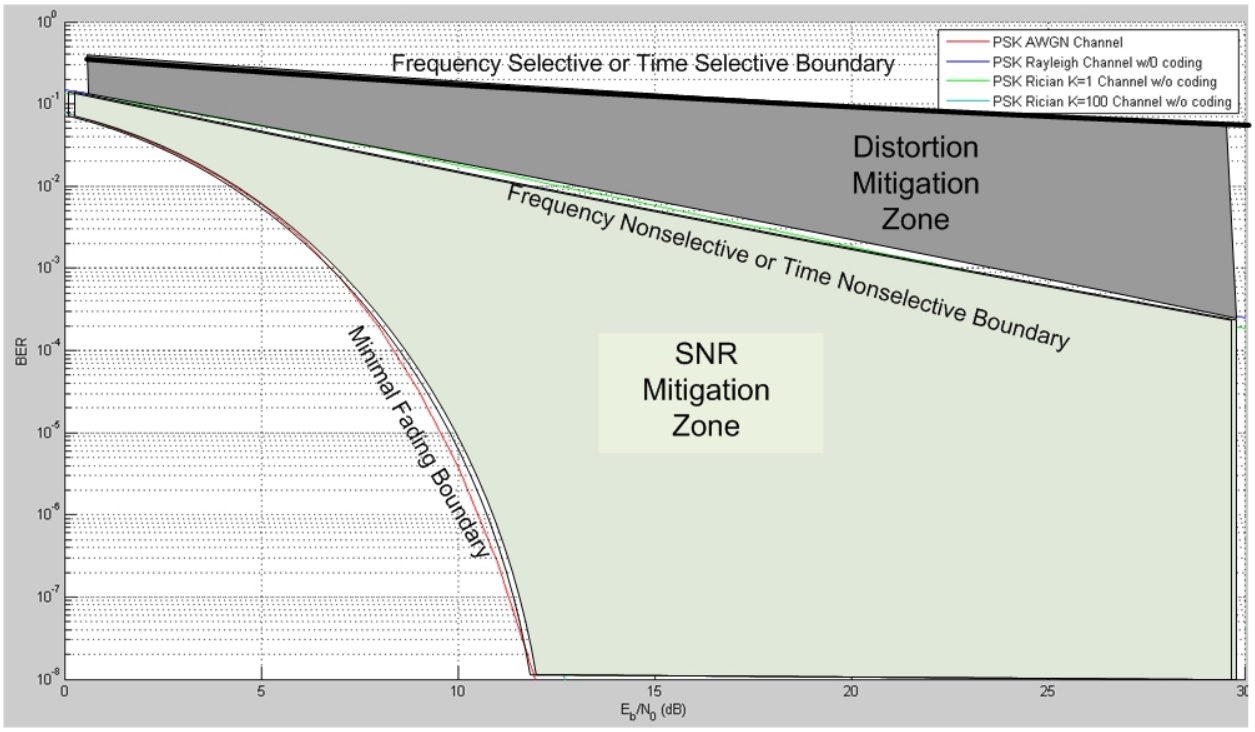

Figure 3.4: Channel State Recognition Processing Zones

mitigation processing.

For example, a coherent processing zone can be established at or near the minimal fading boundary based on CSM state 1 awareness. Under these conditions, the MWC behaves nearly like an AWGN channel. In this region, SNR performance mitigation processing methods would be effective while application of distortion methods would result in wasteful or inefficient communication resource allocations. As a second example, a SNR processing zone can also be established based on CSM state 2 awareness. Under these conditions, in the absence of distortion, effective adaptive SNR mitigation processing selections (i.e. power, coding or processing gain) can be selected to maintain robust performance. In this zone, application of single distortion mitigation strategies are communication resource wasteful and inefficient. As a third example, a distortion mitigation processing zone can be established based on CSM states 3 or 4 awareness (single time or frequency selective conditions). In the case of MWC ISI distortion, adaptive equalization processing selections will be effective at maintaining BER performance while SNR mitigation selections are ineffective, communication resource wasteful, and inefficient. As a fourth example, is an irreducible error zone

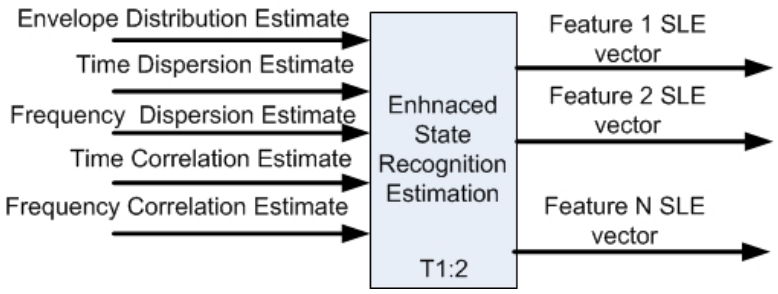

Figure 3.5: State Likelihood Estimation System Model

defined at the dual frequency and time selective boundary. This zone can be established based on awareness of CSM state 5 (dual selective conditions). Attempts to apply SNR and/or single distortion mitigation processing methods in these conditions are ineffective and result in wasteful or inefficient application of communication resources. Rather, alternative processing methods designed for dual dispersive conditions, should be selected. In all these cases, CSM state awareness provides channel state recognition and resulting capabilities to disable ineffective communication processing and to enable selections of alternative effective communication processing methods based on current MWC dynamic conditions.

State Likelihood Estimation

The state likelihood estimation (T1:2) system model shown in Figure 3.5 transforms the parallel input WFV into a SLV comprising a sequence of parallel feature SLEs.

State Decision Estimation

The state decision estimation (T1:3) system model shown in Figure3.6 transforms the parallel feature SLE sequences into a CSE vector.

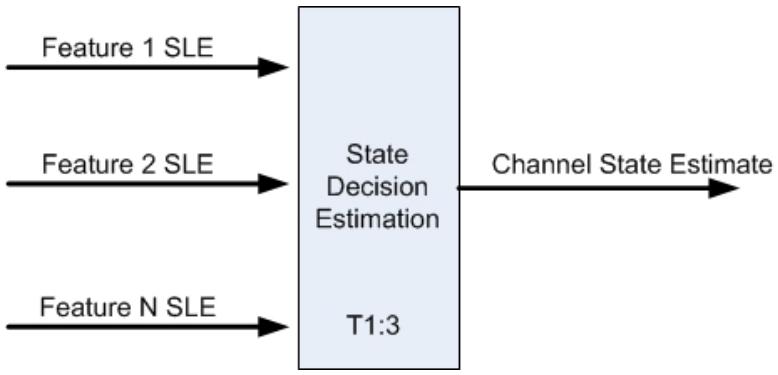

Figure 3.6: State Decision Estimation System Model

3.2.2 Data Model

Waveform Feature Extraction

The waveform FE output is a sequence of WFV defined by equation (3.1),

$$WFV_k = \left[\widehat{CE_k} \;\; \widehat{Tc_k} \;\; \widehat{BWc_k} \;\; \widehat{DS_k} \;\; \widehat{DP_k}\right]. \tag{3.1}$$

The following parameter definitions apply:

Complex envelope estimate $= \widehat{CE_k} \in R$,

and $0 < \widehat{CE_k} < CE_{max}$,

and CE_{max} is the maximum waveform amplitude,

Time Dispersion Estimate = Delay Spread $= \widehat{DS_k} \in R$,

and $0 < \widehat{DS_k} < 5T_s$,

Frequency Dispersion Estimate = Doppler Spread $= \widehat{DP_k} \in R$,

and $0 < \widehat{DP_k} < 5f_s$,

Tc -Time Correlation Estimate $= \widehat{Tc_k} \in R$,

and $0 < \widehat{Tc_k} < 5T_s$,

BWc -Frequency Correlation Estimate $= \widehat{BWc_k} \in R$,

where R is the set of all real numbers,

and $0 < \widehat{BWc}_k < 5f_s$,

Waveform block index = k, where $0 < k < k_{blk}$,

Number of waveform blocks = k_{blk},

Waveform block rate = f_{blk},

Waveform sample rate = f_s,

Complex envelope estimate sequence = $\widehat{CE}_k = \left[\widehat{CE}_1 \quad \widehat{CE}_2 \quad \cdots \quad \widehat{CE}_{x\ N_{blk}}\right]$,

Time dispersion delay spread estimate sequence = $\widehat{DS}_k = \left[\widehat{DS}_1 \quad \widehat{DS}_2 \quad \cdots \quad \widehat{DS}_{N_{blk}}\right]$,

Frequency dispersion Doppler spread estimate sequence = $\widehat{DP}_k = \left[\widehat{DP}_1 \quad \widehat{DP}_2 \quad \cdots \quad \widehat{DP}_{N_{blk}}\right]$,

Time Correlation Tc estimation sequence = $\widehat{Tc}_k = \left[\widehat{Tc}_1 \quad \widehat{Tc}_2 \quad \cdots \quad \widehat{Tc}_{N_{blk}}\right]$,

Frequency Correlation BWc estimation sequence = $\hat{BWc}_k = \left[\hat{BWc}_{s1} \quad \hat{BWc}_{s2} \quad \cdots \quad \hat{BWc}_{sN_{blk}}\right]$,

Number of samples per waveform block = N_{blk}.

On a per feature basis, the Tier 1 state likelihood estimation and the channel state decision estimation process outputs are similar to the baseline data model described in Section 2.2.2.

3.3 Tier 2 Analysis

3.3.1 Architecture

The architecture shown in Figure 3.7 comprises eight subprocesses that have been upgraded from the baseline architecture. Tier 2 enhancements include: 1) waveform feature extraction (T2:1,T2:6-T2:9), 2) state likelihood parameter estimation (T2:10), and 3) state likelihood estimation (T2:11), 4) state decision estimation process (T2:4-T2:5) which will be discussed as part of the Tier 3 analysis. These waveform features were chosen because they are directly related to the MWC coherent nonselective and noncoherent selective states defined in the CSM.

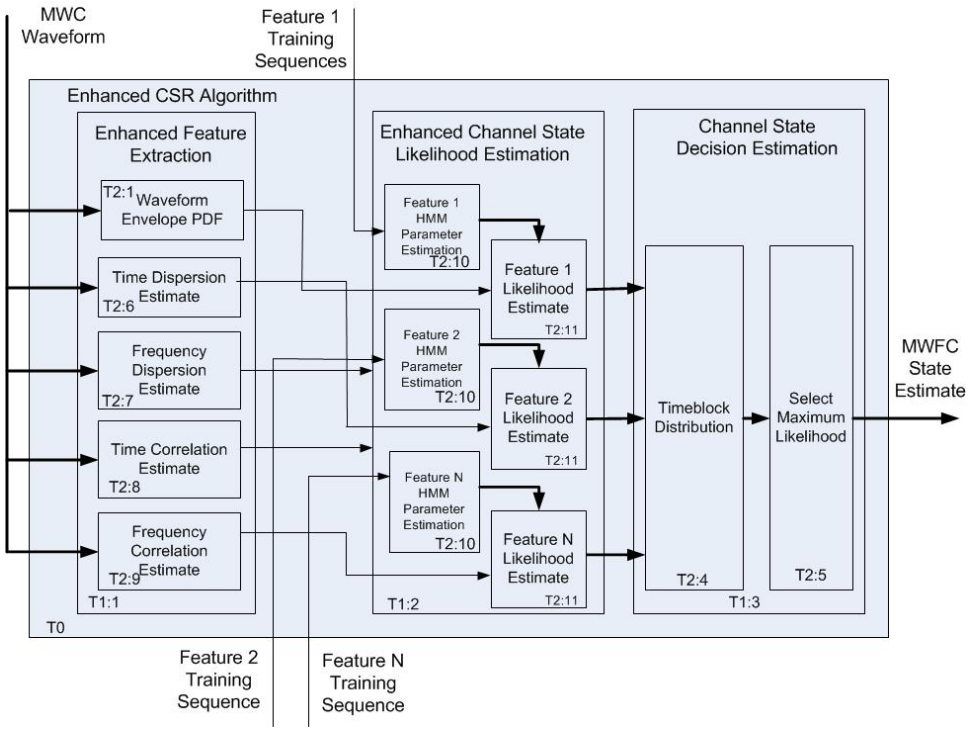

Figure 3.7: Tier 2 Architecture

Waveform Feature Extraction

The FE system model shown in Figure 3.8, transforms the input MWC waveform blocks into a set of parallel statistical WFVs.

Complex Envelope Distribution Estimation The envelope magnitude estimation model (T2:1) shown in Figure 3.9, transforms the input MWC waveform blocks into a WFV comprising a sequence of CE PDF estimates.

Time Dispersion Estimation

The time dispersion estimation model (T2:6) shown in Figure 3.10, transforms the input waveform blocks into a WFV comprising a sequence of DS PDF estimates.

Frequency Dispersion Estimation

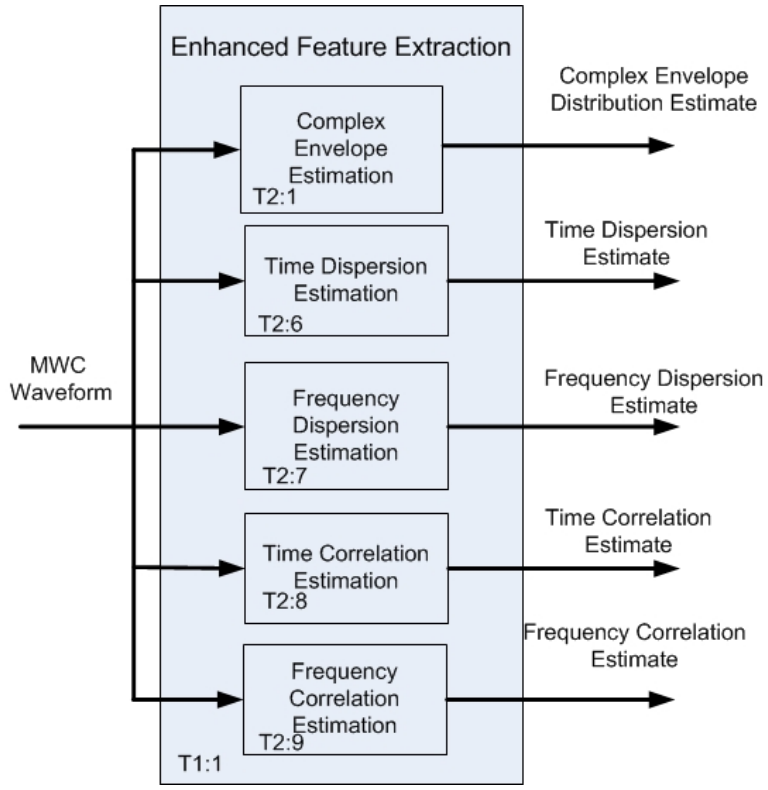

Figure 3.8: Feature Extraction System Model

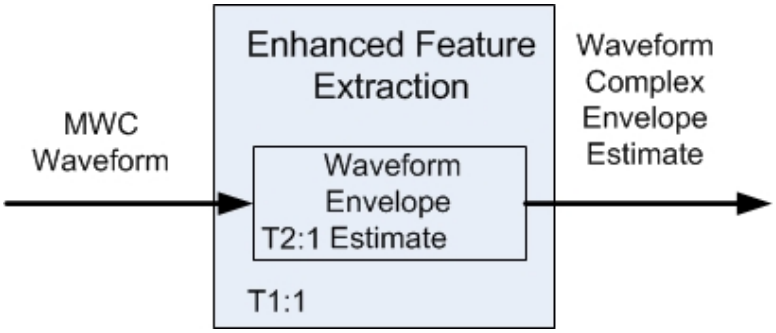

Figure 3.9: Waveform Envelope Distribution Estimation System Model

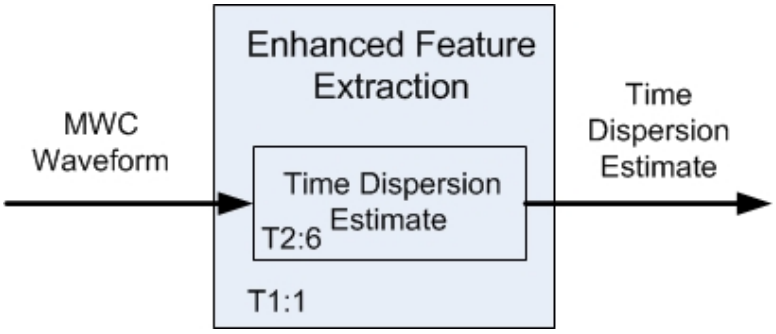

Figure 3.10: Time Dispersion Estimation System Model

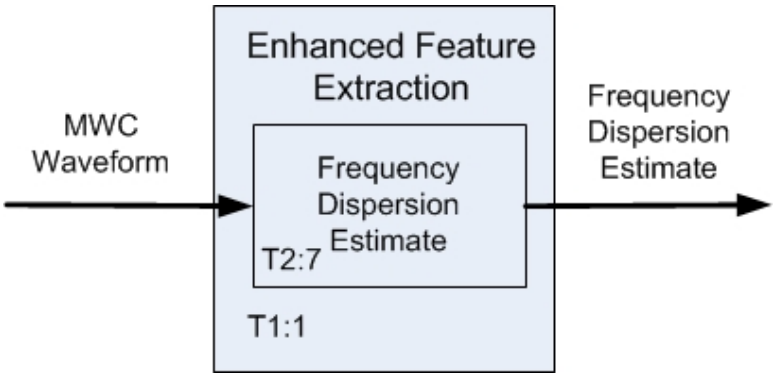

Figure 3.11: Frequency Dispersion Estimation System Model

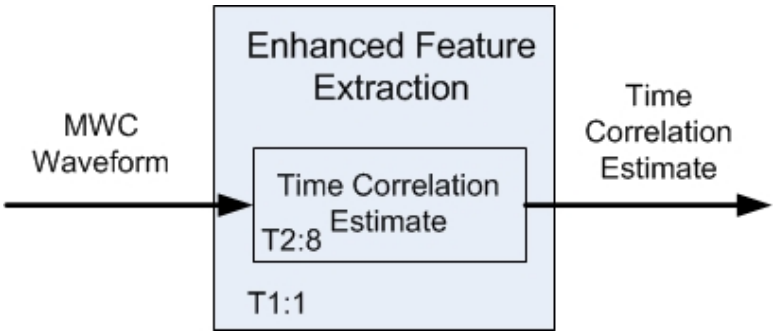

Figure 3.12: Time Correlation Estimation System Model

The frequence dispersion estimation model (T2:7) shown in Figure 3.11, transforms the input waveform blocks into a WFV comprising a sequence of DP estimates.

Time Correlation Estimation

The time correlation estimation model (T2:8) shown in Figure 3.12, transforms the input waveform blocks into a WFV comprising a sequence of Tc estimates.

Frequency Correlation Estimation

The frequency correlation estimation model (T2:9) shown in Figure 3.13, transforms the input waveform blocks into a WFV comprising a sequence of BWc estimates.

Feature State Likelihood Estimation

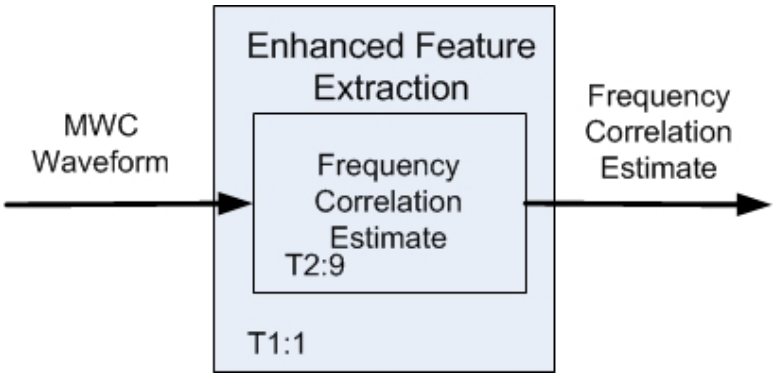

Figure 3.13: Frequency Correlation Estimation System Model

The state likelihood estimation architecture (T1:2) shown in Figure 3.14, transforms the input parallel WFVs into a SLV comprising a sequence of feature SLE. There are two inputs to each HMM for this process: 1) HMM training sequences, and 2) operational WFV sequences.

State Likelihood Parameter Estimation

The feature recognition HMM state likelihood parameter (SLP) estimation model (T2:10) shown in Figure 3.15, transforms the offline feature state training sequence into HMM state transition and output probability matrices. These training processes are computed prior to operating the HMM in recognition mode.

Feature State Likelihood Estimation

The feature state likelihood estimation model (T2:11) shown in Figure 3.16, transforms the input WFV into a sequence of individual feature SLE.

State Decision Estimation

The state decision estimation model (T1:3) shown in Figure 3.17, transforms the parallel SLE sequences into a combined hard decision estimate (HDE) and then into a sequence of CSEs.

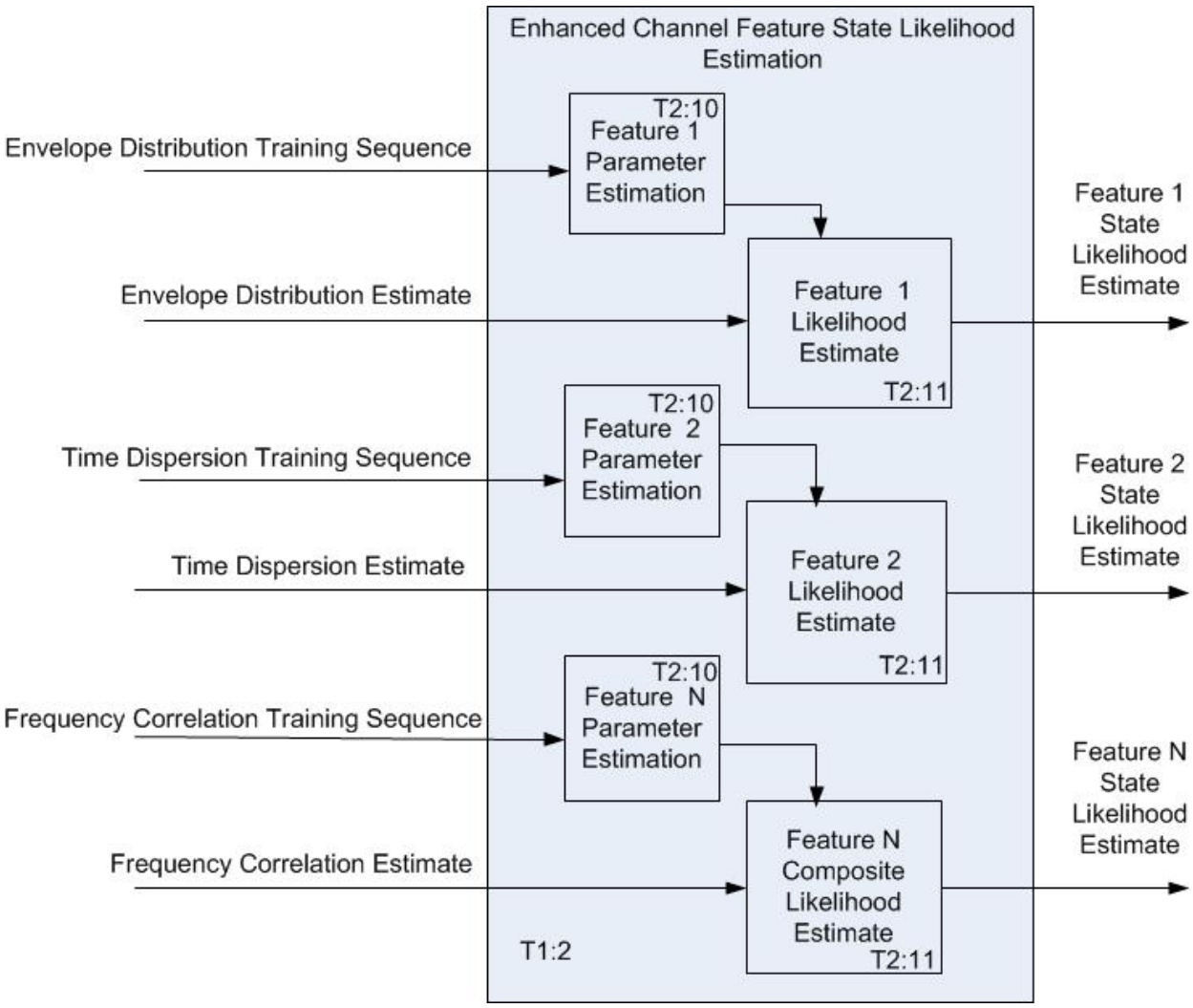

Figure 3.14: Feature State Likelihood Estimation Architecture

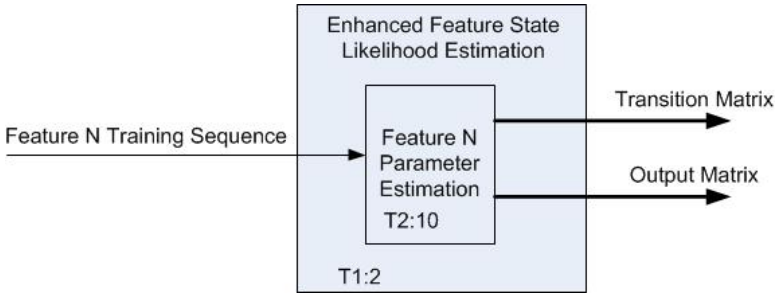

Figure 3.15: State Parameter Estimation System Model

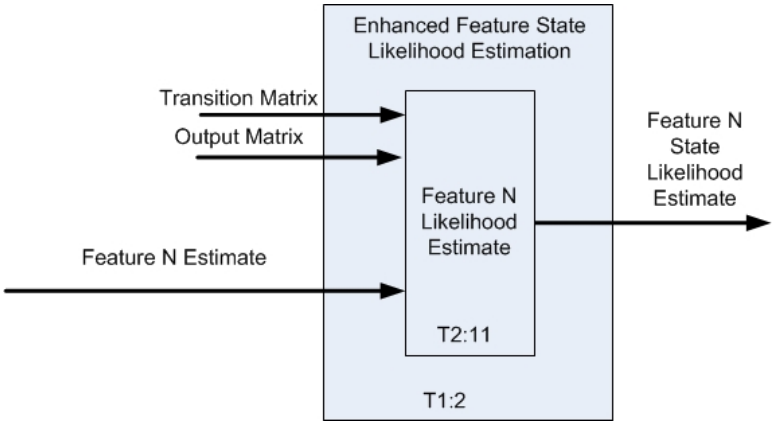

Figure 3.16: Feature State Likelihood Estimation System Model

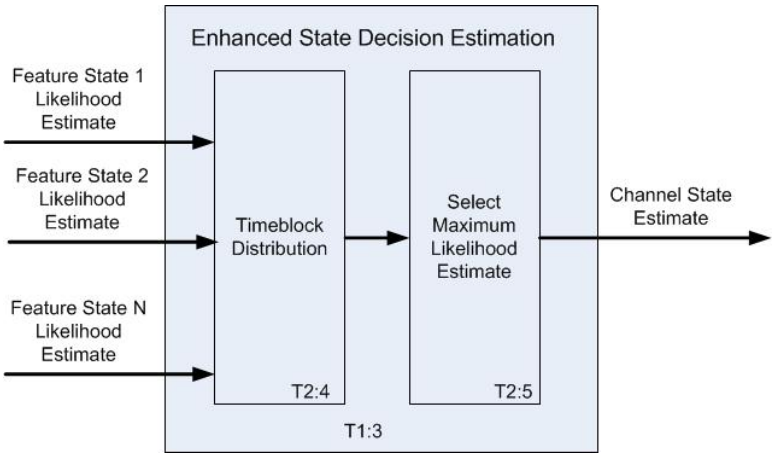

Figure 3.17: State Decision Estimation System Model

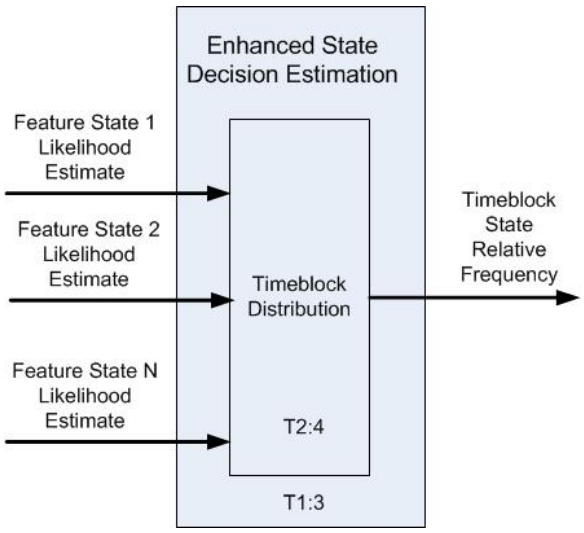

Figure 3.18: Timeblock Distribution System Model

Timeblock Frequency Distribution

The timeblock distribution model (T2:4) shown in Figure 3.18, transforms the parallel SLEs into a sequence of timeblock state relative frequency distribution (RFD) vectors.

Select Maximum

The select maximum likelihood model (T2:5) shown in Figure 3.19, transforms the input timeblock state RFD vector into a sequence of CSEs.

3.4 Tier 3 Analysis

3.4.1 Architecture

The Tier 3 architecture shown in Figure 3.20, provides the fouth level of detail for the Enhanced CSR algorithm. This Section highlights the methods for each feature extraction, state likelihood estimation, and state decision estimation processes.

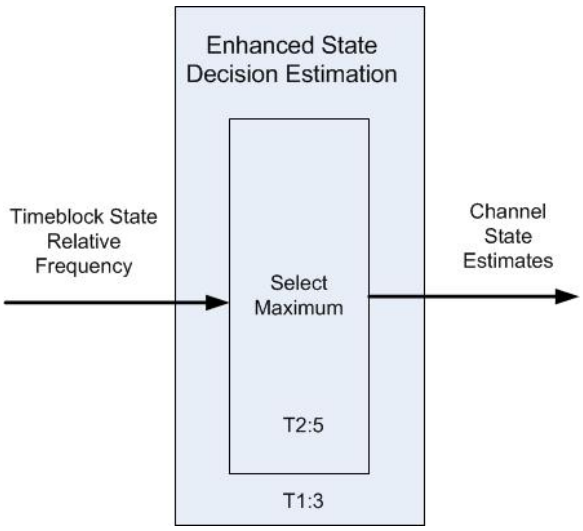

Figure 3.19: Timeblock Distribution System

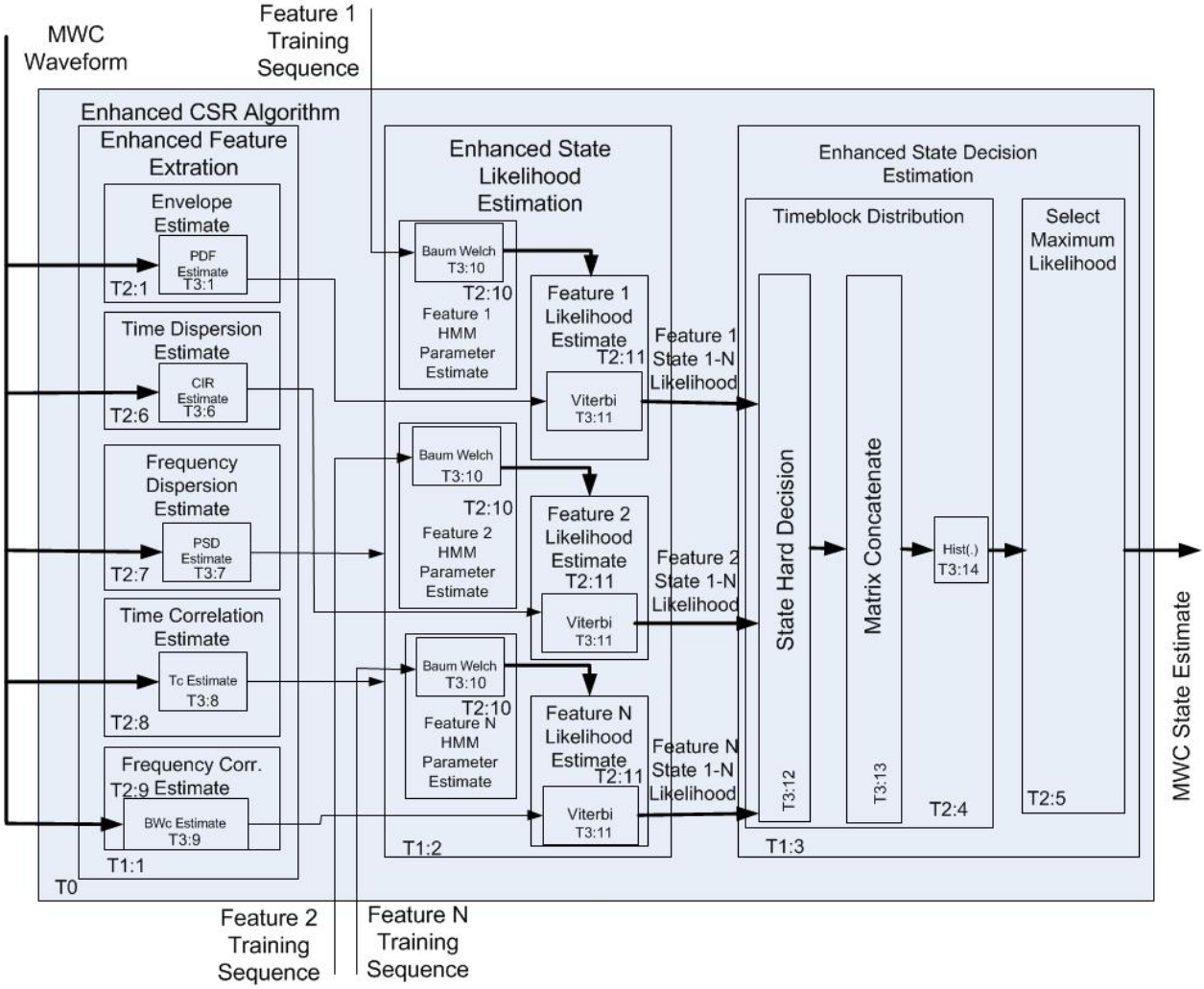

Figure 3.20: Tier 3 Architecture

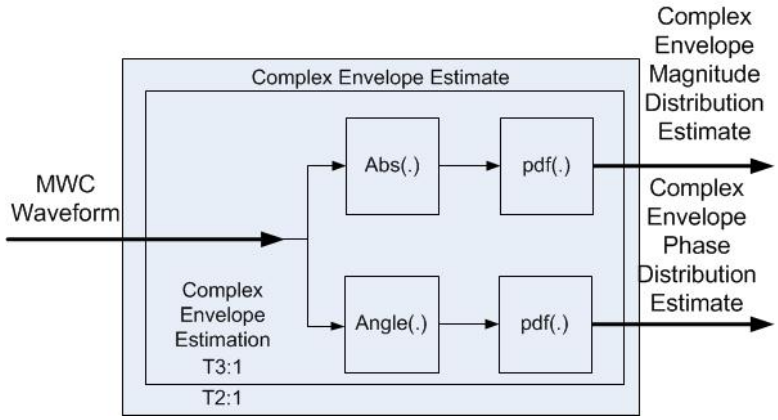

Figure 3.21: Complex Envelope Estimation System Model

Waveform Envelope Estimation

The complex envelope estimation method (T3:1) shown in Figure 3.21, estimates the magnitude and phase of the waveform envelope estimate. The output of this function is a sequence of CEM and complex envelope phase (CEP) estimates. This method is implemented by applying an absolute value and an angle functions to each MWC waveform block.

Waveform Time Dispersion Estimation

The time dispersion estimation method (T3:6) shown in Figure 3.22, estimates the magnitude and phase of the time dispersion estimate (Delay Spread - DS) . The output of this function is a sequence of time dispersion, or delay spread magnitude (DSM) and DS phase (DSP) estimates. This is implemented by applying a Fourier transform followed by a frequency domain correlation, and an inverse Fourier transform followed by an absolute value and an angle functions to each MWC waveform block.

Waveform Frequency Dispersion Estimation

The frequency dispersion estimation method (T3:7) shown in Figure 3.23, estimates the magnitude and phase of the frequency dispersion estimate (Doppler Spread - DP). The output of

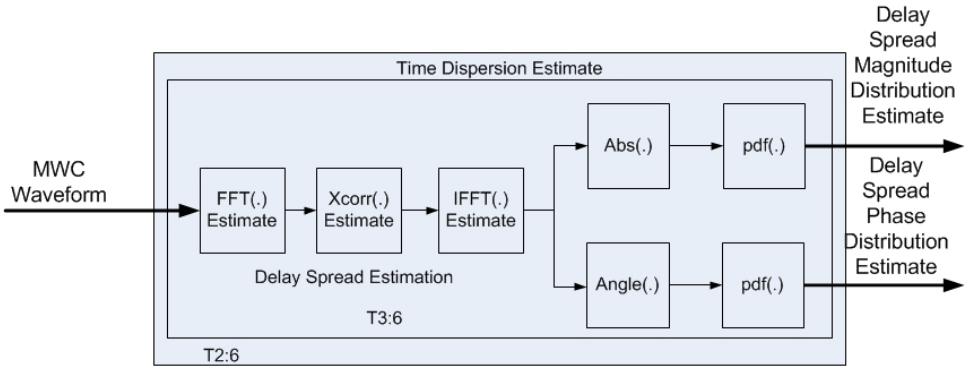

Figure 3.22: Time Dispersion Estimation System Model

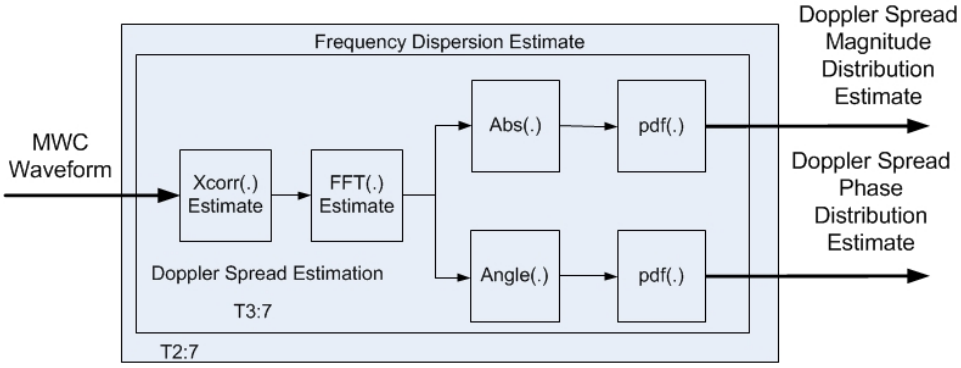

Figure 3.23: Frequency Dispersion Estimation System Model

this function is a sequence of frequency dispersion, or Doppler spread magnitude (DPM) and DP phase (DPP) estimates. This method is implemented by applying a correlation followed by an FFT, absolute value, and angle functions applied to each waveform block.

Waveform Time Correlation Estimation

The time correlation estimation method (T3:8) shown in Figure 3.24, estimates the magnitude and phase of the time correlation estimate (Coherence Time - Tc). The output of this function is a sequence of time correlation, or coherence time magnitude (TcM) and Tc phase (TcP) estimates. This method is implemented by applying a time domain correlation followed by an absolute value and an angle functions applied to each MWC waveform block.

Waveform Frequency Correlation Estimation

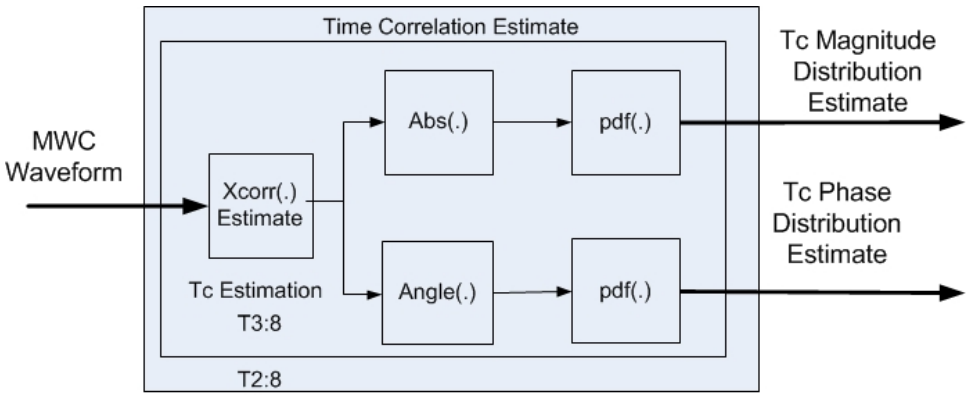

Figure 3.24: Time Correlation Estimation System Model

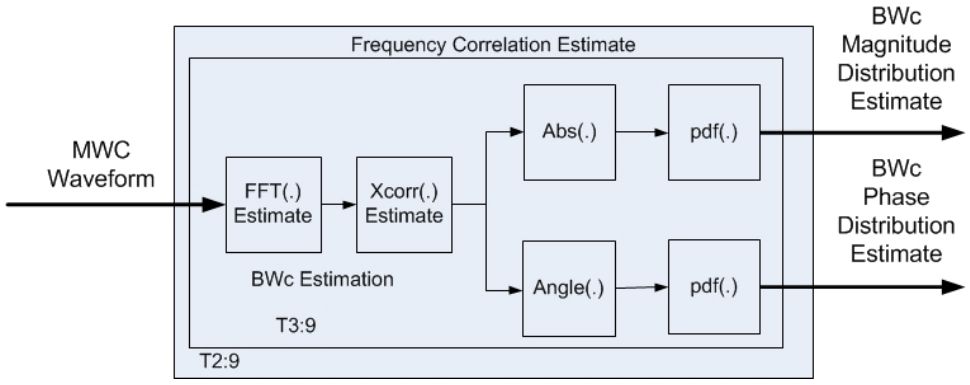

Figure 3.25: Frequency Correlation System Model

The frequency correlation estimation method (T3:9) shown in Figure 3.25, estimates the magnitude and phase of the frequency correlation estimate (Coherence Bandwidth - BWc). The output of this function is a sequence of frequency correlation, or coherence bandwidth magnitude (BWM) and BWc phase (BWP) estimates. This method is implemented by applying a Fourier transform and frequency domain correlation followed by both an absolute value and angle functions applied to each waveform block.

State Likelihood Estimation

The state likelihood estimation architecture (T3:11) shown in Figure 3.26, generates the feature SLPs and the SLEs. The output of the offline training process is a transition and output probability matrices. The output of the online operational process is a sequence of SLE. These

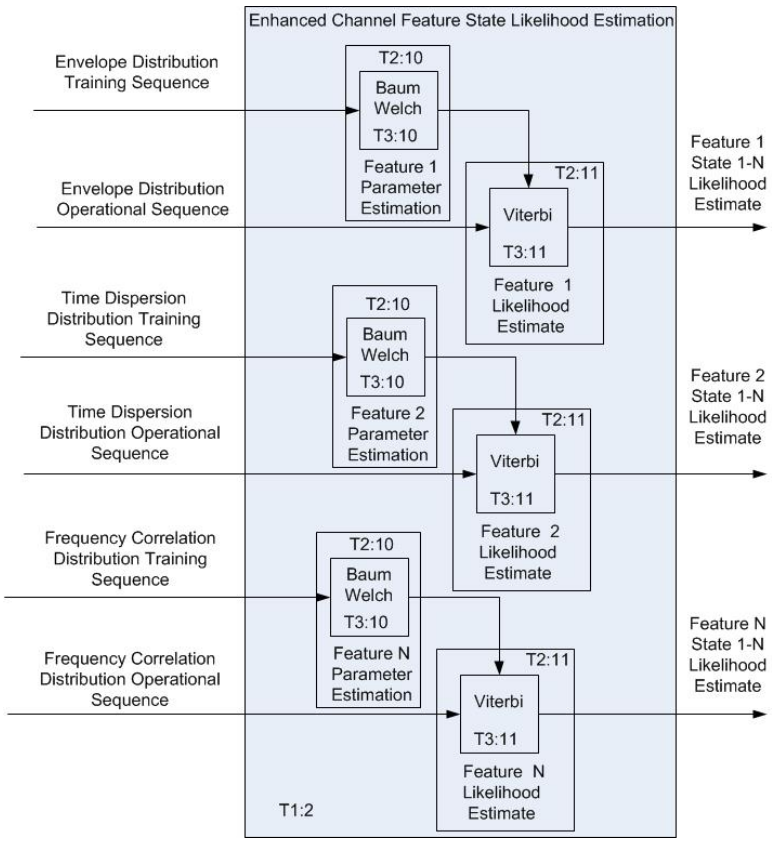

Figure 3.26: State Likelihood Estimate Architecture

methods are implemented by application of the Baum Welch and the Viterbi algorithms respectively to the training and operational WFVs.

State Decision Estimation

The state decision estimation process architecture (T1:3) shown in Figure 3.27, transforms the input SLE into a sequence of HDE, followed by hard decision combining, frequency distribution estimation, and a select maximum likelihood methods applied to each MWC waveform block.

State Hard Decision

The state hard decision (T3:12) model shown in Figure 3.28, transforms the input feature SLE into a sequence of timeblock feature state estimates. This method is implemented by applying a hard decision function to each MWC waveform feature block.

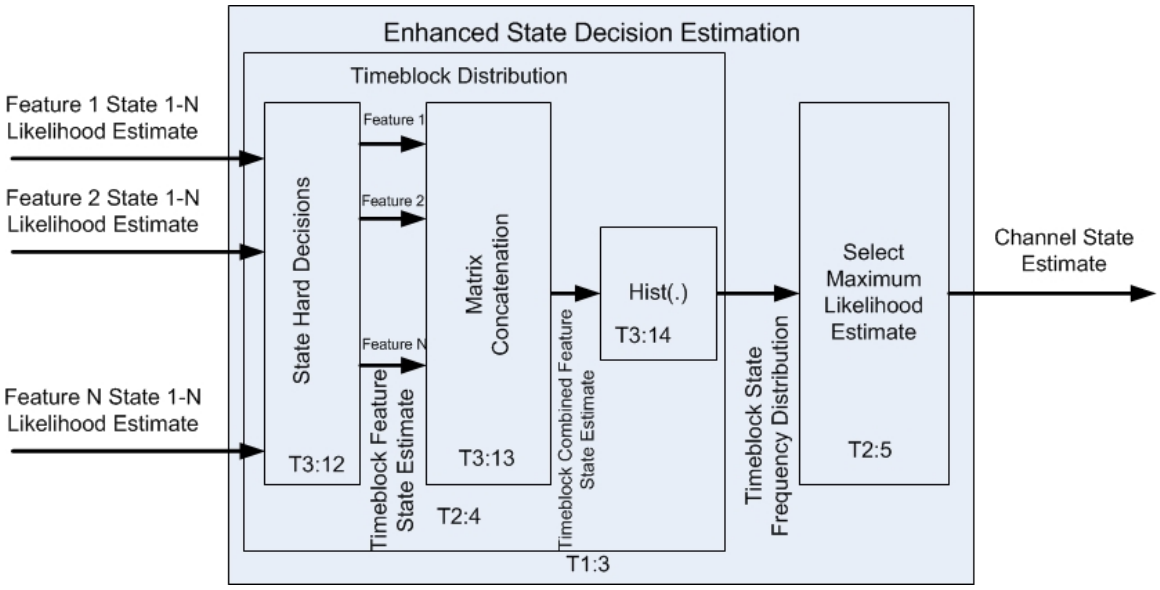

Figure 3.27: State Decision Estimation Architecture

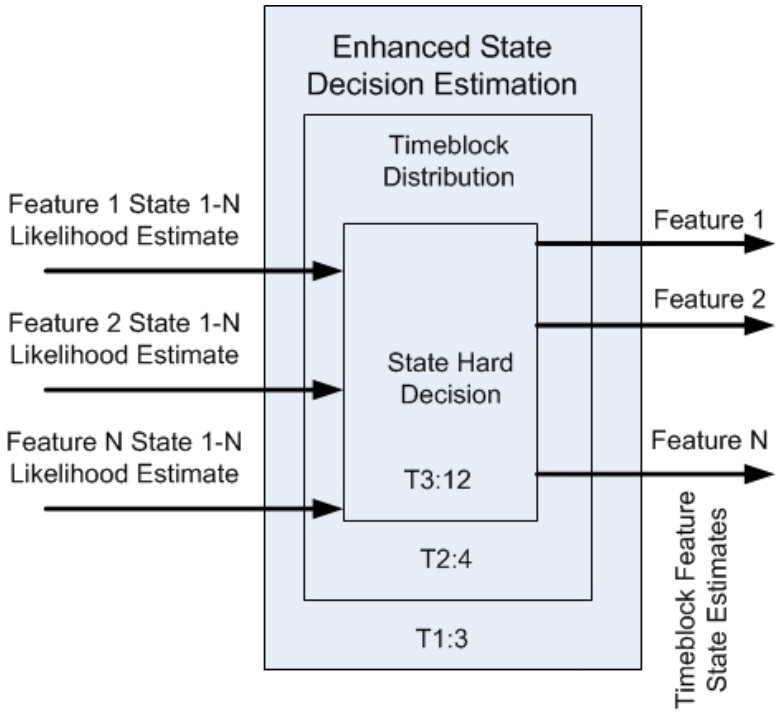

Figure 3.28: State Hard Decision System Model

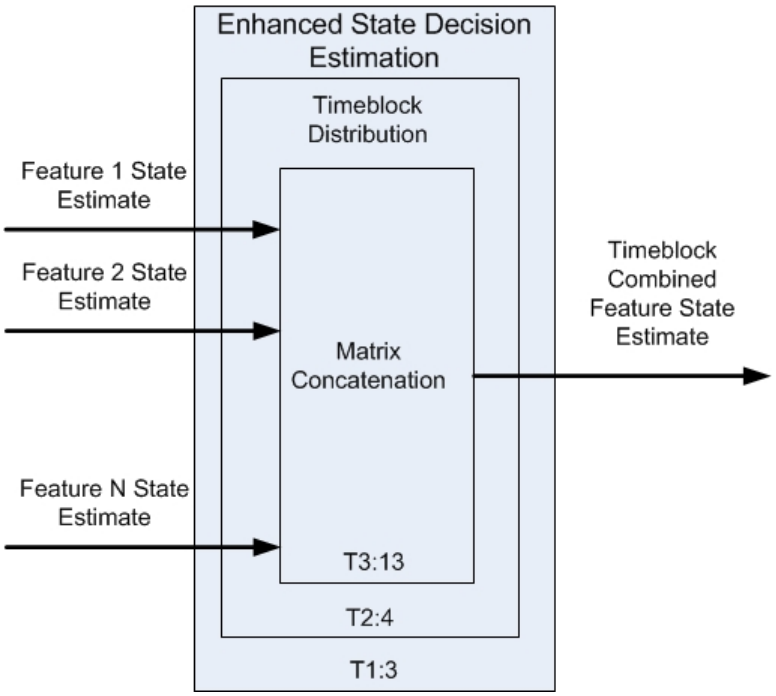

Figure 3.29: Matrix Concatenate System Model

Matrix Concatenation

The matrix concatenation method (T3:13) model shown in Figure 3.29, transforms the input individual feature state estimate vectors into a sequence of combined feature state vectors. This method is implemented by application of a matrix concatenation method.

Timeblock State Frequency Distribution

The timeblock state frequency distribution method (T3:14) shown in Figure 3.30, transforms the input timeblock combined feature state sequence into a sequence of timeblock frequency distribution vectors. This method is implemented by applying a histogram function to each MWC waveform block.

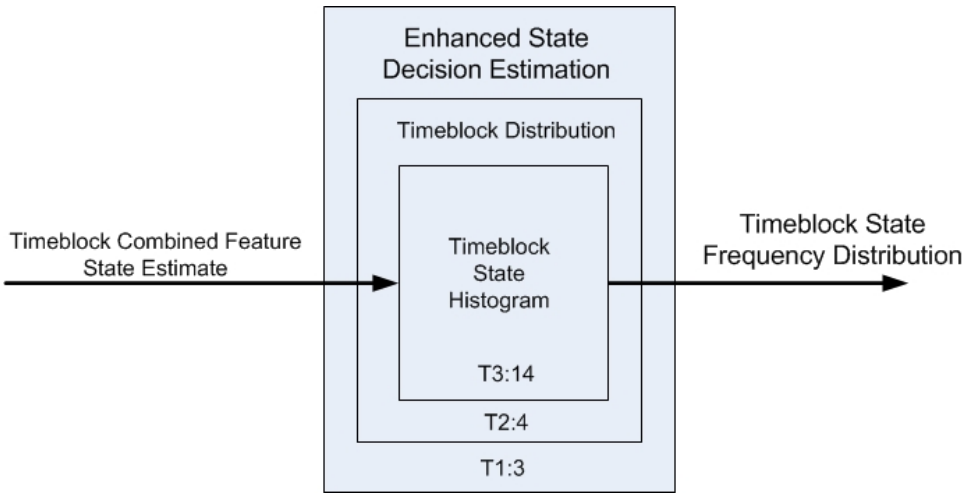

Figure 3.30: Timeblock Frequency Distribution Architecture

3.4.2 Analytical Model

The purpose of the analytical model is to express the behavior of each method in terms of mathematical operators such that its transfer function can be implemented with a floating or fixed-point processor. Refer to the Baseline Algorithm analysis in Chapter 2, and the Enhanced CSR Algorithm system architecture and data models for background for the analytical model.

Waveform Envelope Estimation

Refer to Figures 3.20 and 3.21 for the waveform envelope estimation (T3:1) architecture and system model. Given the input waveform samples, the waveform envelope estimation method computes both the complex envelope magnitude and phase. The waveform magnitude and phase were defined in Chapter 1 and repeated here as equations (3.2) and (3.3) respectively

$$y_{bb}(t) = z(t) = x(t) + y(t) = |z(t)|\, e^{\theta(t)} = \sqrt{x(t) + y(t)}\, e^{\theta(t)}, \tag{3.2}$$

$$\theta(t) = \tan^{-1} \frac{y(t)}{x(t)}. \tag{3.3}$$

The frequency distribution method is applied to the envelope magnitude and phase by applying a histogram PDF estimation method previously defined in Chapter 2 and repeated here as equations (3.4) through (3.6)

The histogram can be defined by equation (3.4),

$$N = \sum_{i=1}^{j} N_{bin}, \tag{3.4}$$

where N is the total number of observations, j is the total number of bins, and N_{bin} are the number of observed discrete waveform envelope magnitude $|R(kT)|$ samples in each bin. For this waveform magnitude distribution estimation the bin width B_{width} is defined by equation (3.5),

$$B_{width} = {}^{R_{magmax} - R_{magmin}}/_{k}. \tag{3.5}$$

Where k is an arbitrary number of bins chosen to produce a smooth and continuous distribution, R_{magmax} is the maximum received waveform magnitude observation, and R_{magmin} is the minimum received waveform magnitude observation.

Next, distribute the waveform envelope magnitude observations into each bin and accumulate the total number of observations (N_{bin}) in each bin. Finally, normalize the magnitude of each bin as defined in equation (3.6),

$$f = {}^{N_{bin}}/_{N}. \tag{3.6}$$

Normalize so that the total area under the curve is equal to one by dividing the total number of observations in each bin by the total number of observations such that the area of each bin approaches the percentile of observations in that bin. With these constraints, the histogram approaches an estimate of probability distribution. The output of this method is a sequence of CEM and CEP estimates as defined in Section 3.2.2. Refer to Appendix Section A.11.2 for additional background for second order statistical feature extraction.

Waveform Time Dispersion Estimation Refer to Figures 3.20 and 3.22 for the waveform DS estimation (T3:6) architecture and system model. As discussed in Chapter 1, time dispersion is related to coherence bandwidth by an inverse Fourier transform. Additionally, channel coherence

bandwidth is directly related to waveform frequency correlation. Therefore, the waveform time dispersion method first applies a Fourier transform, and then a complex autocorrelation, as a waveform indicator feature for the coherence bandwidth BWc. Then an inverse Fourier transform is applied to the BWc estimate to produce the DS result. After these operations, both the delay spread magnitude and phase frequency distributions are computed as previously defined in Section 3.4.2. The output of this method is a stream of delay spread magnitude and phase estimate vectors at the waveform block rate as defined in Section 3.2.2. Refer to Appendix Section A.11.2 for additional background for second order statistical feature extraction.

Waveform Frequency Dispersion Estimation Refer to Figures 3.20 and 3.23 for the waveform DP estimation (T3:7) architecture and system model. As discussed in Chapter 1, frequency dispersion is related to time coherence by a Fourier transform. Additionally, channel time coherence is related to waveform frequency domain correlation. Given the input waveform complex envelope samples, the waveform frequency dispersion method estimates both the frequency dispersion magnitude and phase. Therefore, a time domain autocorrelation is computed followed by a Fourier transform to produce a waveform feature indicator for DP. After these operations, both the DP magnitude and phase frequency distributions are computed as previously defined in Section 3.4.2. The output of this method is a sequence of DP magnitude and phase estimates at the waveform block rate as defined in Section 3.2.2. Refer to Appendix Section A.11.2 for additional background for second order statistical feature extraction.

Waveform Time Correlation Estimation Refer to Figures 3.20 and 3.24 for the waveform Tc estimation (T3:8) architecture and system model. As discussed in Chapter 1, channel coherence is related to waveform time correlation. Given the input waveform complex envelope samples, the time correlation method estimates the Tc magnitude and phase. Therefore, a time domain autocorrelation is computed to produce a waveform indicator feature for Tc. After these operations, both the Tc magnitude and phase frequency distributions are computed as previously defined in Section 3.4.2. The time domain correlation was previously defined in Section 3.22. The output of

this method is a stream of Tc magnitude and phase estimate vectors at the waveform block rate as defined in Section 3.2.2. Refer to Appendix Section A.11.2 for additional background for second order statistical feature extraction.

Waveform Frequency Correlation Estimation Refer to Figures 3.20 and 3.25 for the waveform BWc estimation (T3:9) architecture and system model. As discussed in Chapter 1, frequency coherence is related to waveform frequency correlation. Given the input waveform complex envelope samples, the frequency correlation method estimates both the BWcM and BWcP. Therefore, a frequency domain autocorrelation is computed to produce a waveform indicator feature for BWc. After these operations, both the BWc magnitude and phase frequency distributions are computed as previously defined in Section 3.4.2. The output of this method is a sequence of BWc magnitude and phase estimates at the waveform block rate as defined in Section 3.2.2. Refer to Appendix Section A.11.2 for additional background for second order statistical feature extraction.

State Likelihood Estimation

State Likelihood Parameter Estimation Referring to Figure 3.26, for the state likelihood parameter estimation architecture. As discussed in Chapter 1 and Chapter 2 the HMM training processes have been defined. These processes for the Enhanced CSR Algorithm for a single feature are similar to the HMM training processes as defined for the Baseline HMM Algorithm. Refer to Section 2.4.2 for background and definition of the Enhanced CSR Algorithm SLP analytical model.

State Likelihood Estimation Referring to Figure 3.26, for the state likelihood parameter estimation architecture. As discussed in Chapter 1 and Chapter 2 the HMM state likelihood estimation processes have been defined. These processes for the Enhanced CSR Algorithm for a single feature are similar to the HMM training processes as defined for the Baseline HMM Algorithm. Refer to Section 2.4.2 for background and definition of the Enhanced CSR Algorithm state likelihood

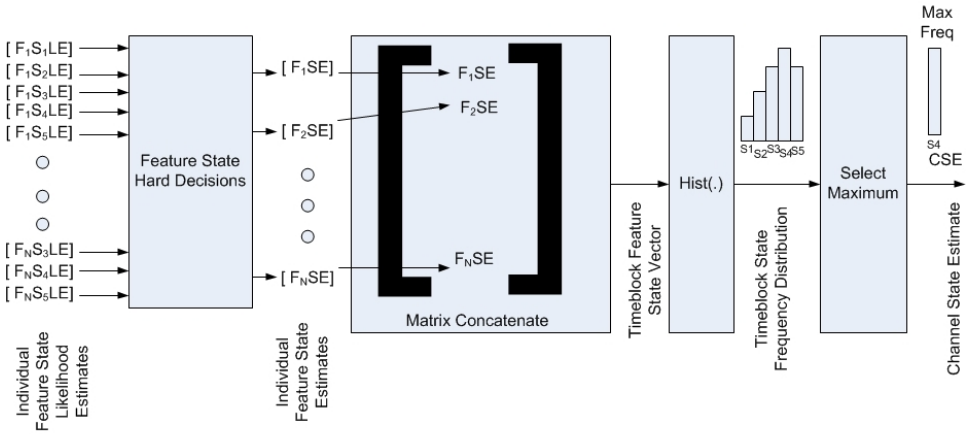

Figure 3.31: CSR-Enhanced Tier 3 State Decision Estimation Computations

estimation analytical model.

State Decision Estimation

The state decision computations shown in Figure 3.31, provides a reference for each of the state decision methods to follow. Refer to Appendix Sections A.11.5 and A.11.6 for additional background for state decision estimation processes.

State Hard Decision Referring to Figures 3.27, 3.28, and 3.31, the state hard decision method is defined by equation (3.7) which defines the feature state estimate (FSE) for each input feature. The hard decision is made as CS_i if the input feature state likelihood is greater than 90% likely, otherwise, FSE is zero. The .90 threshold is arbitrary, and could just as well been established as .98 depending upon the desired accuracy between the operational sequence and the training sequence statistics.

$$FSE_k = \begin{cases} 0 & if SLE < .9 \\ CS_i & if SLE >= .9 \end{cases} \tag{3.7}$$

Matrix Concatenation Referring to Figures 3.27, 3.29, and 3.31, the matrix concatenate method appends the individual feature states into a single column vector.

Timeblock State Frequency Distribution Referring to Figures 3.27,3.30, and 3.31, the time block frequency distribution is achieved by application of the histogram method previously defined in Section 3.4.2.

Select Maximum Referring to Figures 3.27 and 3.31, the select maximum method is achieved by selecting the state with the highest highest number of estimates previously defined in Section 3.4.2.

3.5 Conclusion

The enhanced algorithm is established upon the preliminary results discussed in the previous Chapter 3. In this Chapter, the enhanced algorithm has been decomposed into 4 levels of detail. Within each level analysis of relevant architecture, system, data, and analytical models have been provided. This effort exposes details of the enhanced CSR algorithm. Verification test results for the enhanced CSR algorithm are provided in Chapter 4. The test results in Chapter 4 are to be interpreted consistent with the analysis provided in this chapter.

This Page Intentionally Left Blank

Chapter 4

CSR Algorithm Verification

There are two forms of the CSR algorithm. The baseline version serves as a proof of concept prototype for feasibility evaluation of the CSM and CSR concepts. The first Section of this chapter will cover the verification testbed, approach, and test results from evaluation of the baseline version. The enhanced version of the CSR algorithm is focused on improving limitations discovered in the POC prototype and also in the published literature. The second Section of this chapter will cover the verification testbed, approach, and test results from evaluation of the enhanced version.

4.1 Baseline CSR Algorithm Verification

This Section will cover the verification testbed, approach and results for the Baseline CSR Algorithm.

4.1.1 Baseline Verification Testbed

The CSR verification testbed (CVT) shown in Figure 4.1, has been created for testing of MWC state recognition algorithms. A channel state waveform generator has been designed to provide a source of calibrated MWC state waveforms. After these are applied to the CSR algorithm the output CSEs are monitored for verification against the source waveform generator.

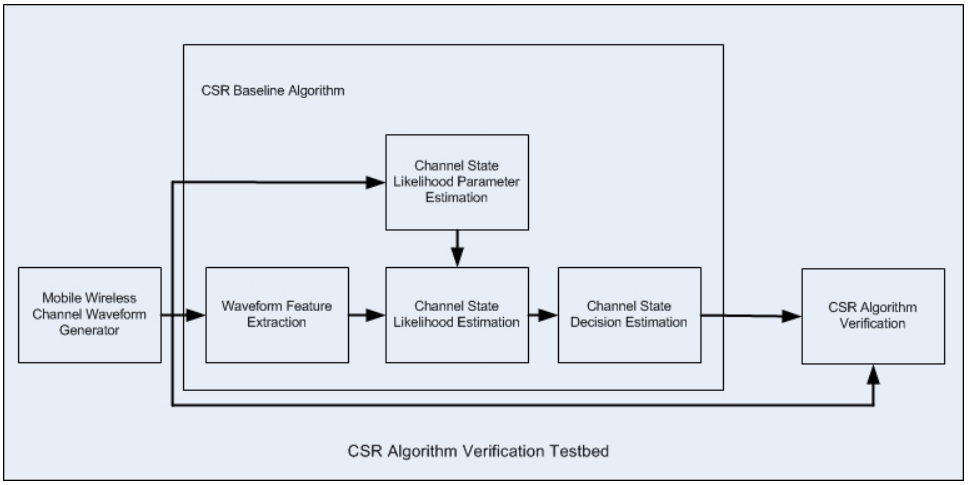

Figure 4.1: CSR Algorithm Testbed

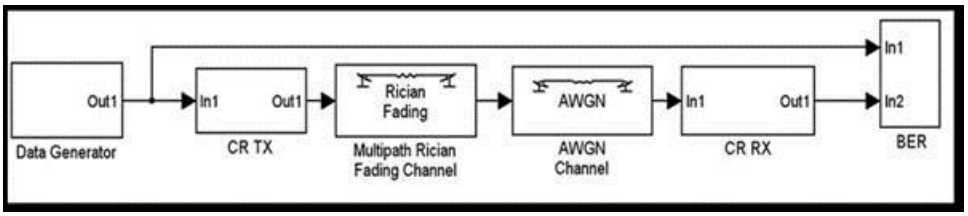

Figure 4.2: Channel State Waveform Generator

State Waveform Generator

The channel state waveform generator (SWG) shown in Figure 4.2, provides a set of MWC state cases based on waveform characteristics, channel parameters, and source bit streams. The SWG enables control of channel hidden process parameters and receive waveform characteristics so that correlated training and operational sequences can be generated for the CSM and the CSR algorithm. Example CSM state parameters have been enumerated in Table 4.1. Observable

Table 4.1: SWG: Enumerated MWC CSM Cases

Typical Waveform Parameters	Typical Channel Parameters	CSM States	Example Transmit Stream	Example Receive Stream	BER	Channel Symbol Sequence
Modulation; Coding; Bit Rate; Amplitude	Amplitude Distribution; CIR; Doppler Spread; Eb/No	AWGN	10110010101...	10110010101...	1.00E-006	1+j, -1-j,...
		FN + TN	10011010101...	10011010101...	1.00E-006	1-j, -1-j,...
		FN + TS	11100010101...	11100010101...	1.00E-006	1+j, -1+j,...
		FS + TN	10111110101...	10111110101...	1.00E-006	1-j, -1+j,...
		FS + TS	10000010101...	10000010101...	1.00E-006	1+j, -1-j,...

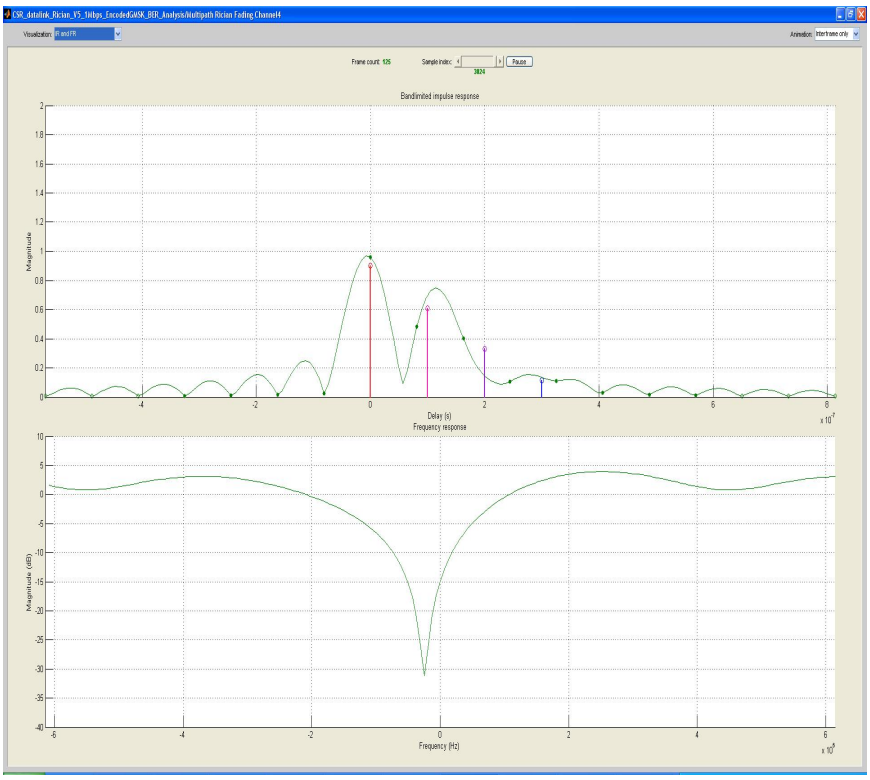

Figure 4.3: MWC Impulse Response with Selective Frequency Response

receive waveform features such as CEM first order statistics and symbol rate are correlated with channel parameters such as time and frequency dispersion. Each case is applied to the baseline CSR algorithm with predictable state sequence recognition results. Given an expected output sequence, performance verification of the baseline CSR algorithms is achievable. Training waveforms are also produced by the SWG for off-line HMM parameter estimation prior to operational testing. Random data streams with statistics similar to operational data are generated for training. Time-variant MWC hidden state sequences are produced for evaluating state tracking. Management of these parameters enables implementation of statistical relationships between MWC hidden states and observable waveform statistics. For example in Figure 4.3, the channel impulse response is shown which provides an indicator of channel time dispersion. A second example is shown in Figure 4.4 which illustrates the MWC scattering function. A third example is shown in Figure 4.5, which provides multipath components with associated CIR and symbol amplitude and phase traces. These waveform and channel features provide sufficient

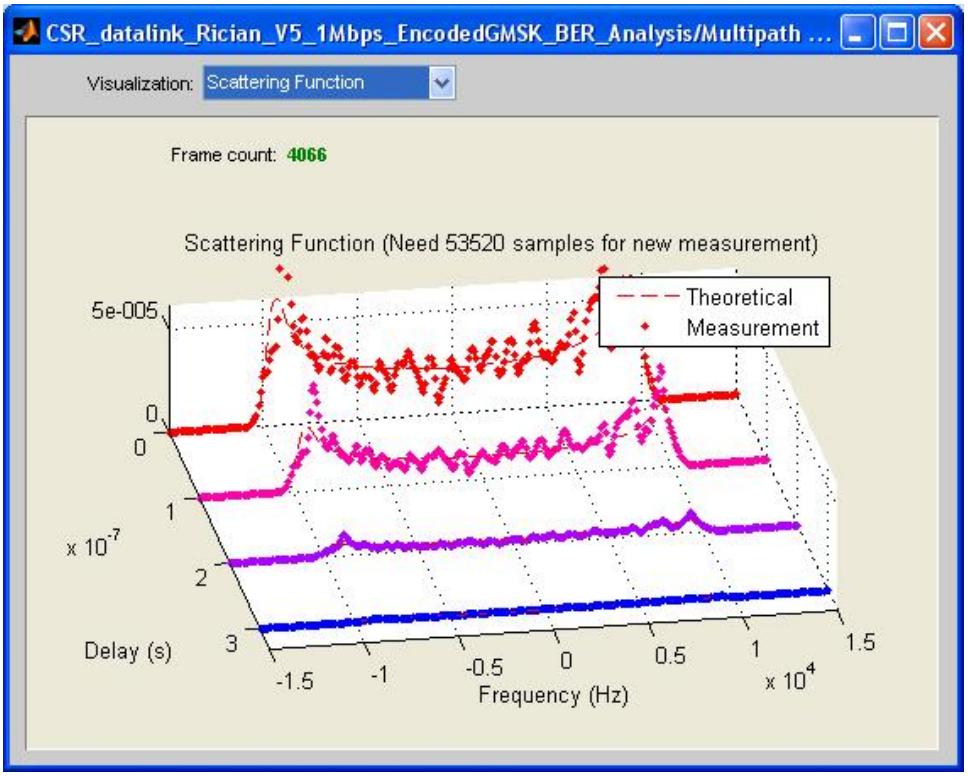

Figure 4.4: MWC Scattering Function

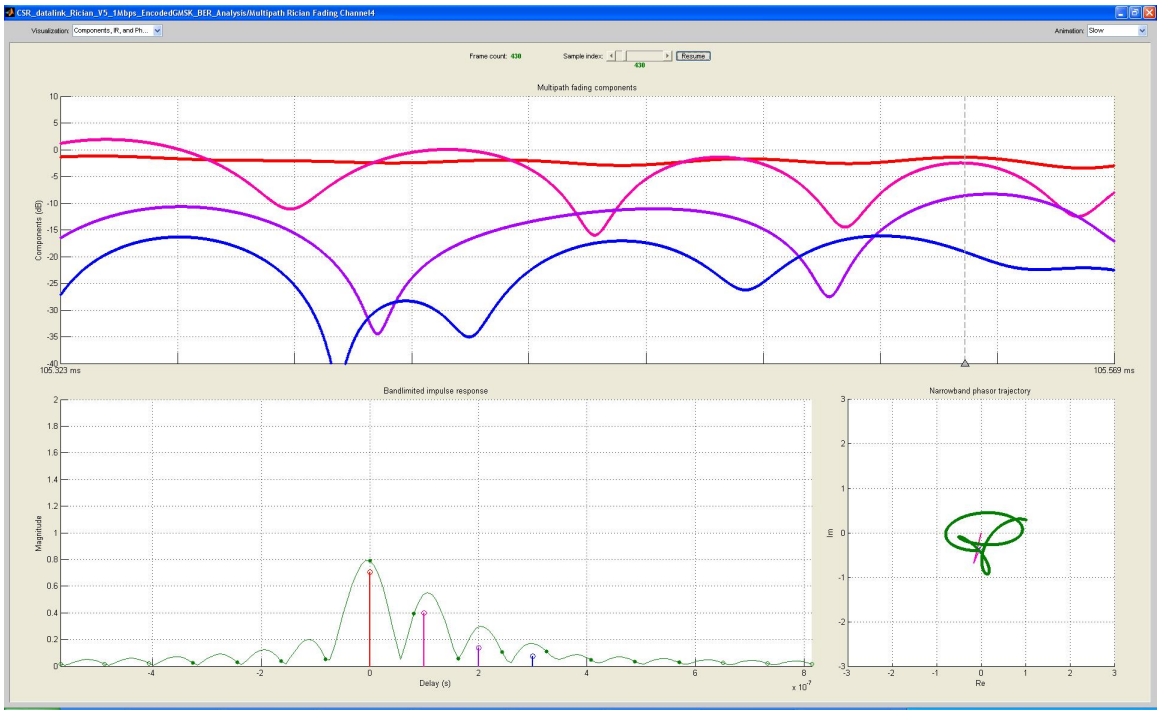

Figure 4.5: MWC CIR, Time Variant Frequency Response and Constellation

information to discriminate MWC states and waveform statistical features which can be recognized by the CSR algorithms. These channel and waveform features, along with input and output waveform symbol sequences, and output CSR state sequences are recorded for analysis and verification. CSR algorithm performance is verified by comparing the experimental CSR algorithm response to the known response of the SWG. Cause and effect relationships between CSR algorithm response and SWG MWC state sequences can be experimentally verified.

4.1.2 Baseline Verification Approach

Coherence State Model

For verification of the baseline algorithm, the CSM has been embedded within the memory parameters of a CSR HMM. This was accomplished by tailoring the training sequences with statistical parameters consistent with the CSM. The CSM trained HMM has been tested in the CVT as shown in Figure 4.1. The intent of this test is to demonstrate the feasibility of HMMs to recognize time-variant channel states. As described in Chapter 2, the HMM is operated as a ML sequence decoder; that is, given an observed sequence of symbols, an estimate is generated of the unobserved hidden state sequence. Recall from Chapter 1 that HMMs have been utilized in several recognition applications including automatic speech recognition systems. Given sufficient MWC waveform feature extraction, and statistical training, this verification test demonstrates that a HMM can be extended to channel state recognition.

Coherence State Cases

SWG symbol sequences with characteristics as defined in Table 4.2 are applied to the CSR HMM for performance verification. Each test case is designed to represent a state in the CSM.

Sequences of 50k symbols were generated for each case in MATLAB [47] and also in SIMULINK [47] and the channel output was stored for post processing analysis. Certification that waveform

Table 4.2: Test Case Definitions

	Channel State					Waveform State			
Test Case	Amplitude PDF	Multipath Delay Profile	Multipath Gain Profile	Doppler Shift	Doppler Spread	Eb/No	Baseband Modulation	Bitrate Mbps	FEC
1	Ricean	[0 .1e-6 .2e-6 .3e-6]	[0 -100 -100 -100]	0	.01	10	BPSK	1	Uncoded
2	Rayleigh	[0 .1e-6 .2e-6 .3e-6]	[0 -3 -10 -20]	0	.01	10	BPSK	1	Uncoded
3	Rayleigh	[0 1e-6 2e-6 3e-6]	[0 -3 -10 -20]	0	.01	10	BPSK	1	Uncoded
4	Rayleigh	[0 1e-6 2e-6 3e-6]	[0 -3 -10 -20]	0	100	10	BPSK	.01	Uncoded
5	Rayleigh	[0 1e-3 2e-3 3e-3]	[0 -3 -10 -20]	0	100	10	BPSK	.01	Uncoded

symbol streams are consistent with wireless channel CSM states is critical. Therefore testing on each waveform sequence has been conducted to verify that specific waveform state and channel state characteristics are reliable. Figures of merit such as SNR levels, chanel impulse response (CIR), channel frequency response (CFR), channel scattering functions (CSF), CEM PDF, and bit error rate (BER) curves have been evaluated to verify the integrity of each waveform sequence.

Waveform Envelope PDF Estimation

Complex waveform magnitude and angle distributions were estimated with a 200 bin histogram. For case 1 and 2, the magnitude distribution is consistent with a theoretical Ricean magnitude distribution. The angle distributions had a small variance with means located at 0 and pi radians. Cases 2-5 had magnitude distributions consistent with cases 1 and 2 as expected. However, the angle distributions demonstrated greatly increased variance around the means of 0 and pi radians. This is consistent with dramatic fading effects on phase and minor impacts to waveform magnitude.

Waveform Eb/No Estimation

E_b/N_o for each test cases was estimated by computing signal power and noise relative to the specified E_b/N_o signal level. All test cases produced an estimated SNR and of 10 dB as specified in Table 4.2.

Waveform Bit Error Rate Computation

Bit error rates were computed by comparing the output data stream to the transmitted bit stream (Refer to SWG Figure 4.2) and enumerating observed errors. For case 1 and 2, BER curves were exponential confirming that state 2 assumptions regarding nonselective behavior is valid. Test cases 3-5 did demonstrate an error floor consistent with more linear BER curves for frequency selective or time selective channels. All BER tests are consistent with theoretical expected results.

Waveform Channel Impulse Response

Cases 1-5 had CIR delay and gain components consistent (refer to Figures 4.3 – 4.5 for examples) with each specified channel state in Table 4.2.

Waveform Frequency Response Estimation

The CFR was estimated for each test case (refer to Figures 4.3 – 4.5 for examples) with consistent results. Case 1-2 demonstrated time invariant CFR however case 2 demonstrated flat frequency fading as expected for the AWGN and Flat Frequency channels. Test case 3 demonstrated frequency selective behavior as expected for a frequency selective channel. Test case 4-5 demonstrated time variant CFR in that for each symbol the CFR was dynamic consistent with a time selective channel. Test case 4 was a time variant flat frequency response while test case 5 was a time variant frequency selective channel response. The CFR were all consistent with expected behavior.

Scattering Function Estimation

The CSF is a 3D graphical display of waveform power as a function of delay spread and Doppler spread. For each test case the Doppler spread and multipath delay components were as specified in Table 4.3. Channel coherence time and coherence bandwidth were computed based on root mean square (RMS) time delay spread and maximum Doppler frequency spread as defined in equation 4.1 to equation 4.5. Case 1 and 2 were designed such that the channel time dispersion is

Table 4.3: MWC Coherence Time/Bandwidth

Channel BW_c and $T_c$computed from CSF				
Case	Channel State	Waveform State	Computed C_{BW} (Hz)	Computed C_T (s)
1	AWGN	1 Mbps uncoded BPSK	3.7417e-12	42.3
2	FN+TN	1 Mbps uncoded BPSK	6.3972e-8	42.3
3	FS+TN	1 Mbps uncoded BPSK	6.3972e-7	42.3
4	FN+TS	10 kbps uncoded BPSK	6.3972e-7	4.23e-4
5	FS+TS	10 kbps uncoded BPSK	6.3972e-4	4.23e-4

much less than the bit period and case 1 represents an AWGN channel with a Ricean distribution. Case 2 is a Rayleigh distribution with flat frequency fading. Case 3 was designed such that the channel time dispersion exceeds 20% of the bit period and therefore is representative of a frequency selective channel. Case 4 is designed such that the channel time dispersion is much less than the bit period however the channel coherence time is approaching the bit period and therefore is representative of mildly time selective channel. Case 5 was designed such that the channel time dispersion exceeds 20% of the bit period and the coherence time is approaching the bit period and therefore is representative of a dual time and frequency selective channel.

Channel BWc and Tc Estimation

The following discussion was introduced in Chapter 1; it is based on several commonly cited wireless communication references such as Rappaport [3], Proakis [48], and Sklar [49]. Equations (4.1) to (4.5) have been repeated here to support the verification testing observations. Tc and BWc are computed from the cases in Table 4.2 and enumerated in Table 4.3. BWc is inversely related to the channel time dispersion due to summation of multipath signals and is defined as the frequency bandwidth where waveform frequencies are highly correlated. The BWc is roughly related to the channel time dispersion through equation (4.1),

$$B_c = \frac{1}{50\sigma_\tau}, \tag{4.1}$$

where σ_t is the rms multipath channel delay spread. This equation estimates the bandwidth where

the frequency components are highly correlated; frequency correlation exceeds .9 in this region. If the frequency correlation is reduced to .5, then equation (4.2),

$$B_c = \frac{1}{5\sigma_\tau}, \tag{4.2}$$

is utilized to estimate the BWc. The rms time delay spread is computed from the multipath CIR from the first and second weighted moments.

Tc is inversely related to the channel frequency dispersion due to Doppler spread induced by motion between transmitter and receivers. Tc is loosely defined as the period of time where waveform signals are highly correlated. The Tc is roughly related to the channel frequency dispersion by equation (4.3),

$$T_c = \frac{9}{16\,\pi f_m}, \tag{4.3}$$

where f_m is the maximum Doppler frequency spread. Equation (4.4),

$$T_c = \frac{1}{f_m}, \tag{4.4}$$

estimates Tc where time samples have correlation coefficients greater than .5. A more restrictive relationship between Tc and Doppler spread is provided by equation (4.4). A more practical estimation of CT is provided by equation (4.5),

$$T_c = \sqrt{\frac{9}{16\,\pi {f_m}^2}} = \frac{.423}{f_m}, \tag{4.5}$$

which is the geometric mean between equation (4.3) and (4.4). Time-variant operational and training symbol sequences with varying combinations of hidden channel states were concatenated to form a set of 250k symbol sequence training vectors and after quantization each is similar in structure to the example shown in Figure 4.6.

Input State Sequence Generation

Five training CSM state sequence vectors are shown for reference:

1. State 1, State 2, State 3, State 4, State 5,
2. State 2, State 3, State 4, State 5, State 1,
3. State 3, State 4, State 5, State 1, State 2,
4. State 4, State 5, State 1, State 2, State 3,
5. State 5, State 1, State 2, State 3, State 4.

This set of state sequences is not exhaustive, but sufficient to prove feasibility of the CSM and the CSR algorithm. It does capture the self state transitions, and forward state transitions of the CSM. Remaining state transitions are left for future confidence testing. The input waveform PDF is estimated by outputting a histogram bin index for each waveform sample. The bin indexes are accumulated to produce an estimated waveform pdf. An example statistical quantized sequence for hidden state sequence 12345 is shown in Figure 4.6. Each hidden state was formulated with controlled waveform and wireless channel properties consistent with the previously defined CSM channel states. These symbol sequences were applied to the statistical quantizer which estimated the waveform envelope PDF with a 200 bin[1] histogram[2].

4.1.3 State Likelihood Parameter Estimation

Refer to chapter 2 for background on HMM training sequences and parameter estimation. A set of CSM training vectors were formed with five different combinations of MWC hidden state sequences. Correlated state vectors were also generated and submitted to the baseline CSM algorithm to estimate HMM memory parameters first with the Viterbi algorithm, and refined by the Baum

[1]Less than 200 bins is inadequate to represent an accurate histogram function

[2]Mathworks, Inc.. MATLAB [20] function histogram(variable_name, bin_size) help pages.

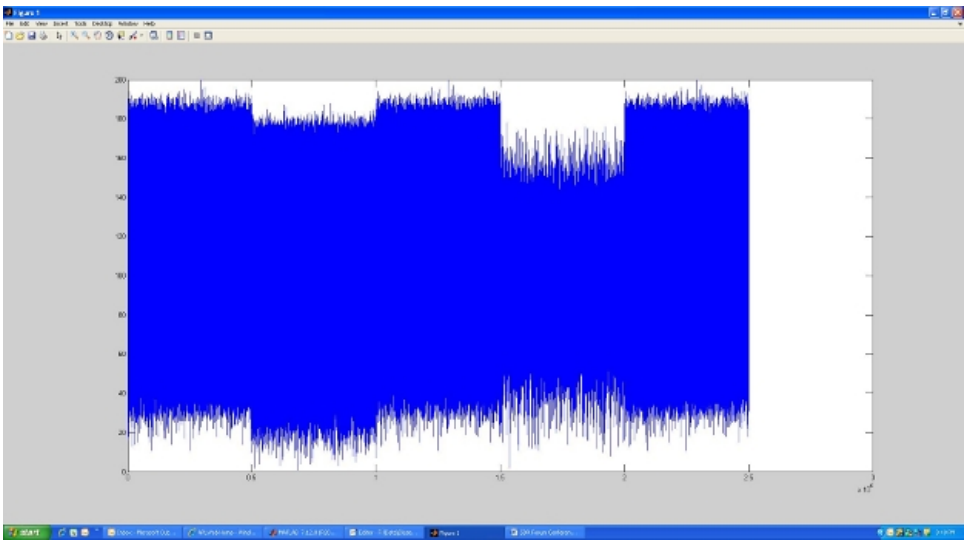

Figure 4.6: Statistically Quantized Waveform for State Sequence 12345

Welch algorithm. Estimates for the HMM transition and output probability matrices are formed by submitting a training symbol sequence statistically similar to the operational symbol sequences with an associated state sequence vector. As an example, a training statistically quantized sequence vector is shown in Figure 4.6 with a hidden state sequence of 12345. This was input to the training algorithm with 50 000 symbols[3] for each hidden state. An associated known state vector was also generated with a correlated state variable for each symbol. For clarification, each state vector is formulated as in equation (4.6),

$$State\_vector = [1_1 \cdots 1_{50000} 2_1 \cdots 2_{50000} 3_1 \cdots 3_{50000} 4_1 \cdots 4_{50000} 5_1 \cdots 5_{50000}]. \tag{4.6}$$

These training vectors were input to the Viterbi training algorithm to formulate an initial rough order estimation of the transition and output parameters. Next these initial transition and output matrices were input into the Baum Welch training algorithm for fine-tuning. The Viterbi training algorithm is available in the MATLAB function hmmestimate [50] and the BW algorithm is available in the MATLAB function hmmtrain [51]. This training parameter estimation process produced estimates for the 5 state transition probability matrix (5x5) shown in Table 4.4. The

[3]Statistical significance is a known HMM limitation, to avoid this problem a substantial number of samples were generated. Future research will investigate shorter training sequences.

Table 4.4: CSR HMM Transition Probability Matrix

.9999	1.999e-5	1.999e-5	1.999e-5	1.999e-5
1.999e-5	.9999	1.999e-5	1.999e-5	1.999e-5
1.999e-5	1.999e-5	.9999	1.999e-5	1.999e-5
1.999e-5	1.999e-5	1.999e-5	.9999	1.999e-5
1.999e-5	1.999e-5	1.999e-5	1.999e-5	.9999

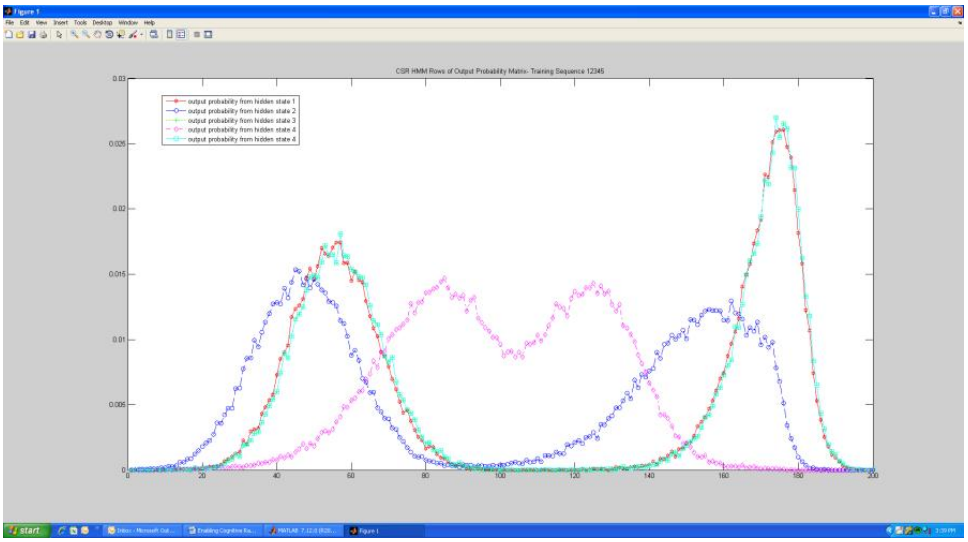

Figure 4.7: CSR HMM Output Probability Matrix Rows

training process also produced an output probability matrix (5x200) shown in Figure 4.7. This figure plots each of the rows of the output matrix similar to a PDF relating the HMM output to each of the CSM hidden states.

4.1.4 State Decision Estimation

As discussed in Chapter 2, the Viterbi algorithm can be applied to the observed symbol sequence to estimate the most probable or the most likely hidden state sequence given an HMM model. The maximum likelihood state sequence is described by equation (4.7),

$$\pi^* = \max_{\pi} P(x, \pi), \tag{4.7}$$

where Π is the ML symbol sequence and Π_i is a specific symbol in the ML sequence.

The Viterbi algorithm is initialized with the most probable state k known for all the states at position i and then backward iterates to the beginning of the state space with equation (4.8),

$$v_l(i) = e_l(x_i)\max_k (v_k(i)a_{kl}. \tag{4.8}$$

This equation is utilized to identify the ML path through the state space, where v_l is the most probable path in the sequence through the state space at observation i, $e_l(x_i)$ is the associated output probability, a_{kl} is the associated transition probability, and $v_k(i)$ is the highest probability state at observation i. The output is a state sequence Π whose elements identify the most likely states associated with the symbol sequence x. The Viterbi decoding algorithm is implemented by the MATLAB hmmdecode function [52].

4.1.5 CSR Baseline Algorithm Verification Results

After training was completed, accuracy testing of the DSR HMM was performed by submitting a single hidden state sequence to each of the 5 trained HMMs. Accuracy performance results from each ML decoding trial were recorded for evaluation. Accuracy performance metrics in terms of sensitivity and specificity coefficients are provided. Decoded HMM output hidden state sequences are shown in Figure 4.8.

Statistical accuracy metrics sensitivity and specificity for the baseline CSM CSR are summarized in Figures 4.9 to 4.13.

For each test case, an operational hidden state sequence 12345 was submitted to each uniquely trained HMM. The HMM model utilized to recognize the sequence was varied as noted in each diagram. Accuracy is defined in terms of statistical tests for sensitivity and specificity as computed by equation (4.9),

$$Sensitivity = \frac{TP}{TP+FN}, \tag{4.9}$$

Figure 4.8: ML Decoded CSM State Sequences

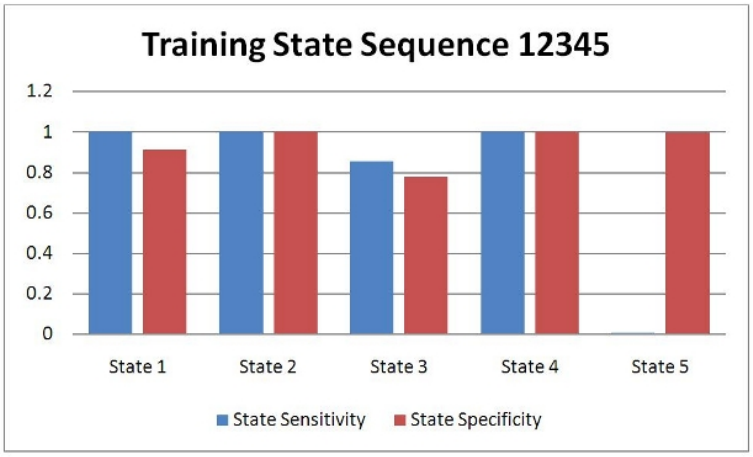

Figure 4.9: Training State Sequence 12345 Results

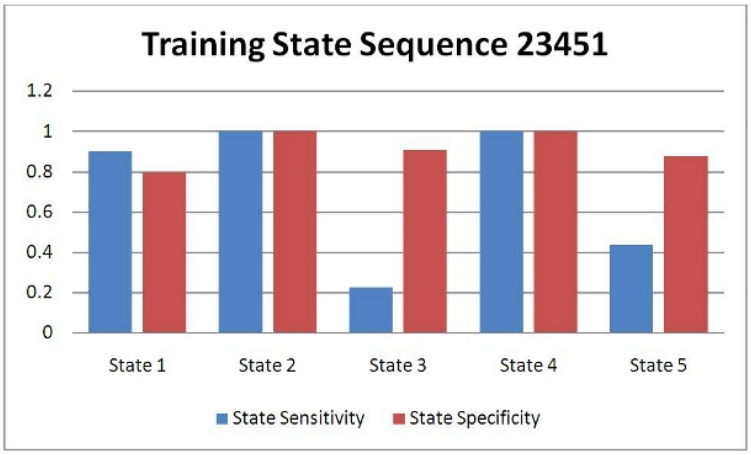

Figure 4.10: Training State Sequence 23451 Results

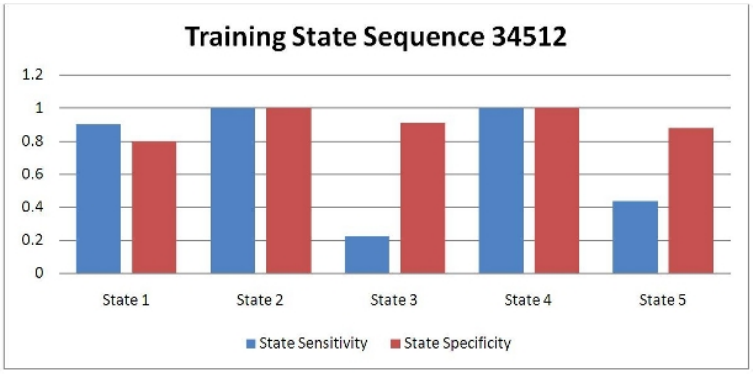

Figure 4.11: Training State Sequence 34512 Results

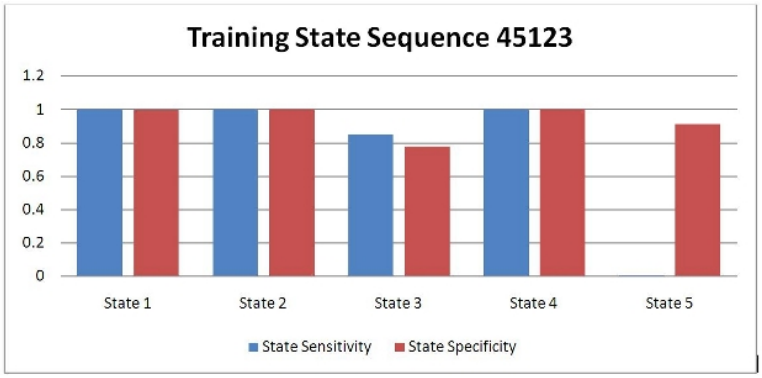

Figure 4.12: Training State Sequence 45123 Results

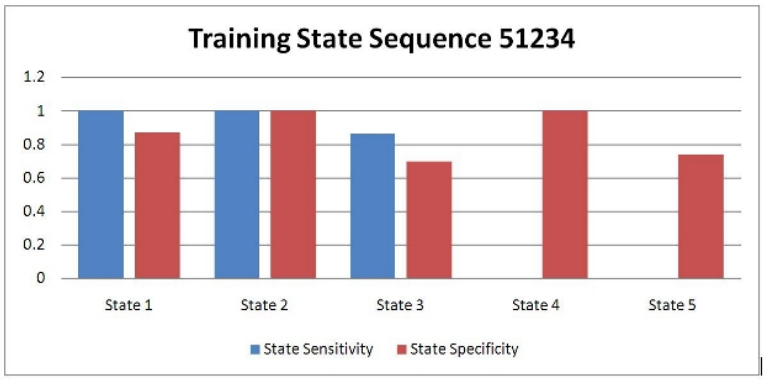

Figure 4.13: Training State Sequence 51234 Results

and (4.10),

$$Specificity = \frac{TN}{TN + FP}. \tag{4.10}$$

Sensitivity is a statistical measure for a binary classification system which identifies the proportion of actual positive decisions that are correct, that is, the number of true positives (TP) as shown in equation (4.9) where, TP = true positives and FN = false negatives. With high sensitivity, a low type II error is expected, and a negative result would suggest a high probability of a negative result. Specificity is a statistical measure for a binary classification system which identifies the proportion of actual negative decisions that are correct as shown in equation (4.10) where TN = true negatives and FP = false positives. The goal is 100% sensitivity (correctly predict all the positive outcomes) and 100% specificity (correctly predict all negative outcomes). With high specificity, a low type I error is expected, and a positive result would indicate a high probability of a positive result.

4.1.6 CSR Baseline Algorithm Verification Findings

Evaluating the results, several conclusions can be formed:

- These results suggest that statistical feature recognition with HMMs is feasible,
- These results suggest that decoding MWC hidden state sequences with HMM is feasible,
- None of the HMMs recognize dual dispersive state 5,

- All of the HMMs recognized the absence of dual dispersive state 5,
- All of the HMMs would accurately predict the presence or the absence of dual non-selective state 2 or singly frequency dispersive state 4,
- All of the HMMs would recognize the presence of AWGN State 1 with greater than 85% accuracy and would recognize the absence of AWGN S state 1 greater than 80% of the time,
- Two of the HMMs would recognize the presence of singly time dispersive state 3 with greater than 80% accuracy while all of the HMMs would recognize the absence of singly time dispersive state 3 with greater than 70% accuracy,
- Preliminary results suggest that the approach is insensitive to waveform parameters such as modulation or data rate,
- If these HMMs were arranged in parallel and their outputs were logically combined, states 1, 2, and 4 could be recognized with 100% accuracy and state 3 could be recognized with greater than 90% accuracy,
- As suggested by this observation, HMM structures for CSR will be a subject for further research,
- It is clear that the dual dispersive state 5 training sequence is not representative of the operational data.

4.2 Enhanced CSR Algorithm Verification

This Section will discuss the CSR enhanced algorithm testbed, verification approach, and accuracy test results.

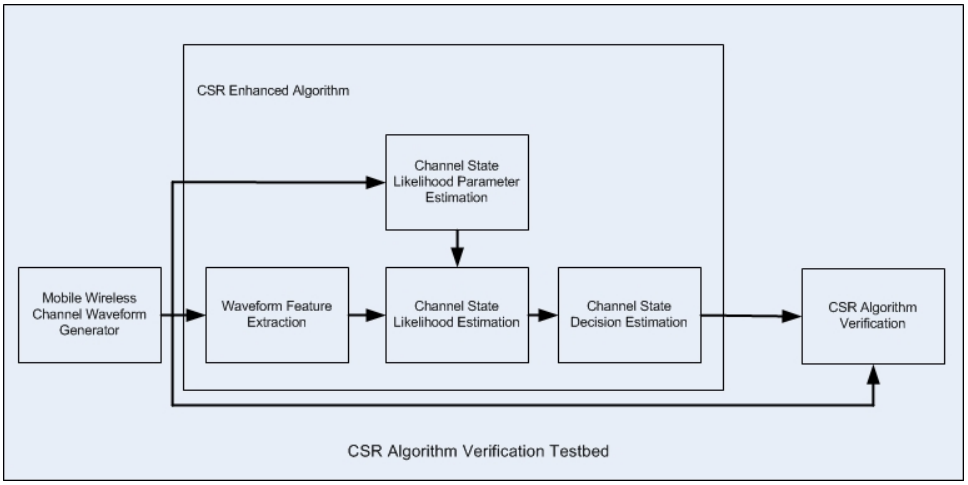

Figure 4.14: CSR Algorithm Testbed

4.2.1 Enhanced Verification Testbed

The Enhanced CVT is shown in Figure 4.14. It is similar to the previously described Baseline CVT discussed in the previous Section 4.1.1 except the architecture and function of the CSR algorithm.

4.2.2 Enhanced Verification Approach

The approach to verify the enhanced algorithm is similar to that described previously in Section 4.1.2. CSM hidden state and observable receive waveform features sequences were generated. These receive waveform sequences were input to the state likelihood and state decision estimation processes and the output CSM state sequences were evaluated for accuracy against the input MWC hidden state sequences. Figure 4.15 highlights the relationship between MWC hidden processes (e.g., time and frequency dispersion) and observable process features receive waveform first and second order statistics (e.g., CEM distribution, time, and frequency correlations). As described in the introduction, the HMM statistical memory links the the MWC hidden state process and the observable process statistics. The waveform generator was utilized to produce calibrated CSM waveforms that were passed through HMMs that had been trained as described in Section 4.2.3. The resulting output MWC state estimates were evaluated for accuracy against the input hidden state sequences.

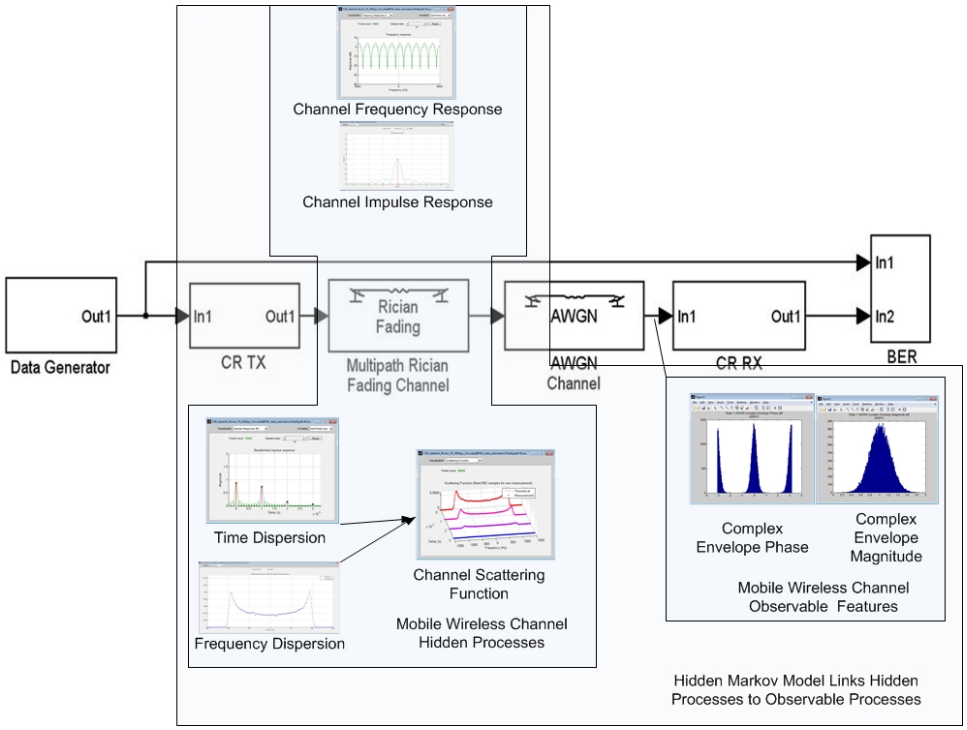

Figure 4.15: HMM Verification

State Feature Sequence Generation

The Enhanced CSR WFV were generated as shown in Figure 4.16. Each feature vector is processed to produce the waveform feature sequences defined in Table 4.2. The WFV generation results can be reviewed in Appendix Section A.11.2.

The WFV from the previous Section were processed to formulate a set of state feature sequence vectors as shown in Figure 4.17. This processing produced test vectors that contain state feature sequences as previously described in Section 4.1.2. Input test sequences were formulated for each of 10 features in each state resulting in 50 unique test sequences that were applied to the state likelihood estimation algorithm.

4.2.3 Enhanced State Likelihood Parameter Estimation Processing

To create the state likelihood HMM transition and output probability parameters, state sequence and feature sequence vector pairs are combined into HMM training sequences. This process is

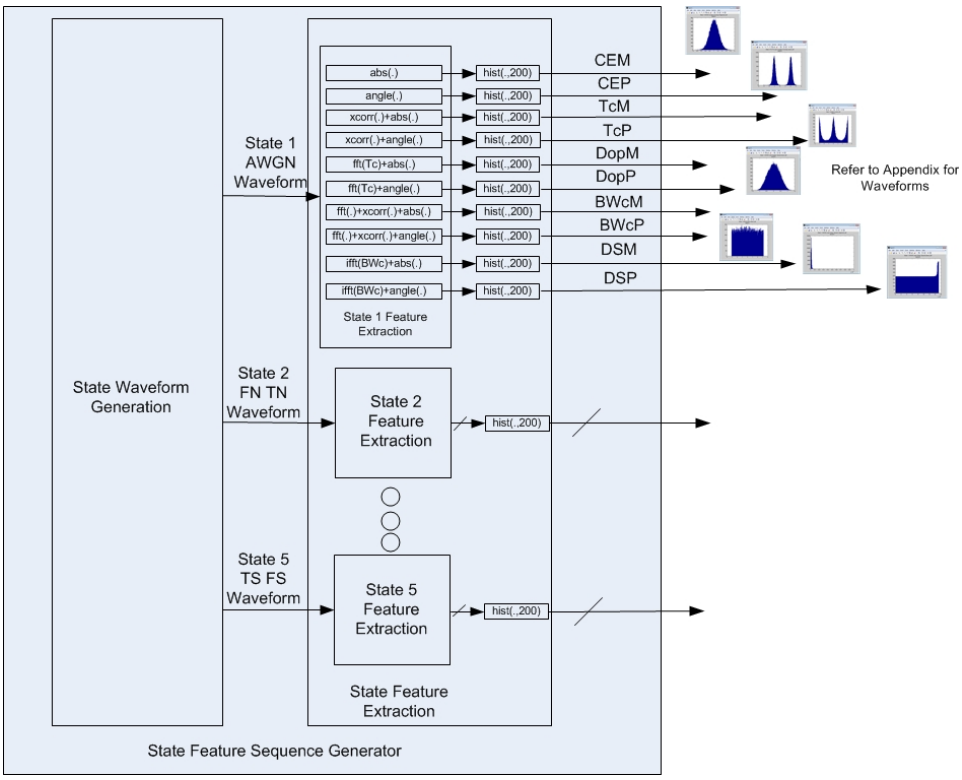

Figure 4.16: State Feature Generator

shown in Figure 4.18. The state feature sequence generator was described in the previous Section while the state sequence generator is a sequence of state vectors that are correlated with the feature sequence. These correlated sequences provide the linkage between the MWC hidden processes and the MWC observable feature sequences. Standard MATLAB matrix and vector operations provide the processes to produce the HMM training sequences.

The HMM training sequences described in the previous Section were supplied to the state likelihood parameter estimation process as shown in Figure 4.19. The HMM parameter estimation generates a transition and output probability matrix. A set of HMM parameters for each HMM can be reviewed in Appendix Section A.11.3.

Refer to Appendix section A.11.3 for additional background for state likelihood parameter estimation.

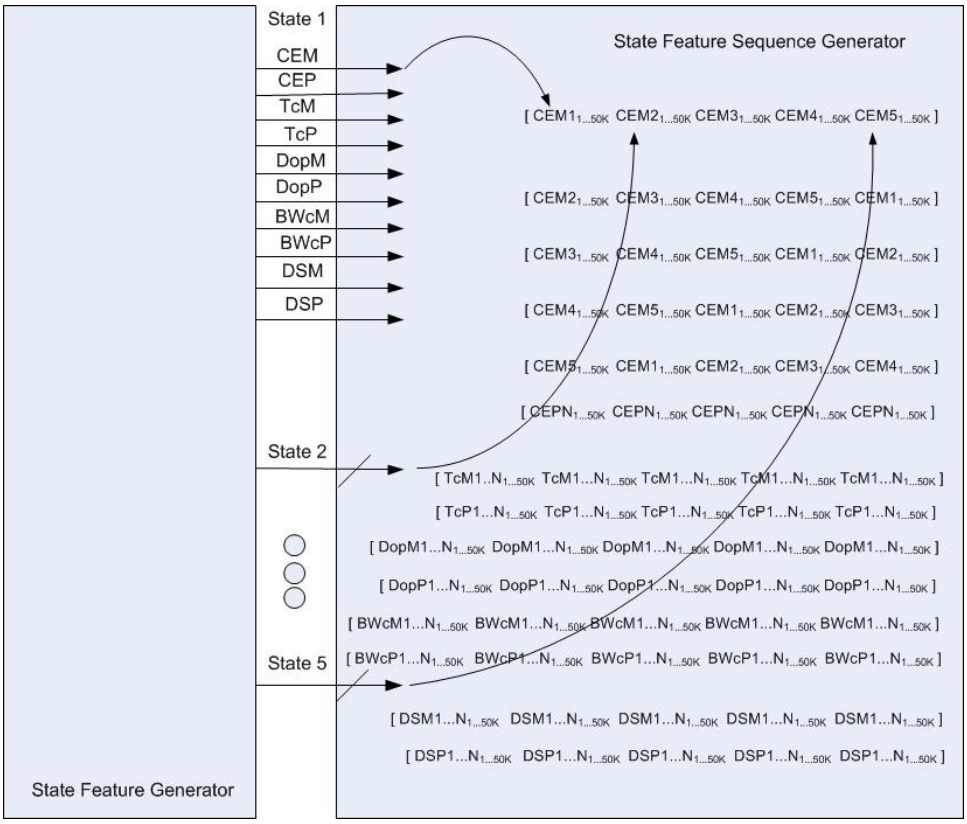

Figure 4.17: Feature State Sequence Generation

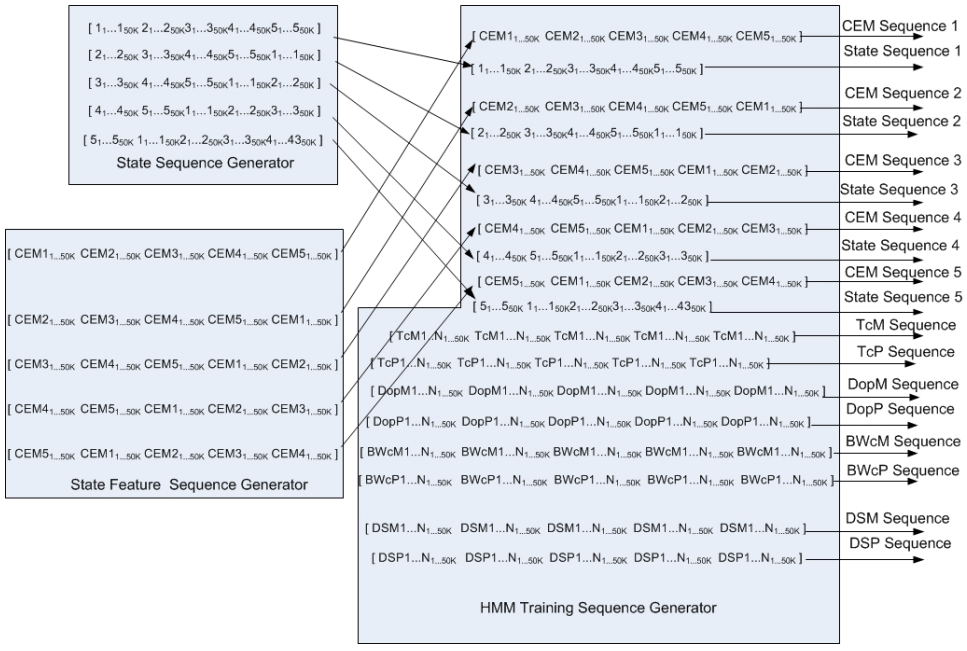

Figure 4.18: HMM Training Sequence Generator

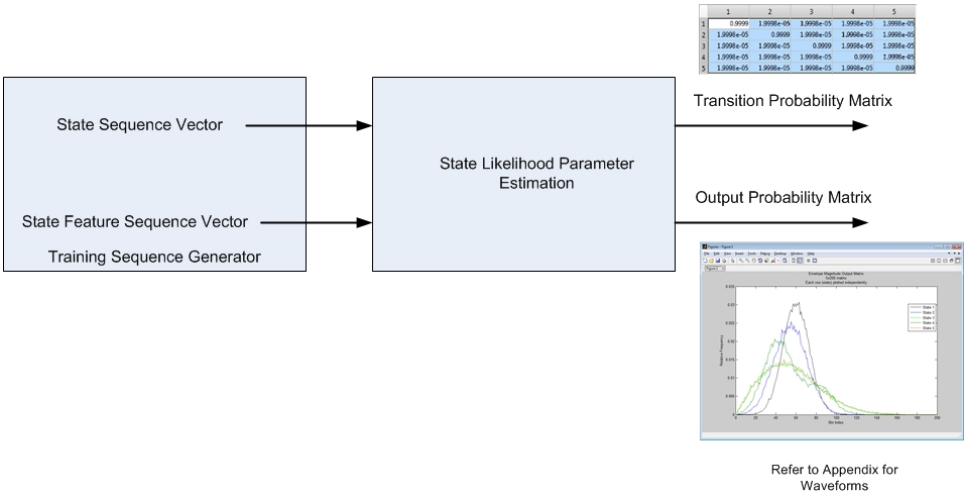

Figure 4.19: HMM Parameter Estimation

4.2.4 Enhanced State Likelihood Estimation Processing

Each of the state feature sequences were input into the state likelihood estimation HMMs to produce a sequence conditional probability sequence as shown in Figure 4.20. The output state feature conditional probability matrices are shown in Appendix Section A.11.4. These conditional probability sequences identify how closely the input sequence agrees with the sequence utilized to estimate the HMM parameters. The first row of the output matrix corresponds to how the hidden state 1 relates to the output waveform while the second row of the matrix corresponds to how state 2 of the hidden process relates to the output waveform. The rest of the rows are mapped to states 3-5 respectively. A value of 1 on any of the outputs indicates that the input sequence and the training sequences possess similar statistical properties while a value of 0 indicates that the two sequences do not have the same statistical properties. By monitoring each of the outputs sequences, the likelihood of the input matching any of the hidden states can be detected. By utilizing the same input sequences that were utilized to train the HMM, likelihood values approaching 1 would be expected when the input sequences match the training sequences.

Refer to Appendix Section A.11.4 for additional background for second order state likelihood estimation.

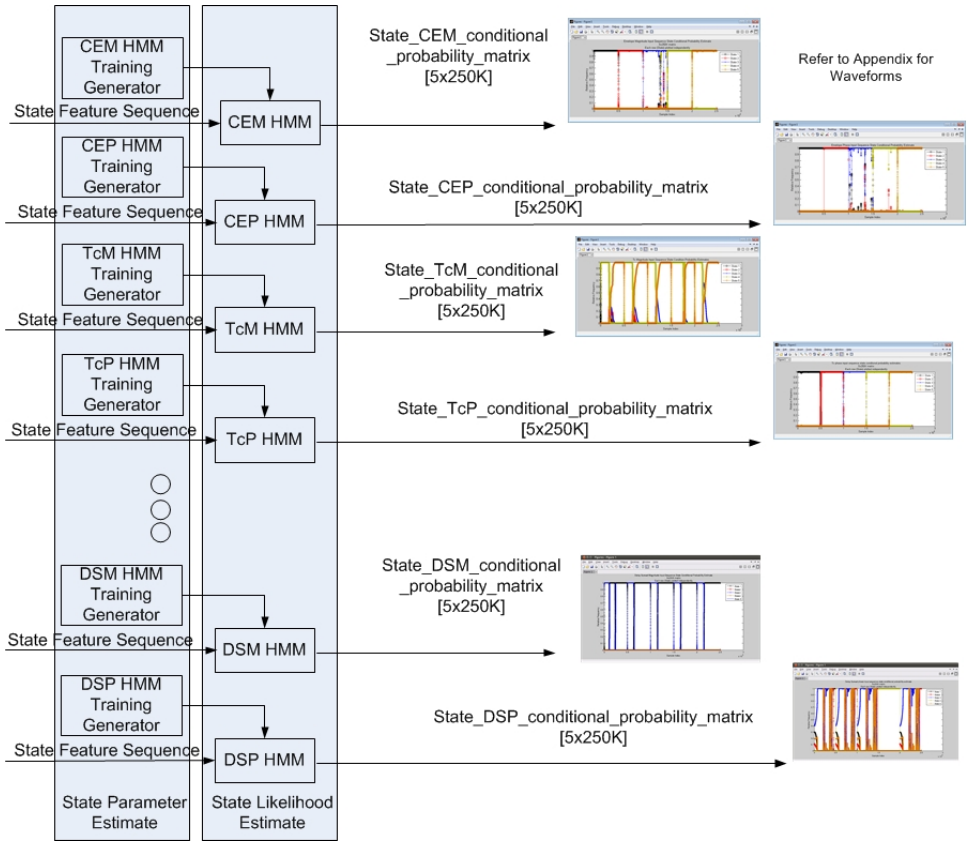

Figure 4.20: State Likelihood Estimation

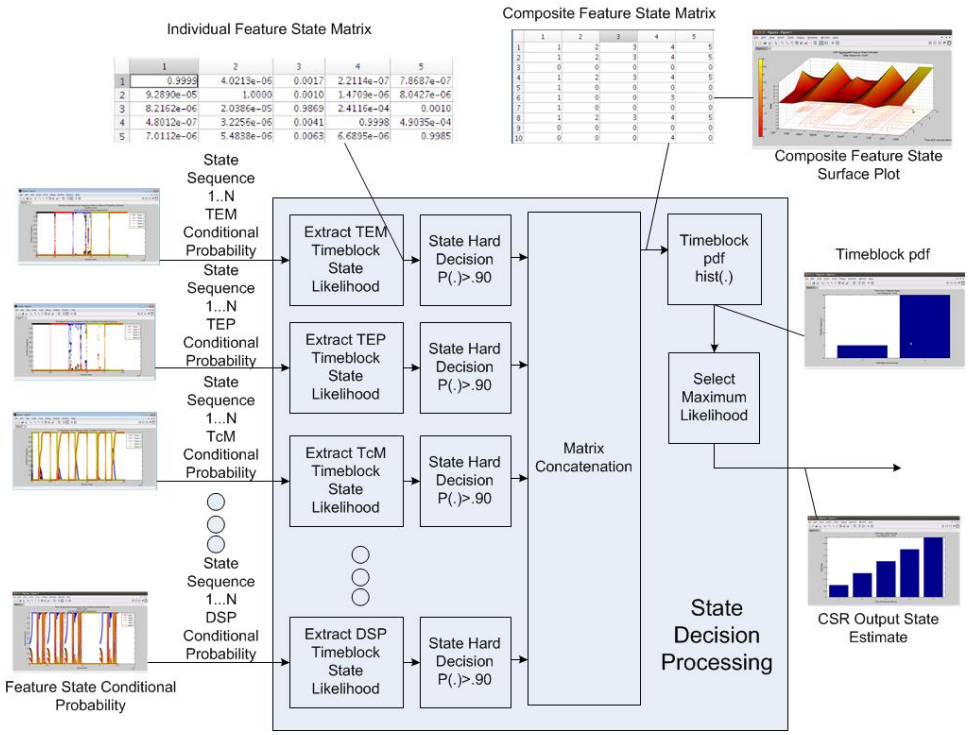

Figure 4.21: State Decision Estimation

4.2.5 State Decision Estimation

The state feature conditional probability matrices produced in the previous Section are input to the state decision estimation process as shown in Figure 4.21. The individual feature states are accumulated within each timeblock and normalized to provide a scalar likelihood estimate for each individual feature state sequence. Any states that exceed a 90% likelihood are extracted into the example individual feature state matrix as shown in Figure 4.21 and Appendix Section A.11.5. Each of the individual feature state matrices are concatenated into a an example composite feature state matrix as shown in Figure 4.21. An example surface plot of the composite feature state estimate matrix is shown in Figure 4.21 while the results are shown in Appendix Section A.11.6. The timeblock state distribution is estimated by accumulating all feature state estimates as shown in Figure 4.21. Finally, as shown in Figure 4.21, the state with the maximum number of detections is selected as the CSR output state. The timeblock state distributions and the CSR output state estimates are provided in Appendix Section A.11.7.

Table 4.5: CSR Accuracy State Sequence 12345

State Sequence 12345										
Feature	State 1 Sensitivity	State 1 Specificity	State 2 Sensitivity	State 2 Specificity	State 3 Sensitivity	State 3 Specificity	State 4 Sensitivity	State 4 Specificity	State 5 Sensitivity	State 5 Specificity
Envelope Magnitude	.9997	.9995	.9999	.9996	.9626	.9998	.9994	.9984	.9992	.9929
Envelope Phase	1	.9993	.9999	.9997	.9946	1	.9997	.9994	.9994	1
Tc Magnitude	2e-5	.9873	0	.9620	0	.8651	.5414	.6170	.4943	.4086
Tc Phase	.9975	.9963	.9849	.9993	.9997	.9999	.9990	1.000	.9998	.9999
Doppler Spread Magnitude	1	.9225	.6901	.8402	.1273	.5000	0	.9253	0	.8326
Doppler Spread Phase	1	.8121	.3093	.9204	.3734	.7138	0	.9312	.0482	.9154
BWc Magnitude	.9957	.7059	.4742	.8496	.2124	.8859	.0619	.8239	.1094	.9472
BWc Phase	.8379	.9833	.9891	.9685	.9671	.9975	.9236	.9954	.9957	.9862
Delay Spread Magnitude	.7595	.2936	0	1	.3007	.7125	0	1	0	1
Delay Spread Phase	.0995	.9091	.1444	.9037	.5709	.4654	.9999	.9951	.1492	.7720

Results Evaluation

CSR Algorithm MWC Hidden State Estimation Accuracy After applying the state sequences to the CSR algorithm, each state likelihood output sequence was evaluated against the input sequence. Each estimated state can be classified into one of four categories : 1) the estimated state is correctly true while the true state was true, 2) the estimated state was incorrectly true while the true state was false (Type I error), 3) the estimated state was incorrectly false while the state was true (Type II error), 4) the estimated state was correctly false while the true state was false. Table 4.5 through Table 4.9 provides the results after evaluating the input state sequences 12345, 23451, 34512, 45123, and 51234 respectively.

Table 4.6: CSR Accuracy State Sequence 23451

State Sequence 23451										
Feature	State 1 Sensitivity	State 1 Specificity	State 2 Sensitivity	State 2 Specificity	State 3 Sensitivity	State 3 Specificity	State 4 Sensitivity	State 4 Specificity	State 5 Sensitivity	State 5 Specificity
Envelope Magnitude	.9998	.9995	.9998	.9996	.9626	.9998	.9994	.9982	.9992	.9929
Envelope Phase	.9998	.9993	1.000	.9997	.9946	1	.9997	.9992	.9994	1.000
Tc Magnitude	0	.9873	0	.9620	0	.8651	.5414	.6308	.4937	.4086
Tc Phase	.9999	.9961	.9846	1.000	.9997	.9999	.9990	.9999	.9996	.9999
Doppler Spread Magnitude	0	1	1	0	0	1	0	1	0	1
Doppler Spread Phase	0	.9440	0	.8849	0	.9697	.7737	.1754	.1146	.9588
BWc Magnitude	.9957	.7059	.4742	.8496	.2124	.8859	.0619	.7312	.1094	.9472
BWc Phase	.8419	.9809	.9850	.9719	.9671	.9975	.9236	.9943	.9902	.9861
Delay Spread Magnitude	1	.0962	0	1	0	.9022	0	1	0	1
Delay Spread Phase	0	.9461	.1101	1	0	.8332	1	.3328	0	.9320

Table 4.7: CSR Accuracy State Sequence 34512

State Sequence 34512										
Feature	State 1 Sensitivity	State 1 Specificity	State 2 Sensitivity	State 2 Specificity	State 3 Sensitivity	State 3 Specificity	State 4 Sensitivity	State 4 Specificity	State 5 Sensitivity	State 5 Specificity
Envelope Magnitude	.9997	.9995	.9999	.9996	.9633	1	1	.9997	.9992	.9929
Envelope Phase	.9999	.9993	.9999	.9997	.9946	1	.9997	.9998	.9994	.9996
Tc Magnitude	0	.9872	0	.9620	0	.8651	.5409	.6268	.4937	.4085
Tc Phase	.9975	.9937	.9849	.9993	.9998	1.000	.9893	1.000	.9996	.9999
Doppler Spread Magnitude	0	1	1	0	0	1	0	1	0	1
Doppler Spread Phase	0	.9435	0	.8849	0	.9778	.3094	.0555	.1146	.9588
BWc Magnitude	.9957	.7059	.4742	.8496	.2124	.8859	.0619	.8435	.1094	.9472
BWc Phase	.8376	.9788	.9891	.9685	.9811	.9999	.9205	.9989	.9902	.9861
Delay Spread Magnitude	.9994	.0962	0	1	0	.9021	0	1	0	1
Delay Spread Phase	0	.9461	.1101	1	0	.8335	1	.3318	0	.9320

Table 4.8: CSR Accuracy State Sequence 45123

State Sequence 45123										
Feature	State 1 Sensitivity	State 1 Specificity	State 2 Sensitivity	State 2 Specificity	State 3 Sensitivity	State 3 Specificity	State 4 Sensitivity	State 4 Specificity	State 5 Sensitivity	State 5 Specificity
Envelope Magnitude	.9997	.9995	.9999	.9996	.9626	.9998	.9994	.9984	.9992	.9929
Envelope Phase	1	.9993	.9999	.9997	.9946	1	.9997	.9994	.9994	1
Tc Magnitude	2e-5	.9873	0	.9620	0	.8651	.5414	.6170	.4943	.4086
Tc Phase	.9975	.9963	.9849	.9993	.9997	.9999	.9990	1.000	.9998	.9999
Doppler Spread Magnitude	1	.9225	.6901	.8402	.1273	.5000	0	.9253	0	.8326
Doppler Spread Phase	1	.8121	.3093	.9204	.3734	.7138	0	.9312	.0482	.9154
BWc Magnitude	.9957	.7059	.4742	.8496	.2124	.8859	.0619	.8239	.1094	.9472
BWc Phase	.8379	.9833	.9891	.9685	.9671	.9975	.9236	.9954	.9957	.9862
Delay Spread Magnitude	.7595	.2936	0	1	.3007	.7125	0	1	0	1
Delay Spread Phase	.0995	.9091	.1444	.9037	.5709	.4654	.9999	.9951	.1492	.7720

Table 4.9: CSR Accuracy State Sequence 51234

State Sequence 51234										
Feature	State 1 Sensitivity	State 1 Specificity	State 2 Sensitivity	State 2 Specificity	State 3 Sensitivity	State 3 Specificity	State 4 Sensitivity	State 4 Specificity	State 5 Sensitivity	State 5 Specificity
Envelope Magnitude	.9997	.9995	.9999	.9996	.9626	.9998	.9994	.9988	1.000	.9929
Envelope Phase	.9999	.9993	.9999	.9997	.9946	1	.9997	.9996	.9998	1.000
Tc Magnitude	0	.9871	0	.9620	0	.8651	.5414	.6246	.4937	.4086
Tc Phase	.9975	.9961	.9849	.9993	.9997	.9999	.9996	1.000	.9995	1.000
Doppler Spread Magnitude	0	1	1	0	0	1	0	1	0	1
Doppler Spread Phase	0	.9461	.1101	1	0	.8335	1	.2488	0	.9320
BWc Magnitude	.9957	.7059	.4742	.8496	.2124	.8859	.0619	.7984	.1094	.9472
BWc Phase	.8376	.9793	.9891	.9685	.9671	.9975	.9323	.9966	.9833	.9876
Delay Spread Magnitude	.9994	.0962	0	1	0	.9021	0	1	0	1
Delay Spread Phase	0	.9461	.1101	1	0	.8335	1	.2488	0	.9320

4.2.6 Enhanced CSR Algorithm Verification Findings

Several conclusions emerge after evaluating the CSR enhanced algorithm verification results as described in teh paragraphs that follow:

1. The sensitivity and specificity over all features, states, and sequences is shown in Table 4.10. This Table displays averages over all features derived from the accuracy data shown in Section 4.2.5 The average over all states is shown in the far right column for each input state sequence. The average over all state sequences is shown in the bottom row. The average over all all features, states, and sequences is displayed in the lower right-hand colums.

2. Referring to Figure 4.22, the enhanced as compared to the baseline algorithm across all states, with the hard decision approach, has improved state recognition sensitivity by over 20% across all state sequences and exceeds 40% for the state sequence 51234. The state recognition specificity has improved by more than 10% across all states and by as much as 12% for state sequence 51234. The enhanced as compared to the baseline algorirthm across all states, without the hard decision approach, suffers from several underperforming feature extractions. The average sensitivity has decreased by almost 20% across all state sequences except 51234. The average specificity has decreased by as much as 2.5% across all state sequences except 51234. Clearly, rejection of under performing waveform features by the decision rule, has increased accuracy performance of the CSR algorithm in terms of

sensitivity and specificity.

3. Referring to Figure 4.23, the enhanced algorithm as compared to the baseline algorithm across all features, without the hard decision approach, suffers from under performing feature extraction. The state recognition sensitivity across all features in most cases has decreased as compared to the baseline algorithm. There are only a few cases where the sensitivity has increased; namely for state 3 and state 5 which the baseline algorithm under performed. The state recognition specificity has improved by more than 5% across states for 2 state sequences and all state sequences for state 5. Clearly the enhanced as compared to the baseline algorithm without the hard decision method, has improved state recognition accuracy for states 3 and 5, while under performing the baseline in all other states.

4. Referring to Figure 4.24, the enhanced algorithm as compared to the baseline algorithm across all state sequences and without the hard decision approach, suffers from under performing feature extraction. The state recognition sensitivity across all state sequences in most cases has decreased as compared to the baseline algorithm. There is only a one case where the sensitivity has increased; namely for state 5 which the baseline algorithm under performed. The state recognition specificity has improved by more than 1% across all state sequences for 3 states, and 25% for state 5. Clearly the enhanced as compared to the baseline algorithm across all state sequences without the hard decision method, has improved state recognition accuracy for states 3 and 5, while under performing the baseline in all other states. The effect of the enhanced hard decision method is clearlypositive across all state sequences increasing state recogntion sensitivity by over 25% and specificity by over 5%.

5. Evaluating input sequence likelihood against HMM memory sequences has been demonstrated to be an effective means of recognizing MWC hidden states,

6. Recognizing MWC hidden processes such as coherence, noncoherent selectivity is feasible with HMMs.

7. Blind Channel state recognition utilizing first and second order observable waveform features is feasible based on HMMs.

8. First order waveform features were more effectively recognized by the HMM.

9. Some second order features were not as effectively recognized by the HMM. Namely, second order magnitude, however, several second order phase sequences were uniquely recognized, but not with likelihoods that achieve the hard decision threshold. This is because either the magnitude, phase, or both, feature extracts were not statistically unique. Alternative second order methods should be reevaluated that produce unique magnitude and phase statistical sequences.

10. The effect of the hard decision method is positive and significant. This is due to rejection of under performing feature extraction methods.

11. The length of the state sequence blocks were conservatively long. There were no observable convergence issues, or asymptotic errors, therefore it is likely that the block lengths could be reduced from 50000 samples to identify any effects on accuracy and/or convergence. The state sequence vectors were intensive on the modeling and simulation testbed memory. Shorter length would improve speed of computations and reduce memory requirements.

12. The coherence state model was effective at recognizing the MWC coherent, single time and frequency selective, and dual selective waveforms.

13. Feature diversity can improve feature recognition accuracy with proper feature extraction design. It can also penalize feature recognition accuracy with improper feature extraction design.

14. HMM computations are intensive on memory and require latency. Parallel computational architectures and/or hardware based computational architectures would be required to implement the CSR algorithm.

Table 4.10: Enhanced CSR Accuracy Across All Features, States, and Sequences

	State 1		State 2		State 3		State 4		State 5		Avg Across All States	
	Sensitivity	Specificity	Sensitivity	Specificity	Sensitivity	Specificity	Sensitivity	Specificity	Sensitivity	Specificity	Sensitivity	Specificity
Seq. 12345 Avg Across All Features	.9988	.9711	.9935	.9647	.9810	.9993	.9843	.9778	.9985	.9773	.9932	.9780
Seq. 23451 Avg Across All Features	.9990	.9795	.9938	.9904	.9810	.9781	.9843	.9986	.9977	.9796	.9911	.9852
Seq 34512 Avg Across All Features	.9981	.9766	.9948	.9905	.9834	.9870	.9869	.9983	.9971	.9777	.9920	.9860
Seq 45123 Avg Across All Features	.9984	.9788	.9947	.9898	.9847	.9828	.9819	.9997	.9971	.9796	.9913	.9886
Seq 51234 Avg Across All Features	.9984	.9816	.9947	.9911	.9810	.9831	.9885	.9978	.9956	.9768	.9916	.9860
Avg across all Sequences	.9985	.9775	.9943	.9853	.9822	.9860	.9851	.9944	.9972	.9782	.9918	.9847

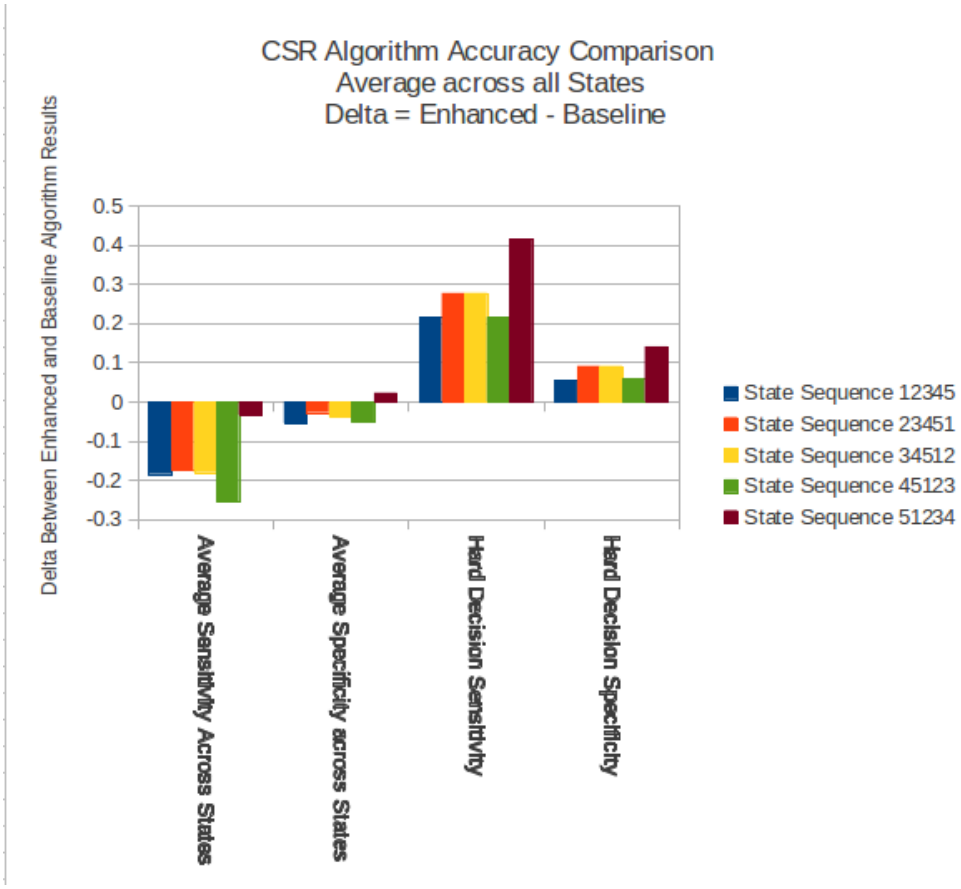

Figure 4.22: CSR Algorithm Accuracy Comparison Across All States

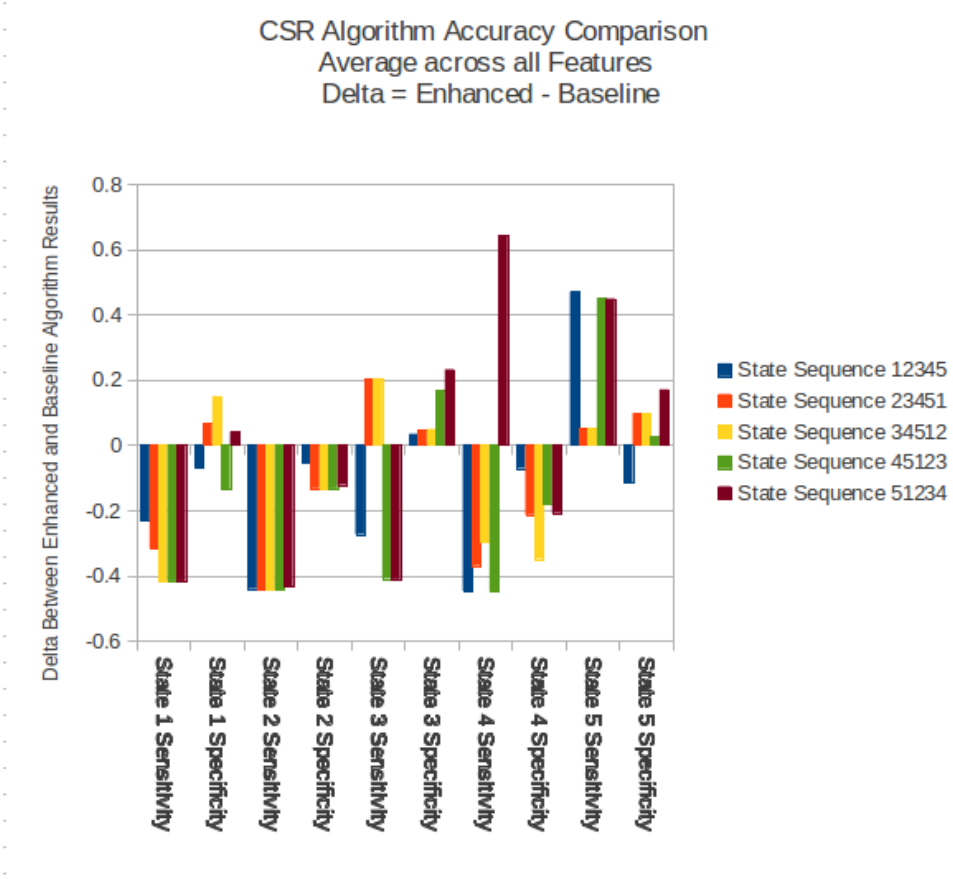

Figure 4.23: CSR Algorithm Accuracy Comparison Across All Features

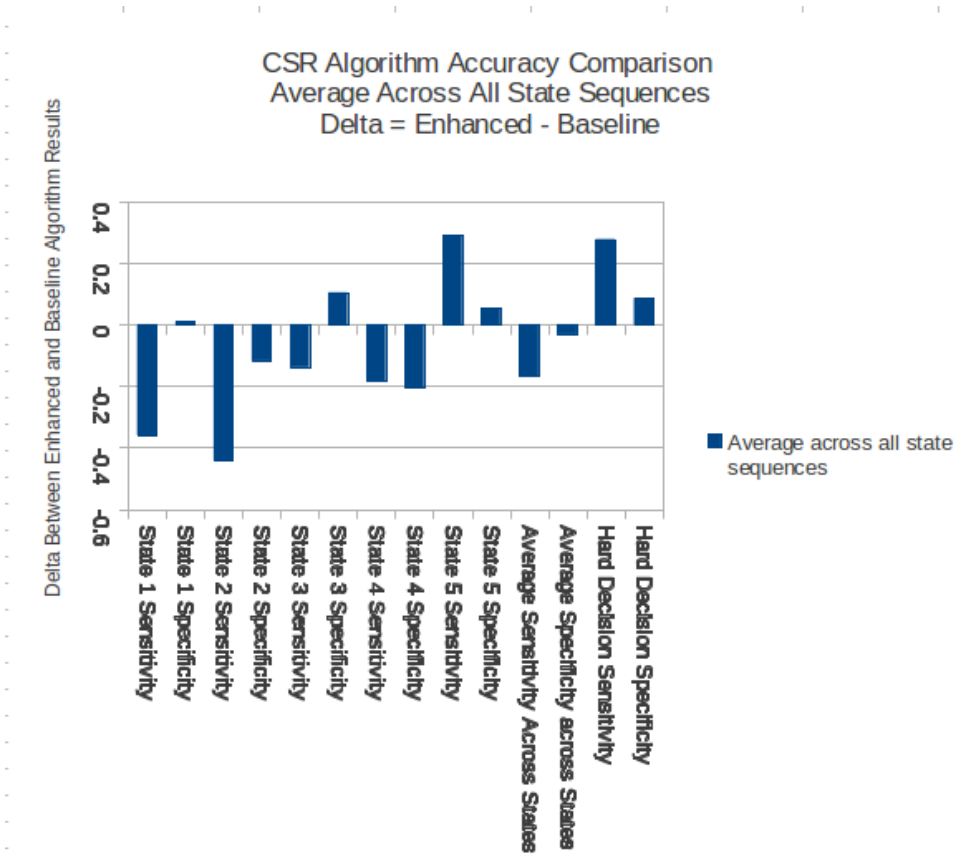

Figure 4.24: CSR Algorithm Accuracy Comparison Across All State Sequences

Chapter 5

Conclusions

5.1 Summary

In summary, this research has produced two forms of a CSR Algorithm based on statistical feature recognition HMMs. The first is a baseline algorithm utilized for POC prototyping, the second integrated enhanced features such as diverse feature extraction, state hard decisions, and combined feature state decisions to improve algorithm accuracy. MWC first order and second order statistical features are extracted as indicators of channel time and frequency dispersion processes and formulated into sample timeblocks. A novel CSM was architected that organizes the MWC features into one of five coherent nonselective or noncoherent selective states. HMMs are utilized to map statistical relationships between the hidden MWC time and frequency dispersion processes and the observable receive waveform processes. The HMM memory parameters were derived from training sequences that were statistically similar to expected operational waveforms. MWC feature state likelihood estimates are produced by parallel HMM feature recognition processes which feed a state hard decision process. The parallel state decisions are combined into a single most likely channel state estimate for each waveform timeblock. A MWC state waveform testbed was designed and implemented to verify the CSR algorithms. CSM state sequences were applied to the algorithms, and performance verified by comparing the sensitivity and specificity of the algo-

Table 5.1: Baseline CSR Algorithm Findings

1	The coherence state model was verified to be accurate in terms of sensitivity and specificity. Results were mixed. Sensitivity and specificity were high for some states while low for other states. This suggests with enhancements, performance might be more consistent.
2	HMM training processes were verified to be mixed. The baseline CSR algorithm utilized a hybrid of Viterbi and Baum Welch training algorithms. An alternative approach might improve the accuracy performance.
3	Recognition of MWC hidden CSM state sequences by HMM decoding methods were mixed suggesting enhancement to the baseline version might improve consistency.
4	The channel state waveform generator was verified to be effective.
5	The CSR verification testbed was verified to be effective.
6	The CSR algorithm accuracy measures of performance were verified to be effective.
7	The CSR algorithm verification testing motivated the enhanced version of the CSR algorithm.

rithm channel hidden state estimates to the input hidden state sequence. It was determined that the enhanced algorithm improved sensitivity by as much as 25% and specificity by as much as 5% over the baseline version because of the enhanced multiple feature extraction and parallel hard decision combining methods. The enhanced algorithm sensitivity was determined to exceed 95% for the best features and the specificity was determined to exceed 98% for the best cases. It was determined that some waveform features were not as effective as others due to lack of statistical uniqueness. Overall, the CSR algorithm was found to be feasible and effective at recognizing the MWC hidden CSM states. A case study based on the WiMAX waveform demonstrated how significant improvements in wireless power efficiency and economic revenues could be achieved if the CSR algorithm were applied.

5.2 Key Findings

Important lessons learned from the design and verification testing of the baseline CSR algorithm are shown in Table 5.1.

Important lessons learned from the design and verification testing of the enhanced CSR algorithm

are shown in Table 5.2.

5.3 Knowledge Contributions

This research effort provided answers to several MWC state recognition questions which are provided in Table 5.3.

5.4 New Research Questions

During the course of researching the CSR algorithm, new questions have emerged which are shown in Table 5.4.

5.5 Recommended Next Steps

Recommended follow on research into MWC state recognition is summarized in Table 5.5:

Table 5.2: Enhanced CSR Algorithm Findings

1	The enhanced CSR algorithm has been demonstrated to be feasible based on accuracy verification results provided in Chapter 4. The verification was designed for proof of concept. A full factorial experiment that includes a full range of hidden transitions and full range of waveform statistical features would be required for full confidence testing.
2	Test results for HMM sequence likelihood computations suggest that it is feasible to track dynamic MWC CSM hidden state sequences such as coherent nonselective and noncoherent selectivity. Further investigation into hidden state transition convergence and a full factorial experiment that includes full range of hidden state transitions would be required for confidence testing.
3	The enhanced CSR algorithm has improved accuracy sensitivity by 25% and specificity by 5% over the baseline CSR approach.
4	Parallel waveform statistical feature extraction adds diversity but at a cost of complexity.
5	Block size was conservative to maintain statistical significance. Decreased block size could improve computational speed and responsiveness while reducing complexity.
6	MWC waveform phase features tend to be more statistically unique than magnitude features.
7	First order statistical features utilized in the CSR algorithm were found to be less complex and more effective than second order statistical waveform features.
8	Some second order statistical features were found to be more unique than others, suggesting feature extraction process design is important and should be investigated for improvements.
9	It is known that HMM training suffers from overfitting and staleness; published approaches suggest that combining Kalman Filtering and HMM training processes could yield dynamic HMM parameter tracking over time to overcome staleness.
10	The demonstrated HMM training was effective, however, additional verification testing is required to investigate the range of MWC waveforms that can be effectively recognized by the CSR HMMS.
11	The verification testing of the enhanced CSR algorithm was designed for a limited proof of concept demonstration. Further confidence testing is required to investigate all transitions in the CSM model.
12	Parallel feature state likelihood was demonstrated to be feasible, however it adds considerable complexity.
13	HMM computations will add latency; although latency was not a primary focus of this research, investigation into HMM latency should be characterized to minimize these effects.
14	Published research into HMM complexity reduction such as ML suboptimal sequence detection approaches can yield reduced complexity recognition methods.
15	Maturation of the CSR algorithm from a collection of batch MATLAB scripts to a recursive monolithic library function could yield a reduced complexity online version of the algorithm.
16	Feature state hard decisions are feasible, however, combining soft decision likelihoods might offer additional benefits.
17	Combining feature state hard decisions increased the CSR algorithm sensitivity and specificity performance.
18	Confidence testing of the enhanced CSR algorithm would require embedding with

Table 5.3: Knowledge Contributions

1	Can MWC hidden states be defined that express the presence of hidden coherent nonselective and noncoherent selective distortion processes? This research demonstrated that this is true.
2	Can a signal processing algorithm based on statistical feature recognition HMMs be architected to recognize MWC hidden states? This research demonstrated that this is true.
3	Can MWC first order and second order statistical features provide sufficient uniqueness that HMMs can discriminate between coherent and noncoherent states? This research demonstrated that this is true.
4	Can blind channel state recognition approaches, without the aid of training symbols or pilot tones, achieve sufficient sensitivity and specificity to be considered feasible? This research demonstrate that this is true.
5	Will diverse parallel waveform statistical feature combining approaches increase recognition accuracy? This research demonstrate that this is true.

Table 5.4: New Research Questions

1	Can complexity and latency be reduced with recursive approaches to achieve a practical CSR algorithm?
2	Can HMM statistical memory parameters be dynamically tracked as MWC states evolve?
3	What are the limits of operational waveform statistics for which HMM training processes provide robust recognition accuracy?
4	What is the practical waveform block size that increases CSR responsiveness without compromising accuracy performance?
5	Cam the waveform block size be dynamically adaptive with MWC conditions?
6	Can soft rather than hard decision combining provide additional performance benefits?
7	Can the CSR algorithm provide sufficient environmental awareness for state based communication controls for operational waveforms such as WiMAX or LTE?
8	Can the CSR algorithm benefits be extended to wired or wireless waveform recognition applications?

Table 5.5: Recommended Follow On Developments

1	Confidence testing of CSR algorithm against a full range of input waveform characteristics and hidden state transitions.
2	Implement waveform feature block size reduction and adaptive processes to dynamically adjust the block size.
3	Implement HMM parameter error tracking.
4	Implement HMM complexity reduction.
5	Implement feature state soft decision combining.
6	Implement a recursive CSR algorithm.
7	Integrate CSR prototype with cognitive state based mobile wireless communication control process.
8	Redesign the coherent state model for wireless or wired waveform states.
9	Redesign and verify a waveform state recognition algorithm.

Bibliography

[1] L.R. Rabiner, "A tutorial on hidden markov models and selected applications in speech recognition," *Proceedings of the IEEE*, vol. 77, no. 2, pp. 257 –286, feb 1989.

[2] G.D. Durgin, *Space-Time Wireless Channels*, Prentice Hall Communications Engineering and Emerging Technologies Series. Prentice Hall PTR, 2003.

[3] T.S. Rappaport, *Wireless communications: principles and practice*, Prentice Hall communications engineering and emerging technologies series. Prentice Hall PTR, 2002.

[4] SeonYeong Han and N.B. Abu-Ghazaleh, "Estimated measurement-based markov models: Towards flexible and accurate modeling of wireless channels," in *Wireless and Mobile Computing, Networking and Communications, 2009. WIMOB 2009. IEEE International Conference on*, oct. 2009, pp. 331 –337.

[5] H.S. Wang and N. Moayeri, "Modeling, capacity, and joint source/channel coding for rayleigh fading channels," in *Vehicular Technology Conference, 1993., 43rd IEEE*, may 1993, pp. 473 –479.

[6] C.C. Tan and N.C. Beaulieu, "On first-order markov modeling for the rayleigh fading channel," *Communications, IEEE Transactions on*, vol. 48, no. 12, pp. 2032 –2040, dec 2000.

[7] F. Babich and G. Lombardi, "A markov model for the mobile propagation channel," *Vehicular Technology, IEEE Transactions on*, vol. 49, no. 1, pp. 63 –73, jan 2000.

[8] L. Rabiner and B. Juang, "An introduction to hidden markov models," *ASSP Magazine, IEEE*, vol. 3, no. 1, pp. 4 –16, jan 1986.

[9] Anders Krogh Graeme Mi Richard Durbin, Sean R. Eddy, *Biological Sequence Analysis: Probabilistic Models Of Proteins And Nucleic Acids*, Cambridge University Press, 1998.

[10] M.M. Olama, S.M. Djouadi, and C.D. Charalambous, "Time varying channel modeling for ad-hoc mobile wireless networks," in *Wireless Communications and Networking Conference, 2006. WCNC 2006. IEEE*, april 2006, vol. 3, pp. 1277 –1282.

[11] V. Wieser and V. Psenak, "Mobile radio channel state prediction for power control in wcdma mobile network," in *Radioelektronika, 2007. 17th International Conference*, april 2007, pp. 1 –4.

[12] Hsiao-Chun Wu and Xiaozhou Huang, "Spc04-2: Semi-blind ici equalization for wireless ofdm systems," in *Global Telecommunications Conference, 2006. GLOBECOM '06. IEEE*, 27 2006-dec. 1 2006, pp. 1 –6.

[13] A.J. Goldsmith and P.P. Varaiya, "Capacity, mutual information, and coding for finite-state markov channels," *Information Theory, IEEE Transactions on*, vol. 42, no. 3, pp. 868 –886, may 1996.

[14] B. Fritchman, "A binary channel characterization using partitioned markov chains," *Information Theory, IEEE Transactions on*, vol. 13, no. 2, pp. 221 –227, april 1967.

[15] A. Chockalingam, L.B. Milstein, and M. Zorzi, "Performance of a wireless media access protocol on a markovian fading channel," in *Global Telecommunications Conference, 1996. GLOBECOM '96. 'Communications: The Key to Global Prosperity*, nov 1996, vol. 3, pp. 1769 –1773 vol.3.

[16] A. Jain, R. Upadhyay, P.D. Vyavahare, and L.D. Arya, "Stochastic modeling and performance evaluation of fading channel for wireless network design," in *Advanced Information*

Networking and Applications Workshops, 2007, AINAW '07. 21st International Conference on, may 2007, vol. 2, pp. 893 –898.

[17] F. Babich, O.E. Kelly, and G. Lombardi, "A context-tree based model for quantized fading," *Communications Letters, IEEE*, vol. 3, no. 2, pp. 46 –48, february 1999.

[18] Wei ho Chung and Kung Yao, "Modified hidden semi-markov model for modelling the flat fading channel," *Communications, IEEE Transactions on*, vol. 57, no. 6, pp. 1806 –1814, june 2009.

[19] F. Babich, G. Lombardi, and E. Valentinuzzi, "Variable order markov modelling for leo mobile satellite channels," *Electronics Letters*, vol. 35, no. 8, pp. 621 –623, apr 1999.

[20] S.R. Kundu, K. Basu, and S.K. Das, "Finite state markov model for effective bandwidth calculation in wireless packet networks," in *Modeling and Optimization in Mobile, Ad Hoc, and Wireless Networks, 2005. WIOPT 2005. Third International Symposium on*, april 2005, pp. 351 – 357.

[21] M. Riediger and E. Shwedyk, "Communication receivers based on markov models of the fading channel," in *Electrical and Computer Engineering, 2002. IEEE CCECE 2002. Canadian Conference on*, 2002, vol. 3, pp. 1255 – 1260 vol.3.

[22] W. Kumwilaisak and C.-C.J. Kuo, "Adaptive variable length markov chain for non-stationary fading channel modeling," in *Global Telecommunications Conference, 2002. GLOBECOM '02. IEEE*, nov. 2002, vol. 3, pp. 2046 – 2050 vol.3.

[23] Qinqing Zhang and S.A. Kassam, "Finite-state markov model for rayleigh fading channels," *Communications, IEEE Transactions on*, vol. 47, no. 11, pp. 1688 –1692, nov 1999.

[24] C. Pimentel, T.H. Falk, and L. Lisboa, "Finite-state markov modeling of correlated rician-fading channels," *Vehicular Technology, IEEE Transactions on*, vol. 53, no. 5, pp. 1491 – 1501, sept. 2004.

[25] Hong Shen Wang, "On verifying the first-order markovian assumption for a rayleigh fading channel model," in *Universal Personal Communications, 1994. Record., 1994 Third Annual International Conference on*, sep-1 oct 1994, pp. 160 –164.

[26] J. Yang, N. Tin, and A.K. Khandani, "Adaptive modulation and coding in 3g wireless systems," in *Vehicular Technology Conference, 2002. Proceedings. VTC 2002-Fall. 2002 IEEE 56th*, 2002, vol. 1, pp. 544 – 548 vol.1.

[27] J. Poikonen, "A finite-state simulation model for ofdm over frequency-selective fast fading channels," in *Broadband Multimedia Systems and Broadcasting, 2009. BMSB '09. IEEE International Symposium on*, may 2009, pp. 1 –6.

[28] Yongjun Xie and Yuguang Fang, "A general statistical channel model for mobile satellite systems," *Vehicular Technology, IEEE Transactions on*, vol. 49, no. 3, pp. 744 –752, may 2000.

[29] J. Arauz and P. Krishnamurthy, "A study of different partitioning schemes in first order markovian models for rayleigh fading channels," in *Wireless Personal Multimedia Communications, 2002. The 5th International Symposium on*, oct. 2002, vol. 1, pp. 277 – 281 vol.1.

[30] H. Wakana, "Propagation model for simulating shadowing and multipath fading in land-mobile satellite channel," *Electronics Letters*, vol. 33, no. 23, pp. 1925 –1926, nov 1997.

[31] F. Swarts and H.C. Ferreira, "Markov characterization of channels with soft decision outputs," *Communications, IEEE Transactions on*, vol. 41, no. 5, pp. 678 –682, may 1993.

[32] Ching-Wan Yuen and On-Ching Yue, "Channel state dependent packet discard policy for 3g networks," in *Vehicular Technology Conference, 2006. VTC 2006-Spring. IEEE 63rd*, may 2006, vol. 1, pp. 405 –409.

[33] C. Lubritto, A. Petraglia, C. Vetromile, S. Curcuruto, M. Logorelli, G. Marsico, and A. D'Onofrio, "Energy and environmental aspects of mobile communication systems," *Energy*, vol. 36, no. 2, pp. 1109 – 1114, 2011.

[34] Steel in the Air Airwave Management LLC, "Cell phone tower statistics," Jul 2012.

[35] U.S. Department of Energy, "List of countries by electricity consumption," 2010.

[36] European Commission and Netherlands Environmental Assessment Agency, "List of countries by 2011 emissions estimates," 2011.

[37] International Electrical and Electronic Engineering Society, "Ieee standard for local and metropolitan area networks; part 16," *IEEE Std. 802.16*, 2009.

[38] Rahman T. A. Osman, W. E., "Optimization of guard time length for mobile wimax system over multipath channel," in *Proceedings of the International MultiConference of Engineers and Computer Scientists*, Hong Kong, mar 2008, vol. II.

[39] Kaiser Family Foundation, "Urban population-percent of total population living in urban areas," 2012.

[40] U.S. Census, "Highway mileage—urban and rural by ownership: 1990 to 2008," 2012.

[41] John; Gates David Sekino, Hamilton; Kwon, "Wimax outlook in the us market:implications for service providers," Tech. Rep., Diamond Management and Technology Consultants, Jan 2007.

[42] Wikipedia, "Clearwire inc.," .

[43] A. P. Dempster, N. M. Laird, and D. B. Rubin, "Maximum likelihood from incomplete data via the em algorithm," *JOURNAL OF THE ROYAL STATISTICAL SOCIETY, SERIES B*, vol. 39, no. 1, pp. 1–38, 1977.

[44] Thomas H. Cormen, Charles E. Leiserson, Ronald L. Rivest, and Clifford Stein, *Introduction to Algorithms, Third Edition*, The MIT Press, 3rd edition, 2009.

[45] S. A. Teukolsky W. T. Vetterling W. H. Press, B. P. Flannery, *Numerical Recipes, The Art of Scientific Computing*, Cambridge University Press, 1986.

[46] M.J. V. Estivill-Castro; Atallah and M. Editors Blanton, *Sorting and Order Statistics: article found in Foundations of Algorithms and Theory of Computation*, Applied Algorithms and Data Structures. Taylor & Francis, 2009.

[47] MATLAB, *version 7.10.0 (R2012a)*, The MathWorks Inc., Natick, Massachusetts, 2011.

[48] J. Proakis, *Digital Communications*, McGraw-Hill series in electrical and computer engineering. McGraw-Hill, 2000.

[49] B. Sklar, *Digital communications: fundamentals and applications*, Prentice Hall Communications Engineering and Emerging Technologies Series. Prentice-Hall PTR, 2001.

[50] MATLAB, *hmmestimate function, version 7.10.0 (R2012a)*, The MathWorks Inc., Natick, Massachusetts, 2011.

[51] MATLAB, *hmmtrain function, version 7.10.0 (R2012a)*, The MathWorks Inc., Natick, Massachusetts, 2011.

[52] MATLAB, *hmmdecode function, version 7.10.0 (R2012a)*, The MathWorks Inc., Natick, Massachusetts, 2011.

[53] M. Lopez-Guerrero and J. Gomez, "A mobility-based channel model for wireless systems with adaptive modulation," in *Electrical and Computer Engineering, 2009. CCECE '09. Canadian Conference on*, may 2009, pp. 750 –755.

[54] F. Babich, O.E. Kelly, and G. Lombardi, "Generalized markov modeling for flat fading," *Communications, IEEE Transactions on*, vol. 48, no. 4, pp. 547 –551, apr 2000.

[55] A. Richter, J. Salmi, and V. Koivunen, "An algorithm for estimation and tracking of distributed diffuse scattering in mobile radio channels," in *Signal Processing Advances in Wireless Communications, 2006. SPAWC '06. IEEE 7th Workshop on*, july 2006, pp. 1 –5.

[56] R.K.H. Galvao, A. Izhac, V.M. Becerra, J.W. Bowen, and S. Hadjiloucas, "Mimo wiener model identification for large scale fading of wireless mobile communications links," *Communications Letters, IEEE*, vol. 11, no. 6, pp. 513 –515, june 2007.

[57] M.M. Olama, S.M. Djouadi, and C.D. Charalambous, "Stochastic differential equations for modeling, estimation and identification of mobile-to-mobile communication channels," *Wireless Communications, IEEE Transactions on*, vol. 8, no. 4, pp. 1754 –1763, april 2009.

[58] Xiaozhou Huang and Hsiao-Chun Wu, "Robust and efficient intercarrier interference mitigation for ofdm systems in time-varying fading channels," *Vehicular Technology, IEEE Transactions on*, vol. 56, no. 5, pp. 2517 –2528, sept. 2007.

[59] Tao Su, Hao Ling, and W.J. Vogel, "Markov modeling of slow fading in wireless mobile channels at 1.9 ghz," *Antennas and Propagation, IEEE Transactions on*, vol. 46, no. 6, pp. 947 –948, jun 1998.

[60] J.L. Cuevas-Ruiz and J.A. Delgado-Penin, "Channel model based on semi-markovian processes. an approach for haps systems," in *Electronics, Communications and Computers, 2004. CONIELECOMP 2004. 14th International Conference on*, feb. 2004, pp. 52 – 56.

[61] P. Burzigotti, R. Prieto-Cerdeira, A. Bolea-Alamanac, F. Perez-Fontan, and I. Sanchez-Lago, "Dvb-sh analysis using a multi-state land mobile satellite channel model," in *Advanced Satellite Mobile Systems, 2008. ASMS 2008. 4th*, aug. 2008, pp. 149 –155.

[62] E. Inaty, "A finite state markov chain-based umbrella cell channel model for fast mobile users," in *Wireless Communications, Networking and Mobile Computing, 2006. WiCOM 2006.International Conference on*, sept. 2006, pp. 1 –5.

[63] Shen Dongya, Rong Jian, Yang Yihuai, Quo Yong, Cao Hongliang, and Fu Shigang, "The six-state markov model for land mobile satellite channels," in *Microwave, Antenna, Propagation and EMC Technologies for Wireless Communications, 2005. MAPE 2005. IEEE International Symposium on*, aug. 2005, vol. 2, pp. 1619 – 1622 Vol. 2.

[64] D.A. Sanchez-Salas and J.L. Cuevas-Ruiz, "N-states channel model using markov chains," in *Electronics, Robotics and Automotive Mechanics Conference, 2007. CERMA 2007*, sept. 2007, pp. 342 –347.

[65] M. Zorzi, R.R. Rao, and L.B. Milstein, "On the accuracy of a first-order markov model for data transmission on fading channels," in *Universal Personal Communications. 1995. Record., 1995 Fourth IEEE International Conference on*, nov 1995, pp. 211 –215.

[66] Q. Du and X. Zhang, "Time-sharing based rate adaptation for multicast over wireless fading channels in mobile wireless networks," in *Information Sciences and Systems, 2006 40th Annual Conference on*, march 2006, pp. 1385 –1390.

[67] F. Babich and G. Lombardi, "A measurement based markov model for the indoor propagation channel," in *Vehicular Technology Conference, 1997, IEEE 47th*, may 1997, vol. 1, pp. 77 –81 vol.1.

[68] H. Steffan, "Adaptive generative radio channel models," in *Personal, Indoor and Mobile Radio Communications, 1994. Wireless Networks - Catching the Mobile Future., 5th IEEE International Symposium on*, sep 1994, vol. 1, pp. 268 –273 vol.1.

[69] Hamza Abdelkrim, Kazem Ali, Salut Gerard, Chitroub Salim, and Touhami Rachida, "Blind detection in idma systems," in *Wireless Information Networks and Systems (WINSYS), Proceedings of the 2010 International Conference on*, july 2010, pp. 1 –5.

[70] S. Bellini and F. Rocca, "Near optimal blind deconvolution," in *Acoustics, Speech, and Signal Processing, 1988. ICASSP-88., 1988 International Conference on*, apr 1988, pp. 2236 –2239 vol.4.

[71] G. Caire and K.R. Kumar, "Information theoretic foundations of adaptive coded modulation," *Proceedings of the IEEE*, vol. 95, no. 12, pp. 2274 –2298, dec. 2007.

[72] F. Chan, J. Choi, P. Rapajic, and J. Yuan, "Information theoretic comparisons of training based channel estimation and semi-blind estimation in fading channels with memory," in *Intelligent Signal Processing and Communication Systems, 2004. ISPACS 2004. Proceedings of 2004 International Symposium on*, nov. 2004, pp. 6 – 10.

[73] Dongsik Kim, Ui-Kun Kwon, Gi-Hong Im, and Changyong Shin, "A pilot design technique for single-carrier transmission over fast fading relay channels," in *Global Telecommunications Conference, 2008. IEEE GLOBECOM 2008. IEEE*, 30 2008-dec. 4 2008, pp. 1 –5.

[74] Duel-Hallen A. Hallen H. Eyceoz, T., "Deterministic channel modeling and long range prediction of fast fading mobile radio channels," *Communications Letters, IEEE*, vol. 2, no. 9, pp. 254 –256, sept. 1998.

[75] S. Semmelrodt and R. Kattenbach, "Investigation of different fading forecast schemes for flat fading radio channels," in *Vehicular Technology Conference, 2003. VTC 2003-Fall. 2003 IEEE 58th*, oct. 2003, vol. 1, pp. 149 – 153 Vol.1.

[76] Songnan Xi and Hsiao-Chun Wu, "Robust automatic modulation classification using cumulant features in the presence of fading channels," in *Wireless Communications and Networking Conference, 2006. WCNC 2006. IEEE*, april 2006, vol. 4, pp. 2094 –2099.

[77] K. Umebayashi, S. Ishii, and R. Kohno, "Blind adaptive estimation of modulation scheme for software defined radio," in *Personal, Indoor and Mobile Radio Communications, 2000. PIMRC 2000. The 11th IEEE International Symposium on*, 2000, vol. 1, pp. 43 –47 vol.1.

[78] G.M. Vitetta, D.P. Taylor, and U. Mengali, "Blind receivers for psk signals transmitted over rayleigh frequency-flat fading channels," in *Global Telecommunications Conference, 1995. GLOBECOM '95., IEEE*, nov 1995, vol. 2, pp. 1034 –1038 vol.2.

[79] K. Abed-Meraim, Wanzhi Qiu, and Yingbo Hua, "Blind system identification," *Proceedings of the IEEE*, vol. 85, no. 8, pp. 1310 –1322, aug 1997.

[80] Bao-Yun Wang and Wei Xing Zheng, "Blind adaptive channel identification/equalization in chaotic communications by using nonlinear prediction technique," in *Signal Processing, 2004. Proceedings. ICSP '04. 2004 7th International Conference on*, aug.-4 sept. 2004, vol. 1, pp. 372 – 375 vol.1.

[81] C. Carlemalm and A. Logothetis, "Blind channel estimation for fading channels with markov inputs," in *Statistical Signal and Array Processing, 1998. Proceedings., Ninth IEEE SP Workshop on*, sep 1998, pp. 292 –295.

[82] H.A. Cirpan and M.K. Tsatsanis, "Maximum likelihood blind channel estimation in the presence of doppler shifts," *Signal Processing, IEEE Transactions on*, vol. 47, no. 6, pp. 1559 –1569, jun 1999.

[83] S. Falahati, A. Svensson, M. Sternad, and T. Ekman, "Adaptive modulation systems for predicted wireless channels," in *Global Telecommunications Conference, 2003. GLOBECOM '03. IEEE*, dec. 2003, vol. 1, pp. 357 – 361 Vol.1.

[84] Fu Li, Heng Xiao, Yibing Guo, and Jin Yang, "On modeling of a mobile multipath fading channel," in *Statistical Signal and Array Processing., IEEE Seventh SP Workshop on*, jun 1994, pp. 445 –448.

[85] T. Ghirmai, M.F. Bugallo, J. Miguez, and P.M. Djuric, "A sequential monte carlo method for adaptive blind timing estimation and data detection," *Signal Processing, IEEE Transactions on*, vol. 53, no. 8, pp. 2855 – 2865, aug. 2005.

[86] Meng Cai, Kefeng Zhang, and Xuecheng Zou, "Low complexity channel estimation and tracking method for high speed mobile communication systems," in *Solid-State and Integrated-Circuit Technology, 2008. ICSICT 2008. 9th International Conference on*, oct. 2008, pp. 1629 –1632.

[87] I. Nevat and Jinhong Yuan, "Error propagation mitigation for iterative channel tracking, detection and decoding of bicm-ofdm systems," in *Wireless Communication Systems, 2007. ISWCS 2007. 4th International Symposium on*, oct. 2007, pp. 75 –80.

[88] C. Ramesh and V. Vaidehi, "Imm based kalman filter for channel estimation in uwb ofdm systems," in *Signal Processing, Communications and Networking, 2007. ICSCN '07. International Conference on*, feb. 2007, pp. 320 –325.

[89] J.K. Tugnait, "Blind estimation of digital communication channel impulse response," *Communications, IEEE Transactions on*, vol. 42, no. 234, pp. 1606 –1616, feb/mar/apr 1994.

[90] J.K. Tugnait, Lang Tong, and Zhi Ding, "Single-user channel estimation and equalization," *Signal Processing Magazine, IEEE*, vol. 17, no. 3, pp. 16 – 28, may 2000.

[91] R. Wang, N. Jindal, T. Bruns, A.R.S. Bahai, and D.C. Cox, "Comparing rls and lms adaptive equalizers for nonstationary wireless channels in mobile ad hoc networks," in *Personal, Indoor and Mobile Radio Communications, 2002. The 13th IEEE International Symposium on*, sept. 2002, vol. 3, pp. 1131 – 1135 vol.3.

[92] Xi-Bin Han and Wei-Ping Zhu, "Variable step-size adaptive channel estimation for wcdma receiver," in *Intelligent Multimedia, Video and Speech Processing, 2004. Proceedings of 2004 International Symposium on*, oct. 2004, pp. 85 – 88.

[93] Xin Li and Tan F. Wong, "Turbo equalization with nonlinear kalman filtering for time-varying frequency-selective fading channels," *Wireless Communications, IEEE Transactions on*, vol. 6, no. 2, pp. 691 –700, feb. 2007.

[94] Yunxin Zhao, "An em algorithm for linear distortion channel estimation based on observations from a mixture of gaussian sources," *Speech and Audio Processing, IEEE Transactions on*, vol. 7, no. 4, pp. 400 –413, jul 1999.

[95] Zhengyuan Xu, "Effects of imperfect blind channel estimation on performance of linear cdma receivers," *Signal Processing, IEEE Transactions on*, vol. 52, no. 10, pp. 2873 – 2884, oct. 2004.

[96] Hanbing Zhou, Daoben Li, and Gang Li, "A simplified kalman-mlsd receiver over fast fading channel," in *Wireless, Mobile and Multimedia Networks, 2006 IET International Conference on*, nov. 2006, pp. 1 –4.

[97] E. Aktas and U. Mitra, "Blind channel estimation for multi-user cdma systems," in *Communications, 1998. ICC 98. Conference Record. 1998 IEEE International Conference on*, jun 1998, vol. 2, pp. 1064 –1068 vol.2.

[98] N. Ammar and Z. Ding, "Frequency selective channel estimation in time-reversed space-time coding," in *Wireless Communications and Networking Conference, 2004. WCNC. 2004 IEEE*, march 2004, vol. 3, pp. 1838 – 1843 Vol.3.

[99] N. Ammar and Zhi Ding, "On blind channel identifiability under space-time coded transmission," in *Signals, Systems and Computers, 2002. Conference Record of the Thirty-Sixth Asilomar Conference on*, nov. 2002, vol. 1, pp. 664 –668 vol.1.

[100] S. Ariyavistakul, J.H. Winters, and N.R. Sollenberger, "Joint equalization and interference suppression for high data rate wireless systems," in *Vehicular Technology Conference, 1999 IEEE 49th*, jul 1999, vol. 1, pp. 700 –706 vol.1.

[101] S. Buzzi and H.V. Poor, "A multi-pass strategy for channel estimation and data detection in long-code uplink cdma systems," in *Personal, Indoor and Mobile Radio Communications, 2002. The 13th IEEE International Symposium on*, sept. 2002, vol. 4, pp. 1535 – 1539 vol.4.

[102] Changyong Shin and E.J. Powers, "Doubly selective channel estimation for ofdm systems," in *Signals, Systems and Computers, 2005. Conference Record of the Thirty-Ninth Asilomar Conference on*, 2005, pp. 509 –513.

[103] Ching-Shyang Maa, Chin-Tseng Huang, Yeong-Cheng Wang, and Jiunn-Tsair Chen, "Blind joint channel estimation and signal decoding for systems with time-varying rayleigh-fading channels," in *Vehicular Technology Conference, 2003. VTC 2003-Spring. The 57th IEEE Semiannual*, april 2003, vol. 4, pp. 2575 – 2578 vol.4.

[104] H.A. Cirpan and E. Panayirci, "Blind channel estimation for space-time coding systems with baum-welch algorithm," in *Communications, 2002. ICC 2002. IEEE International Conference on*, 2002, vol. 3, pp. 1579 – 1583 vol.3.

[105] Dongxin Xu and Hsiao-Chun Wu, "Blind channel equalization based on iterative weighted least-mean squared algorithm," in *Vehicular Technology Conference, 2004. VTC2004-Fall. 2004 IEEE 60th*, sept. 2004, vol. 6, pp. 3833 – 3837 Vol. 6.

[106] M. Enescu and V. Koivunen, "Estimating the fading coefficient in mobile ofdm systems using state-space model," in *Circuits and Systems, 2005. ISCAS 2005. IEEE International Symposium on*, may 2005, pp. 6094 – 6097 Vol. 6.

[107] H. Gerlach, D. Dahlhaus, M. Pesce, and Wen Xu, "Joint kalman channel estimation and equalization for the umts fdd downlink," in *Vehicular Technology Conference, 2003. VTC 2003-Fall. 2003 IEEE 58th*, oct. 2003, vol. 2, pp. 1263 – 1267 Vol.2.

[108] He Zhongqiu and Yannan Xing, "Pilot aided channel estimation of mimo ofdm systems," in *Wireless Communications, Networking and Mobile Computing, 2008. WiCOM '08. 4th International Conference on*, oct. 2008, pp. 1 –5.

[109] Jae Choong Han and C.N. Georghiades, "Maximum-likelihood sequence estimation for fading channels via the em algorithm," in *Global Telecommunications Conference, 1993, including a Communications Theory Mini-Conference. Technical Program Conference Record, IEEE in Houston. GLOBECOM '93., IEEE*, nov-2 dec 1993, pp. 133 –137 vol.4.

[110] Jenhui Chen and Chiang-Wei Chang, "A signal-aware uplink resource allocation strategy in

ieee 802.16 systems," in *Wireless and Mobile Computing, Networking and Communications, 2007. WiMOB 2007. Third IEEE International Conference on*, oct. 2007, p. 15.

[111] Jinho Choi, "Equalization and semi-blind channel estimation for space-time block coded signals over a frequency-selective fading channel," *Signal Processing, IEEE Transactions on*, vol. 52, no. 3, pp. 774 – 785, march 2004.

[112] Joon-Hyuk Chang, Dong Jin Seo, Young-Joon Kim, and Nam Soo Kim, "Pre-rejection of distorted speech for speech recognition in wireless communication channel," in *Vehicular Technology Conference, 2003. VTC 2003-Spring. The 57th IEEE Semiannual*, april 2003, vol. 4, pp. 2803 – 2806 vol.4.

[113] S. Kadambe and Q. Jiang, "Classification of modulation of signals of interest," in *Digital Signal Processing Workshop, 2004 and the 3rd IEEE Signal Processing Education Workshop. 2004 IEEE 11th*, aug. 2004, pp. 226 – 230.

[114] V. Krishnamurthy, S. Dey, and J.P. LeBlanc, "Blind equalization of iir channels using hidden markov models and extended least squares," *Signal Processing, IEEE Transactions on*, vol. 43, no. 12, pp. 2994 –3006, dec 1995.

[115] Kyeong Jin Kim and R.A. Iltis, "Joint detection and channel estimation algorithms for qs-cdma signals over time-varying channels," *Communications, IEEE Transactions on*, vol. 50, no. 5, pp. 845 –855, may 2002.

[116] S. Lasaulce, P. Loubaton, and E. Moulines, "Performance of a subspace based semi-blind technique in the umts tdd mode context," in *Acoustics, Speech, and Signal Processing, 2000. ICASSP '00. Proceedings. 2000 IEEE International Conference on*, 2000, vol. 5, pp. 2481 –2484 vol.5.

[117] F. Lehmann, "Blind soft-output decoding of space-time trellis coded transmissions over time-varying rayleigh fading channels," *Wireless Communications, IEEE Transactions on*, vol. 8, no. 4, pp. 2088 –2099, april 2009.

[118] Y. Li, C.N. Georghiades, and G. Huang, "Em-based sequence estimation for space-time codes systems," in *Information Theory, 2000. Proceedings. IEEE International Symposium on*, 2000, p. 315.

[119] Luo Tao, Li Jianfeng, Hao Jianjun, and Yue Guangxin, "Performance analysis for orthogonal space-time block codes in the absence of perfect channel state information," in *Personal, Indoor and Mobile Radio Communications, 2003. PIMRC 2003. 14th IEEE Proceedings on*, sept. 2003, vol. 2, pp. 1012 – 1016 vol.2.

[120] L. Mucchi, T. Palandri, R. Fantacci, and E. Del Re, "Space x2013;time mmse advanced detector for multisatellite systems under nonideal conditions," *Vehicular Technology, IEEE Transactions on*, vol. 56, no. 4, pp. 1716 –1726, july 2007.

[121] M.B. Noune and A. Nix, "Impact of channel estimation errors on the performance of dfe equalizers with space time block codes in wideband fading channels," in *Wireless Communications and Networking Conference, 2007.WCNC 2007. IEEE*, march 2007, pp. 2241 –2246.

[122] S. Ratanamahatana and H.M. Kwon, "Channel estimation for power controlled 3g cdma," in *Vehicular Technology Conference Proceedings, 2000. VTC 2000-Spring Tokyo. 2000 IEEE 51st*, 2000, vol. 3, pp. 2429 –2433 vol.3.

[123] D. Samardzija and N. Mandayam, "Unquantized and uncoded channel state information feedback in multiple-antenna multiuser systems," *Communications, IEEE Transactions on*, vol. 54, no. 7, pp. 1335 –1345, july 2006.

[124] D. Schafhuber, G. Matz, and F. Hlawatsch, "Kalman tracking of time-varying channels in wireless mimo-ofdm systems," in *Signals, Systems and Computers, 2003. Conference Record of the Thirty-Seventh Asilomar Conference on*, nov. 2003, vol. 2, pp. 1261 – 1265 Vol.2.

[125] Shengli Zhou, B. Muquet, and G.B. Giannakis, "Subspace-based (semi-) blind channel estimation for block precoded space-time ofdm," *Signal Processing, IEEE Transactions on*, vol. 50, no. 5, pp. 1215 –1228, may 2002.

[126] Subhadeep Roy and Tolga M. Duman, "Soft input soft output kalman equalizer for mimo frequency selective fading channels," *Wireless Communications, IEEE Transactions on*, vol. 6, no. 2, pp. 506 –514, feb. 2007.

[127] A.L. Swindlehurst and G. Leus, "Blind and semi-blind equalization for generalized space-time block codes," *Signal Processing, IEEE Transactions on*, vol. 50, no. 10, pp. 2489 – 2498, oct 2002.

[128] S. Tsai, T.F. Wong, and J.S. Lehnert, "Ds-cdma system with joint channel estimation and map detection in time-selective fading channels," *Selected Areas in Communications, IEEE Journal on*, vol. 19, no. 1, pp. 121 –131, jan 2001.

[129] M.K. Teatsanis and Zhengyuan Xu, "Performance analysis of minimum variance cdma receivers," in *Digital Signal Processing Proceedings, 1997. DSP 97., 1997 13th International Conference on*, jul 1997, vol. 1, pp. 379 –382 vol.1.

[130] Wei Chen and Ruifeng Zhang, "Kalman-filter channel estimator for ofdm systems in time and frequency-selective fading environment," in *Acoustics, Speech, and Signal Processing, 2004. Proceedings. (ICASSP '04). IEEE International Conference on*, may 2004, vol. 4, pp. iv–377 – iv–380 vol.4.

[131] Weiwei Yang, Yueming Cai, and Yunpeng Cheng, "Pilot embedded channel estimation for ofdm systems," in *Wireless Communications, Networking and Mobile Computing, 2007. WiCom 2007. International Conference on*, sept. 2007, pp. 81 –84.

[132] Xiaofei Dong and Zhi Ding, "Downlink wireless channel estimation for linear mimo transmission precoding," *Communications, IEEE Transactions on*, vol. 57, no. 4, pp. 1151 –1161, april 2009.

[133] M. Yalcin and A. Akan, "Doubly-selective channel estimation for ofdm systems," in *Communications (MICC), 2009 IEEE 9th Malaysia International Conference on*, dec. 2009, pp. 6 –10.

[134] T. Yucek and H. Arslan, "A novel sub-optimum maximum-likelihood modulation classification algorithm for adaptive ofdm systems," in *Wireless Communications and Networking Conference, 2004. WCNC. 2004 IEEE*, march 2004, vol. 2, pp. 739 – 744 Vol.2.

[135] Yuming Zhu, Xiuming Shan, and Yong Ren, "A power efficient adaptive modulation scheme over fading channel," in *Communications, Circuits and Systems and West Sino Expositions, IEEE 2002 International Conference on*, june-1 july 2002, vol. 1, pp. 257 – 261 vol.1.

[136] Zhiqiang Liu, Xiaoli Ma, and G.B. Giannakis, "Space-time coding and kalman filtering for time-selective fading channels," *Communications, IEEE Transactions on*, vol. 50, no. 2, pp. 183 –186, feb 2002.

[137] Zi-Zhe Ding, Xian-Da Zhang, and Xiao-Long Zhu, "A low complexity rls-pastd algorithm for blind multiuser detection in dispersive cdma channels," *Wireless Communications, IEEE Transactions on*, vol. 6, no. 4, pp. 1187 –1192, april 2007.

[138] Du Jiang and Song Ting, "A low-complexity adaptive moving target tracking algorithm over time-varying scattering channel," in *Wireless Communications, Networking and Mobile Computing, 2007. WiCom 2007. International Conference on*, sept. 2007, pp. 1171 –1175.

[139] E. Eleftheriou and D. Falconer, "Tracking properties and steady-state performance of rls adaptive filter algorithms," *Acoustics, Speech and Signal Processing, IEEE Transactions on*, vol. 34, no. 5, pp. 1097 – 1110, oct 1986.

[140] M. Kiessling, J. Speidel, I. Viering, and M. Reinhardt, "Statistical prefiltering for mmse and ml receivers with correlated mimo channels," in *Wireless Communications and Networking, 2003. WCNC 2003. 2003 IEEE*, march 2003, vol. 2, pp. 919 –924 vol.2.

[141] M.B. Loiola and R.R. Lopes, "A state-space approach to semi-blind signal detection in fast frequency-selective fading mimo channels," in *Signal Processing Advances in Wireless Communications, 2008. SPAWC 2008. IEEE 9th Workshop on*, july 2008, pp. 276 –280.

[142] Nam-Soo Kim and Ye Hoon Lee, "Effect of channel estimation errors and feedback delay on the performance of closed-loop transmit diversity system," in *Signal Processing Advances in Wireless Communications, 2003. SPAWC 2003. 4th IEEE Workshop on*, june 2003, pp. 542 – 545.

[143] S. Prakriya, "Eigenanalysis-based blind methods for identification, equalization, and inversion of linear time-invariant channels," *Signal Processing, IEEE Transactions on*, vol. 50, no. 7, pp. 1525 –1532, jul 2002.

[144] A. Richter, M. Enescu, and V. Koivunen, "State-space approach to propagation path parameter estimation and tracking," in *Signal Processing Advances in Wireless Communications, 2005 IEEE 6th Workshop on*, june 2005, pp. 510 – 514.

[145] T. Eyceoz, A. Duel-Hallen, and H. Hallen, "Prediction of fast fading parameters by resolving the interference pattern," in *Signals, Systems amp; Computers, 1997. Conference Record of the Thirty-First Asilomar Conference on*, nov. 1997, vol. 1, pp. 167 –171 vol.1.

[146] T.L. Hemminger, "Signal estimation with neural networks for multipath mobile communications," in *Neural Networks,1997., International Conference on*, jun 1997, vol. 1, pp. 138 –141 vol.1.

[147] Hsiao-Chun Wu, M. Saquib, and Zhifeng Yun, "Novel automatic modulation classification using cumulant features for communications via multipath channels," *Wireless Communications, IEEE Transactions on*, vol. 7, no. 8, pp. 3098 –3105, august 2008.

[148] Jinho Choi, "Data detection with imperfect csi using averaged likelihood function," *Wireless Communications, IEEE Transactions on*, vol. 7, no. 11, pp. 4117 –4121, november 2008.

[149] R.J. Lyman and A. Sikora, "Prediction of bandlimited fading envelopes with arbitrary spectral shape," *Wireless Communications, IEEE Transactions on*, vol. 6, no. 4, pp. 1560 –1567, april 2007.

[150] Xiaoli Ma, G.B. Giannakis, and S. Ohno, "Optimal training for block transmissions over doubly selective wireless fading channels," *Signal Processing, IEEE Transactions on*, vol. 51, no. 5, pp. 1351 – 1366, may 2003.

[151] A. Duel-Hallen, "Fading channel prediction for mobile radio adaptive transmission systems," *Proceedings of the IEEE*, vol. 95, no. 12, pp. 2299 –2313, dec. 2007.

[152] Dong Chunli, Dong Yuning, and Wang Li, "Autoregressive channel prediction model for cognitive radio," in *Wireless Communications, Networking and Mobile Computing, 2009. WiCom '09. 5th International Conference on*, sept. 2009, pp. 1 –4.

[153] K.E. Baddour and N.C. Beaulieu, "Autoregressive models for fading channel simulation," in *Global Telecommunications Conference, 2001. GLOBECOM '01. IEEE*, 2001, vol. 2, pp. 1187 –1192 vol.2.

[154] V. Krishnamurthy and A. Logothetis, "Hidden markov model signal processing for errors-in-variables communication channels," in *Global Telecommunications Conference, 1995. GLOBECOM '95., IEEE*, nov 1995, vol. 2, pp. 1049 –1053 vol.2.

[155] A. Logothetis and V. Krishnamurthy, "Expectation maximization algorithms for map estimation of jump markov linear systems," *Signal Processing, IEEE Transactions on*, vol. 47, no. 8, pp. 2139 –2156, aug 1999.

[156] H. Zamiri-Jafarian and S. Pasupathy, "Adaptive mlsde using the em algorithm," *Communications, IEEE Transactions on*, vol. 47, no. 8, pp. 1181 –1193, aug 1999.

[157] Zhiwen Zhu and H. Leung, "Adaptive blind equalization for chaotic communication systems

using extended-kalman filter," *Circuits and Systems I: Fundamental Theory and Applications, IEEE Transactions on*, vol. 48, no. 8, pp. 979 –989, aug 2001.

[158] R. Raheli, A. Polydoros, and Ching-Kae Tzou, "Per-survivor processing: a general approach to mlse in uncertain environments," *Communications, IEEE Transactions on*, vol. 43, no. 234, pp. 354 –364, feb/mar/apr 1995.

[159] Lang Tong and S. Perreau, "Multichannel blind identification: from subspace to maximum likelihood methods," *Proceedings of the IEEE*, vol. 86, no. 10, pp. 1951 –1968, oct 1998.

[160] I.A. Akbar and W.H. Tranter, "Order estimation of binary hidden markov wireless channel models in rayleigh fading," in *SoutheastCon, 2007. Proceedings. IEEE*, march 2007, pp. 202 –207.

[161] A. Swami and B.M. Sadler, "Hierarchical digital modulation classification using cumulants," *Communications, IEEE Transactions on*, vol. 48, no. 3, pp. 416 –429, mar 2000.

[162] S.E. Goodman and S.T. Hedetniemi, *Introduction to the design and analysis of algorithms*, McGraw-Hill computer science series. McGraw-Hill, 1977.

Appendix A

A.1 Time Variant, Invariant, and Mobile Models

The transmission of a baseband signal $\tilde{s}$(t) through a linear time-varying channel such that the received signal varies as a function of time and space can be modeled in the time domain by equation (A.1) or the frequency domain by equation (A.2) ,

$$\tilde{y}(t,r) = \frac{1}{2}\int_{-\infty}^{+\infty} \tilde{H}(\tau;t,r)\tilde{s}(t-\tau)\,d\tau, \tag{A.1}$$

$$\tilde{y}(t,r) = \frac{1}{2}\int_{-\infty}^{+\infty} \tilde{h}(f;t,r)\tilde{S}(f)\,e^{(j2\pi ft)}df. \tag{A.2}$$

The transmission of a baseband signal $\tilde{s}$(t) through a linear time-invariant channel such that a received signal varies as a function of only frequency and position can be modeled by equation (A.3) and equivalently equations (A.4) and (A.5),

$$\tilde{y}(t,r) = \frac{1}{2}\int_{-\infty}^{+\infty} \tilde{H}(\tau;r)\tilde{s}(t-\tau)\,d\tau, \tag{A.3}$$

$$\tilde{y}(t,r) = \frac{1}{2}\left[\tilde{H}(\tau;r)\,|\,\tau = t \otimes \tilde{x}(t)\right], \tag{A.4}$$

$$\tilde{Y}(f,r) = \frac{1}{2}\left[\tilde{h}(f;r)\,\tilde{S}(f)\right]. \tag{A.5}$$

The mobile case where position r = vt is a function of a constant velocity and time. In this case the received signal can be expressed only as a function of time as defined in equations (A.6) and (A.7) ,

$$\tilde{y}(t) = \tilde{y}(t,r)\,|r = vt\ , \tag{A.6}$$

$$\tilde{y}(t) = \frac{1}{2}\int_{-\infty}^{+\infty}\left[\tilde{H}(\tau;r,t)\,|r = vt\ \right]\tilde{s}(t-\tau)\,d\tau. \tag{A.7}$$

A.2 Stationarity

Stationarity is an important attribute to characterize stochastic processes; there are at least three defined types of stationarity. First order stationarity exists if all first order statistics- mean, variance, and probability density function (PDF) are invariant with regard to time, frequency, and space. Wide sense stationarity requires that first order and second order statistics are invariant. In this case the autocorrelation by definition, depends only on the difference in time so that the correlation behavior is time invariant. Additionally the mean is expected to be invariant[2] as defined in equation (A.8),

$$C_{\tilde{h}}(t_1,t_2) \doteq C_{\tilde{h}}(t_0+t_1,t_0+t_2)\ \ for\ all\ t_0. \tag{A.8}$$

Here a WSS processes is equivalent to equation (A.9),

$$C_{\tilde{h}}(t) \doteq E\left\{\tilde{h}(t_1)\tilde{h}^*(t_1-t)\right\}\ \ for\ all\ t_0. \tag{A.9}$$

Strict-sense stationarity describes a process that is invariant across all orders of time, frequency, and space.

A.3 Spectral Model

The effects of spatial selectivity can be defined within a local area with relatively constant mean power in contrast to a macro area where mean power would vary. Durgin defines a spectral model based on a local area model. The local area is the largest volume of free-space that can be modeled accurately as the sum of homogeneous plane waves. In this volume plane waves are dominate so that inhomogeneous plane waves are insignificant. Furthermore, specular, nonspecular, and diffuse waveform components are described by a sum of specular waves and a diffuse nonspecular component as defined by equation (A.10),

$$\tilde{h}(f,\vec{r}) = \sum_{i=1}^{N} V_i e^{\left(j\left[\varphi_i - \vec{k_i}\vec{r} - 2\pi f \tau_i\right]\right)} + \widetilde{h_{diff}}(f,\vec{r}). \tag{A.10}$$

Here N is the number of specular components and this equation reduces a local area channel of any arbitrary complexity to the sum of a few large specular components and nonspecular components that are diffuse[2].

A.3.1 Local Area Specular Component Mathematical Model

The local area specular component defined by equation (A.11),

$$\Phi_{\mathrm{XY}}(v) = \rho \int_{0}^{\infty} J_o\left(V_o v\right), \tag{A.11}$$

is based on a zero-order Bessel function which only depends on the amplitude of the specular component[2].

A.3.2 Local Area Diffuse Component Mathematical Model

The local area diffuse component defined by equation (A.12),

$$\Phi_{\mathrm{XY}}(v) = e^{\left(\frac{-v^2 P_{diff}}{4}\right)}, \tag{A.12}$$

is a Gaussian function that depends only on the average power of the voltage component, $\mathrm{P_{diff}}$.

A.3.3 Local Area Complex Envelope PDF Model

The envelope PDF in terms of specular and diffuse terms is defined by equation (A.13),

$$\mathrm{f_R}(\rho) = \rho \int_0^{\infty} J_o(v\rho) e^{\left(\frac{-v^2 P_{diff}}{4}\right)} \left[\prod_{i=1}^{N} J_o(V_i v)\right] v dv, \tag{A.13}$$

for $\mathrm{R} = \left|\tilde{V}_{\mathrm{diff}} + \sum_{\mathrm{i}=1}^{\mathrm{N}} \mathrm{V_i} e^{(\mathrm{j}\Phi_\mathrm{i})}\right|$ and $\mathrm{E}\left\{\left|\tilde{V}_{\mathrm{diff}}\right|^2\right\} = \mathrm{P_{diff}}$, which is valid for $\rho \geq 0$[2] .

A.4 First Order Statistical Model

The probability density function (PDF) is a common first-order tool for characterizing mobile wireless fading channels. The mean received power is a common statistics given the relationship between received power and error rate. Independent, uniformly distributed phases, have a specific phase PDF [2]. Application of the specular model enables an approach that ignores the fine waveform structure with a focus on mean-squared power of specular and nonspecular components. The waveform PDF $f_p(\rho)$ can be defined in terms of received voltage envelope with conversions to and from envelope power defined in equations (A.14),

$$f_P(p) = \frac{1}{2\sqrt{p}} f_R(\sqrt{p}), \tag{A.14}$$

and (A.15)

$$f_R(\rho) = 2\rho f_P\left(\rho^2\right). \tag{A.15}$$

A.4.1 MWC Closed Form PDF Model

Six closed form PDFs can be defined [2]: 1) single wave, 2) two wave, 3) three wave, 4) Rayleigh, 5) Ricean, and 6) two wave plus diffuse power (TWDP). The single wave is a primitive case generated by integration of equation (A.13) with $N = 1$ and $P_{diff} = 0$. The two wave case is common and well researched and is generated by integration of equation (A.11) with$N = 2$ and $P_{diff} = 0$. While case three is more complicated, it provides insight into differences in behavior between the specular and nonspecular components and is generated with $N = 3$ and $P_{diff} = 0$. The central limit theorem begins to dominate the PDF in the three wave case; additional nonspecular components move the PDF toward a Gaussian distribution based on the central limit theorem and results approach the Rayleigh case.

MWC Rayleigh PDF First Order Statistical Model

The Rayleigh case is most popular for computation of fading margins in wireless fading links can be generated by equation A.13 with $N = 0$ and $P_{diff} > 0$. The Rayleigh PDF is nonzero over the entire range of $\rho \geq 0$ and is defined by equation (A.16),

$$f_R(\rho) = \frac{2\rho}{P_{diff}} e^{\left(\frac{-\rho^2}{P_{diff}}\right)} for\ \rho \geq 0. \tag{A.16}$$

MWC Ricean PDF First Order Statistical Model

The more general case is the Ricean distribution generated by equation A.13 with $N = 1$ and $P_{diff} > 0$. This PDF is nonzero over the range of K and Δ where K is the ratio of specular power to diffuse power and Δ is the difference in power between the specular components which are zero for the Ricean case. As K approaches one, the Ricean PDF approaches the Rayleigh PDF. The

Ricean PDF is defined by equation (A.17),

$$\mathrm{f_R}(\rho) = \frac{2\rho}{P_{diff}} e^{\left(\frac{-\rho^2 - V_1^2}{P_{diff}}\right)} I_o\left(\frac{2\rho V_1}{P_{diff}}\right) for\ \rho \geq 0, \tag{A.17}$$

where $\mathrm{I_o}(\ldots)$ is a zero-order modified Bessel function and $\mathrm{K} = \frac{\text{Specular Power}}{\text{Nonspecular Power}} = \frac{\mathrm{V_1^2}}{\mathrm{P_{diff}}}$. As K becomes much larger than one, the Ricean PDF approaches a pure Gaussian with an mean that is increasingly greater than one. In this case, the Ricean PDF can be approximated by a pure Gaussian distribution as defined in equation (A.18),

$$\mathrm{f_R}(\rho) = \frac{1}{\sqrt{\pi P_{diff}}} e^{\left(\frac{-(\rho - V_1)^2}{P_{diff}}\right)}. \tag{A.18}$$

MWC Two Wave plus Diffuse Component PDF First Order Statistical Model

The TWDP case is generated by equation A.13 with $\mathrm{N} = 2$ and $\mathrm{P_{diff}} > 0$. While this model is the most complicated, it represents a range of fading behavior[2]. For the TWDP case, K and Δ are used to classify the shape of the PDF as defined in equations (A.19) and (equation (A.20)),

$$K = \frac{\mathrm{V_1^2} + \mathrm{V_2^2}}{P_{diff}}, \tag{A.19}$$

$$\Delta = \frac{2V_1V_2}{V_1^2 + V_1^2}. \tag{A.20}$$

The TWDP PDF is defined by equation (A.21),

$$\mathrm{f_R}(\rho) = \frac{2\rho}{P_{diff}} e^{\left(\frac{-\rho^2}{P_{diff}} - K\right)} \sum_{i=1}^{M} a_i \left[\frac{1}{2} e^{\propto K} I_o(x\sqrt{2K(1-\alpha)} + \frac{1}{2} e^{-\propto K} I_o(x\sqrt{2K(1+\alpha)}\right], \tag{A.21}$$

where $\alpha = \cos(\frac{\pi(\mathrm{i}-1)}{2\mathrm{M}-1})$, $\mathrm{x} = \frac{\rho}{\sqrt{\frac{\mathrm{P_{diff}}}{2}}}$, M is the order of the approximation and $\mathrm{a_i}$ is defined by table A.1 .

The product of K and Δ determine the order of equation (A.21) as defined by equation (equa-

Table A.1: TWDP approximate PDF coefficients

Order	a_1				
1	1	a_2			
2	$\frac{1}{4}$	$\frac{3}{4}$	a_3		
3	$\frac{10}{144}$	$\frac{25}{48}$	$\frac{25}{72}$	a_4	
4	$\frac{751}{8640}$	$\frac{3577}{8640}$	$\frac{49}{320}$	$\frac{2080}{8640}$	a_5
5	$\frac{2857}{44800}$	$\frac{15741}{44800}$	$\frac{27}{1120}$	$\frac{1209}{2800}$	$\frac{2880}{22400}$

tion (A.22))

$$\text{Order } (M) = ceiling\left[\frac{1}{2}K\Delta\right]. \tag{A.22}$$

Here $ceiling[\ldots]$ is a function that rounds up to nearest integer. The approximation will deviate from the actual PDF if K is large and Δ approaches unity. The family of resulting PDFs have the following characteristics:

- Mathematically exact PDFs which integrate to unit over the interval of $0 \leq \rho \leq \infty$,
- Accurate over upper and lower tails,
- Second order moments are preserved (average local power),
- Compact description based on P_{diff}, K, and Δ,
- Proper limiting behavior with $\Delta = 0$ approaching Ricean PDF and with $K = 0$ the Rayleigh PDF.

A.5 Second Order Statistical Models

Autocorrelation functions are common for characterizing stochastic processes such as wireless fading channels. The autocorrelation function $C_{\tilde{h}}(t_1, t_2)$ of a time-varying stochastic channel $\tilde{h}(t)$ is defined by equation (A.23),

$$C_{\tilde{h}}(t_1,t_2) \doteq E\left\{\tilde{h}(t_1)\tilde{h}^*(t_2)\right\}. \tag{A.23}$$

The autocorrelation characterizes the time evolution averaging the products of all samples in the random process a two different points in time. The autocorrelation, $C_{\tilde{h}}(t_1,t_2)$ is a snapshot of the correlation behavior of a wireless channel random process defined by equation (A.24),

$$C_{\tilde{h}}(t_1,t_2) \doteq C_{\tilde{h}}(t_0+t_1,t_0+t_2) \;\; for\ all\ t_0. \tag{A.24}$$

For WSS processes equation (A.24) is equivalent to equation (A.25),

$$C_{\tilde{h}}(t) \doteq E\left\{\tilde{h}(t_1)\tilde{h}^*(t_1-t)\right\} \;\; for\ all\ t_0. \tag{A.25}$$

The MWC autocovariance is defined by equation (A.26),

$$C_{\tilde{h}}(t) = E\left\{\left[\tilde{h}(t_0-\tilde{\mu})\right]\left[\tilde{h}^*(t_0+t)-\tilde{\mu}^*\right]\right\} \;\; where\ \tilde{\mu} = E\left\{\tilde{h}(t)\right\}. \tag{A.26}$$

This equation is useful for characterizing processes of envelope and power which have a positive mean value. Recall that the mean power of a time varying process is equal to the autocorrelation evaluated at $\Delta t = 0$ as defined in equations (A.27) and (A.28),

$$C_{\tilde{h}}(0) \doteq E\left\{\tilde{h}(t)\tilde{h}^*(t)\right\} = E\left\{\left|\tilde{h}(t)\right|^2\right\}, \tag{A.27}$$

$$\rho_{\tilde{h}}(\Delta) \doteq \frac{C_{\tilde{h}}(t)-|\tilde{\mu}|^2}{C_{\tilde{h}}(0)-|\tilde{\mu}|^2} \;\; where\ \tilde{\mu} = E\left\{\tilde{h}(t)\right\}. \tag{A.28}$$

The normalized unit autocovariance is an important dimensionless measure of correlation. A unit autocorrelation value of 1 indicates complete correlation while a value of 0 indicates a lack correlation independent of the magnitude of $\tilde{h}(t)$. In addition to characterizing random processes with

autocorrelation in the time domain, spectral analysis via Fourier transforms enable characterization in the frequency domain. Mathematical operations on a random process produce another random process and this is the case when a Fourier transform is applied to a time-varying mobile wireless fading channel. This results in a frequency-varying process $\tilde{H}(\omega)$. A frequency domain autocorrelation $C_{\tilde{H}}(\omega_1, \omega_2)$ is defined by equation (A.29),

$$C_{\tilde{H}}(\omega_1, \omega_2) = E\left\{\tilde{H}(\omega_1)\tilde{H}^*(\omega_2)\right\}, \tag{A.29}$$

characterizing correlation in the frequency domain. If a process is WSS in the time domain, then the spectral components must be uncorrelated as defined by equation (A.30),

$$C_{\tilde{H}}(\omega_1, \omega_2) = 2\pi S_{\tilde{h}}(\omega_1)\,\delta(\omega_1 - \omega_2), \tag{A.30}$$

which evaluates to zero whenever $\omega_1 \neq \omega_2$. The function $S_{\tilde{h}}(\omega_1)$ is known as the power spectral density (PSD) and it describes how the spectral power is distributed in the Doppler spread domain.

A.5.1 Second Order Statistical Models- Time and Bandwidth Coherence

Envelope autocovariance can be related to channel coherence time and bandwidth. The autocorrelation is calculated from its Doppler spectrum by performing an inverse Fourier transform as defined in equation (A.21),

$$S_{\tilde{h}}(\omega) \rightarrow C_{\tilde{h}}(t) \rightarrow \rho_{\tilde{h}}(t). \tag{A.31}$$

The first Fourier transform converts the Doppler spectrum $S_{\tilde{h}}(\omega)$ into a autocorrelation $C_{\tilde{h}}(t)$ and the unit autocovariance $\rho_{\tilde{h}}(t)$ is computed by normalizing by the average power $C_{\tilde{h}}(0)$. A similar set of relationships is developed for Doppler spectrum of received envelope as defined in equation (A.32),

$$S_R(\omega) \rightarrow C_R(t) \rightarrow \rho_R(t). \tag{A.32}$$

Here the envelope and complex baseband channels are related by equation (A.33),

$$\mathrm{R}(\mathrm{t}) = \left|\tilde{h}(\mathrm{t})\right|. \tag{A.33}$$

Coherence Time and Time Domain Unit Autocovariance

An approximation for envelope unit autocovariance that is based only on the root mean square (RMS) spectral spread of the channel process as defined in equation (A.34),

$$\rho_{\mathrm{R}}(\mathrm{t}) \approx \mathrm{e}^{\left(\frac{-23}{2\pi^2}\sigma_{\omega}^2\mathrm{t}^2\right)}, \tag{A.34}$$

where σ_{ω} is the RMS Doppler spread. In this expression, the Doppler spread is the only factor that determines the temporal correlation behavior. It provides a close approximation of unit autocovariance when the time separation Δt is small. Error grows after the time-varying envelope is uncorrelated. The coherence time $\mathrm{T_c}$ is the time period when the complex envelope is a constant. The coherence time can be defined as the time when envelope decorrelates to a value of e^{-1}defined by equation (A.35),

$$\mathrm{T_c} = \frac{2\pi}{\sqrt{46}\sigma_{\omega}} = \frac{1.08}{\sigma_{\omega}}. \tag{A.35}$$

Coherence Bandwidth and Frequency Domain Unit Autocovariance

Applying duality to equation (A.34) results in equation (A.36),

$$\rho_{\mathrm{R}}(\mathrm{f}) \approx \mathrm{e}^{\left(-46\sigma_{\tau}^2\mathrm{f}^2\right)}. \tag{A.36}$$

This equation produces an expression for frequency unit autocovariance given that $\sigma_{\omega} \rightarrow 2\pi\sigma_{\tau}$ and $\Delta\mathrm{t} \rightarrow \Delta\mathrm{f}$ such that the envelope unit autocovariance in the frequency domain. Here σ_{τ} is the RMS delay spread which is the only factor that determines the frequency correlation behavior. Coherence bandwidth, B_c , will be based on the frequency separation Δf where the envelope

decorrelates to a level of e^{-1} as defined in equation (A.37),

$$B_c = \frac{1}{\sqrt{46}\sigma_\tau} = \frac{1}{6.78\sigma_\tau} \approx \frac{1}{5\sigma_\tau}. \tag{A.37}$$

A.6 Time and Frequency Duality

The Wiener-Khintchine theorem defines the autocorrelation of a WSS process and the PSD of an uncorrelated spectrum as Fourier transform pairs defined in equation (A.38),

$$C_{\tilde{h}}(\Delta t) = \frac{1}{2\pi}\int_{-\infty}^{+\infty} S_{\tilde{h}}(\omega)e^{(j\omega\Delta t)}d\omega, \tag{A.38}$$

and (A.39),

$$S_{\tilde{h}}(\omega) = \int_{-\infty}^{+\infty} C_{\tilde{h}}(\Delta t)\ e^{(-j\omega\Delta t)}d\Delta t. \tag{A.39}$$

This implies that characterizing time correlation via the autocorrelation function is equivalent to characterizing average signal power distribution in the spectral domain.

A.7 Coherence State Model Literature Review

Several authors have published historical development of wireless fading channel modeling with multistate Markov chains (MMC). Seon Yeong et al. [4] report that the earliest accounts of multistate MWC models based on the HMM was Gilbert and Elliott in a 1960 publication. Tan [6] provided a historical overview of amplitude quantized finite state Markov Models (FSMM). Since the 1960's, Markov models have been widely utilized to represent simple error and signal strength behavior[4]. Lopez-Guerrero [53] provide development of error state models. Kundu [20] asserts that n-state FSMM are required to achieve sufficient accuracy. Reidiger [21] provides overview of information theoretic based FSMM. Kumwilaisak [22] proposed variable length FSMM to better

model dynamic channel conditions. Qinqing and Kassam [23] proposed partitioned SNR defined not by amplitude but rather average dwell time in each state to model time-variant conditions. Wang and Moayeri [5] state "by partitioning the range of the received signal to noise ratio (SNR) into a finite number of intervals, we build a finite-state model for the Rayleigh fading channel. Each state of the channel corresponds to a specific interval and the Rayleigh fading channel can be modeled by a binary symmetric channel (BSC) in that state". Pimental [24] looked at high-order FSMMs for modeling error behavior with significant memory. Babich [54, 7] reaffirms the need for higher order FSMM for accuracy, however acknowledges the computational complexity and offers order reduction methods to reduce complexity to a 1st order model while maintaining accuracy. Yongjun [28] asserts the need for higher order methods for accurate time-variant behavior and traced prior development of fading envelope distribution models and develops a general distribution model for all channel environments to overcome limitations of the Ricean distribution. Richter et al. [55] and Olama et al. [10] provide general wireless channel state variable models. Galvao et al.[56] assert that state space models are an important alternative to channel impulse response with better accuracy than traditional convolutional methods. Richter, et al., [55] formulated a time variant state-space channel model to track the state-space wireless mobile channel dynamic parameters with a Kalman filter. Olama et al. [57] present a higher order dynamic ad-hoc channel model that estimates parameters from the Doppler PSD. The remainder of the literature search is summarized here. Two articles have been published with multistate wireless channel models which map states to channel impulse response [10] or FIR coefficients [11]. Several papers have been published with multistate Markov chains which associate states with bit error statistics [58, 13]. Several papers have been published with multistate Markov chains which map states to block error statistics [14, 15]. Several published articles present finite state Markov chains with states defined as quantized signal strength [4, 16, 17, 18, 19]. Several published articles present finite state Markov chains with states defined as quantized SNR [20, 21, 22, 23, 5, 24, 25, 26, 27]. In the literature there are a few examples of multistate Markov chain wireless channel models with states derived based on partitioned statistical distributions [28, 29, 25]. Several published articles with multistate

Markov chain wireless channel models define states based on partitioned shadowing. Several papers have been published that include multistate Markov chains which define states as partitioned fading level . Wakana [30] published an example of hidden Markov chain with states defined with channel fading level. Swarts and Ferreira [31] present HMM research for a frequency nonselective, slow time varying MWC model. Yuen and Yue [32] published research based on a four-state Markov model representing variable bit rates partioned into good and bad states. Multistate Markov models have been applied to correlated channels with many channel distributions including: 1) AWGN [13, 14], 2) Log Normal [59], 3) Rayleigh [4, 20, 22, 23, 5, 11, 58, 16, 29, 25, 30], 4) Ricean [5, 54, 7, 15, 17, 18, 19], and 5) Hybrid combinations [27, 60, 61, 62, 63]. Finite state Markov chains have been applied to many communication applications including: 1)CDMA and OFDM cellular networks [53, 11, 58, 26, 31, 32], 2) GEO and LEO Satellite [28, 19, 64, 61, 62], 3) Wireless personal area networks [58, 65], 4) Mobile cellular networks [16, 18, 59, 66], 5) Wireless multimedia networks [22, 24, 29, 27, 61], 6) Indoor propagation channels [54, 7, 32, 67], and 7) Multiple input multiple output channels [56]. Finite state Markov models have been applied to the following types of channel fading: 1) Large scale fading [59], 2) Small scale dual time and frequency non selective fading [20, 21, 22, 23, 5, 24, 16, 29, 64], 3) Small scale frequency non-selective and time selective fading [68], 4) Small scale dual time and frequency selective fading po[27], and 5) Hybrid combinations [18].

Based on this considerable literature survey, the proposed CSM and application of HMMs to CSR is novel and unique.

A.8 Channel State Recognition Literature Review

Table A.2 summaries a substantial, broad, temporally diverse, body of keyword indexed research literature collected primarily from the IEEE Xplorer database on the topics of mobile wireless channel state models and mobile wireless channel state distortion estimation.

There are a number of assumptions given in this body of literature summarized below:

Table A.2: CSR Literature Review Summary

Keyword Topic	Source Type	Source Qty	Article Qty	Years
Channel Blind Distortion Estimation	IEEE Journals	6	12	1993-2004
Channel Blind Distortion Estimation	IEEE Symposium	1	1	2000
Channel Blind Distortion Estimation	IEEE Intrntnl. Conference	1	2	1988
Channel Blind Distortion Estimation	IEEE Workshop	1	1	1993
Channel Blind Distortion Detection	IEEE Intrntnl. Conference	2	3	1995-1998
Wireless Channel Blind State Estimation	IEEE Intrntnl. Conference	6	6	1998-2010
Wireless Channel Blind State Estimation	IEEE Workshop	1	1	2008
Wireless Channel Blind State Estimation	IEEE Journal	2	3	1998-2009
Wireless Channel State	Published Books	4	4	1977-1999
Mobile Wireless Channel State Model	Published Books	23	23	1969-2007
Mobile Wireless Channel State Model	IEEE Intrntnl. Conference	12	15	1993-2009
Mobile Wireless Channel State Model	IEEE Journal	9	24	1967-2009
Mobile Wireless Channel State Model	IEEE Workshop	1	1	2006
Mobile Wireless Channel State Model	IEEE Symposium	5	5	2004
Mobile Wireless Fading Channel Blind State Estimation	IEEE Intrntnal. Conference	6	17	1995-2009
Mobile Wireless Fading Channel Blind State Estimation	IEEE Journal	4	13	1986-2009
Mobile Wireless Fading Channel Blind State Estimation	IEEE Workshop	3	5	1998-2005
Mobile Wireless Fading Channel Blind State Estimation	IEEE Symposium	2	2	2002-2007
Total		84	138	

- Quasi-static channel conditions– ten of these articles assume a length of time when the channel is stationary and unchanging [69, 70, 71, 72, 73, 74, 75, 76, 77, 78],

- Channel state definition– 23 of these articles directly assume a channel state defined by finite impulse response gain given as the ratio of the channel output amplitude to the channel input amplitude [79, 80, 81, 82, 73, 74, 83, 84, 85, 12, 86, 87, 88, 89, 90, 91, 58, 92, 93, 94, 95, 96],

- Specific waveform or channel configuration– 56 of these articles directly assume a specific waveform characteristics (e.g. OFDM, CDMA, BPSK, etc.) [97, 98, 99, 100, 101, 71, 81, 102, 103, 104, 105, 106, 83, 107, 108, 12, 109, 110, 111, 112, 113, 114, 22, 115, 116, 117, 118, 119, 86, 120, 87, 121, 57, 122, 123, 124, 125, 126, 127, 128, 129, 91, 130, 131, 132, 92, 93, 133, 134, 135, 94, 95, 136, 96, 137] while 35 assume a specific channel configuration (e.g. MIMO, MISO, SISO, etc.) [100, 101, 104, 105, 138, 139, 106, 83, 84, 85, 108, 109, 110, 140, 117, 141, 119, 120, 142, 121, 143, 88, 144, 123, 124, 75, 125, 126, 127, 91, 130, 132, 93, 135, 136] and 42 assume a specific channel state (ie. Nondispersive, Frequency nonselective, Frequency Selective, etc.) [69, 97, 99, 81, 72, 102, 103, 73, 74, 145, 84, 107, 85, 146, 147, 12, 109, 148, 111, 140, 117, 149, 142, 121, 143, 88, 122, 124, 128, 90, 77, 78, 130, 131, 150, 58, 93, 133, 95, 136, 96, 137],

- Dependence upon accurate channel state estimates at RX or TX– 18 of these articles assume a critical dependence upon accurate and timely channel state estimates at the receiver with/or without feedback to the transmitter [98, 71, 151, 74, 83, 147, 12, 110, 148, 22, 118, 149, 123, 125, 129, 132, 92, 135],

- Channel state prediction– four of these articles assume channel state prediction which projects past data samples into the future up to one wavelength [152, 151, 149, 75],

- Channel state tracking– 34 of these articles assume channel state tracking which enables adaptive processing based on the current value of channel state [153, 80, 102, 103, 82, 152, 105, 138, 139, 106, 145, 83, 107, 114, 154, 115, 155, 141, 86, 87, 57, 88, 144, 124, 75, 126,

128, 91, 130, 93, 156, 157, 96, 137],

- Training symbol sequence or pilot tone assisted channel state estimation– 19 of these articles propose methods which rely upon sequences of time domain training symbols or presence of frequency domain pilot tones [100, 101, 72, 106, 107, 108, 111, 118, 158, 122, 124, 125, 127, 131, 150, 58, 92, 93, 133],

- Blind channel state estimation– 14 of these articles propose methods which rely upon only received channel output sequences. Semi-blind channel state estimation– four of these articles propose methods which rely upon a hybrid combining both training symbol sequences and blind channel estimation approaches [70, 103, 104, 147, 159, 57, 76, 128, 129, 90, 78, 131, 134, 157],

- Semi-blind channel state estimation– four of these articles propose methods which rely upon a hybrid approach that combines both data directed or pilot tone assisted and blind channel state estimation [72, 111, 116, 141],

- Hidden Markov model (HMM) methods– six of these articles propose methods which are based on hidden Markov models [82, 114, 154, 155, 18, 160],

- Cognitive or software defined radio architecture– three of these articles assume a cognitive or software defined radio architecture [152, 76, 77],

- Neural Network methods– two of these articles assume a method based on neural networks [146, 113],

- Adaptive processing applications– three of these articles propose a direct application to adaptive transmitter processing or resource allocation [110, 76, 71],

- Modulation classification applications– two of these articles propose modulation classification [161, 134],

- Distortion estimation– one of these articles propose distortion estimation [78].

There are a number of channel state processing advantages that are claimed by this body of literature including:

- Maximum Likelihood channel state estimation– one of these articles claims results based on the maximum likelihood algorithm [79],
- High order HMM– one of these articles claims advantages of high order HMM processing [160],
- Frequency selective wireless channels– four of these articles claim stable data rates under frequency selective channel conditions [98, 108, 146, 93],
- Time invariant channel conditions– one of these articles claim consistent error rates with time invariant channel conditions [137],
- Small time dispersion (Flat frequency) and Low mobility (slow time-varying conditions)– eight of these articles claim robust performance under flat frequency and slow time varying conditions [99, 83, 84, 115, 86, 129, 130, 134],
- Time dispersive (Flat frequency and frequency selective channel conditions) with low mobility (small frequency dispersion)– nine of these articles claim robust capacity and BER across both frequency nonselective and frequency selective cases [100, 145, 111, 116, 142, 121, 58, 107, 110],
- Fast time-varying conditions– one of these articles claim consistent error rates with fast time-varying channel conditions [161],
- NonGaussian sources– one of these articles claim performance under nonGaussian signal distribution [152],
- Channel state tracking– 16 of these articles claim a method which can track dynamic changes in channel state [153, 138, 106, 114, 141, 149, 87, 57, 122, 144, 124, 75, 125, 128, 91, 157],

- Robust synchronization– two of these articles claim stable synchronization under fading channel conditions [85, 109],
- Robust spectral efficiency– two of these articles claim stable spectral efficiency under fading conditions [127, 135],
- Reduced computational complexity– 13 of these articles claimed reduced computational complexity [70, 104, 138, 147, 140, 118, 119, 143, 158, 76, 126, 90, 137] and two of these articles claim reduced computational complexity while minimizing computational error [80, 96],
- Increased throughput– five of these articles claimed reduction of data overhead leading to increases in throughput [147, 159, 120, 77, 131],
- Joint channel state estimation and data detection– nine of these articles claim joint channel state estimation and data detection [111, 100, 101, 81, 103, 105, 107, 115, 116],
- Transmitter channel state estimation– two of these articles claim channel state information at the transmitter for adaptive process control [71, 151],
- Low SNR conditions– one of these articles claim improved accuracy with low signal to noise ratio cases [72],
- Fast time-varying conditions– seven of these articles claim channel state tracking in fast time-varying conditions [102, 73, 139, 150, 133, 136, 96],
- Shortened training sequences– two of these articles claim minimum squared error performance with shorter training sequences [82, 89],
- Convergence– five of these articles claim advantages of faster convergence for channel state estimation methods [105, 154, 155, 143, 92],
- Global maximum– one of these articles claim advantages of converging to a global maximum when estimating channel state [105],

- Closed loop feedback– three of these articles claim timely and accurate channel state closed loop feedback from the receiver to a transmitter [74, 22, 123],
- Reduced latency– two of these articles claim advantages of reduced channel state processing latency [89, 132],
- Reduced channel state bandwidth– one of these articles claim the advantages of reduced channel state bandwidth [132],
- Reduced error– two of these articles claim advantages from reduced channel state estimation error [92, 94].

There are a number of channel state processing weaknesses that emerge from this body of literature including:

- Degraded performance under dynamic channel conditions– 58 of these articles propose performance with constraints defined by specific channel configurations such that if the channel condition change, performance claims would be degraded [79, 98, 99, 100, 153, 80, 70, 101, 71, 152, 73, 105, 151, 74, 145, 83, 84, 107, 85, 108, 146, 147, 109, 110, 111, 116, 118, 119, 86, 120, 142, 87, 121, 57, 123, 124, 75, 125, 76, 126, 161, 127, 128, 129, 89, 91, 130, 18, 132, 150, 58, 93, 133, 135, 94, 136, 96],
- Degraded performance under dynamic waveform conditions– 34 of these articles propose performance with constraints defined by specific waveform configurations such that if the waveform changes, performance claims would be degraded [79, 98, 70, 101, 72, 152, 73, 147, 110, 111, 115, 116, 118, 86, 120, 142, 121, 57, 143, 122, 144, 123, 124, 125, 76, 127, 129, 89, 130, 132, 58, 133, 134, 137],
- Resource allocation– 11 of these articles propose methods that impact resource allocations constrained by channel state such that if the channel state is dynamic, resource allocations would be suboptimum [71, 73, 106, 145, 83, 84, 107, 146, 109, 119, 87],

- Complexity– seven of these articles suffer from channel state estimation computational complexity [160, 105, 138, 112, 159, 77, 157],
- Latency– three of these articles suffer from excessive channel state estimation latency [160, 106, 149],
- Accurate and timely channel state estimation– two of these articles assume that channel state estimations are perfect and available when required [102, 138],
- Channel state estimate error– five of these articles ignore channel state estimation error [104, 139, 149, 92, 134],
- Constant velocity– one of these articles claim performance gains under constraint of constant velocity such that if a mobile node does not maintain constant velocity performance would be degraded [82],
- Neural Networks– one of these articles claim performance with neural network methods which have limitations [113],
- Offline methods– three of these articles claim performance with offline or nonadaptive channel state estimation methods [154, 155],
- Reduced capacity– 16 of these articles rely upon online training symbols or pilot tones which reduce throughput capacity, Training sequence length– one of these articles suffers from long training sequence length [136, 100, 101, 73, 12, 148, 111, 140, 121, 158, 88, 124, 125, 150, 58, 92],
- Channel state estimation convergence– two of these articles suffer from channel state estimation convergence [92, 94],
- Local maximum– one of these articles suffers from convergence to local maximum rather than global maximum [94].

There are a number of similarities to the Channel State Recognition algorithm that emerge from this literature including:

- General channel state estimation– similar to the CSR algorithm, three of these articles claim general channel state estimation [101, 145, 94],
- Block channel state estimation– similar to the CSR algorithm, 49 of these articles propose block channel state estimation rather than streaming channel state estimation [69, 97, 99, 153, 80, 70, 81, 72, 102, 103, 73, 105, 138, 151, 74, 83, 84, 107, 108, 147, 12, 109, 110, 148, 111, 112, 140, 114, 22, 159, 117, 119, 149, 142, 57, 88, 123, 75, 76, 126, 89, 90, 77, 78, 131, 133, 156, 157, 96],
- Online feature recognition– similar to the CSR algorithm, 52 of these articles propose online feature recognition [79, 153, 71, 72, 102, 105, 138, 74, 83, 84, 147, 12, 109, 110, 148, 111, 112, 140, 22, 115, 159, 117, 118, 141, 149, 86, 120, 142, 57, 158, 88, 122, 144, 123, 75, 125, 76, 126, 161, 127, 128, 129, 77, 130, 132, 93, 133, 156, 95, 136, 157, 96],
- HMM based processing– similar to the CSR algorithm, 7 of these articles propose HMM based processing [160, 82, 114, 154, 159, 155, 18],
- Adaptive channel state estimation–similar to the CSR algorithm, 49 of these articles claim some form of adaptive processing [98, 99, 100, 153, 80, 70, 71, 72, 102, 104, 105, 151, 139, 106, 83, 84, 107, 108, 146, 110, 114, 116, 118, 119, 86, 120, 87, 121, 143, 122, 123, 124, 125, 161, 127, 128, 129, 91, 130, 131, 132, 58, 92, 93, 134, 135, 156, 136, 137],
- Channel state tracking– similar to the CSR algorithm, 15 of these articles claim some form of channel state tracking [81, 103, 82, 152, 107, 159, 141, 87, 158, 124, 125, 76, 126, 91, 157],
- Offline training– similar to the CSR algorithm, three of these articles propose methods that require offline training sequences [138, 154, 155],

- Feature recognition– similar to the CSR algorithm, 11 of these articles propose approaches with waveform or channel feature recognition [74, 146, 147, 12, 148, 113, 140, 22, 57, 131, 134],

- Maximum likelihood (ML) methods– similar to the CSR algorithm, at least one of these articles is based on the ML algorithm [158],

- Cognitive radio (CR) and/or software defined radio (SDR) architecture– similar to the CSR algorithm, three of these articles are based on a CR or SDR architecture [77, 152, 76],

- Dual dispersive channel state estimation– similar to the CSR algorithm, one of these articles propose dual dispersive channel estimation [150].

There are some observable differences between this body of literature and the Channel state recognition (CSR) algorithm including:

- Channel state definition– unlike the CSR algorithm, 94 of these articles are based on a wireless channel finite impulse response definition of channel state [69, 79, 99, 100, 153, 80, 70, 101, 71, 72, 102, 103, 104, 82, 152, 73, 105, 138, 151, 139, 106, 74, 145, 83, 84, 107, 85, 108, 146, 147, 12, 109, 110, 148, 111, 112, 113, 140, 114, 154, 22, 115, 159, 116, 117, 118, 155, 141, 119, 149, 86, 120, 142, 87, 121, 57, 143, 158, 88, 122, 144, 123, 124, 75, 125, 76, 126, 161, 127, 128, 129, 89, 90, 77, 78, 91, 130, 18, 131, 132, 150, 58, 92, 93, 133, 134, 135, 94, 156, 95, 136, 157, 96, 137] which is significantly different than the CSR distortion state definition,

- HMM processing– unlike the CSR algorithm, 92 of these articles are not based on any form of an HMM [69, 79, 98, 99, 100, 80, 70, 101, 71, 72, 102, 103, 104, 82, 152, 73, 105, 138, 151, 139, 106, 74, 145, 83, 84, 107, 85, 108, 146, 147, 12, 109, 110, 148, 111, 112, 113, 140, 114, 22, 115, 159, 116, 117, 118, 141, 119, 149, 86, 120, 142, 87, 121, 57, 143, 158, 88, 122, 144, 123, 124, 75, 125, 76, 126, 161, 127, 128, 129, 89, 90, 77, 78, 91, 130, 18, 131, 132, 150, 58, 92, 93, 133, 134, 135, 94, 156, 95, 136, 157, 96, 137],

- High order HMM– unlike the CSR algorithm, one of these articles is based on higher order HMM processing [160],

- Distortion state awareness– unlike the CSR algorithm, 89 of these articles are not distortion state aware [79, 98, 99, 153, 80, 70, 101, 71, 72, 102, 104, 152, 73, 105, 138, 151, 139, 106, 74, 145, 83, 84, 107, 85, 108, 146, 12, 109, 110, 111, 112, 113, 140, 114, 154, 22, 115, 159, 116, 118, 155, 141, 119, 149, 86, 120, 142, 87, 121, 57, 143, 158, 88, 122, 144, 123, 124, 125, 76, 126, 161, 127, 128, 129, 89, 90, 77, 78, 91, 130, 18, 131, 132, 150, 58, 92, 93, 133, 134, 135, 94, 156, 95, 136],

- Offline training– unlike the CSR algorithm, 41 of these articles propose methods which do not require offline training [79, 98, 153, 102, 103, 152, 74, 84, 12, 109, 148, 140, 117, 141, 119, 149, 120, 87, 158, 88, 144, 123, 124, 75, 125, 76, 126, 127, 129, 130, 131, 132, 92, 93, 133, 134, 94, 156, 136, 96],

- Offline processing– unlike the CSR algorithm, six of these articles propose offline channel state processing methods [160, 81, 154, 155, 90, 94],

- HMM training– unlike the CSR algorithm, one of these articles does not utilize the Baum Welch algorithm for training [160],

- Online training– unlike the CSR algorithm, 15 of these articles describes methods which utilize online training sequences or pilot tones which reduce throughput capacity [100, 101, 73, 12, 148, 111, 140, 121, 158, 88, 124, 125, 150, 58, 92],

- Adaptive channel state tracking– unlike the CSR algorithm, at least four of these articles do not claim any type of channel state tracking [80, 117, 88, 77],

- HMM generators– unlike the CSR algorithm, two of these articles feature HMM as waveform generators rather than waveform recognition [81, 18],

- Frequency dispersion– unlike the CSR algorithm, at least two of these articles claims only time dispersion to the exclusion of frequency dispersion [146, 84],

- Exploitation of specific waveform or channel features– unlike the CSR algorithm, at least 18 of these articles exploit specific waveform or specific channel features [69, 97, 98, 81, 103, 106, 12, 148, 112, 140, 117, 141, 119, 86, 88, 122, 78, 95],

- Joint channel state estimation and symbol detection processing– unlike the CSR algorithm, at least nine of these articles propose joint channel state estimation with symbol detection processing [111, 100, 101, 81, 103, 105, 107, 115, 116].

From this body of literature, the following CSR claimed contributions are summarized below:

- CSR Channel State definition– The CSR algorithm uniquely defines wireless channel state in terms of five distortion states (two distortionless and three distortion states): 1) nondispersive, 2) time nonselective+ frequency nonselective, 3) frequency nonselective and time selective 4) frequency selective and time nonselective 5) time selective and frequency selective. Distortion state awareness– Most if not all of the proposed processing methods in this body of literature, are environmentally sensitive. That is, they claim performance that depends upon accurate and timely channel state awareness, and they assume favorable wireless channel conditions. However, as traditionally defined, channel state models do not accurately represent channel distortion, but rather wireless channel input to output gain. Wireless channel distortion is a tacit assumption in most if not all of these processing methods given that they constrain the application of their methods to either nondispersive, time, or frequency dispersive channel conditions. By recognizing distortion state, the CSR algorithm provides these environmentally sensitive processing methods environmental awareness; indicating when channel conditions are favorable, and eliminating degraded performance when applied under unfavorable channel conditions.

- Adaptive processing performance– Most if not all of these environmentally sensitive processing methods assume a specific channel distortion state, which can be related to magnitude of

time and frequency dispersion. Given that wireless channel dispersion is dynamic, if a processing algorithm is only applied under favorable channel conditions, then peak performance can be maintained. Furthermore, by eliminating application when unfavorable conditions exist, degraded performance is minimized. The CSR algorithm thus adaptively maintains peak processing performance in a dynamic wireless channel state, while eliminating wasteful suboptimal performance if these processing methods are applied under unfavorable channel state conditions.

- Adaptive resource allocation– Most if not all of these proposed processing methods consume resources including: 1) memory, 2) processing cycles, 3) capacity, 4) bandwidth, 5) power, and 6) spectrum. Given that wireless channel conditions are dynamic, some dispersive states are favorable and others are unfavorable to performance. If an environmentally sensitive processing method is applied under unfavorable channel conditions, peak performance degrades while associated resources are fixed, resulting in suboptimum resource utilization. The CSR algorithm enables adaptive maintenance of peak resource allocation while eliminating wasteful suboptimal resource allocation if these processing methods are applied under unfavorable channel state conditions.

- Adaptive processing latency– Most if not all of these environmentally sensitive processing methods require varying degrees of latency. Given that wireless channel state is dynamic, degraded performance results if these methods are applied in unfavorable conditions, and if associated latency is fixed, inefficient processing latency results. The CSR algorithm enables adaptive maintenance of optimum processing latency while eliminating wasteful suboptimal processing latency if these processing methods are applied under unfavorable channel state conditions.

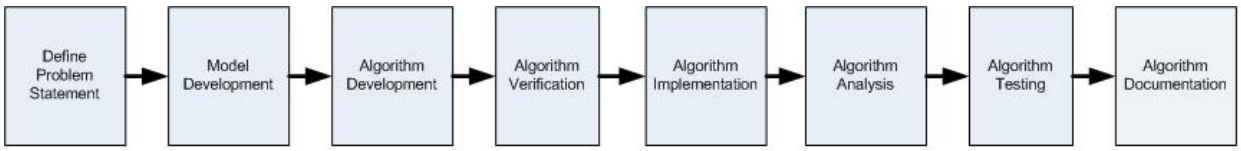

Figure A.1: Algorithm Development Process

A.9 Algorithm Development

An algorithm is a defined computational procedure, that is a sequence of computational steps, that transforms input data into output data. An algorithm can be considered as a tool for solving well-specified computational problems. The problem statement specifies in general terms the desired input/output relationship. Cormen et al. [44] explain the importance of algorithms for design of efficient advanced computing processes such as networking, software compilation, GUIs, and parallel computing architectures. The general algorithm development process shown in Fig. A.1 has been developed by Goodman and Hedetniemi[162].

A.10 Prescriptive Mitigation Selections

Environmental sensing processes provide MWC waveform feature extraction and recognition; feature extraction and state recognition functions effectively translate observable MWC features into meaningful channel states which can be can be processed by the CPA. Given current MWC distortion state, a cognitive processor can implement time-variant distortion mitigation policy. This can be accomplished with a mitigation transform (Refer to FigureA.2) which maps channel distortion states to associated mitigation processing. Refer to Sklar [49], Rappaport [3], and Proakis [48] for discussion of fading mitigation. The distortion mitigation zones are defined as regions of power efficiency for which common mitigation strategies will be effective. For example, regions of QoS where SNR mitigation would be effective is labeled as the SNR zone.

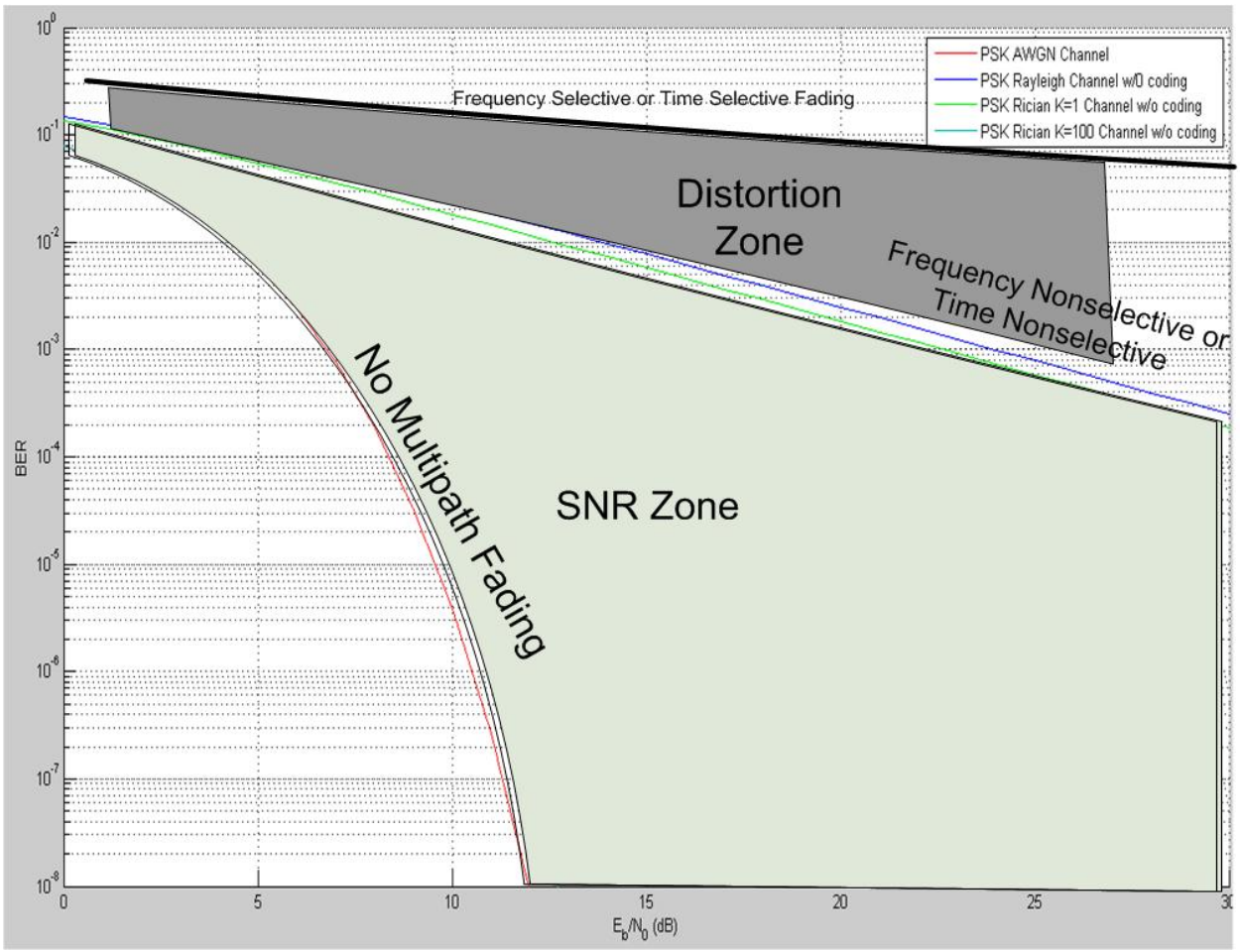

Figure A.2: Distortion Mitigation Transform

This zone is characterized by non-dispersive channel characteristics and selections that increase signal energy or decrease noise power would be sufficient to maintain or improve link quality. In this zone, distortion mitigation methods would waste resources. A second zone is associated with nonselective dispersion states; in this zone equalization or interleaving mitigation would compensate for distortion. In this zone, SNR mitigation methods would waste resources. A third zone is associated with single or dual selective distortion states; in this zone switching to noncoherent or OFDM modulation would be sufficient to mitigate distortion. In this zone, SNR or nonselective distortion mitigation methods would waste resources. By recognizing the distortion state, the cognitive processor can apply effective distortion mitigation selections to the adaptive transmitter and/or receiver to maintain link quality based on current MWC conditions.

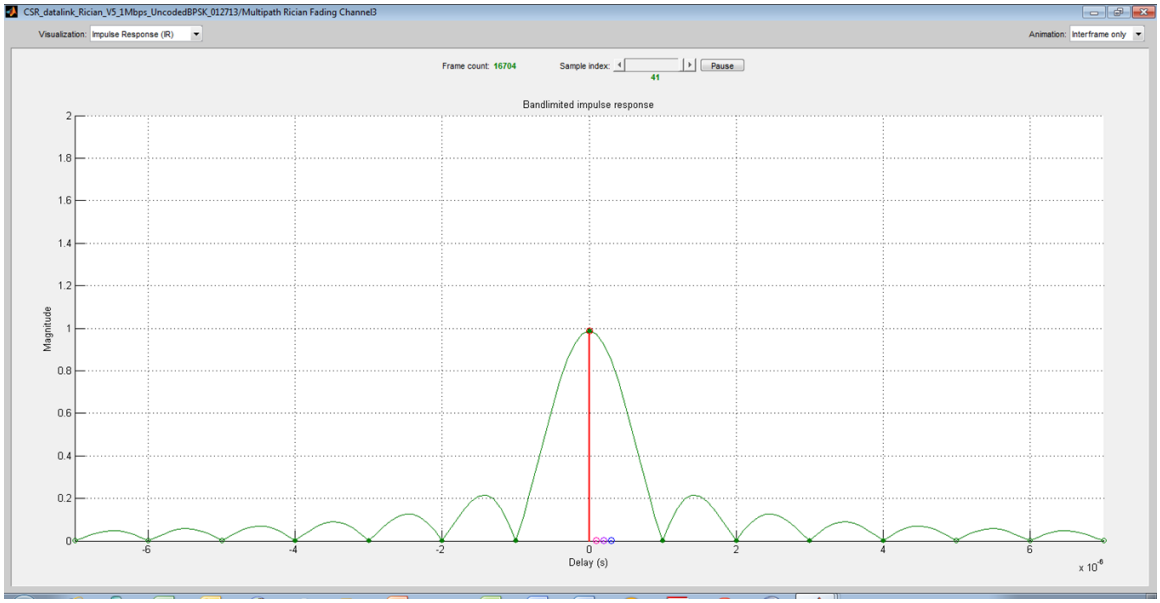

Figure A.3: State 1 AWGN CIR

A.11 Enhanced CSR Test Results

A.11.1 Channel State Waveform Generation

The discussion in this section is about the design of channel state waveforms that have been processed through specific channel state characteristics. Each of these waveforms has been designed in accordance with the Channel Coherence Model (CSM).

State 1 has been designed to be minimally time and frequency dispersive representative of AWGN conditions. In Figure A.3 the state 1 CIR is shown. This CIR has been designed to provide minimal time dispersion effects due to the low gain of delay components two through four. This results in a channel that is frequency coherent because the channel frequency gain does not vary less than the block rate of 20 KHz. The multipath delay vector is [0 .1e-6 .2e-6 .3e-6] while the multipath gain vector is [0 -100 -100 -100] dB. The rms delay spread (DS) of state 1 is .294 e-6 seconds and the associated BWc is ~68 KHz.

In Figure A.4 the state 1 scattering function (SF) is shown. This SF reflects the minimal frequency dispersion effects due to the small diffuse Doppler spread (DP). The channel is considered time

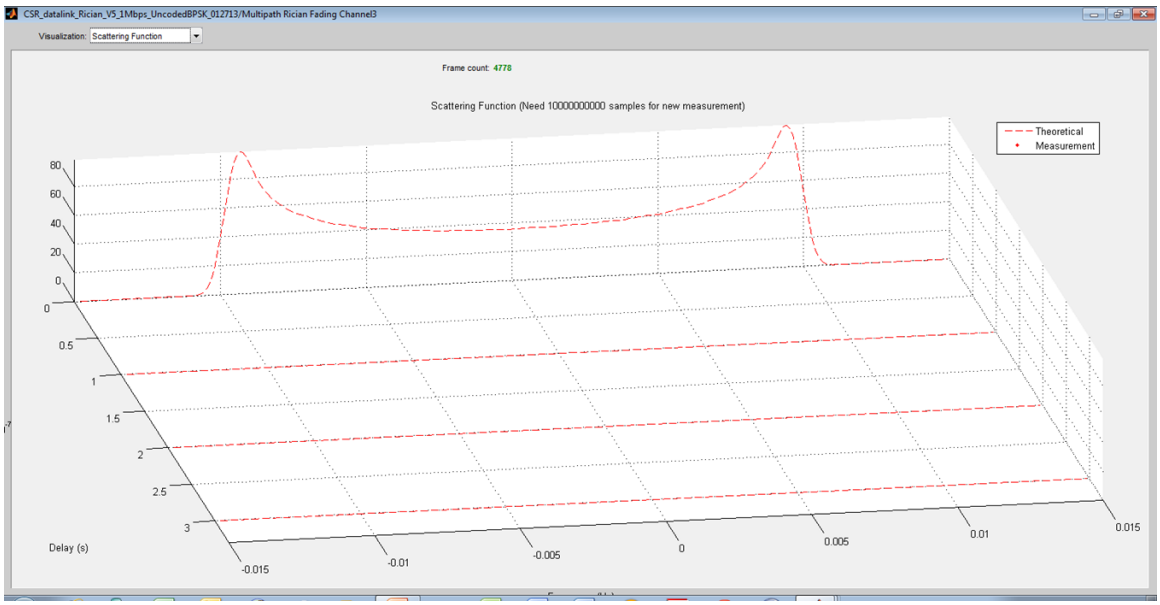

Figure A.4: State 1 AWGN Scattering Function

coherent due because the channel gain does not vary less than the block rate of 50 e-6 seconds. The DP is .01 Hz and the associated Tc of this state is ~42 seconds.

State 2 has been designed to be time nonselective (TN) and frequency nonselective (FN). In Figure A.5 the state 2 CIR is shown. This CIR has been designed to provide low time dispersion effects resulting in FN (flat) conditions (refer to Figure A.6) due to the small delay of the multipath components while the gain of these components has grown relative to state 1. While the frequency response of state 2 does vary, it does not vary substantially less than the block rate of 20 Hhz. The multipath delay vector is [0 .1e-6 .2e-6 .3e-6] while the multipath gain vector is [0 -3 -10 -20] dB. The RMS DS of state 2 is .175 e-6 seconds and the associated BWc is ~114 KHz.

In Figure A.7 the state 2 SF is observed. This SF reflects the minimal time and frequency dispersion effects due to the small diffuse Doppler spread (DP). Similar to state 1, the diffuse DP is .01 Hz and the associated Tc of this state is ~42 seconds..

State 3 has been designed to be TS and FN. In Figures A.8 and A.9 a snapshot of the state 3 time-variant CIR is shown while in Figures A.10 and A.11 a snapshot of the state 3 FR is shown. These Figures highlight how the channel gain changes over time however the FR is nonselective. These CIRs are designed similar to state 2 to provide low time dispersion effects resulting in FN (flat)

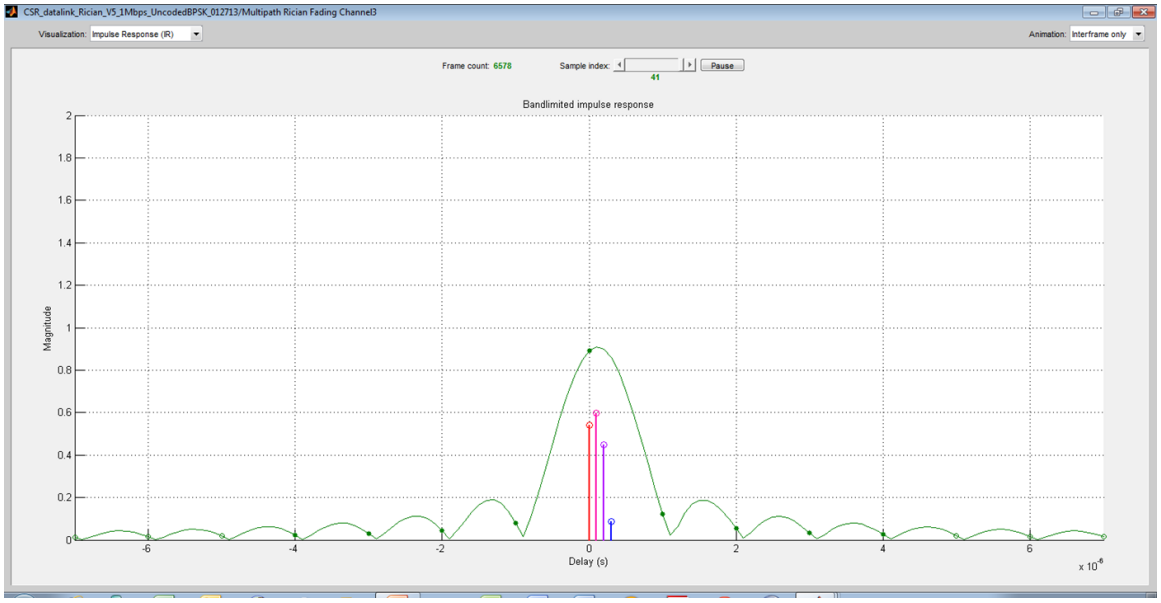

Figure A.5: State 2 Channel Impulse Response

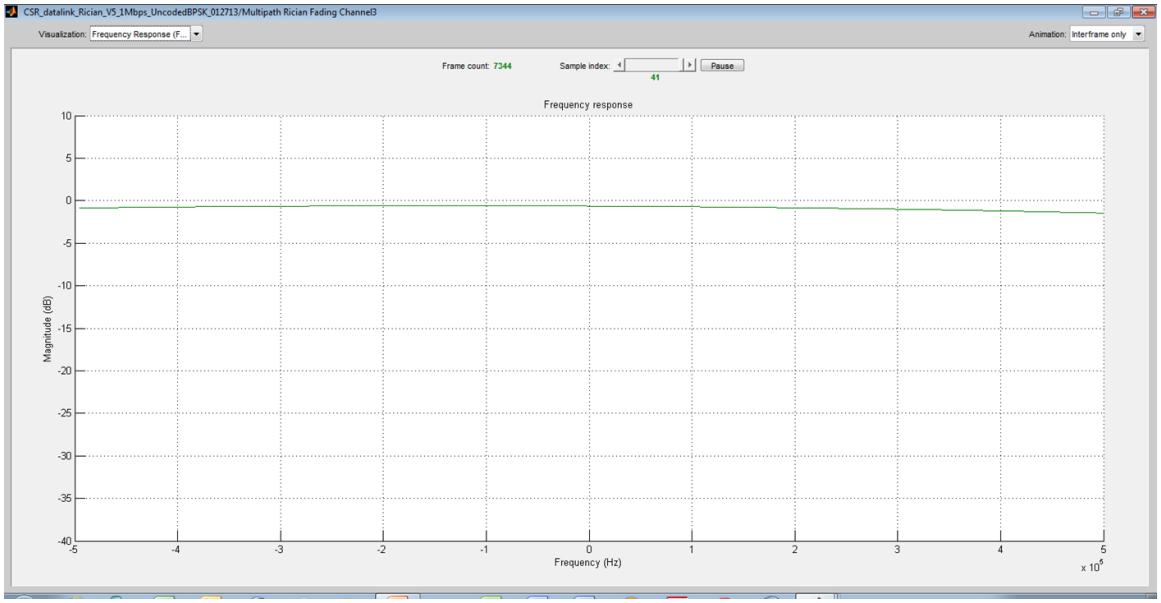

Figure A.6: State 2 Channel Frequency Response

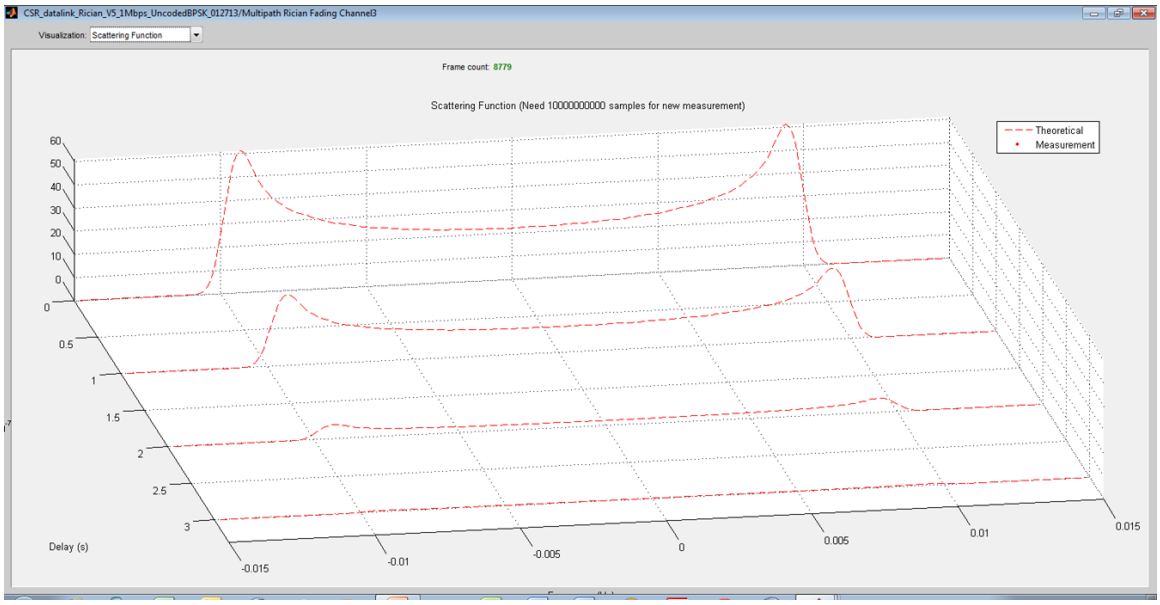

Figure A.7: State 2 Scattering Function

conditions due to the small delay of the multipath components relative to the block rate of 20 KHz. The multipath delay vector is [0 .1e-6 .2e-6 .3e-6] while the multipath gain vector is [0 -3 -10 -20] dB. Similar to state 2, the rms DS of state 3 is .175e-6 seconds and the associated BWc is ~114 KHz.

In Figure A.12 the state 3 SF is observed. This SF reflects the moderate frequency dispersion effects due to the diffuse DP which is a substantial percentage of the block period of 50e-6 seconds. For this state, the diffuse DP is 1 KHz and the associated Tc of this state is ~423e-6 seconds.

State 4 has been designed to be TN and FS. In Figure A.13 the state 4 CIR is shown while in Figure A.14 FR is shown. These figures highlight how the channel gain does not vary over the block period however the frequency response is selective less than the block rate of 20 KHz. For this state, the multipath delay of this CIR has increased 10x over the previous states, and the resulting time dispersion is a significant percentage of the block period resulting in FS conditions. The multipath delay vector is [0 1e-6 2e-6 3e-6] while the multipath gain vector is [0 -3 -10 -20] dB. For this case, the rms DS of state 4 is 1.75 e-6 seconds and the associated BWc is ~11.4 KHz.

In Figure A.15 the state 4 SF is observed. This SF reflects the minimal frequency dispersion effects due to the diffuse DP which is a small percentage of the block rate of 20 KHz. Similar to states

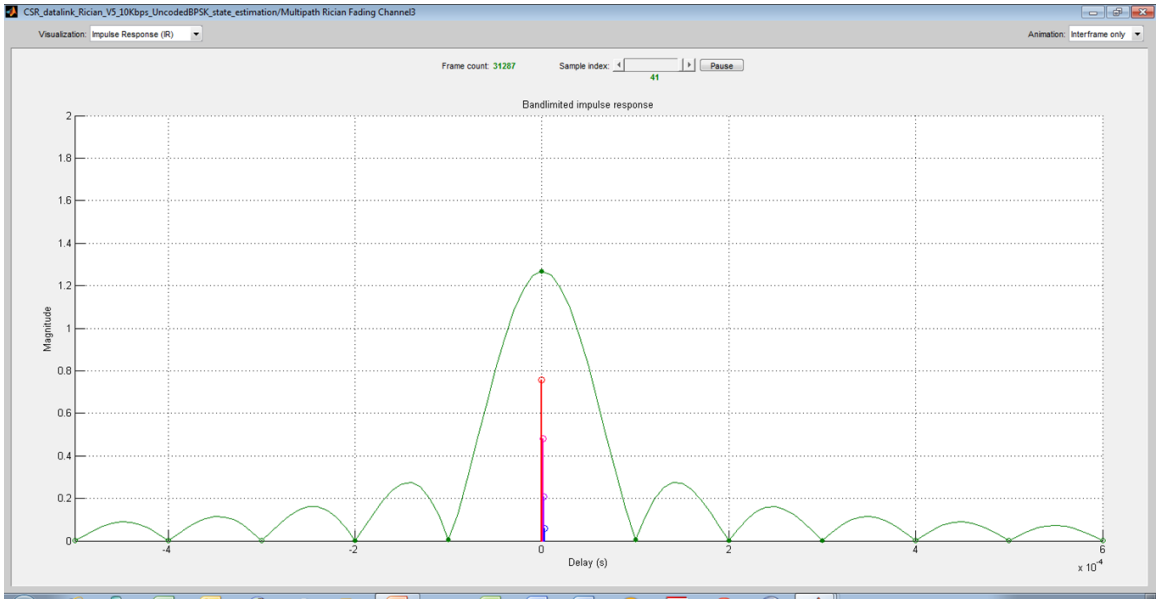

Figure A.8: State 3 Time-Variant Channel Impulse Response

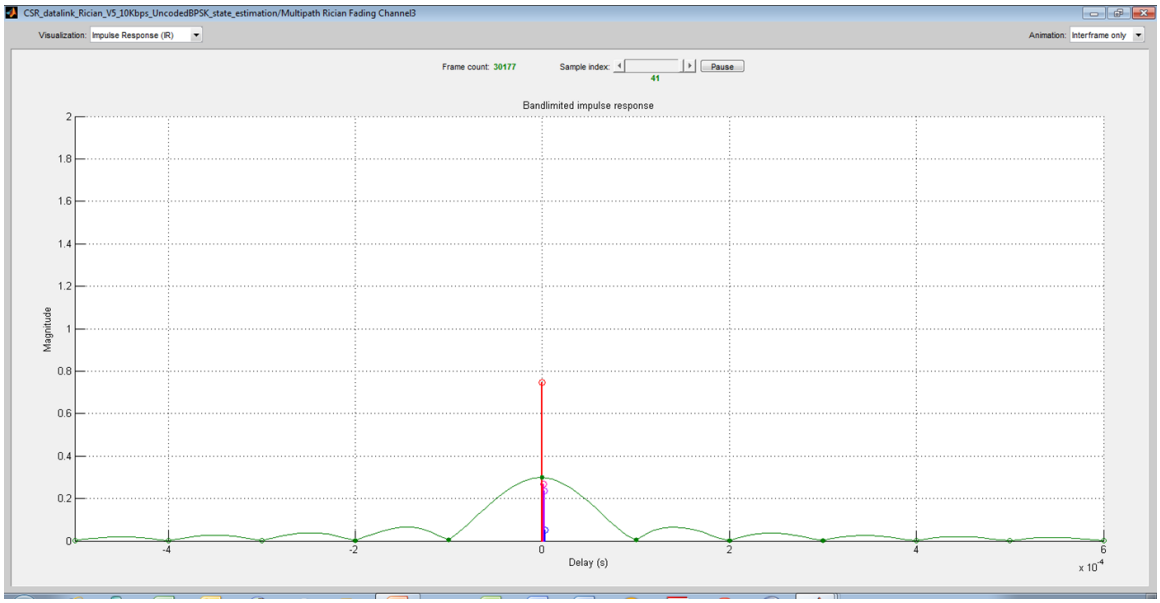

Figure A.9: State 3 Time-Variant Channel Impulse Response

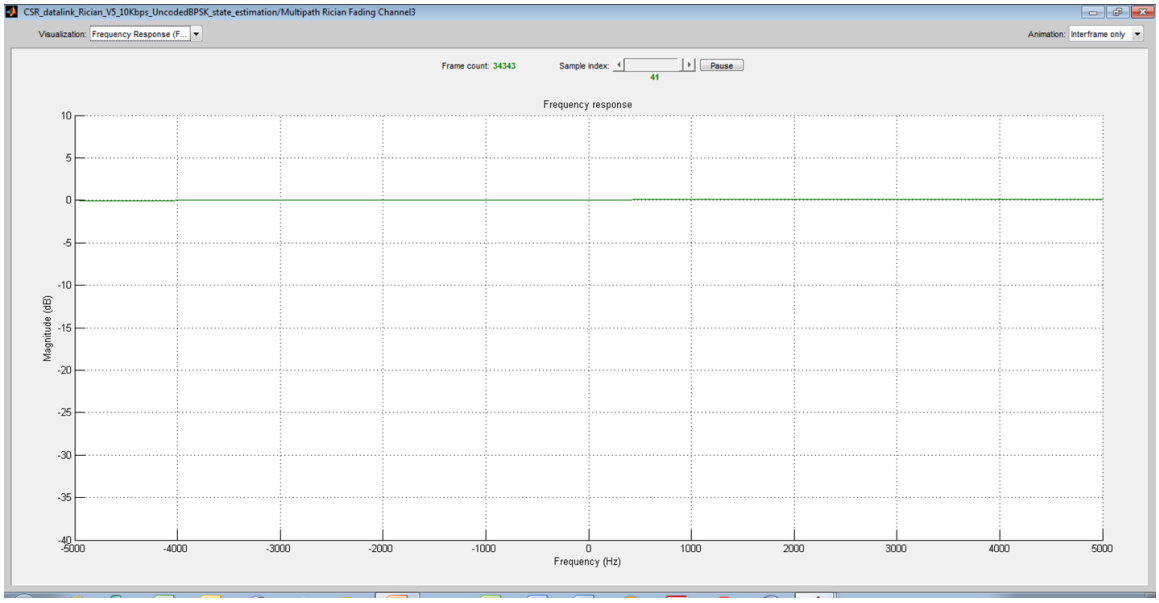

Figure A.10: State 3 Channel Frequency Response

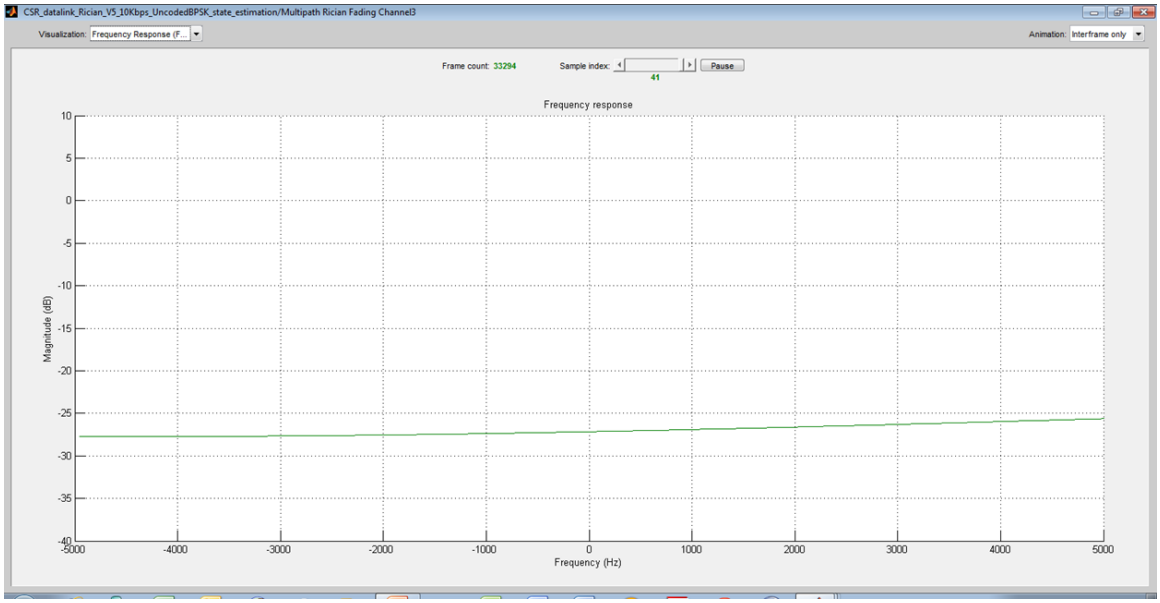

Figure A.11: State 3 Channel Frequency Response

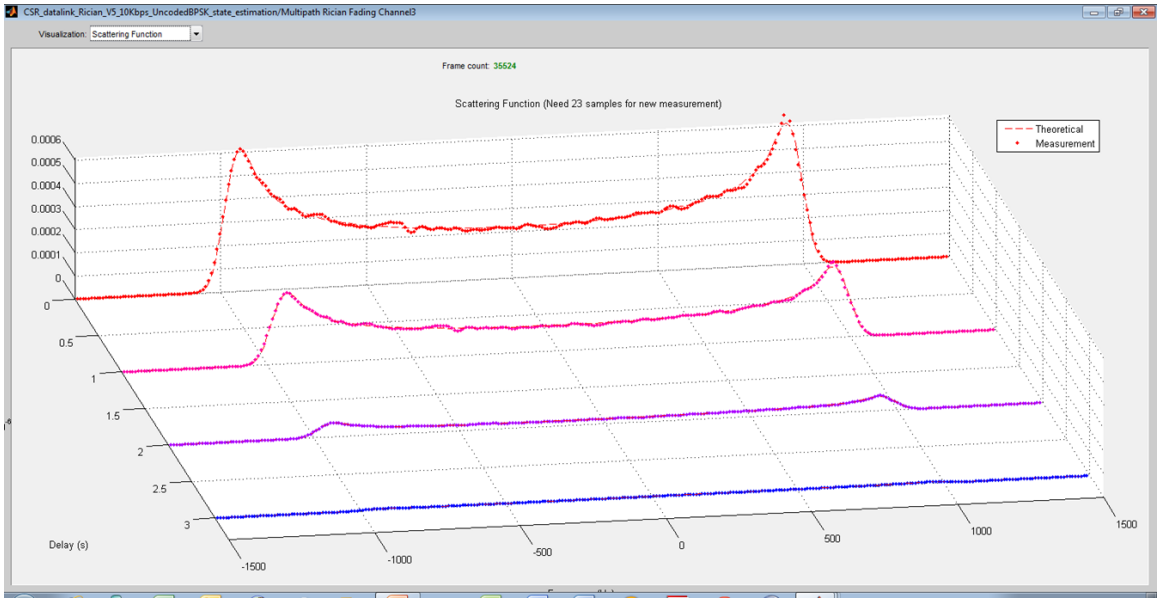

Figure A.12: State 3 Scattering Function

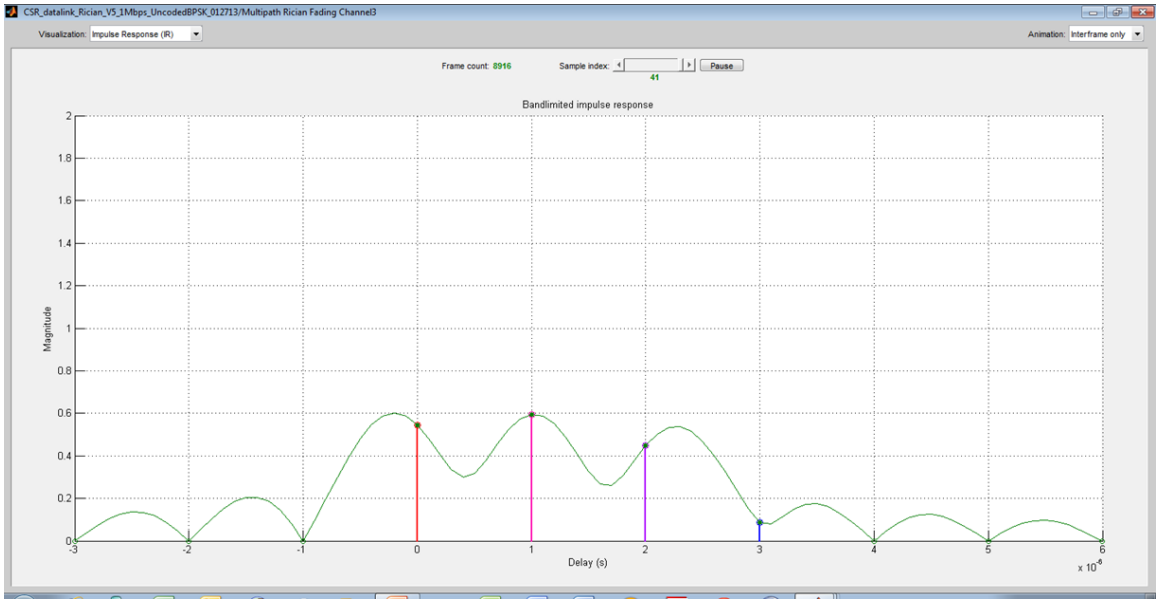

Figure A.13: State 4 Channel Impulse Response

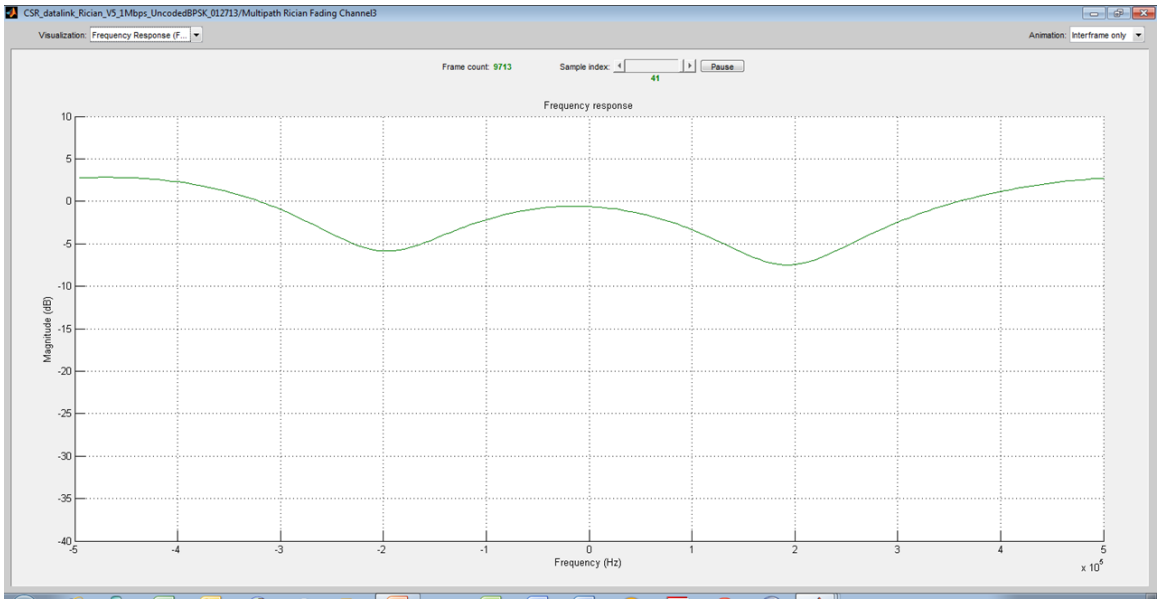

Figure A.14: State 4 Frequency Response

1-3, the diffuse DP is .01 KHz and the associated Tc of this state is ~42 seconds.

State 5 has been designed to be TS and FS. In Figures A.16 and A.17 snapshots of the state 5 time variant CIR is shown while in Figures A.18 and A.19 snapshots of the time-variant FR is shown. These figures highlight how the channel gain varies over the block period and how the frequency response is selective less than the block rate of 20 KHz. For this state, the multipath delay of this CIR is similar to state 3, and the resulting time dispersion is a significant percentage of the block period resulting in FS conditions. The multipath delay vector is [0 1e-3 2e-3 3e-3] while the multipath gain vector is [0 -3 -10 -20] dB. For this case, the RMS DS of state 3 is 1.75 e-3 seconds and the associated BWc is ~11.4 Hz.

In Figure A.20 the state 5 SF is observed. This SF reflects the frequency dispersion effects due to the diffuse DP which is a significant percentage of the block rate of 20 KHz. Similar to state 3 the diffuse DP is 1 KHz and the associated Tc of this state is ~423e-6 seconds.

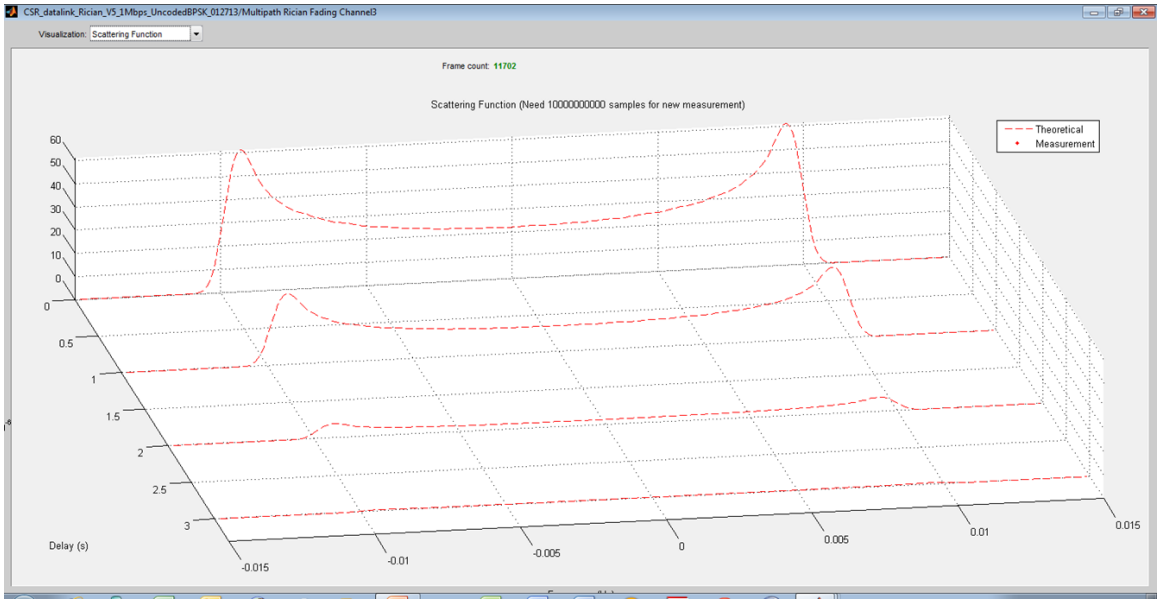

Figure A.15: State 4 Scattering Function

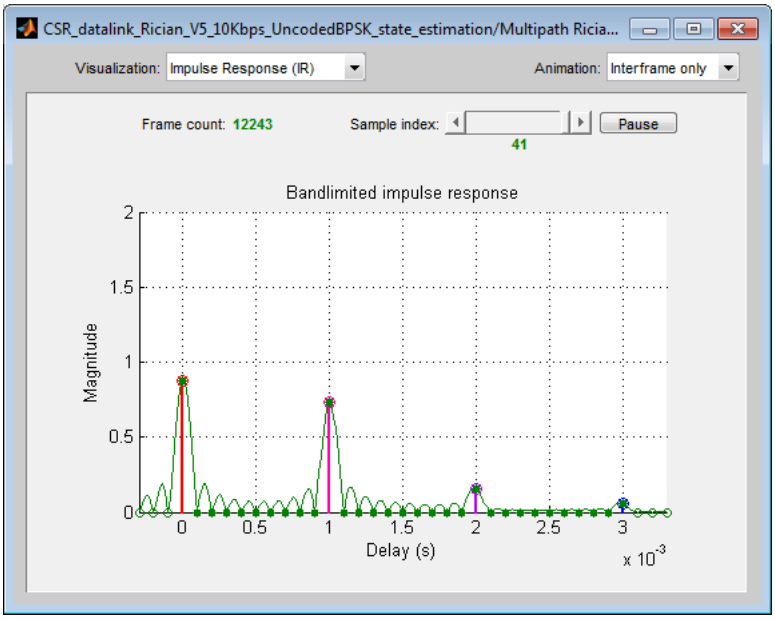

Figure A.16: State 5 Time-Variant Channel Impulse Response

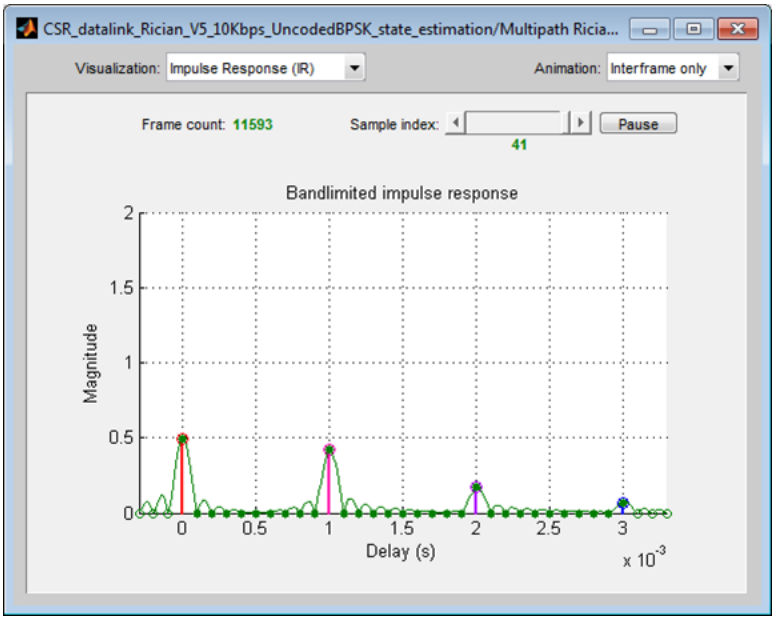

Figure A.17: State 5 Time-Variant Channel Impulse Response

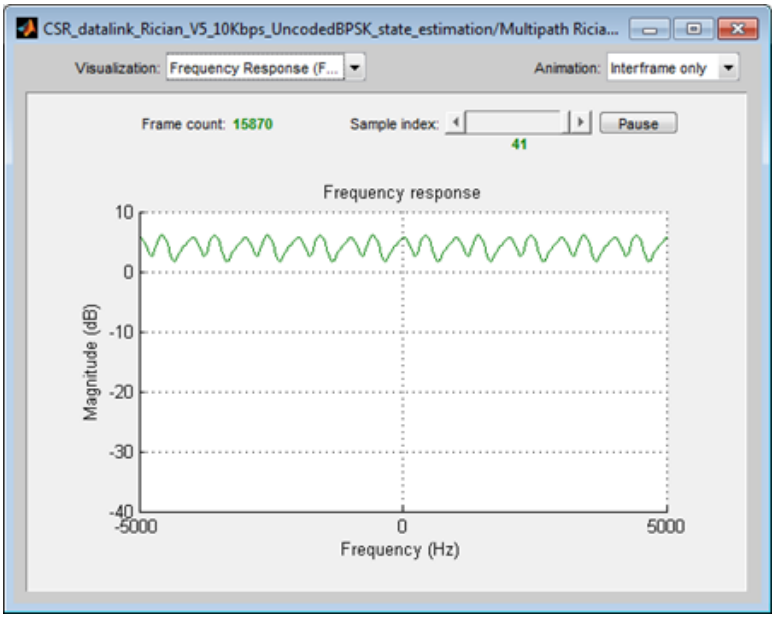

Figure A.18: State 5 Channel Frequency Response

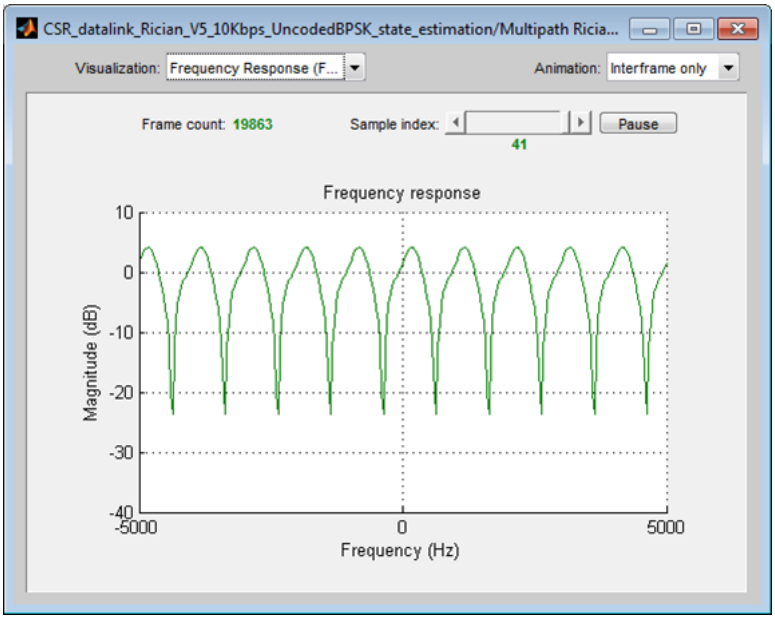

Figure A.19: State 5 Channel Frequency Response

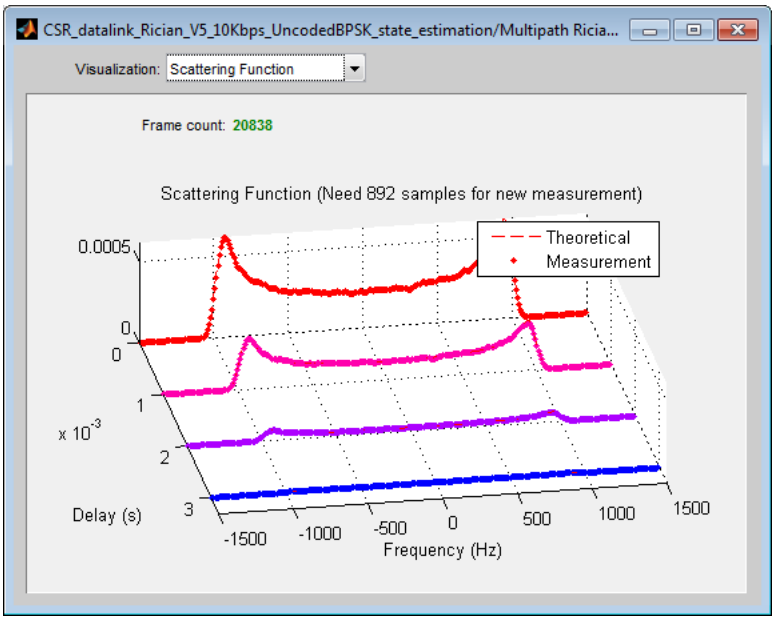

Figure A.20: State 5 Scattering Function

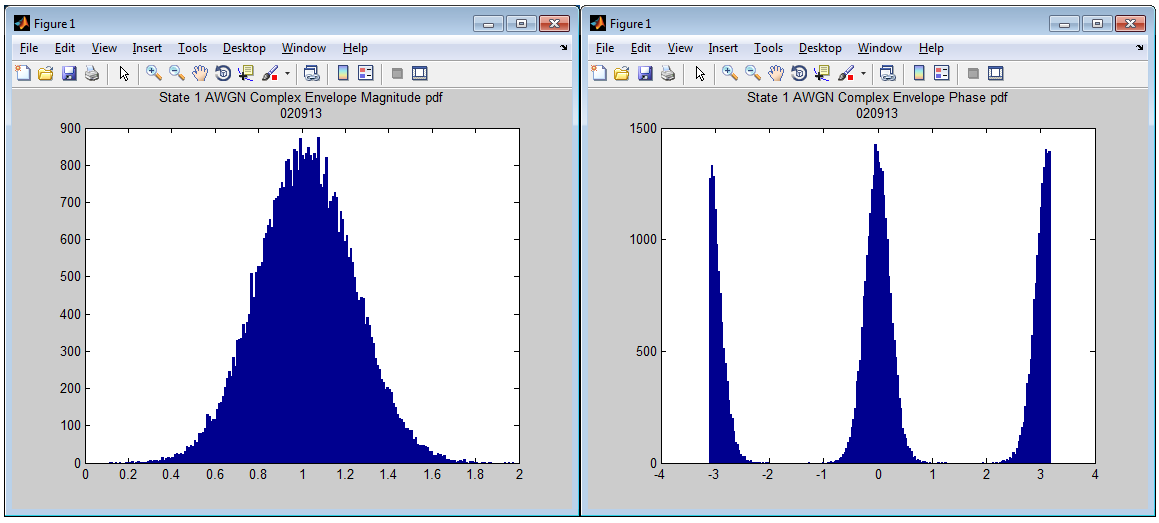

Figure A.21: State 1 Envelope

A.11.2 Waveform Statistical Feature Extraction

First Order Statistical Features

First order statistical features for the Coherence State Model (CSM), state 1 through state 5, are shown in Figures A.21 to A.25. Each of these figures display the complex envelope magnitude and phase PDF.

Waveform Second Order Statistical Features

State 1 Distributions The state 1 extracted waveform second order statistical features are shown in FiguresA.26 to Figure A.29. The estimated Tc magnitude and phase PDF shown in Figure A.26 were computed by an autocorrelation applied to the time domain waveform samples.

The state 1 estimated DP magnitude and phase are shown in Figure A.27. These were computed by applying an FFT to the Tc estimate.

The state 1 estimated BWc magnitude and phase are shown in Figure A.28. The BWc was estimated by an autocorrelation applied to the frequency domain waveform which was computed by applying an FFT the input waveform.

The state 1 estimated DS magnitude and phase are shown in Figure A.29. The DS was estimated

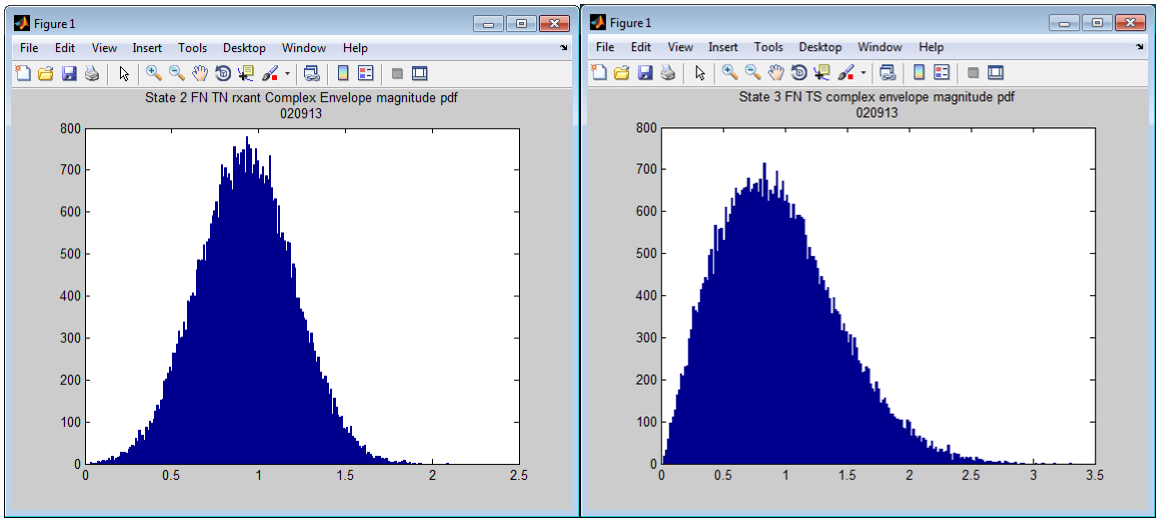

Figure A.22: State 2 Envelope

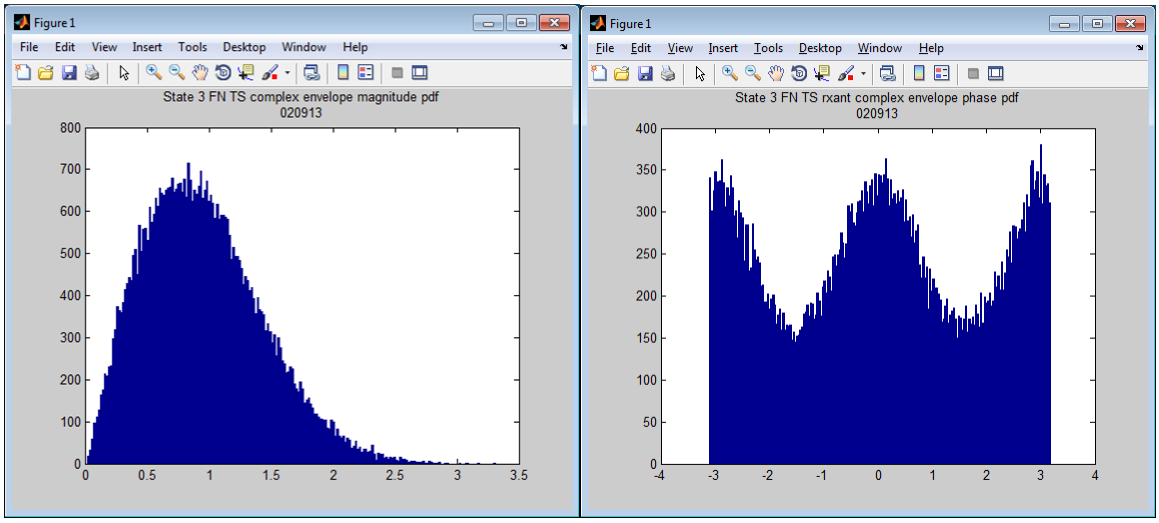

Figure A.23: State 3 Envelope

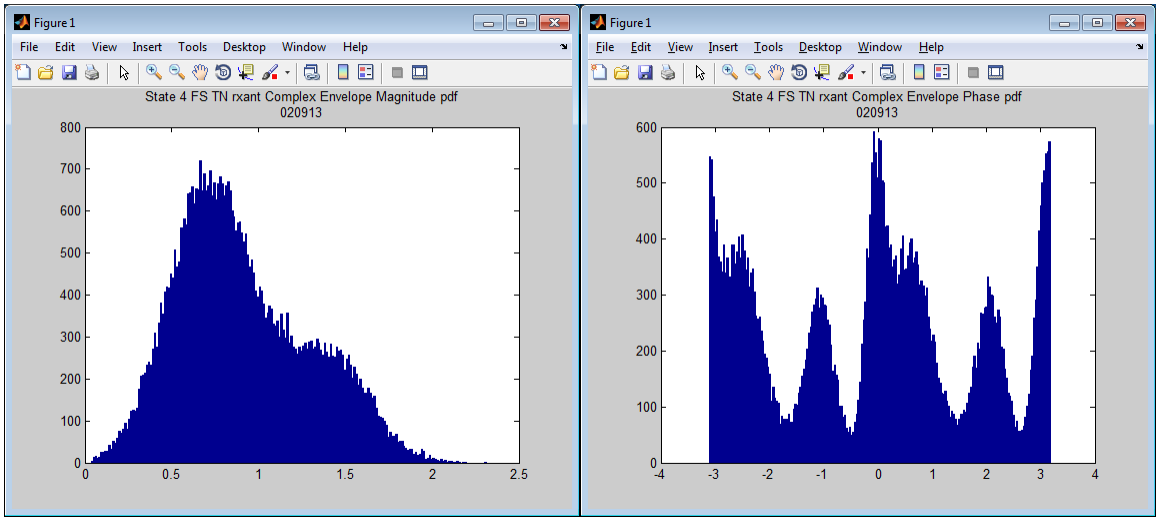

Figure A.24: State 4 Envelope

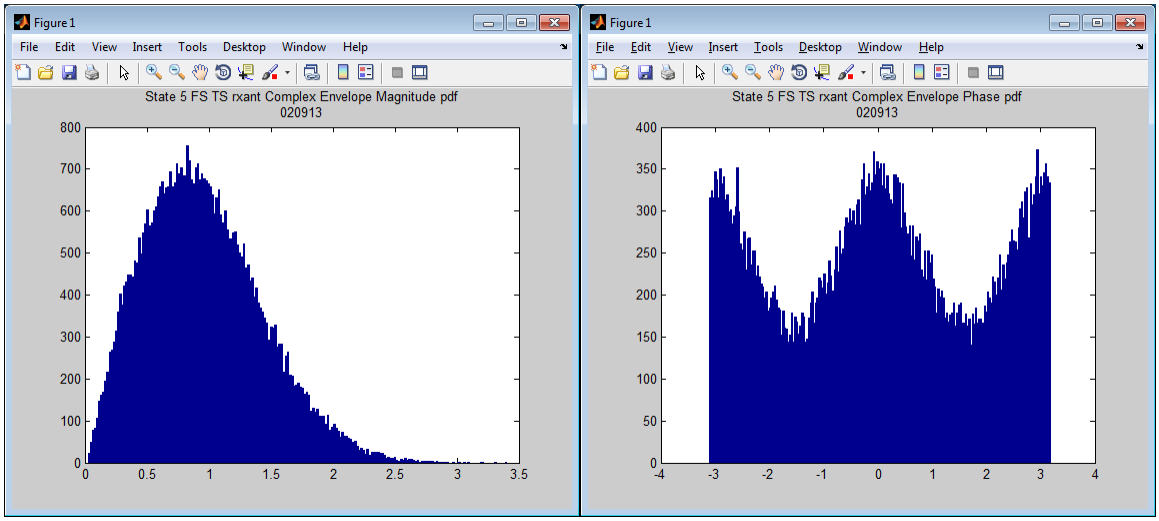

Figure A.25: State 5 Envelope

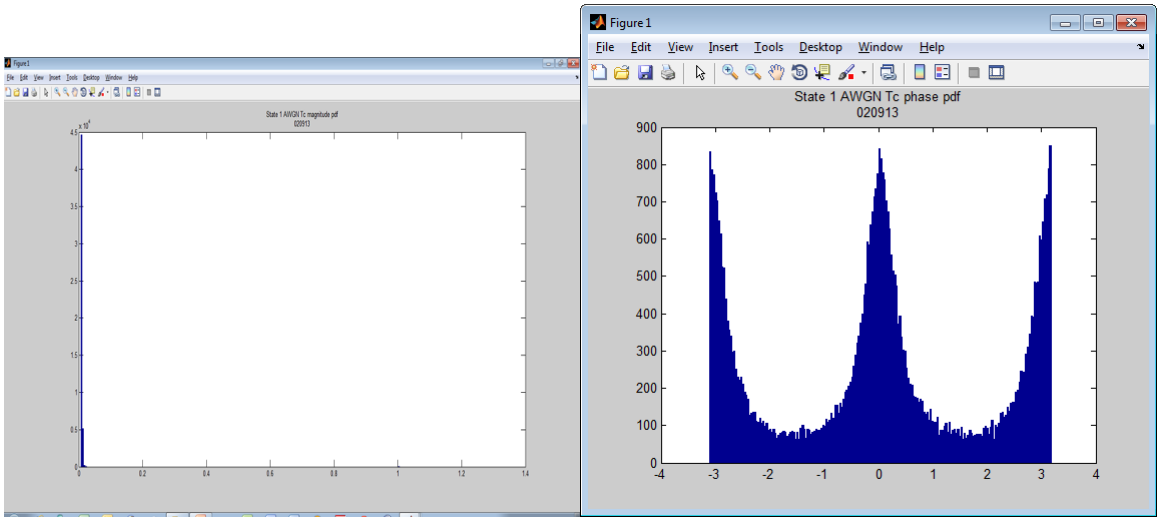

Figure A.26: State 1 Tc

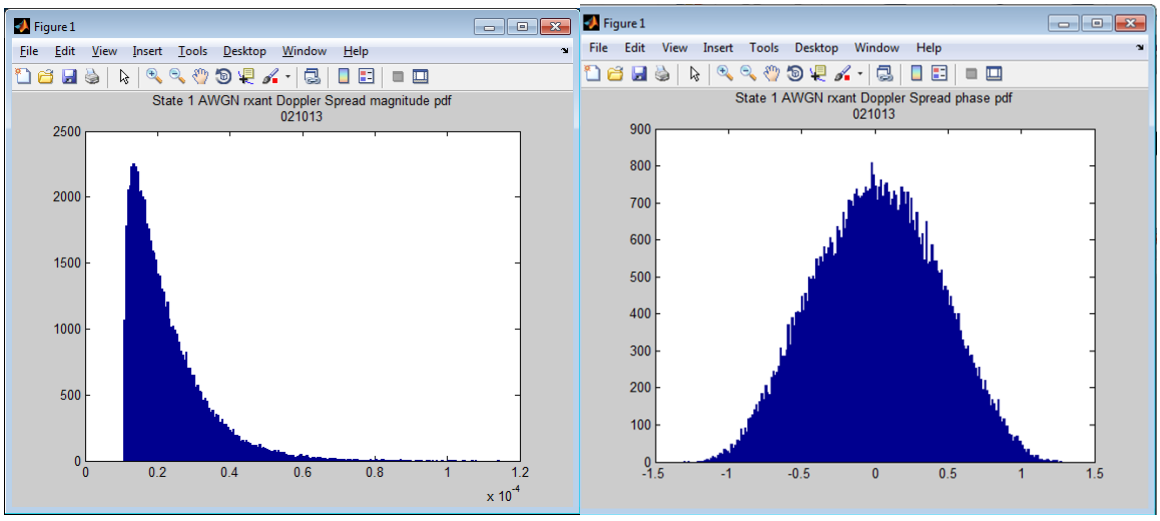

Figure A.27: State 1 DP

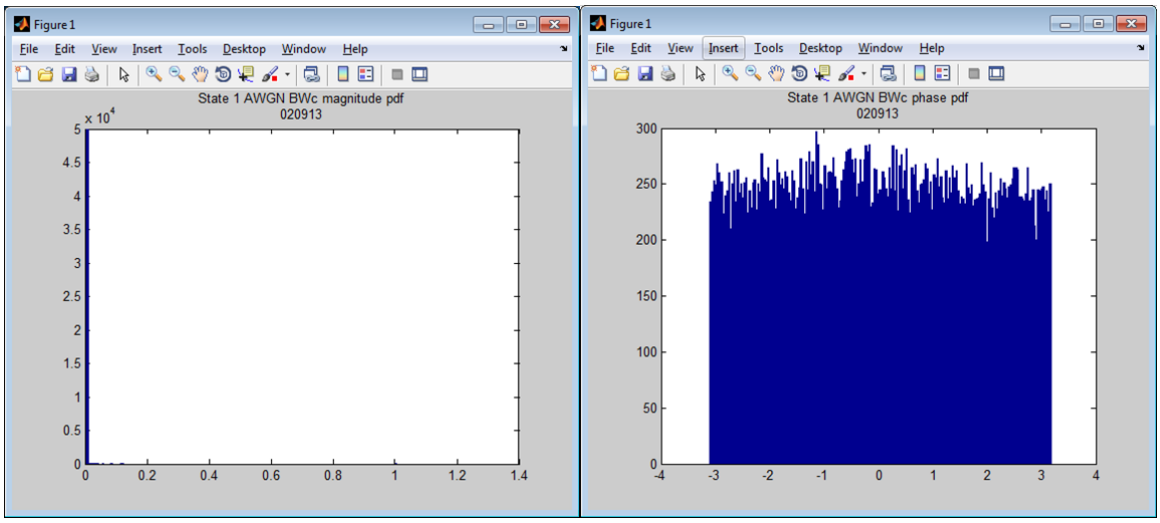

Figure A.28: State 1 BWc

by an inverse FFT applied to the BWc estimate.

State 2 Distributions The state 2 estimated Tc magnitude and phase PDFs are shown in Figure A.30 which were computed by an autocorrelation applied to the time domain input waveform samples.

The state 2 estimated DP magnitude and phase are shown in Figure A.31. These were computed by applying an FFT to the Tc estimate.

The state 2 estimated BWc magnitude and phase are shown in Figure A.32. The BWc was estimated by applying an autocorrelation to the frequency domain waveform which was computed by an FFT of the input waveform.

The state 2 estimated DS magnitude and phase are shown in Figure A.33. The DS was estimated by an inverse FFT applied to the BWc estimate.

State 3 Distributions The state 3 estimated Tc magnitude and phase pdfs are shown in Figure A.34 which were computed by an autocorrelation applied to the time domain input waveform samples.

The state 3 estimated DP magnitude and phase are shown in Figure A.35. These were computed

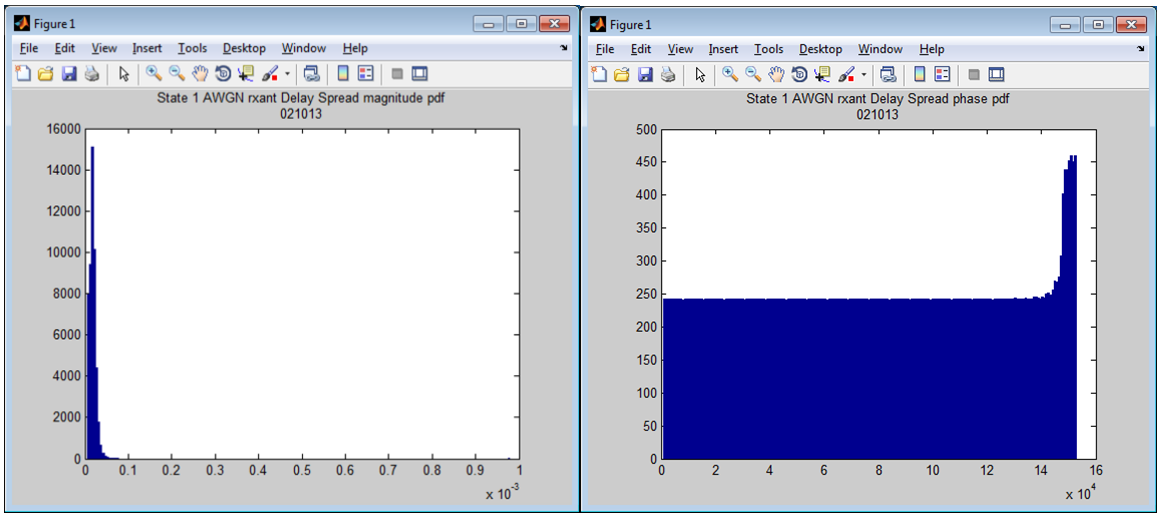

Figure A.29: State 1 DS

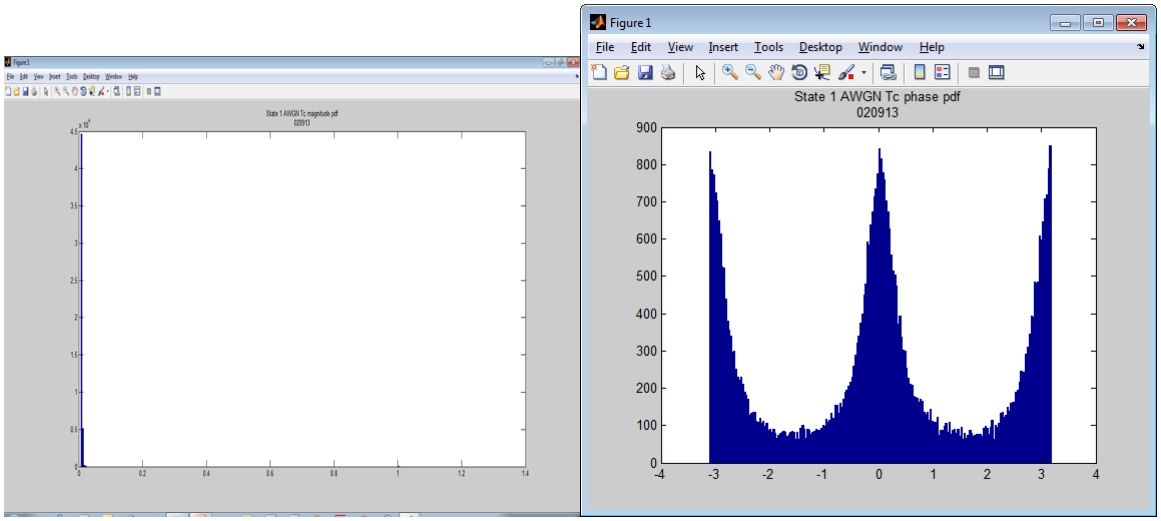

Figure A.30: State 2 Tc

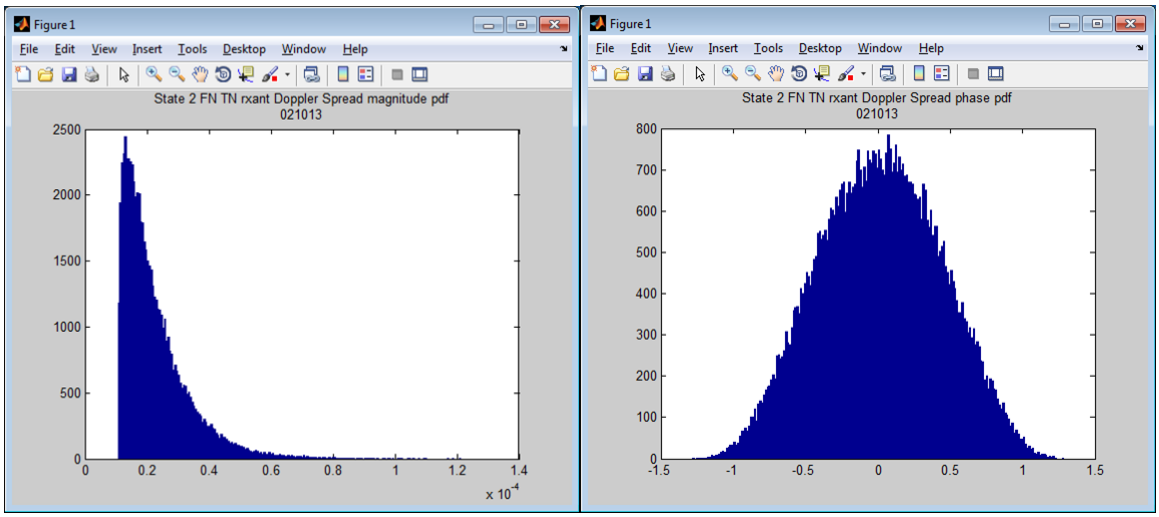

Figure A.31: State 2 DP

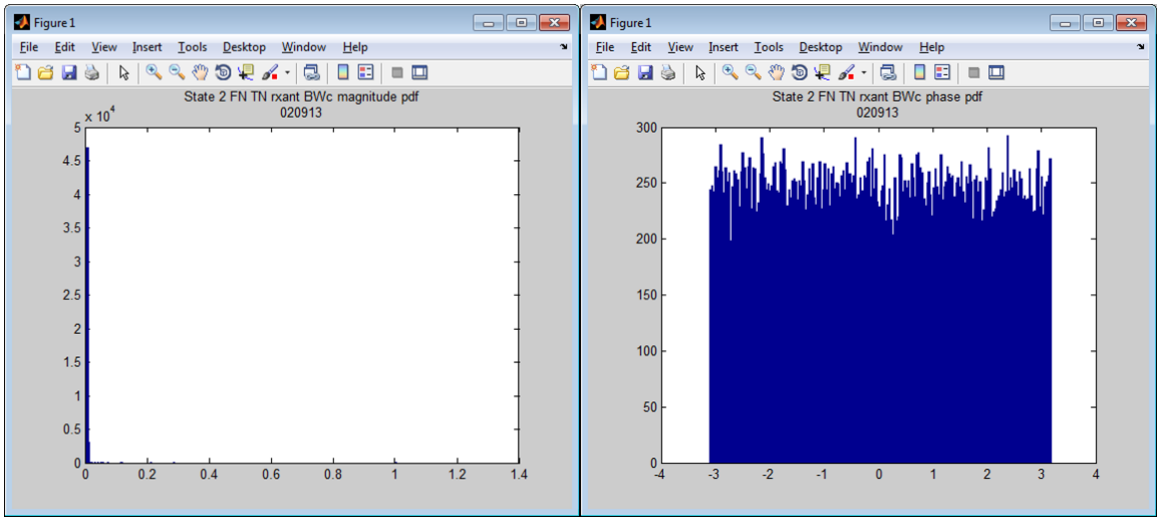

Figure A.32: State 2 BWc

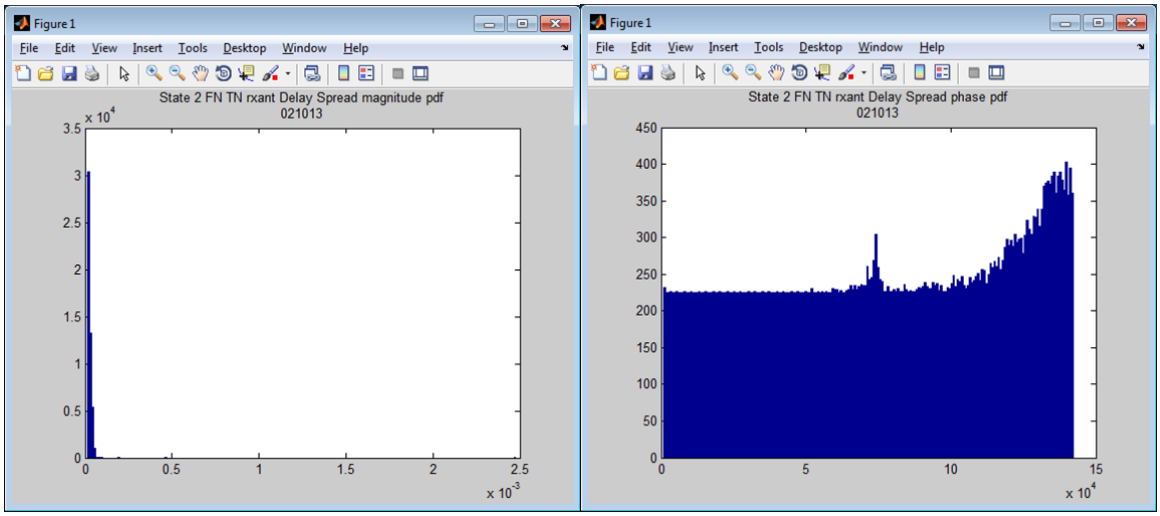

Figure A.33: State 2 DS

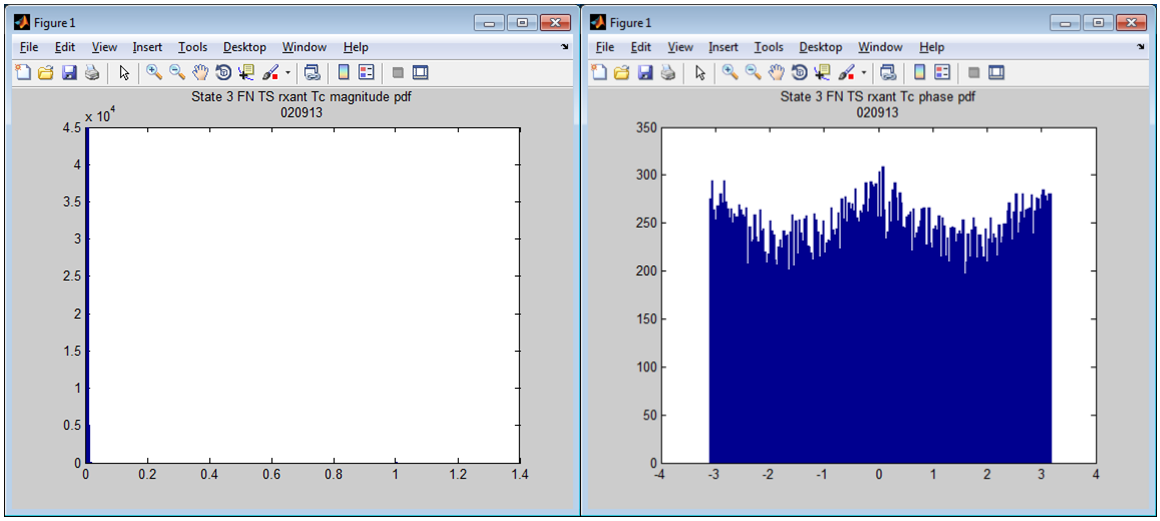

Figure A.34: State 3 Tc

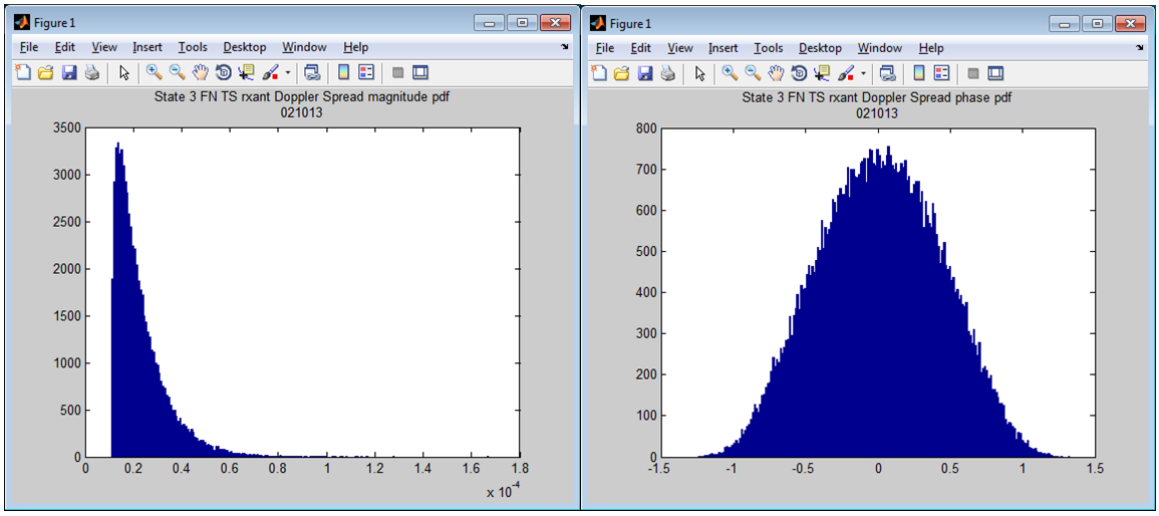

Figure A.35: State 3 DP

by applying an FFT to the Tc estimate.

The state 3 estimated BWc magnitude and phase are shown in Figure A.36. The BWc was estimated by applying an autocorrelation to the frequency domain waveform which was computed by an FFT of the input waveform.

The state 3 estimated DS magnitude and phase are shown in Figure A.37. The DS was estimated by an inverse FFT applied to the BWc estimate.

State 4 Distributions The state 4 estimated Tc magnitude and phase PDFs are shown in Figure A.38 which were computed by an autocorrelation applied to the time domain input waveform samples.

The state 4 estimated DP magnitude and phase are shown in Figure A.39. These were computed by applying an FFT to the Tc estimate.

The state 4 estimated BWc magnitude and phase are shown in Figure A.40. The BWc was estimated by applying an autocorrelation to the frequency domain waveform which was computed by an FFT of the input waveform.

The state 4 estimated DS magnitude and phase are shown in Figure A.41. The DS was estimated by an inverse FFT applied to the BWc estimate.

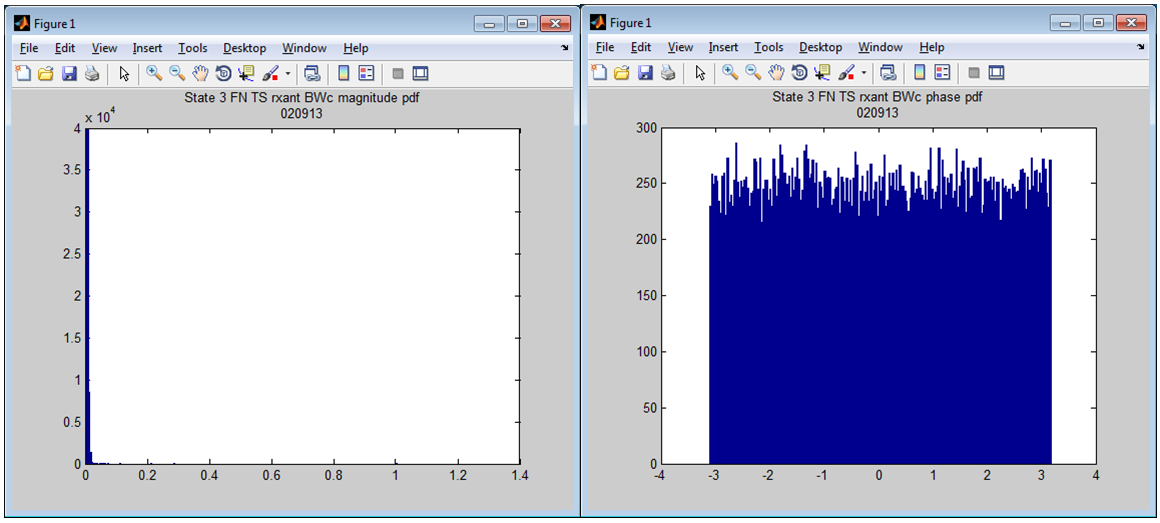

Figure A.36: State 3 BWc

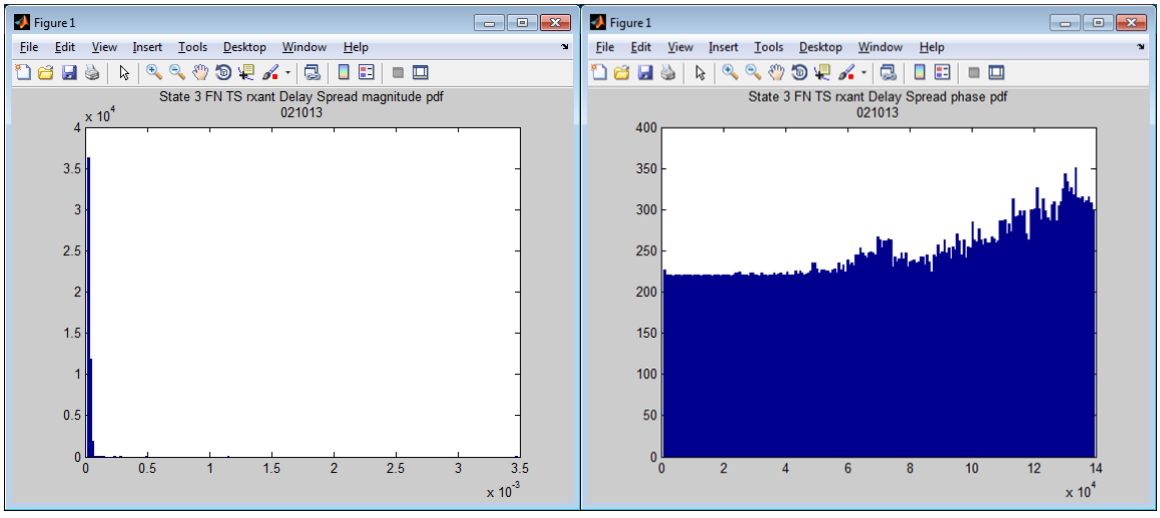

Figure A.37: State 3 DS

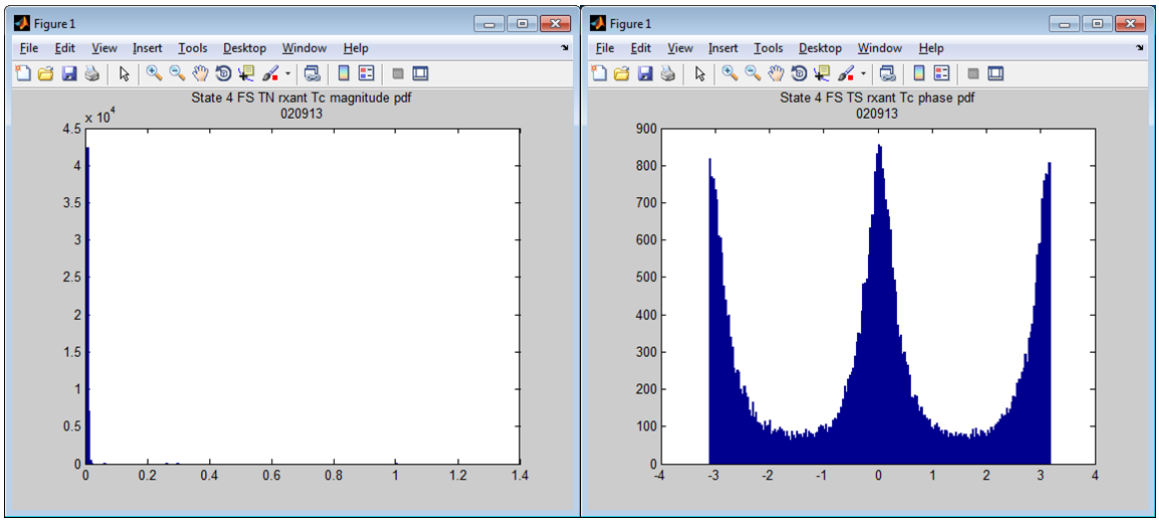

Figure A.38: State 4 Tc

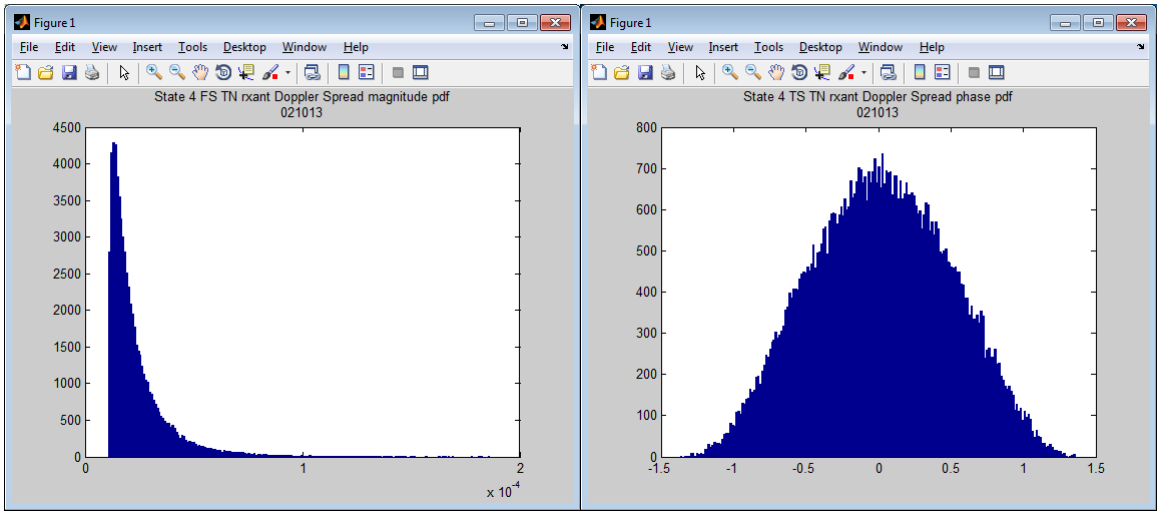

Figure A.39: State 4 DP

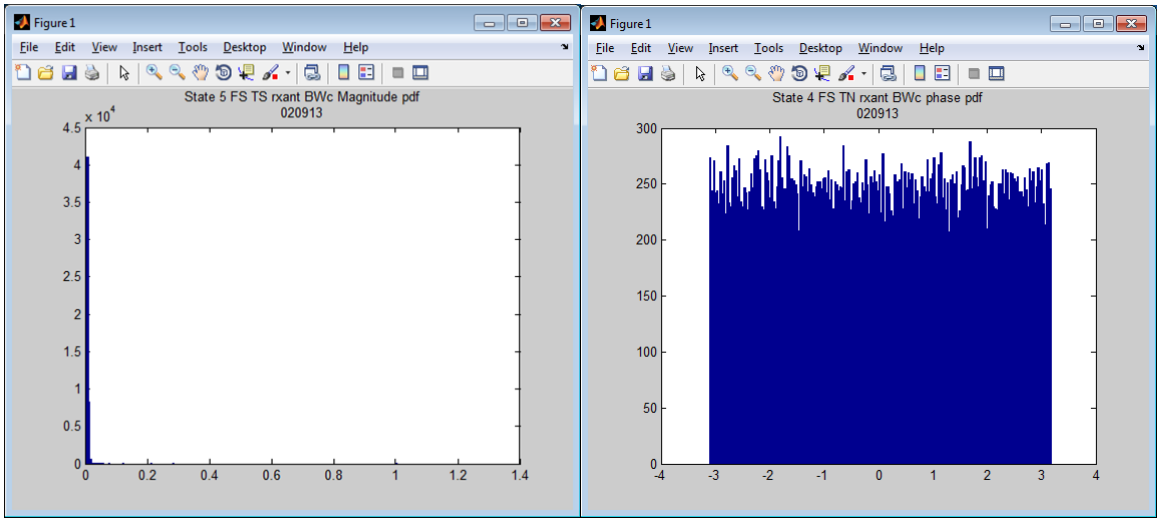

Figure A.40: State 4 BWc

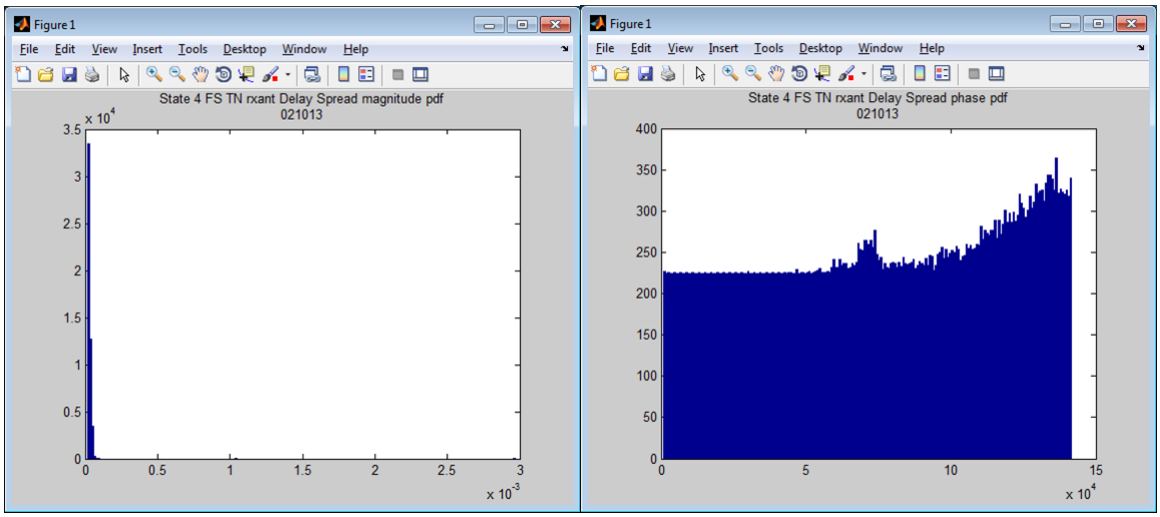

Figure A.41: State 4 DS

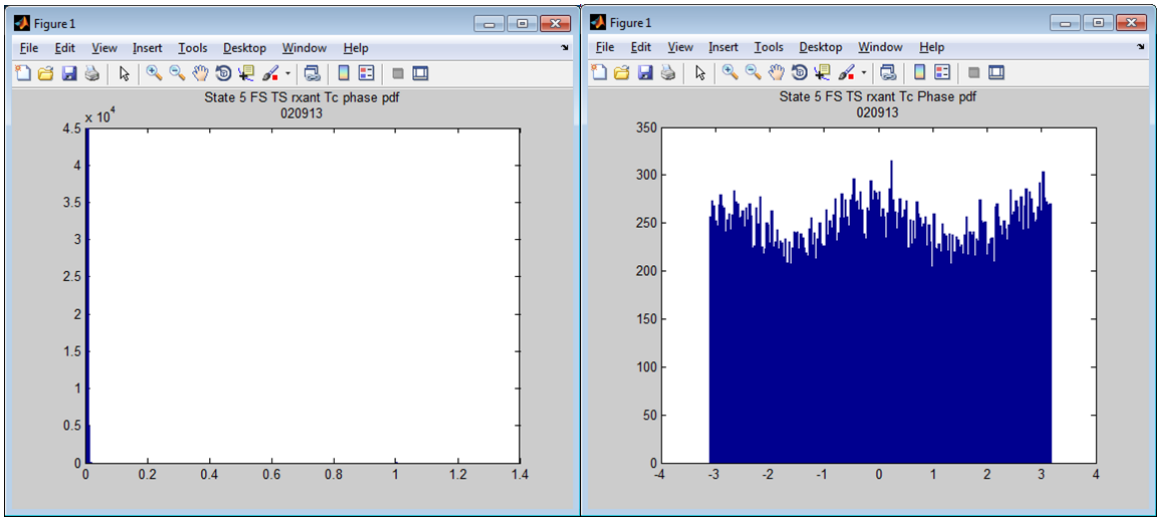

Figure A.42: State 5 Tc

State 5 Distributions The state 5 estimated Tc magnitude and phase PDFs are shown in Figure A.42 which were computed by an autocorrelation applied to the time domain input waveform samples.

The state 5 estimated DP magnitude and phase are shown in Figure A.43. These were computed by applying an FFT to the Tc estimate.

The state 5 estimated BWc magnitude and phase are shown in Figure A.44. The BWc was estimated by applying an autocorrelation to the frequency domain waveform which was computed by an FFT of the input waveform.

The state 5 estimated DS magnitude and phase are shown in Figure A.45. The DS was estimated by an inverse FFT applied to the BWc estimate.

A.11.3 State Likelihood Parameter Estimation

This section provides results for training each of the waveform statistical feature recognition HMMs. Training an HMM is a process of submiting input sequences to the HMM and estimating the probability of transitions between states, and also estimating the conditional probability between a state and the observable output. Two inputs were provided for each HMM training

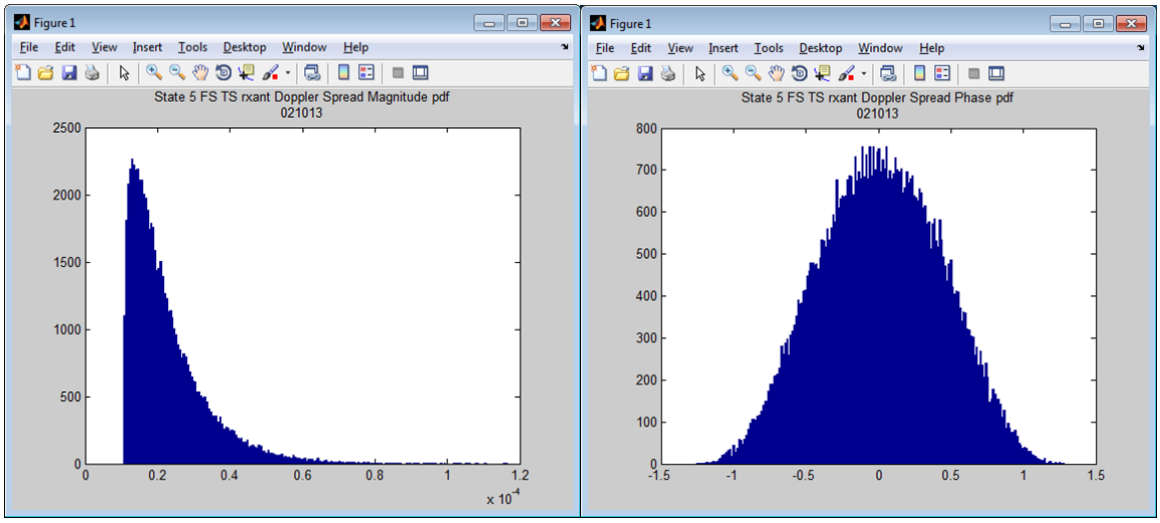

Figure A.43: State 5 DP

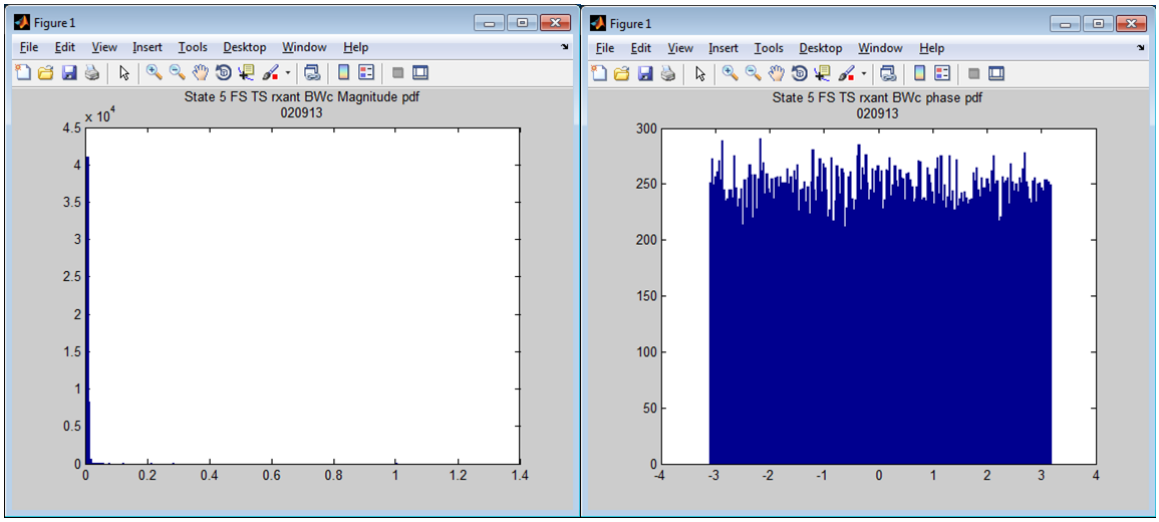

Figure A.44: State 5 BWc

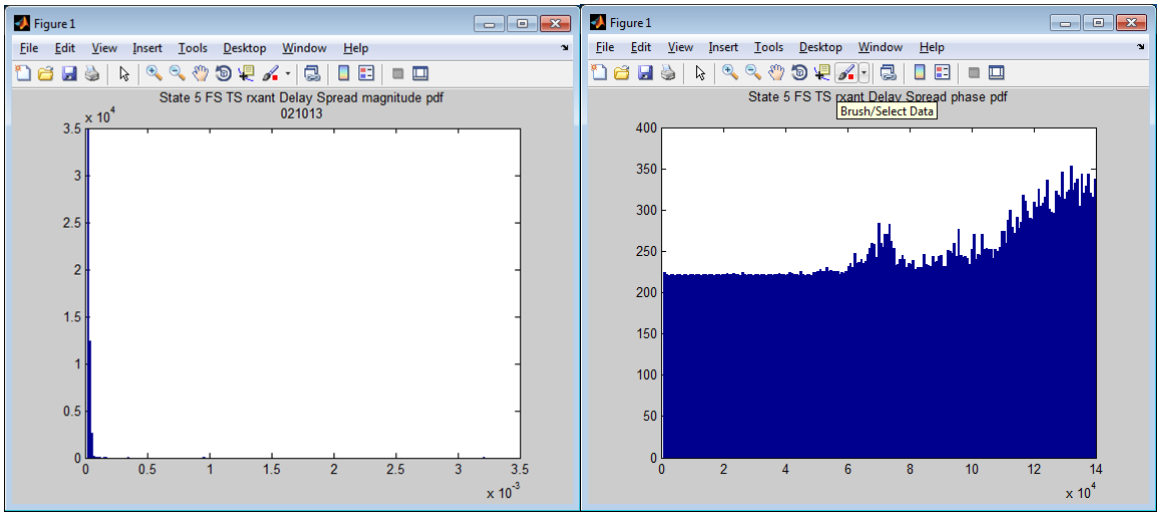

Figure A.45: State 5 DS

session: 1) sequence of symbols selected from a finite state alphabet with 200 symbols, and 2) sequence of associated hidden states. The output of the training process is the state transition and output probability matrices.

Complex Envelope Magnitude HMM

Figure A.46 provides the results of training the CEM HMM. The transition and output matrix are shown after training the HMM with a 250K sample sequence comprising waveform CEM features from state 1, 2, 3, 4, and 5. The output matrix is a 5x 200 element matrix whose rows have been plotted independently. Note the diversity in the output matrix which enhances the sensitivity of this HMM to changes between the MWC hidden states.

Envelope Phase HMM

Figure A.47provides the results of training the CEP HMM. The transition and output matrix are shown after training the HMM with a 250K sample sequence comprising waveform envelope phase features from state 1, 2, 3, 4, and 5. The output matrix is a 5x 200 element matrix whose rows have been plotted independently. Note the diversity in the output matrix which enhances the sensitivity of this HMM to changes between the MWC hidden states.

	1	2	3	4	5
1	0.9999	1.9998e-05	1.9998e-05	1.9998e-05	1.9998e-05
2	1.9998e-05	0.9999	1.9998e-05	1.9998e-05	1.9998e-05
3	1.9998e-05	1.9998e-05	0.9999	1.9998e-05	1.9998e-05
4	1.9998e-05	1.9998e-05	1.9998e-05	0.9999	1.9998e-05
5	1.9998e-05	1.9998e-05	1.9998e-05	1.9998e-05	0.9999

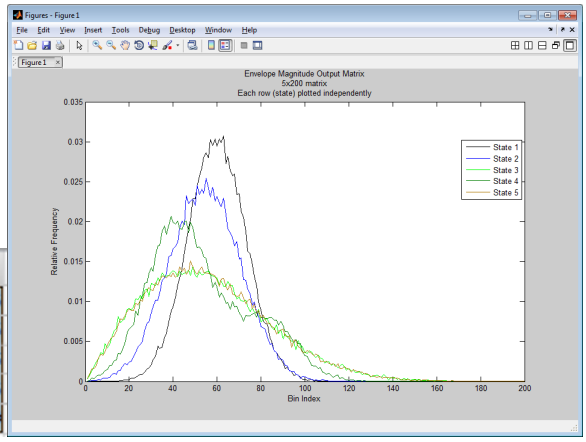

Figure A.46: CEM HMM Parameters

	1	2	3	4	5
1	0.9999	1.9998e-05	1.9998e-05	1.9998e-05	1.9998e-05
2	1.9998e-05	0.9999	1.9998e-05	1.9998e-05	1.9998e-05
3	1.9998e-05	1.9998e-05	0.9999	1.9998e-05	1.9998e-05
4	1.9998e-05	1.9998e-05	1.9998e-05	0.9999	1.9998e-05
5	1.9998e-05	1.9998e-05	1.9998e-05	1.9998e-05	0.9999

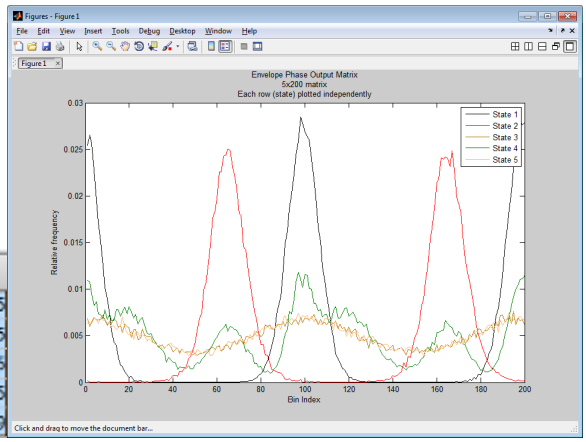

Figure A.47: CEM

	1	2	3	4	5
1	0.9999	1.9998e-05	1.9998e-05	1.9998e-05	1.9998e-05
2	1.9998e-05	0.9999	1.9998e-05	1.9998e-05	1.9998e-05
3	1.9998e-05	1.9998e-05	0.9999	1.9998e-05	1.9998e-05
4	1.9998e-05	1.9998e-05	1.9998e-05	0.9999	1.9998e-05
5	1.9998e-05	1.9998e-05	1.9998e-05	1.9998e-05	0.9999

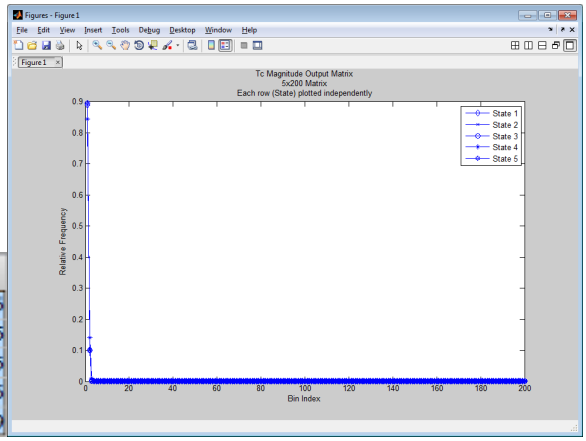

Figure A.48: TcM HMM Parameters

Tc Magnitude HMM

Figure A.48provides the results of training the TcM HMM. The transition and output matrix are shown after training the HMM with a 250K sample sequence comprising waveform Tc magnitude features from state 1, 2, 3, 4, and 5. The output matrix is a 5x 200 element matrix whose rows have been plotted independently. Note the lack of diversity in the magnitude output matrix which degrades the sensitivity of this HMM to changes between the MWC hidden states reducing its effectiveness.

Tc Phase HMM

Figure A.49provides the results of training the TcP HMM. The transition and output matrix are shown after training the HMM with a 250K sample sequence comprising waveform TcP features from state 1, 2, 3, 4, and 5. The output matrix is a 5x 200 element matrix whose rows have been plotted independently. Note the partitioning of the output response into two groups that lack diversity in the phase output matrix. This will degrade the sensitivity of this HMM to changes between the MWC hidden states within each group reducing its effectiveness.

	1	2	3	4	5
1	0.9999	1.9998e-05	1.9998e-05	1.9998e-05	1.9998e-05
2	1.9998e-05	0.9999	1.9998e-05	1.9998e-05	1.9998e-05
3	1.9998e-05	1.9998e-05	0.9999	1.9998e-05	1.9998e-05
4	1.9998e-05	1.9998e-05	1.9998e-05	0.9999	1.9998e-05
5	1.9998e-05	1.9998e-05	1.9998e-05	1.9998e-05	0.9999

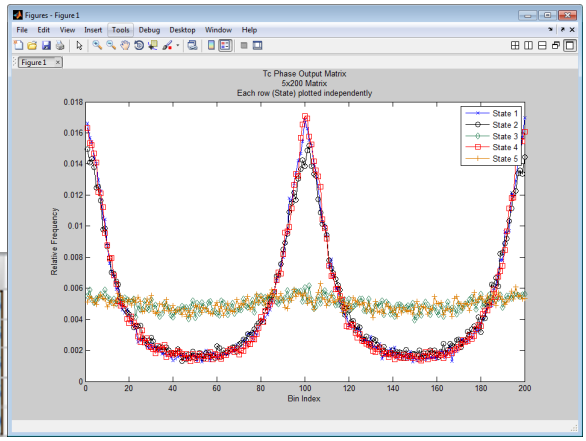

Figure A.49: TcP HMM Parameters

	1	2	3	4	5
1	0.9999	1.5258e-05	1.5258e-05	1.5258e-05	1.5258e-05
2	1.5258e-05	0.9999	1.5258e-05	1.5258e-05	1.5258e-05
3	1.5258e-05	1.5258e-05	0.9999	1.5258e-05	1.5258e-05
4	1.5258e-05	1.5258e-05	1.5258e-05	0.9999	1.5258e-05
5	1.5258e-05	1.5258e-05	1.5258e-05	1.5258e-05	0.9999

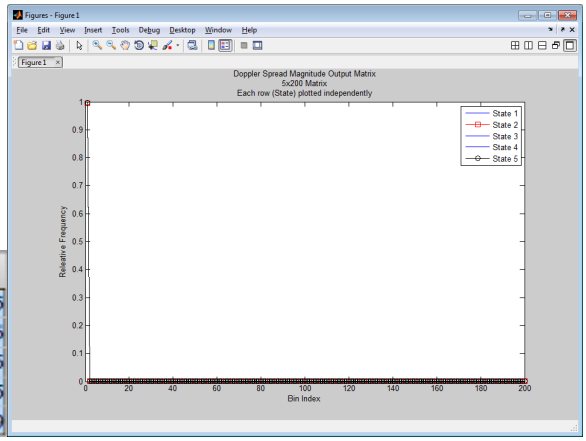

Figure A.50: DPM HMM Parameters

Doppler Spread Magnitude HMM

Figure A.60provides the results of training the envelope magnitude HMM. The transition and output matrix are shown after training the HMM with a 250K sample sequence comprising waveform Doppler spread features from state 1, 2, 3, 4, and 5. The output matrix is a 5x 200 element matrix whose rows have been plotted independently. Note the lack of diversity in the magnitude output matrix which degrades the sensitivity of this HMM to changes between the MWC hidden states reducing its effectiveness.

	1	2	3	4	5
1	0.9999	1.5258e-05	1.5258e-05	1.5258e-05	1.5258e-05
2	1.5258e-05	0.9999	1.5258e-05	1.5258e-05	1.5258e-05
3	1.5258e-05	1.5258e-05	0.9999	1.5258e-05	1.5258e-05
4	1.5258e-05	1.5258e-05	1.5258e-05	0.9999	1.5258e-05
5	1.5258e-05	1.5258e-05	1.5258e-05	1.5258e-05	0.9999

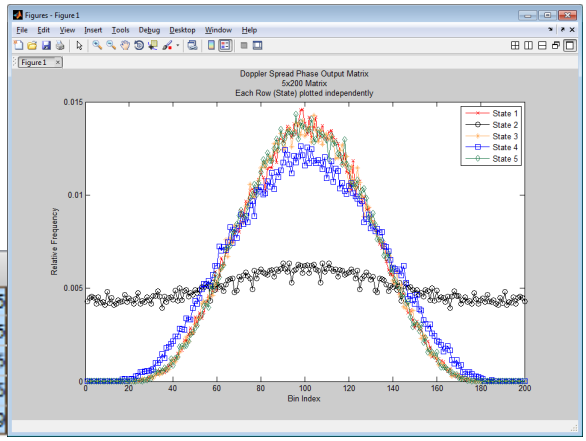

Figure A.51: DPP HMM Parameters

Doppler Spread Phase HMM

Figure A.51provides the results of training the envelope magnitude HMM. The transition and output matrix are shown after training the HMM with a 250K sample sequence comprising waveform Doppler spread phase features from state 1, 2, 3, 4, and 5. The output matrix is a 5x 200 element matrix whose rows have been plotted independently. Note the stratification of the magnitude output matrix into two groups with similar features which degrades the sensitivity of this HMM to changes between the MWC hidden states within each group reducing its effectiveness.

BWc Magnitude HMM

Figure A.52provides the results of training the envelope magnitude HMM. The transition and output matrix are shown after training the HMM with a 250K sample sequence comprising waveform BWM features from state 1, 2, 3, 4, and 5. The output matrix is a 5x 200 element matrix whose rows have been plotted independently. Note the lack of diversity in the magnitude output matrix which degrades the sensitivity of this HMM to changes between the MWC hidden states reducing its effectiveness.

	1	2	3	4	5
1	0.9999	1.9998e-05	1.9998e-05	1.9998e-05	1.9998e-05
2	1.9998e-05	0.9999	1.9998e-05	1.9998e-05	1.9998e-05
3	1.9998e-05	1.9998e-05	0.9999	1.9998e-05	1.9998e-05
4	1.9998e-05	1.9998e-05	1.9998e-05	0.9999	1.9998e-05
5	1.9998e-05	1.9998e-05	1.9998e-05	1.9998e-05	0.9999

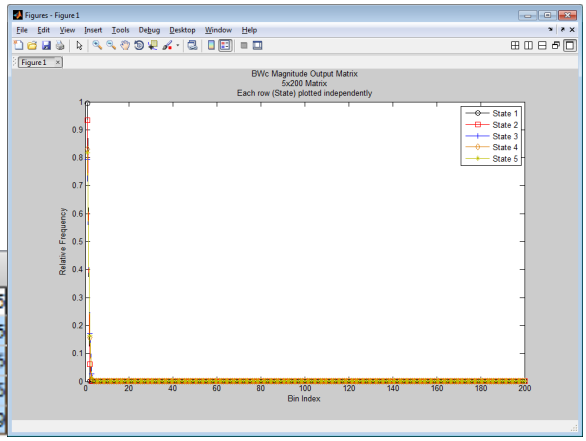

Figure A.52: BWM HMM Parameters

	1	2	3	4	5
1	0.9999	1.9998e-05	1.9998e-05	1.9998e-05	1.9998e-05
2	1.9998e-05	0.9999	1.9998e-05	1.9998e-05	1.9998e-05
3	1.9998e-05	1.9998e-05	0.9999	1.9998e-05	1.9998e-05
4	1.9998e-05	1.9998e-05	1.9998e-05	0.9999	1.9998e-05
5	1.9998e-05	1.9998e-05	1.9998e-05	1.9998e-05	0.9999

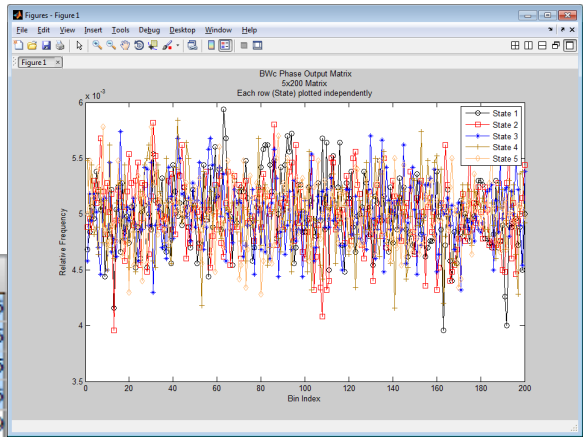

Figure A.53: BWP HMM Parameters

BWc Phase HMM

Figure A.53provides the results of training the envelope magnitude HMM. The transition and output matrix are shown after training the HMM with a 250K sample sequence comprising waveform BWP features from state 1, 2, 3, 4, and 5. The output matrix is a 5x 200 element matrix whose rows have been plotted independently. Note the diversity in the output matrix which enhances the sensitivity of this HMM to changes between the MWC hidden states.

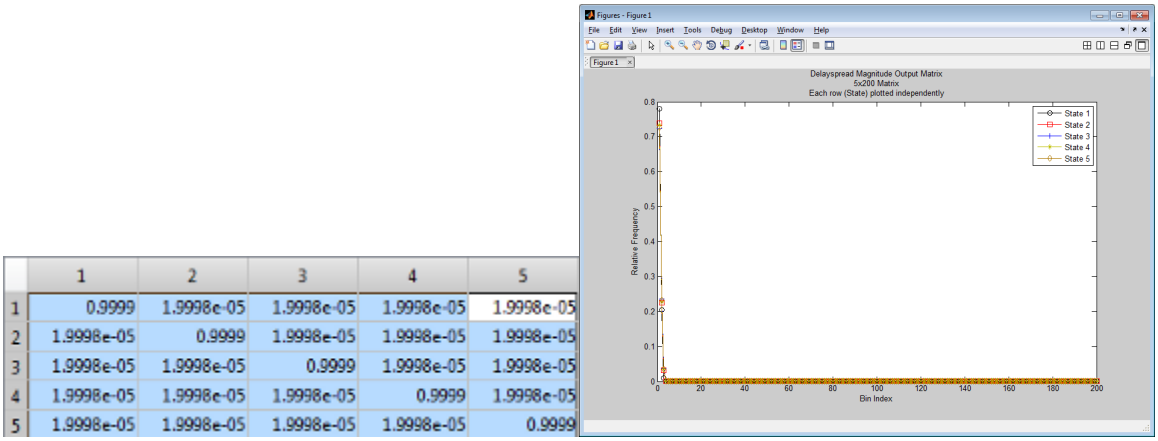

	1	2	3	4	5
1	0.9999	1.9998e-05	1.9998e-05	1.9998e-05	1.9998e-05
2	1.9998e-05	0.9999	1.9998e-05	1.9998e-05	1.9998e-05
3	1.9998e-05	1.9998e-05	0.9999	1.9998e-05	1.9998e-05
4	1.9998e-05	1.9998e-05	1.9998e-05	0.9999	1.9998e-05
5	1.9998e-05	1.9998e-05	1.9998e-05	1.9998e-05	0.9999

Figure A.54: DSM HMM Parameters

Delay Spread Magnitude HMM

Figure A.64provides the results of training the envelope magnitude HMM. The transition and output matrix are shown after training the HMM with a 250K sample sequence comprising waveform delay spread features from state 1, 2, 3, 4, and 5. The output matrix is a 5x 200 element matrix whose rows have been plotted independently. Note the lack of diversity in the magnitude output matrix which degrades the sensitivity of this HMM to changes between the MWC hidden states reducing its effectiveness.

Delay Spread Phase HMM

Figure A.65provides the results of training the envelope magnitude HMM. The transition and output matrix are shown after training the HMM with a 250K sample sequence comprising waveform delay spread features from state 1, 2, 3, 4, and 5. The output matrix is a 5x 200 element matrix whose rows have been plotted independently. Note the lack of diversity in the magnitude output matrix which degrades the sensitivity of this HMM to changes between the MWC hidden states reducing its effectiveness.

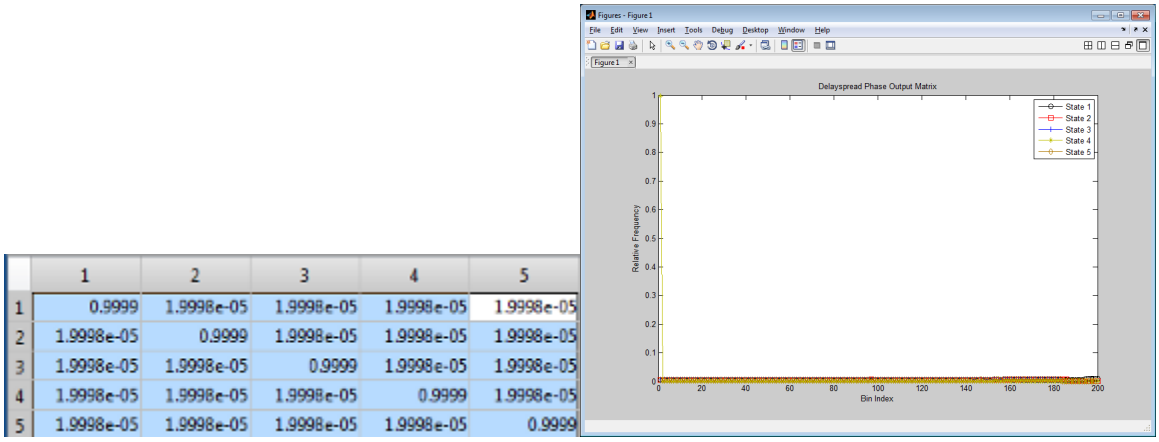

	1	2	3	4	5
1	0.9999	1.9998e-05	1.9998e-05	1.9998e-05	1.9998e-05
2	1.9998e-05	0.9999	1.9998e-05	1.9998e-05	1.9998e-05
3	1.9998e-05	1.9998e-05	0.9999	1.9998e-05	1.9998e-05
4	1.9998e-05	1.9998e-05	1.9998e-05	0.9999	1.9998e-05
5	1.9998e-05	1.9998e-05	1.9998e-05	1.9998e-05	0.9999

Figure A.55: DSP HMM Parameters

A.11.4 CSM State Likelihood Estimation

This section provides results generated by passing 5 different state sequences through each of the trained HMMs. Given that each HMM has been trained with a sequence of features, any input sequence to the HMM can be compared for likelihood that the input statistically matches the training sequences. Responses that approach a value of 1 indicate a strong likelihood that the two sequences stastically are similar will a value approaching 0 indicate a strong likelihood that the two sample sequences are dissimilar.

State Sequence 12345

The results in this section show HMM recognition of states within the statistics of each feature sequence.

Complex Envelope Magnitude Figure A.76 illustrates the detection of each state in the CEM sequence. Note that this HMM successfully recognized the first 50K samples as state 1, the next 50K samples as state 2, etc. Note that there are some fluctuations within each state and false detections within other states reducing accuracy and contributing to Type I and Type II errors.

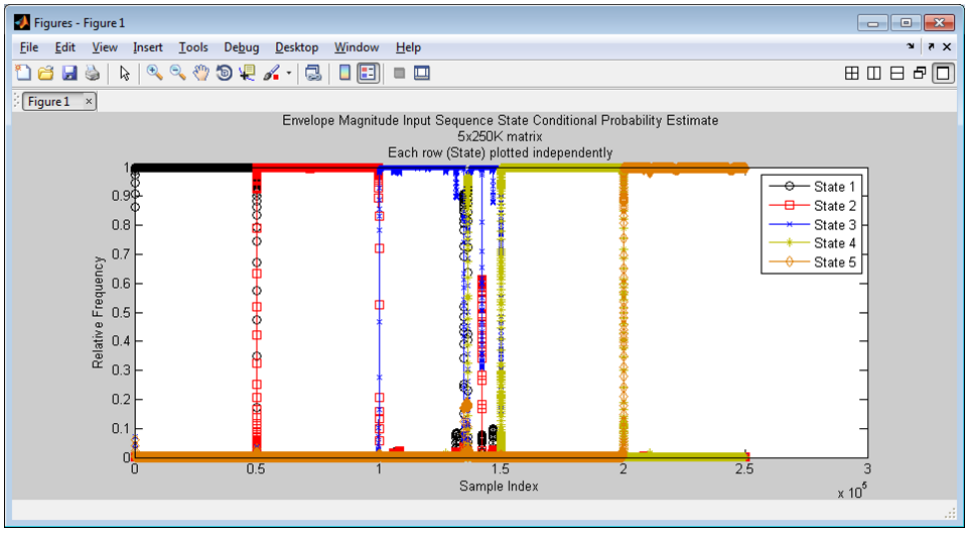

Figure A.56: CEM Sequence Recognition

Complex Envelope Phase Figure A.57 illustrates the detection of each state in the CEP sequence. Note that this HMM successfully recognized the first 50K samples as state 1, the next 50K samples as state 2, etc. Note that there are some fluctuations within each state and false detections within other states reducing accuracy and contributing to Type I and Type II errors.

Tc Magnitude Figure A.58 illustrates the detection of each state in the TcM sequence. Note that this HMM did not recognize the first 50K samples as state 1, the next 50K samples were not recognized as state 2, etc. Note that there is only a partial detection within each state and false detections within other states reducing accuracy and contributing to Type I and Type II errors.

Tc Phase Figure A.59 illustrates the detection of each state in the TcP sequence. Note that this HMM recognized the first 50K samples as state 1, the next 50K samples were recognized as state 2, etc. Note that there are fluctuations within each state and false detections within other states reducing accuracy and contributing to Type I and Type II errors.

Doppler Spread Magnitude Figure A.60 illustrates the detection of each state in the DPM sequence. Note that this HMM recognized the first 50K samples as state 1, and the next 50K samples were recognized as state 2, however, did not recognize states 3, 4, or 5. Note that there are partial

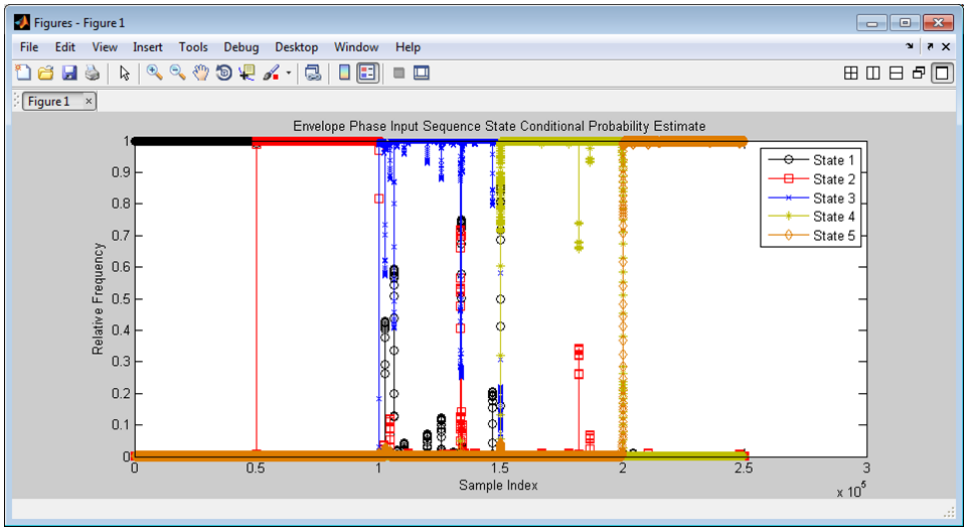

Figure A.57: CEP Sequence Recognition

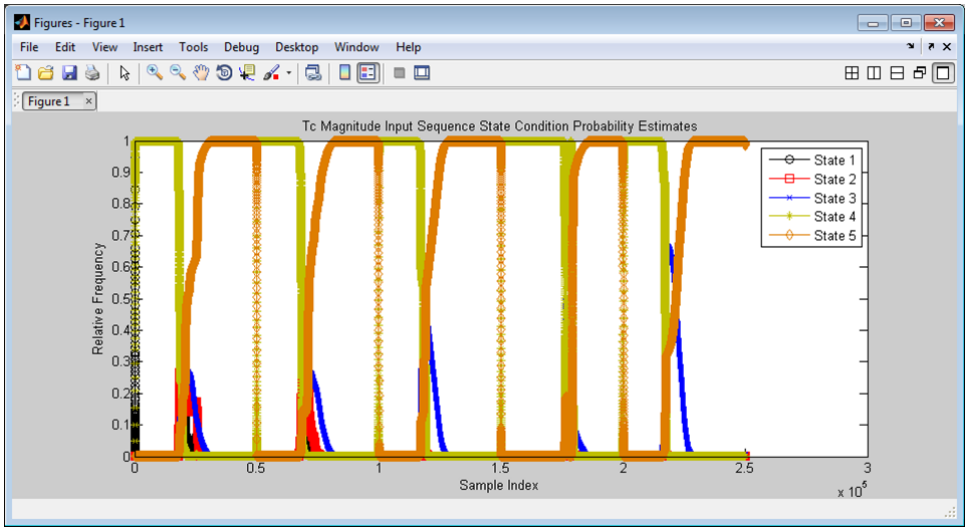

Figure A.58: TcM Sequence Recognition

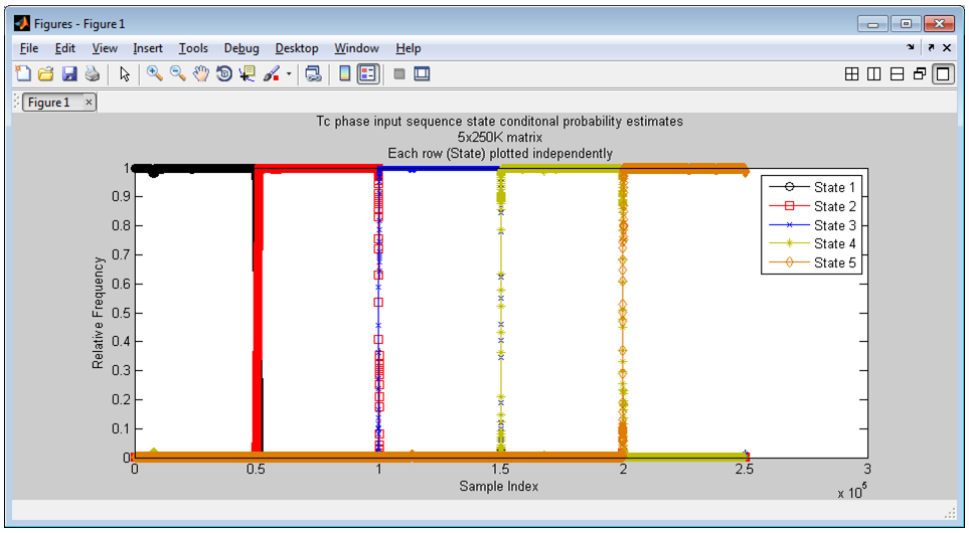

Figure A.59: TcP Sequence Recognition

responses within each state and false detections within other states reducing accuracy and contributing to Type I and Type II errors.

Doppler Spread Phase Figure A.61 illustrates the detection of each state in the DPP sequence. Note that this HMM successfully recognized state 1, 3, and 5, however the performance for state 2, and 4 was poor. Note that there are partial responses within each state and false detections within other states reducing accuracy and contributing to Type I and Type II errors.

BWc Magnitude Figure A.72 illustrates the detection of each state in the BWM sequence. Note that this HMM recognized the first 50K samples as state 1, but did poorly for state 2, 3, 4, and 5. Note that there are partial responses within each state and false detections within other states reducing accuracy and contributing to Type I and Type II errors.

BWc Phase Figure A.60 illustrates the detection of each state in the BWP sequence. Note that this HMM larely recognized the first 50K samples as state 1, and the next 50K samples were recognized as state 2, etc.. Note that there are partial responses within each state and false detections within other states reducing accuracy and contributing to Type I and Type II errors.

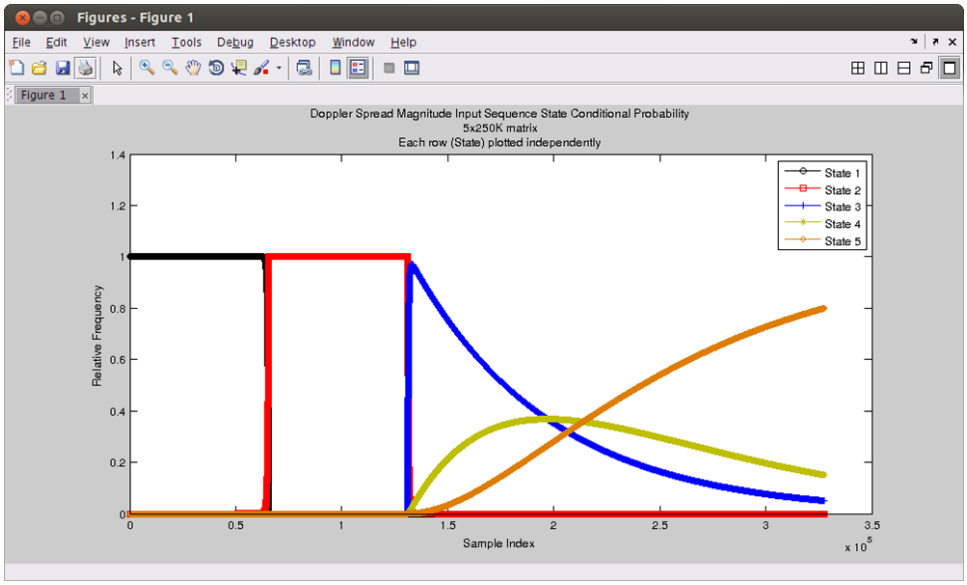

Figure A.60: DPM Sequence Recognition

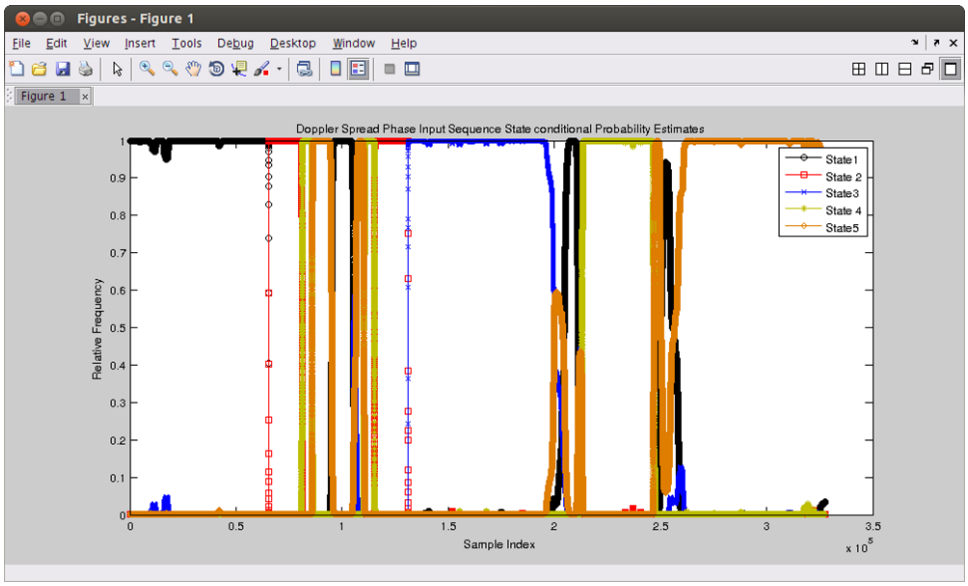

Figure A.61: DPP Sequence Recognition

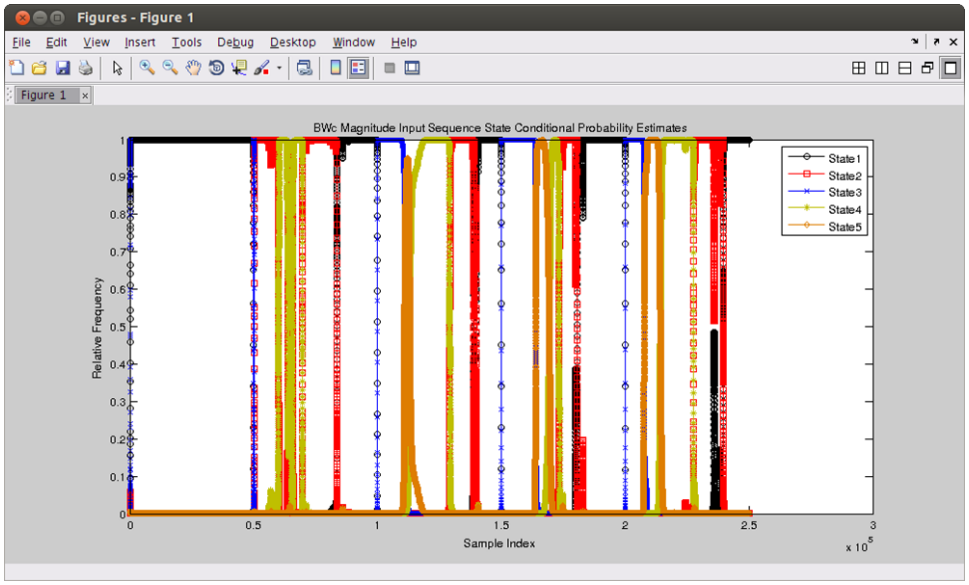

Figure A.62: BWM Sequence Recognition

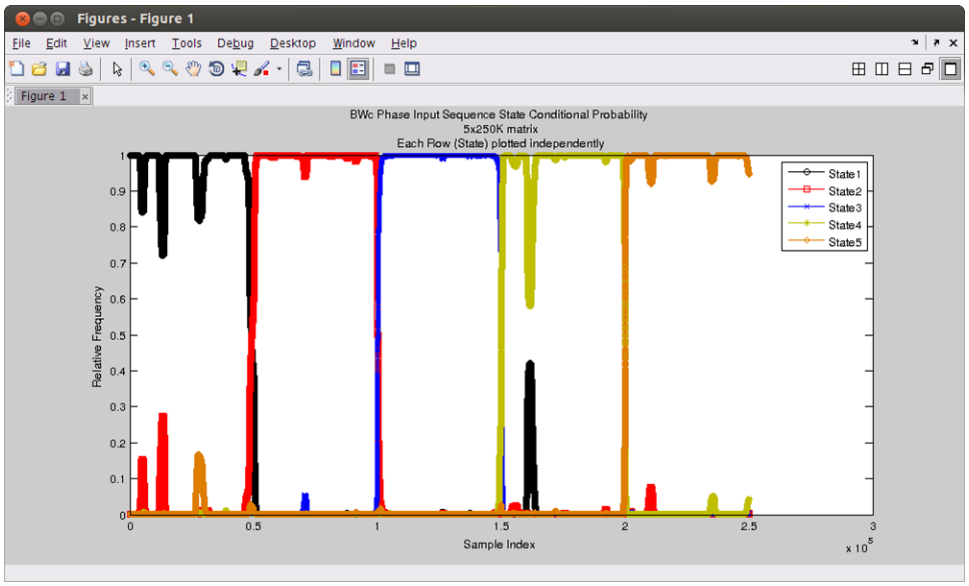

Figure A.63: BWP

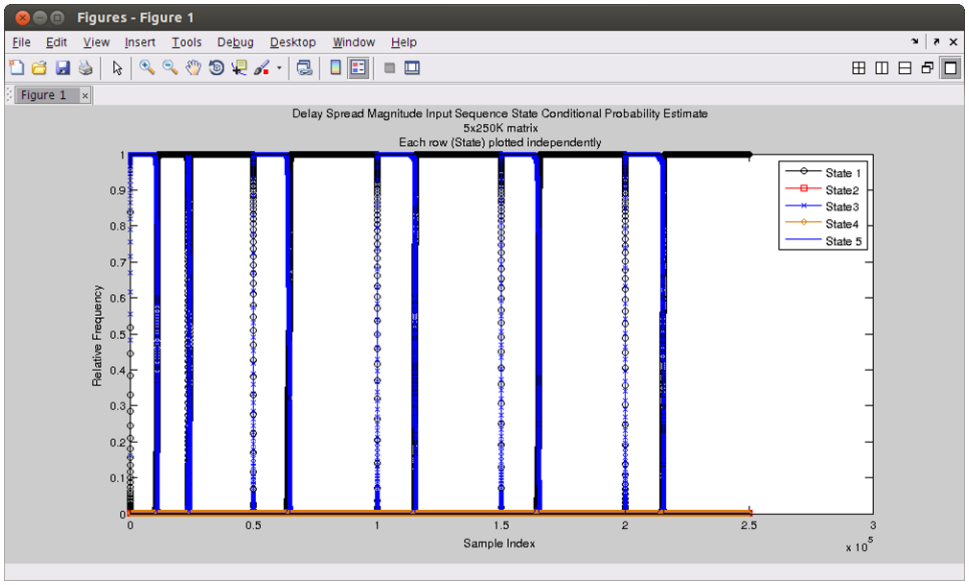

Figure A.64: DSM Sequence Recognition

Delay Spread Magnitude Figure A.64 illustrates the detection of each state in the DSM sequence. Note that this HMM recognized a portion of the first 50K samples as state 1, however did a poor job discriminating state 1 from the other states and did as poorly with all the other states. Note that there are partial responses within each state and false detections within other states reducing accuracy and contributing to Type I and Type II errors.

Delay Spread Phase Figure A.65 illustrates the detection of each state in the DSP sequence. Note that this HMM a partial response to state 1, however did a poor job discriminating state 1 from the other states. It did however, recognize a high percentage of state 4, but performed poorly with all the other states. Note that there are partial responses within each state and false detections within other states reducing accuracy and contributing to Type I and Type II errors.

State Sequence 23451

Figure A.86 illustrates the detection of each state in the CEM sequence. Note that this HMM recognized the first 50K samples as state 2, the next 50K samples as state3, etc. Note that there are partial responses within each state and false detections within other states reducing accuracy and

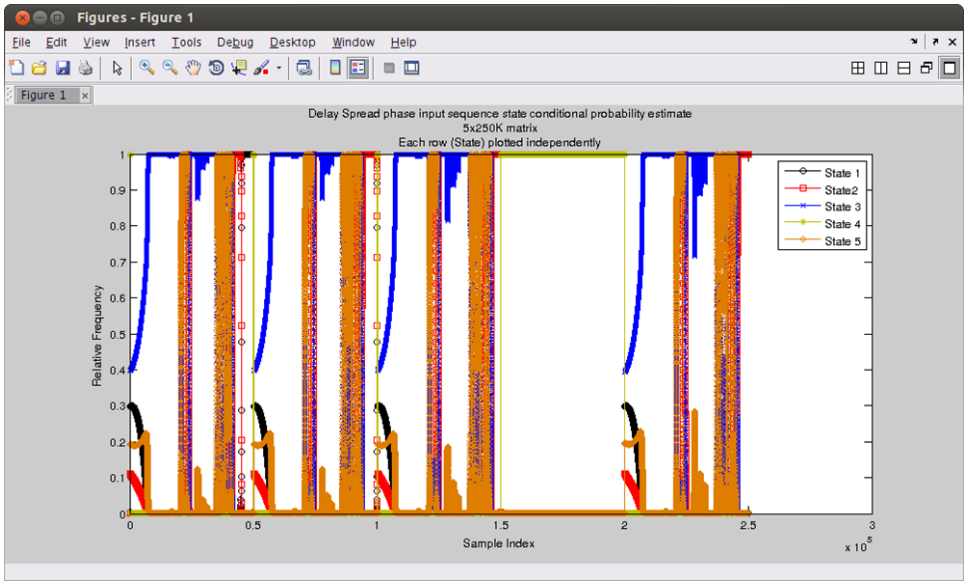

Figure A.65: DSP Sequence Recognition

contributing to Type I and Type II errors.

Complex Envelope Magnitude

Complex Envelope Phase Figure A.77 illustrates the detection of each state in the CEP sequence. Note that this HMM recognized the first 50K samples as state 2, the next 50K samples as state3, etc. Note that there are partial responses within each state and false detections within other states reducing accuracy and contributing to Type I and Type II errors.

Tc Magnitude Figure A.78 illustrates the detection of each state in the TcM sequence. Note that this HMM had only a partial response in the first 50K samples as state 2, and did a poor job of discriminating state 2 from state 1. It did with the all the other states also. Note that there are partial responses within each state and false detections within other states reducing accuracy and contributing to Type I and Type II errors.

Tc Phase Figure A.79 illustrates the detection of each state in the TcP sequence. Note that this HMM did recognize the first 50K samples as state 2, and the next 50K samples as state 3, etc. Note

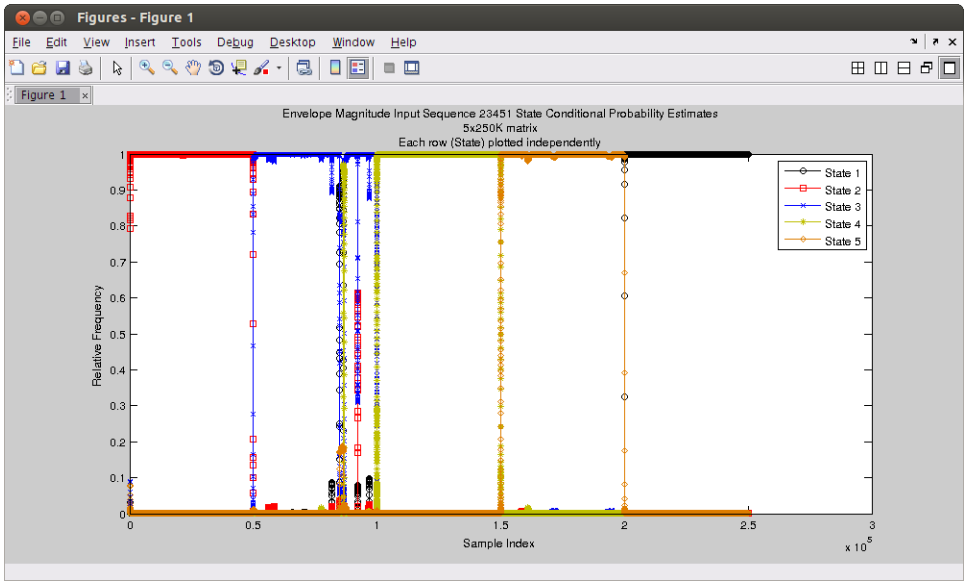

Figure A.66: CEM Sequence Recognition

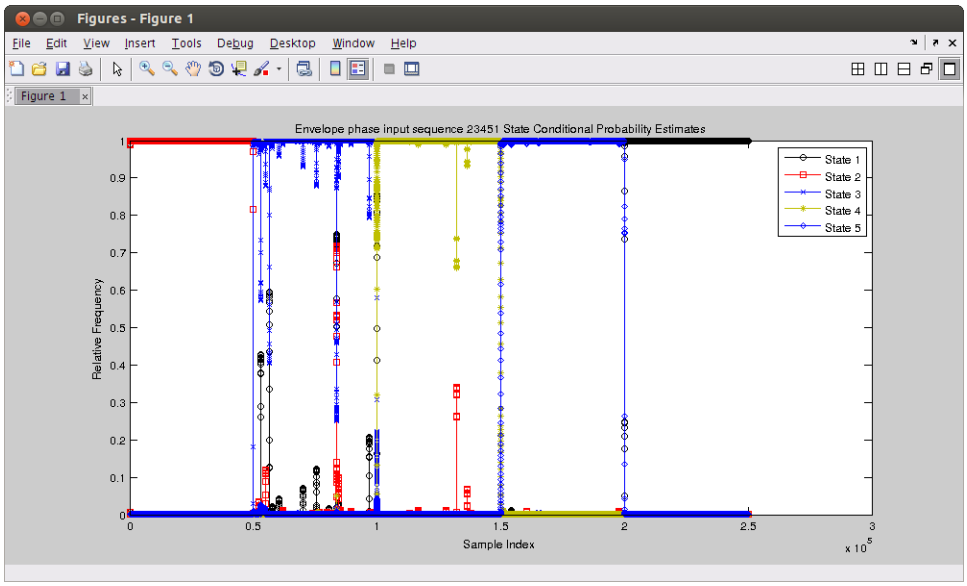

Figure A.67: CEP Sequence Recognition

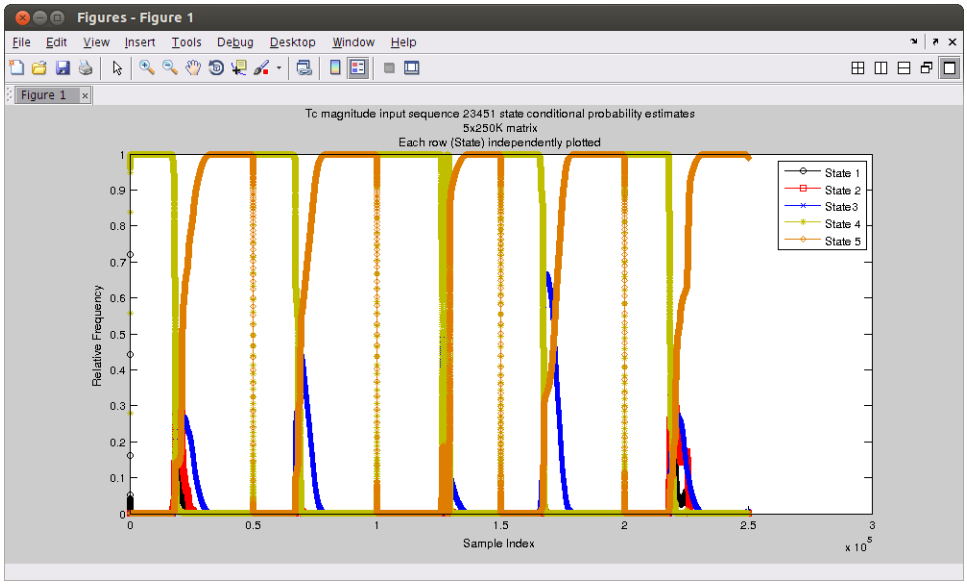

Figure A.68: TcM Sequence Recognition

that there are partial responses within each state and false detections within other states reducing accuracy and contributing to Type I and Type II errors.

Doppler Spread Magnitude Figure A.70 illustrates the detection of each state in the DPM sequence. Note that this HMM did a very poor job of recognizing any of the states in this feature sequence and also did a poor job of discriminating between states.

Doppler Spread Phase Figure A.71 illustrates the detection of each state in the DPP sequence. Note that this HMM performed poorly at recognizing any state and poorly at discriminating between states. Note that there are partial responses within each state and false detections within other states reducing accuracy and contributing to Type I and Type II errors.

BWc Magnitude Figure A.72 illustrates the detection of each state in the BWM sequence. Note that this HMM recognized a portion of the first 50K samples as state 2, but did not discriminate between state 2 and the other states. It performed poorly on all the other states as well. Note that there are partial responses within each state and false detections within other states reducing accuracy and contributing to Type I and Type II errors.

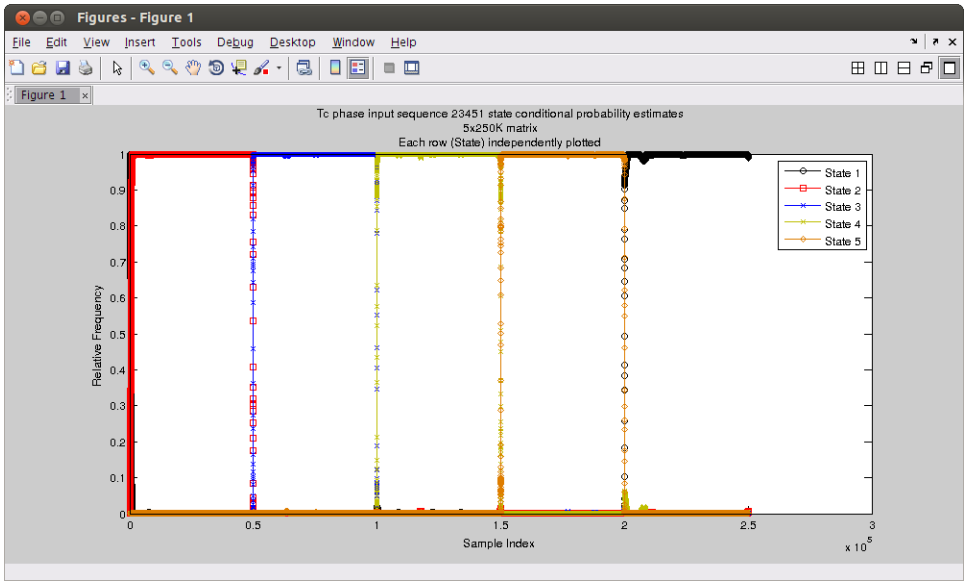

Figure A.69: TcP Sequence Recognition

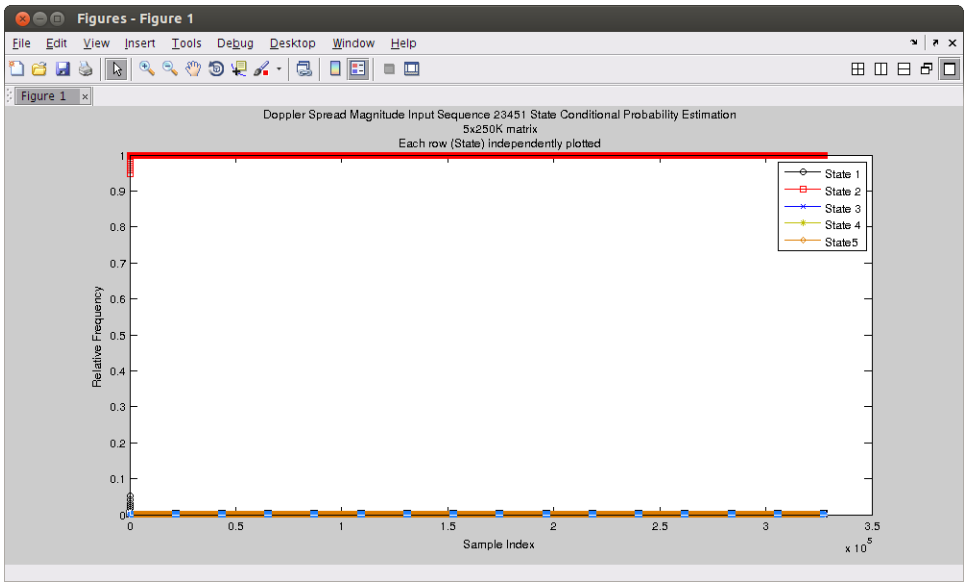

Figure A.70: DPM Sequence Recognition

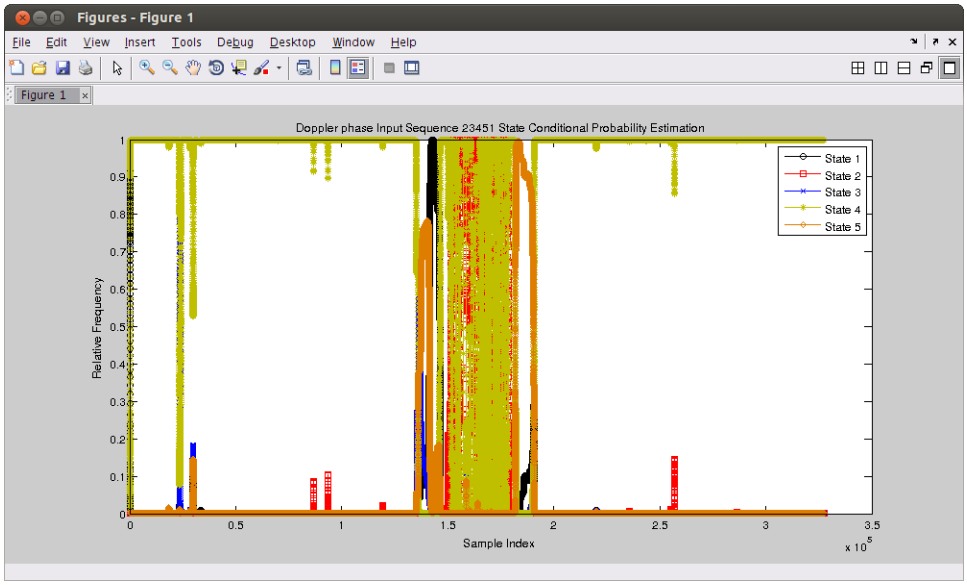

Figure A.71: DPP Sequence Recognition

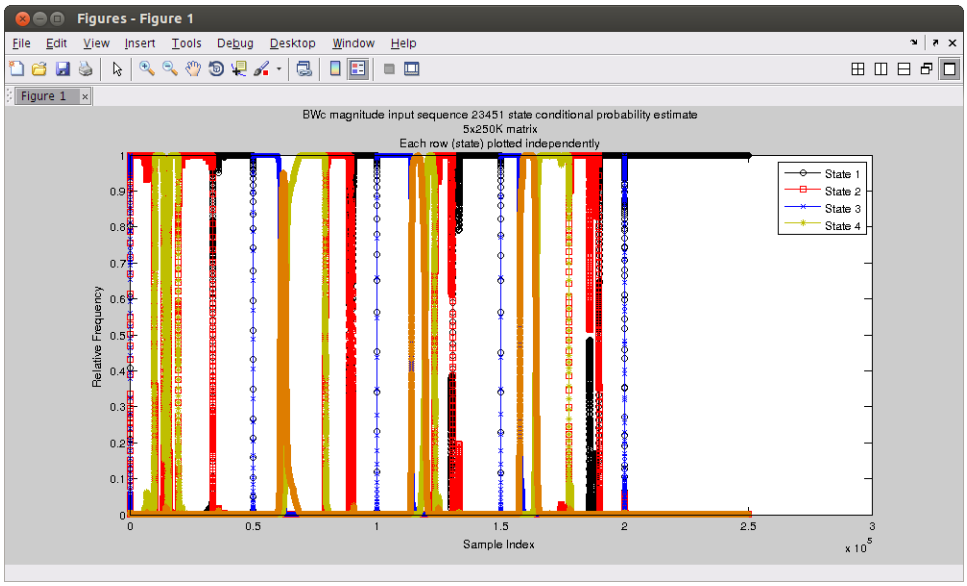

Figure A.72: BWM Sequence Recognition

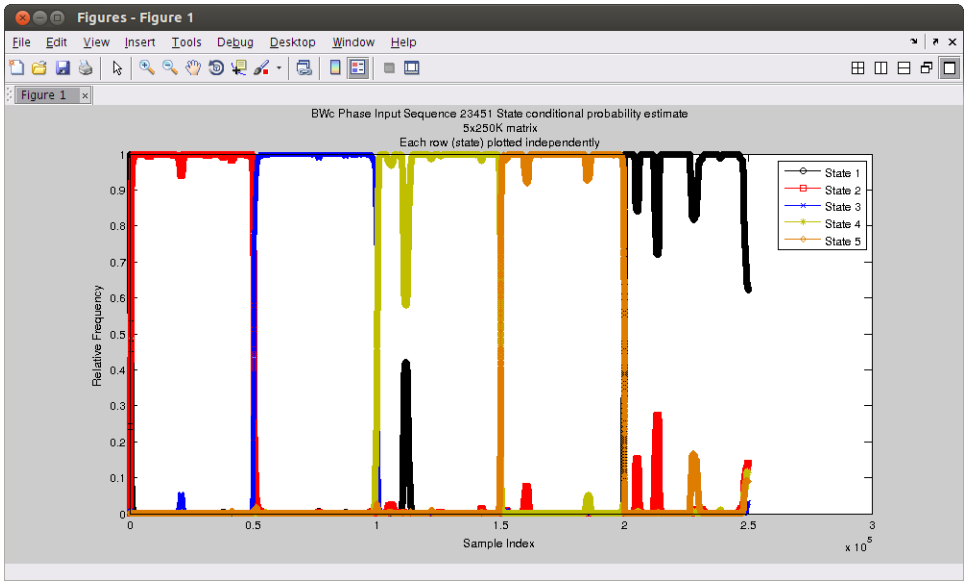

Figure A.73: BWP Sequence Recognition

BWc Phase Figure A.83 illustrates the detection of each state in the BWP sequence. Note that this HMM recognized the first 50K samples as state 2, and the next 50K samples as state three, etc.. Note that there are partial responses within each state and false detections within other states reducing accuracy and contributing to Type I and Type II errors.

Delay Spread Magnitude Figure A.74 illustrates the detection of each state in the DSM sequence. Note that this HMM performed poorly at recognizing any state and poorly at discriminating between states.

Delay Spread Phase Figure A.75 illustrates the detection of each state in the DSP sequence. Note that this HMM performed poorly at recognizing any state and poorly at discriminating between states.

State Sequence 34512

Figure A.76 illustrates the detection of each state in the CEM sequence. Note that this HMM recognized the first 50K samples as state 3, the next 50K samples as state 4, etc.. Note that there

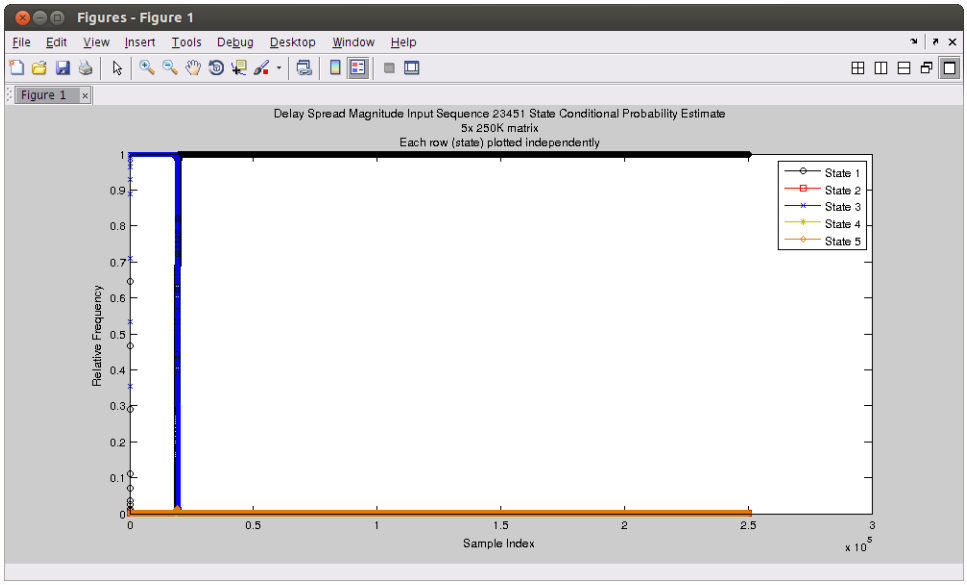

Figure A.74: DSM

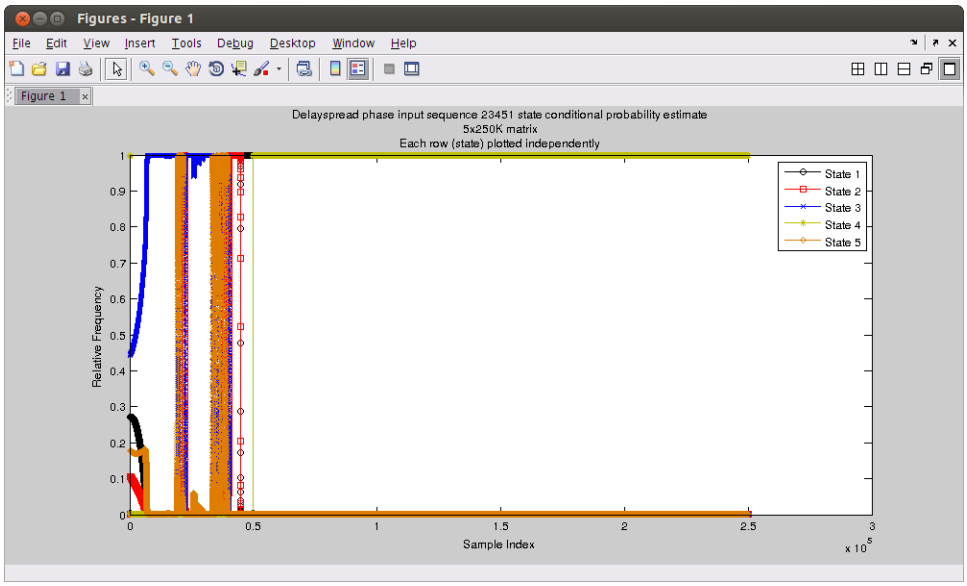

Figure A.75: DSP Sequence Recognition

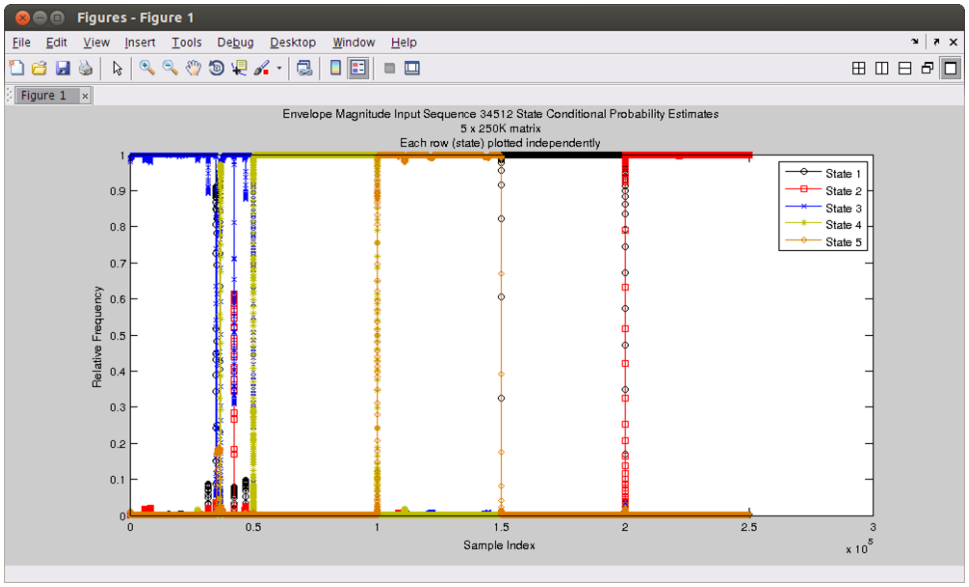

Figure A.76: CEM Sequence Recognition

are partial responses within each state and false detections within other states reducing accuracy and contributing to Type I and Type II errors.

Complex Envelope Magnitude

Complex Envelope Phase Figure A.77 illustrates the detection of each state in the CEP sequence. Note that this HMM recognized the first 50K samples as state 3, the next 50K samples as state 4, etc.. Note that there are partial responses within each state and false detections within other states reducing accuracy and contributing to Type I and Type II errors.

Tc Magnitude Figure A.78 illustrates the detection of each state in the TcM sequence. Note that this HMM partially recognized state 3 in the first 50K samples, but could not discriminate between state 3 and the other states. It also performed poorly at recognizing any of the other states in the TcM sequence. Note that there are partial responses within each state and false detections within other states reducing accuracy and contributing to Type I and Type II errors.

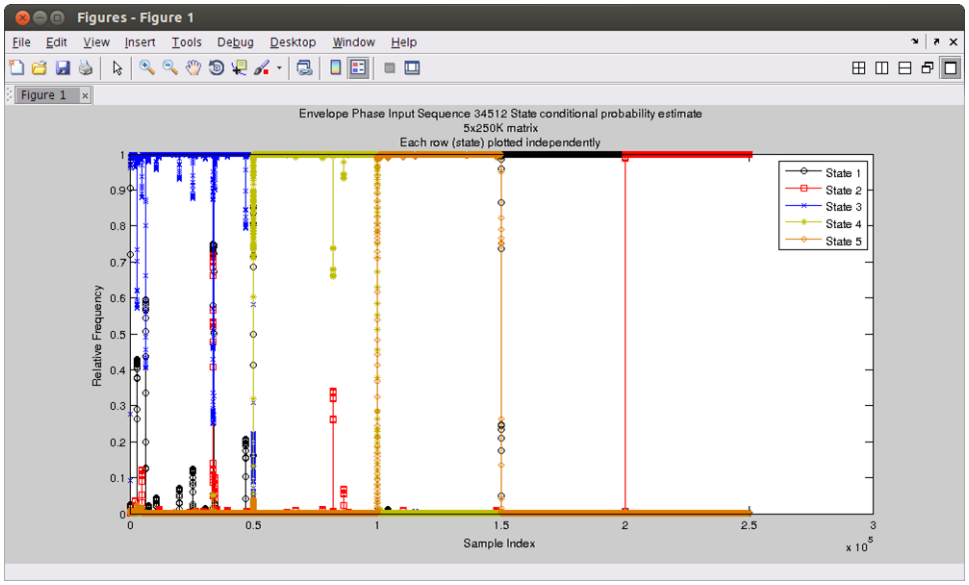

Figure A.77: CEP Sequence Recognition

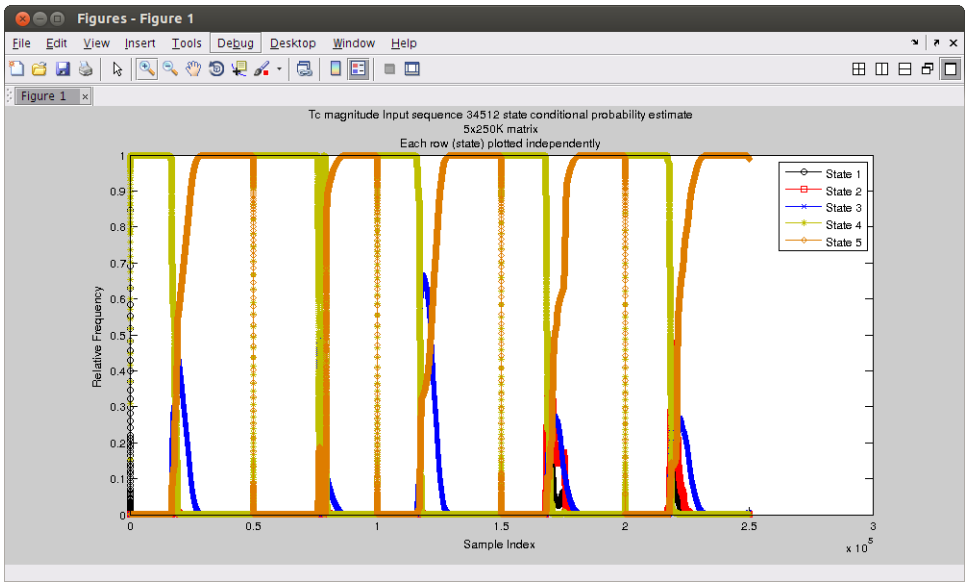

Figure A.78: TcM Sequence Recognition

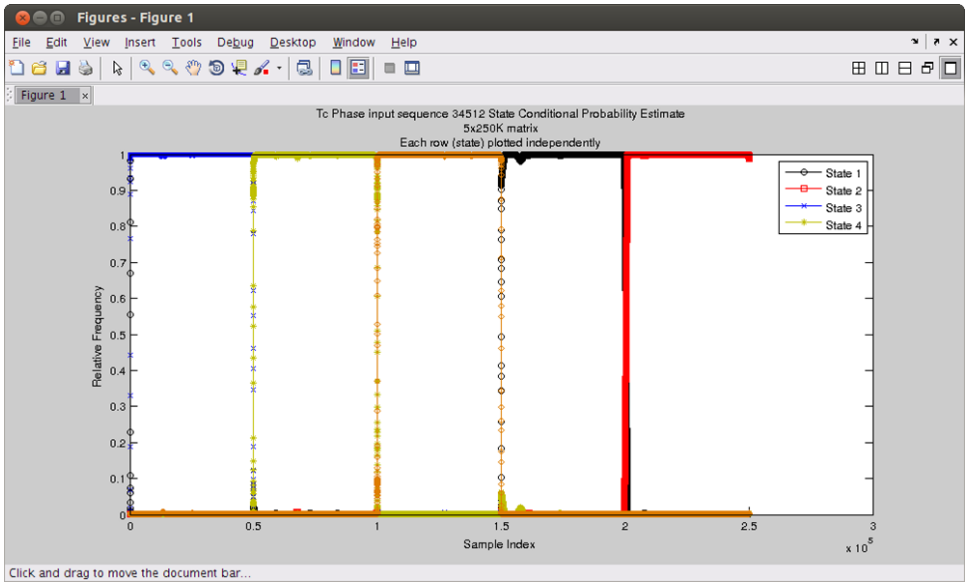

Figure A.79: TcP Sequence Recognition

Tc Phase Figure A.79 illustrates the detection of each state in the TcP sequence. Note that this HMM recognized the 50K samples as state 3, and the next 50K samples as state 4, etc.. Note that there are partial responses within each state and false detections within other states reducing accuracy and contributing to Type I and Type II errors.

Doppler Spread Magnitude Figure A.80 illustrates the detection of each state in the DPM sequence. Note that this HMM performed poorly at recognizing state 3 in the first 50K samples and was unable to discriminate between states.

Doppler Spread Phase Figure A.81 illustrates the detection of each state in the DPP sequence. Note that this HMM performed poorly at recognizing any of the states in the DPP sequence.

BWc Magnitude Figure A.82 illustrates the detection of each state in the BWM sequence. Note that this HMM partially recognized state 3 in the first 50K samples, but could not discriminate between state 3 and the other states. It also performed poorly at recognizing any of the other states in the Tc magnitude sequence.

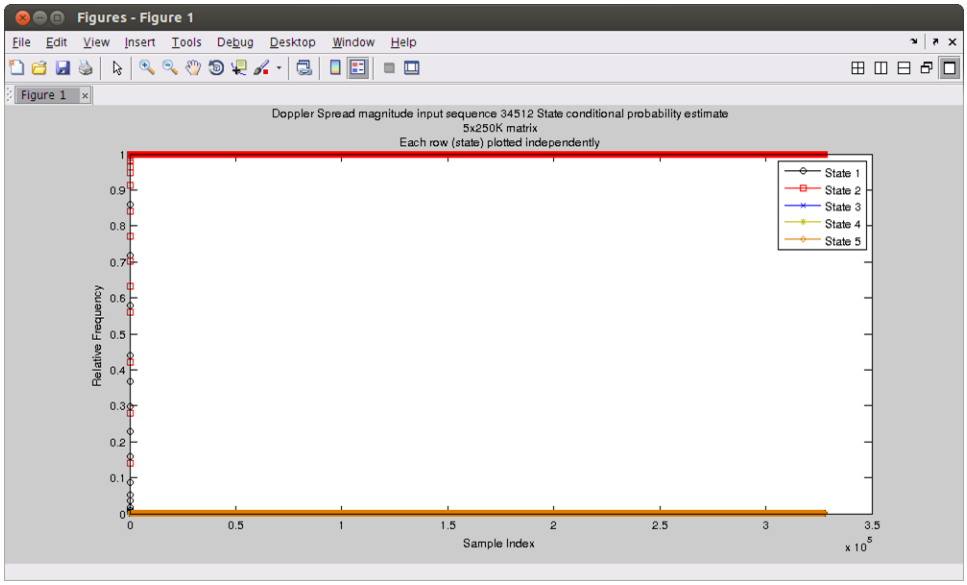

Figure A.80: DPM Sequence Recognition

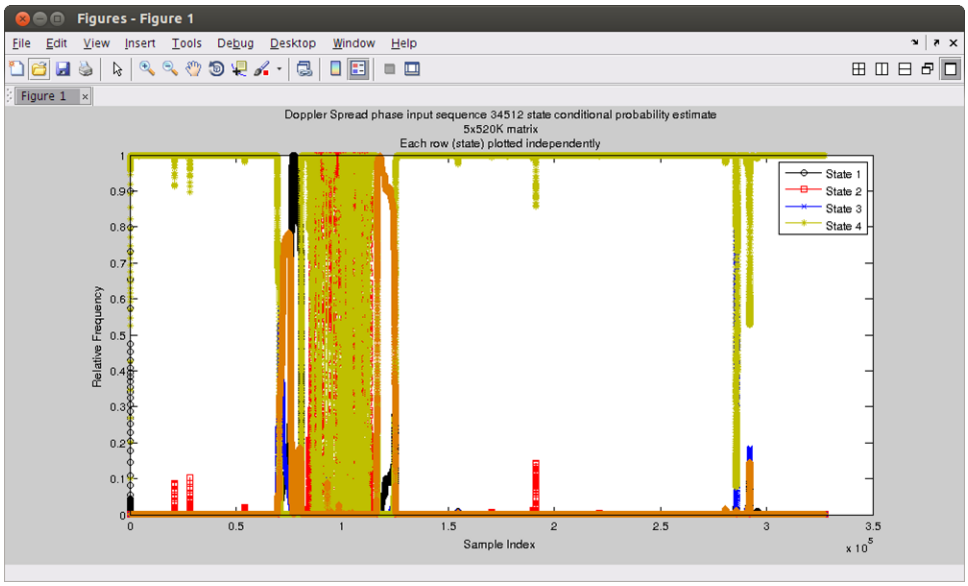

Figure A.81: DPP Sequence Recognition

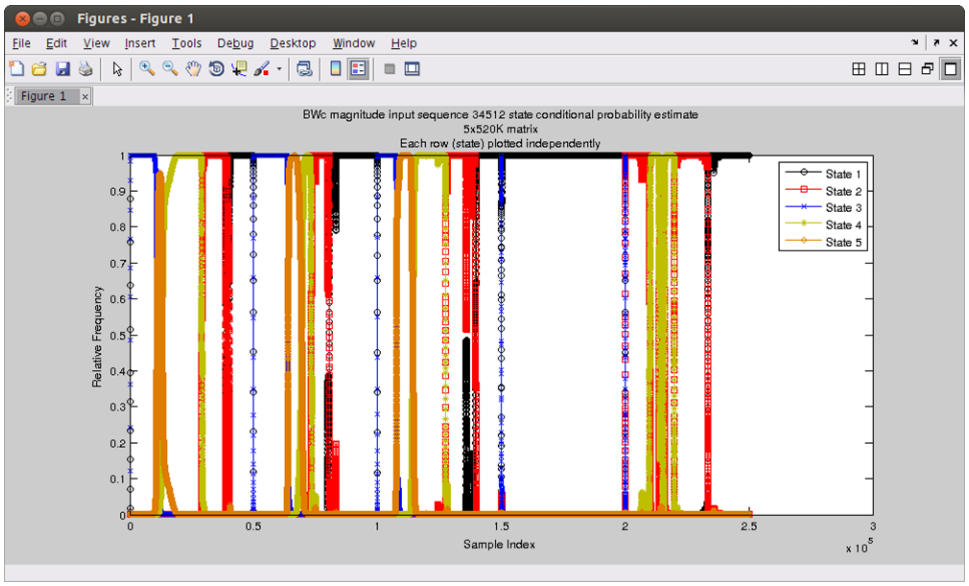

Figure A.82: BWM Sequence Recognition

BWc Phase Figure A.83 illustrates the detection of each state in the BWP sequence. Note that this HMM partially recognized state 3 in the first 50K samples, and state 4 in the next 50K samples, etc.. Note that there are partial responses within each state and false detections within other states reducing accuracy and contributing to Type I and Type II errors.

Delay Spread Magnitude Figure A.84 illustrates the detection of each state in the DSM sequence. Note that this HMM performed poorly at recognizing any of the states in the DSM sequence.

Delay Spread Phase Figure A.85 illustrates the detection of each state in the Delay spread sequence. Note that this HMM performed poorly at recognizing any of the states in the DSP sequence.

State Sequence 45123

Complex Envelope Magnitude Figure A.86 illustrates the detection of each state in the CEM sequence. Note that this HMM recognized the first 50K samples as state 4, the next 50K samples

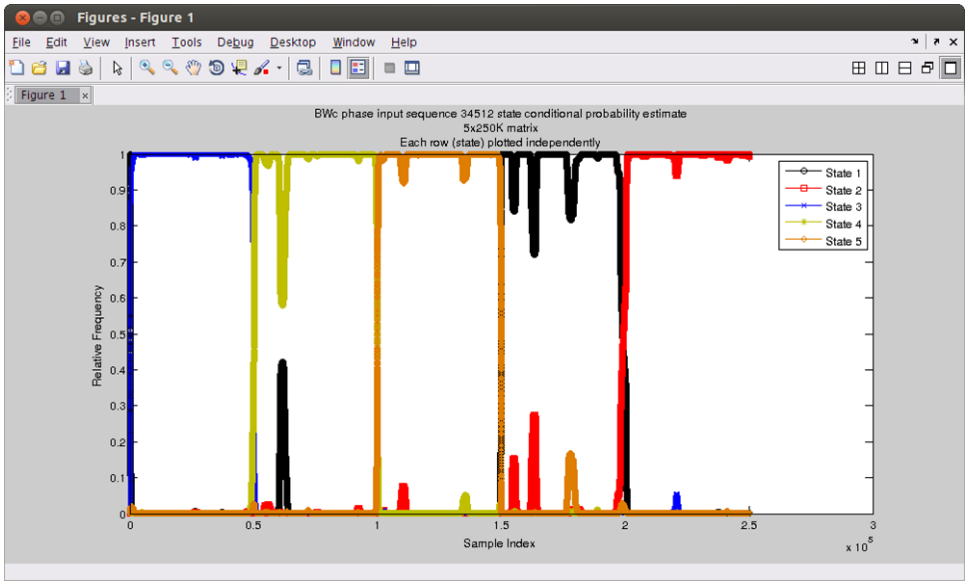

Figure A.83: BWP Sequence Recogntion

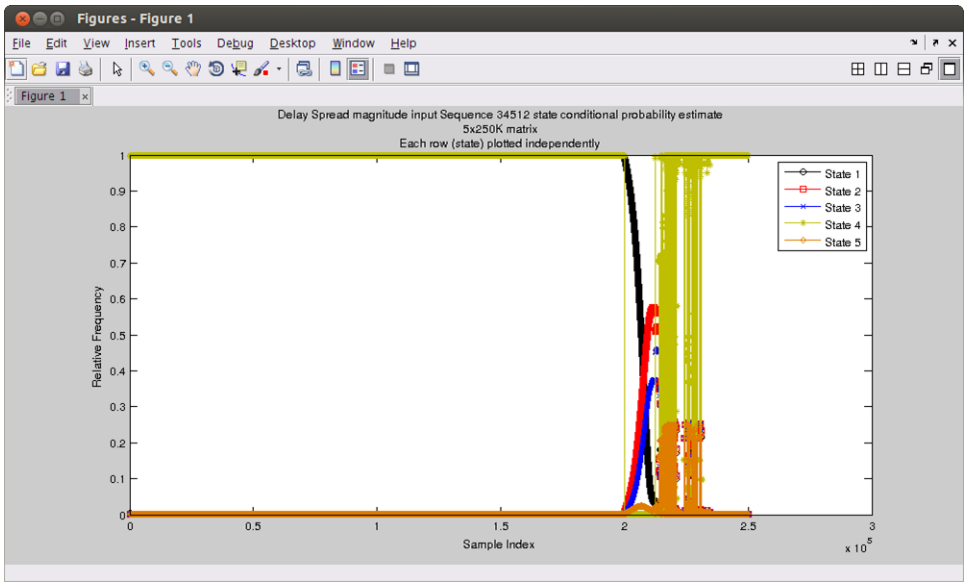

Figure A.84: DSM Sequence Recognition

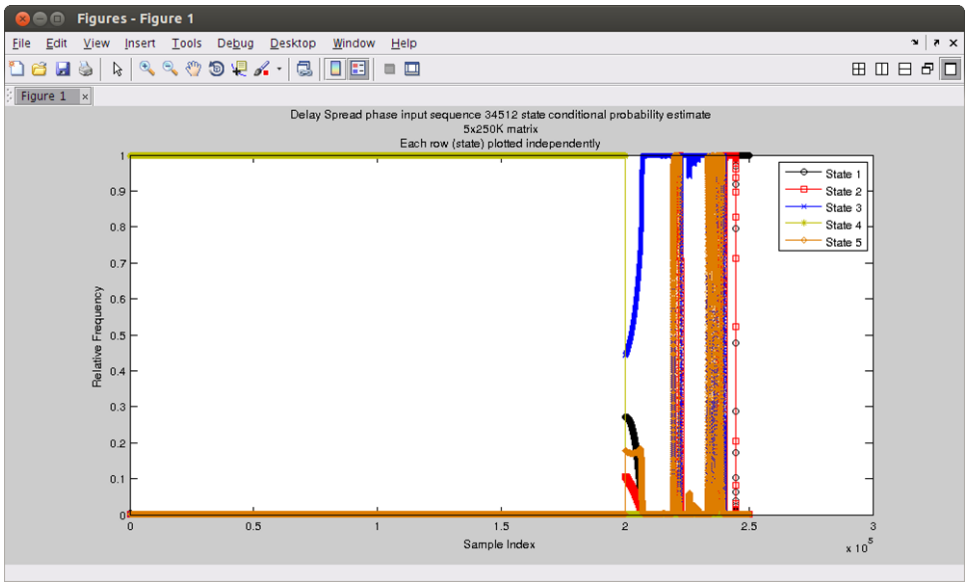

Figure A.85: DSP Sequence Recognition

as state5, etc. Note that there are partial responses within each state and false detections within other states reducing accuracy and contributing to Type I and Type II errors.

Complex Envelope Phase Figure A.87 illustrates the detection of each state in the CEP sequence. Note that this HMM recognized the first 50K samples as state 4, the next 50K samples as state5, etc. Note that there are partial responses within each state and false detections within other states reducing accuracy and contributing to Type I and Type II errors.

Tc Magnitude Figure A.88 illustrates the detection of each state in the TcM sequence. Note that this HMM recognized a portion of the first 50K samples as state 4, but did not effectively discriminate between state 4 and other states. This HMM also performed poorly at recognizing all the remaining states. Note that there are partial responses within each state and false detections within other states reducing accuracy and contributing to Type I and Type II errors.

Tc Phase Figure A.89 illustrates the detection of each state in the TcP sequence. Note that this HMM recognized the first 50K samples as state 4, the next 50K samples as state 5, etc. Note that there are partial responses within each state and false detections within other states reducing

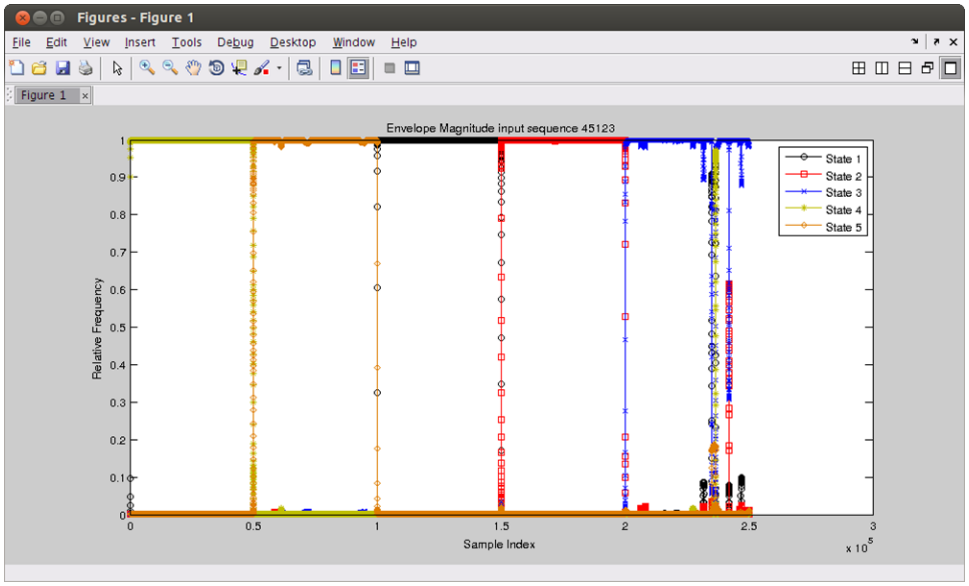

Figure A.86: CEM Sequence Recognition

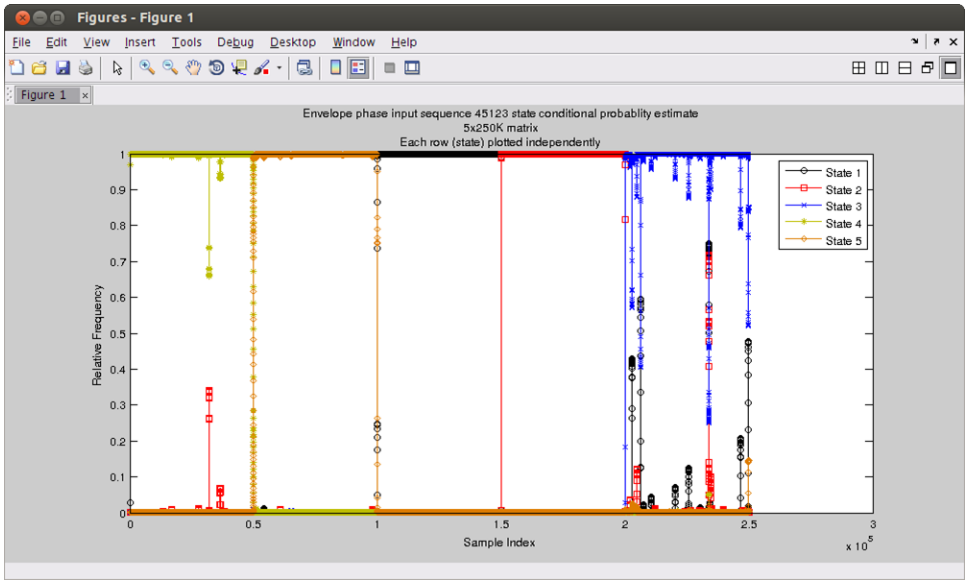

Figure A.87: CEP Sequence Recognition

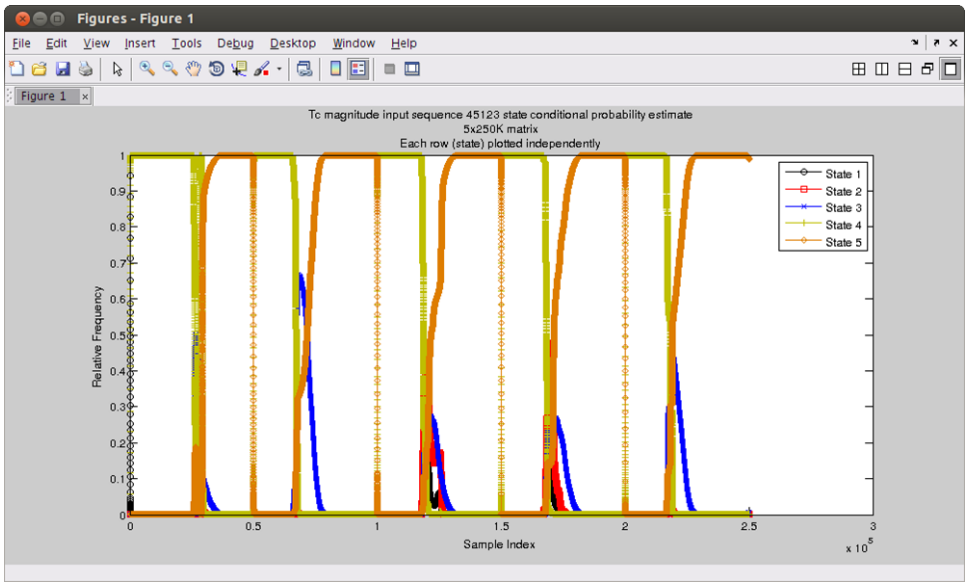

Figure A.88: TcM Sequence Recognition

accuracy and contributing to Type I and Type II errors.

Doppler Spread Magnitude Figure A.90 illustrates the detection of each state in the DPM sequence. Note that this HMM performed poorly at recognizing and discriminating between all the states.

Doppler Spread Phase Figure A.91 illustrates the detection of each state in the DPP sequence. Note that this HMM recognized a significant portion of the first 50K samples as state 4, but was unable to discriminate between state 4 and the remaining states. This HMM also performed poorly with the other states.

BWc Magnitude Figure A.92 illustrates the detection of each state in the BWM sequence. Note that this HMM recognized a portion of the first 50K samples as state 4, but did not effectively discriminate between state 4 and the remaining states. This HMM also performed poorly for the other states.

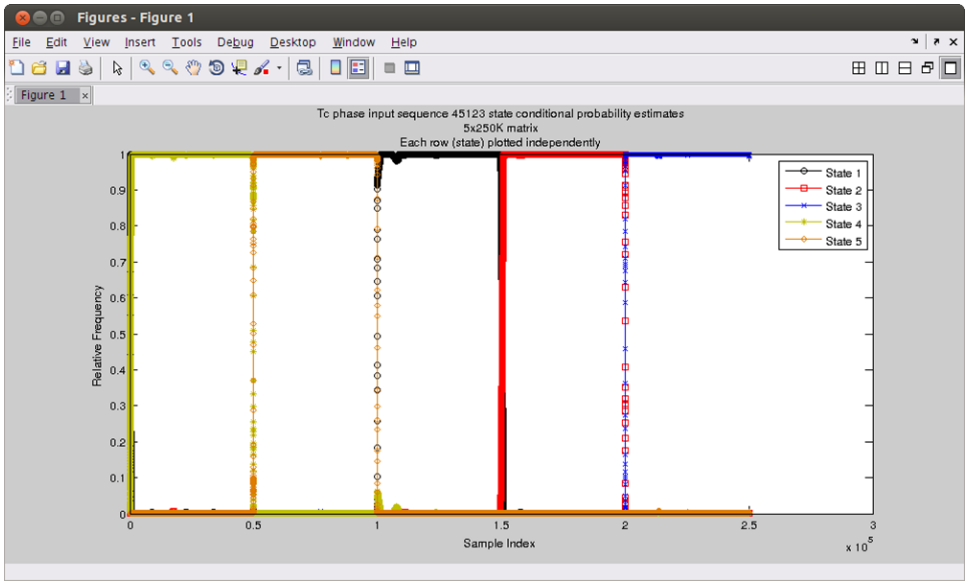

Figure A.89: TcP Sequence Recognition

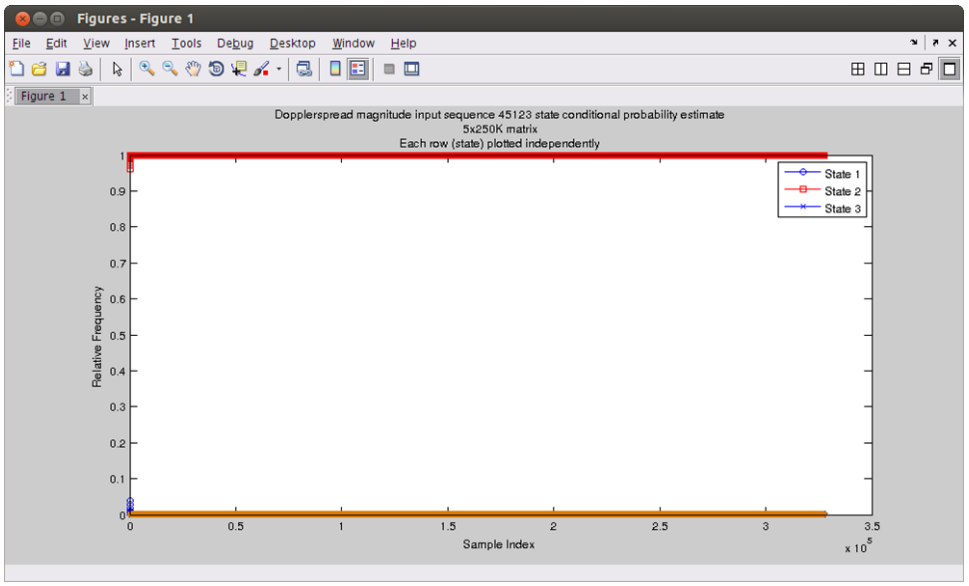

Figure A.90: DPM Sequence Recognition

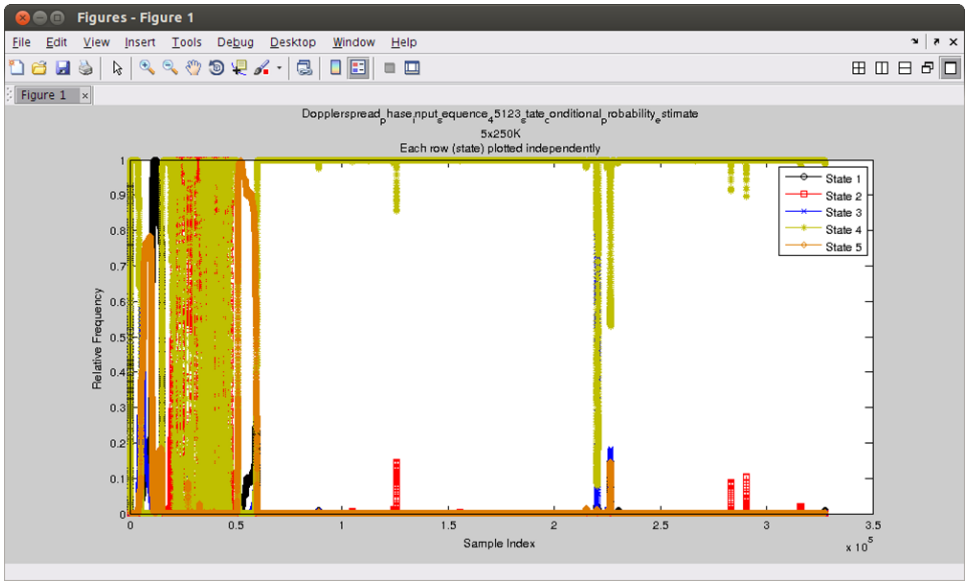

Figure A.91: DPP Sequence Recognition

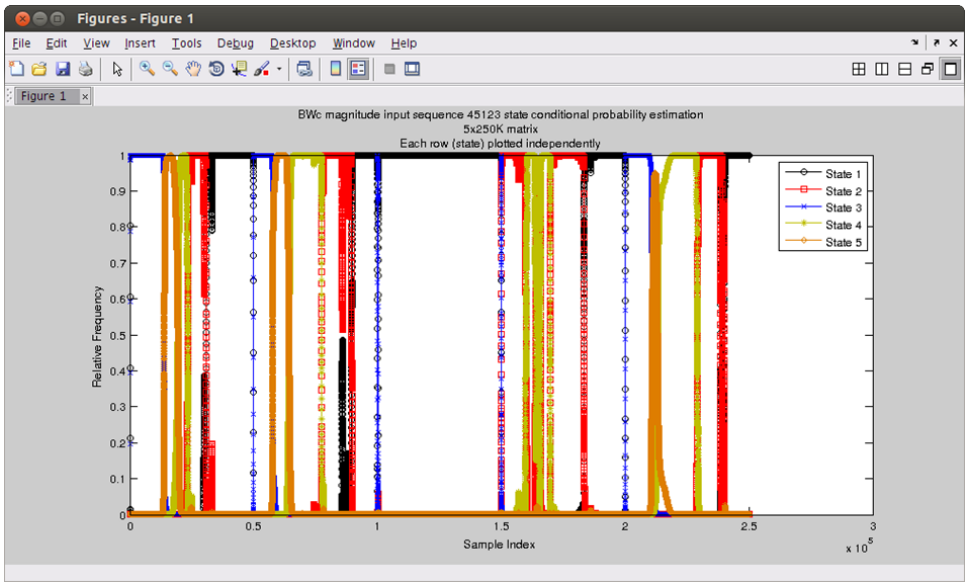

Figure A.92: BWM Sequence Recognition

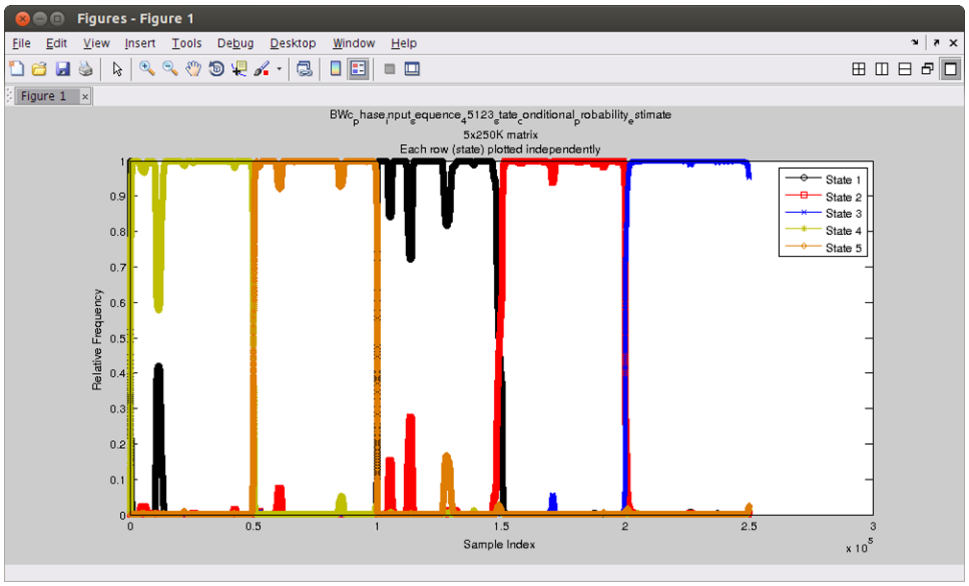

Figure A.93: BWP Sequence Recognition

BWc Phase Figure A.93 illustrates the detection of each state in the BWP sequence. Note that this HMM recognized the first 50K samples as state 4, the next 50K samples as state5, etc. Note that there are partial responses within each state and false detections within other states reducing accuracy and contributing to Type I and Type II errors.

Delay Spread Magnitude Figure A.94 illustrates the detection of each state in the DSM sequence. Note that this HMM performed poorly at recognizing the first 50K samples as state 4 and also did not discriminate between states.

Delay Spread Phase Figure A.95 illustrates the detection of each state in the DSP sequence. Note that this HMM did recognize the first 50K samples as state 4, but did not discriminate between state 4 and the remaining states. This HMM also performed poorly for all the other states.

State Sequence 51234

Figure A.96 illustrates the detection of each state in the CEM sequence. Note that this HMM recognized the first 50K samples as state 2, the next 50K samples as state3, etc. Note that there are

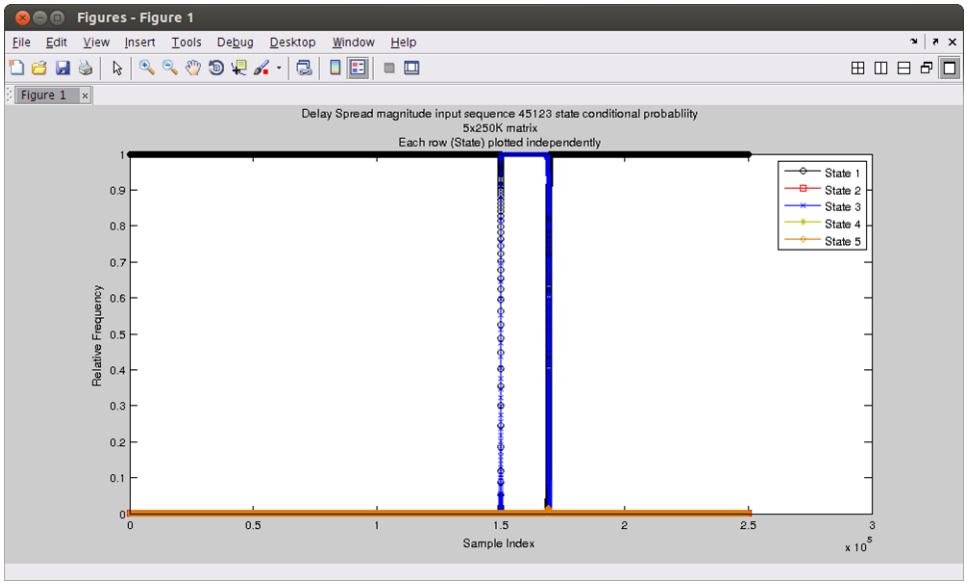

Figure A.94: DSM Sequence Recognition

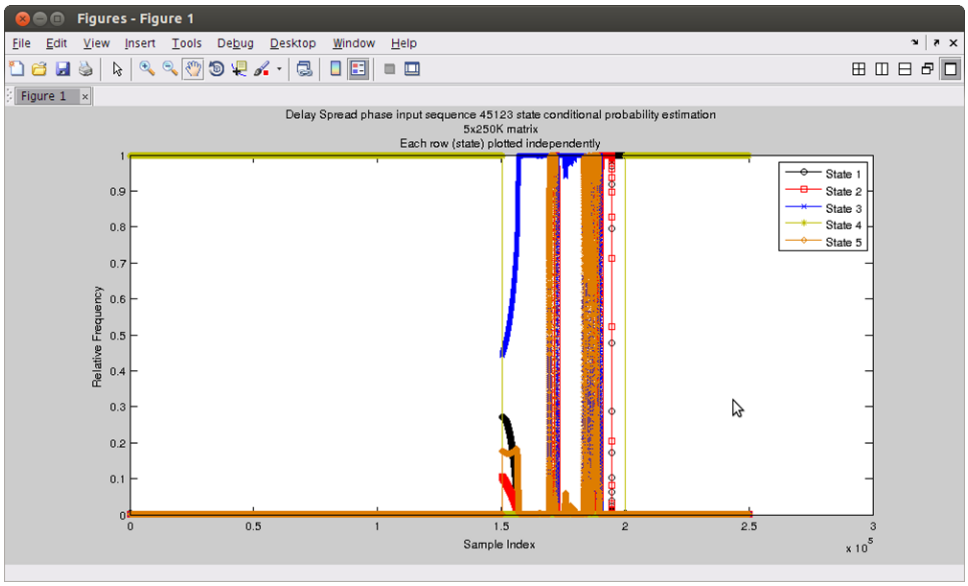

Figure A.95: DSP Sequence Recognition

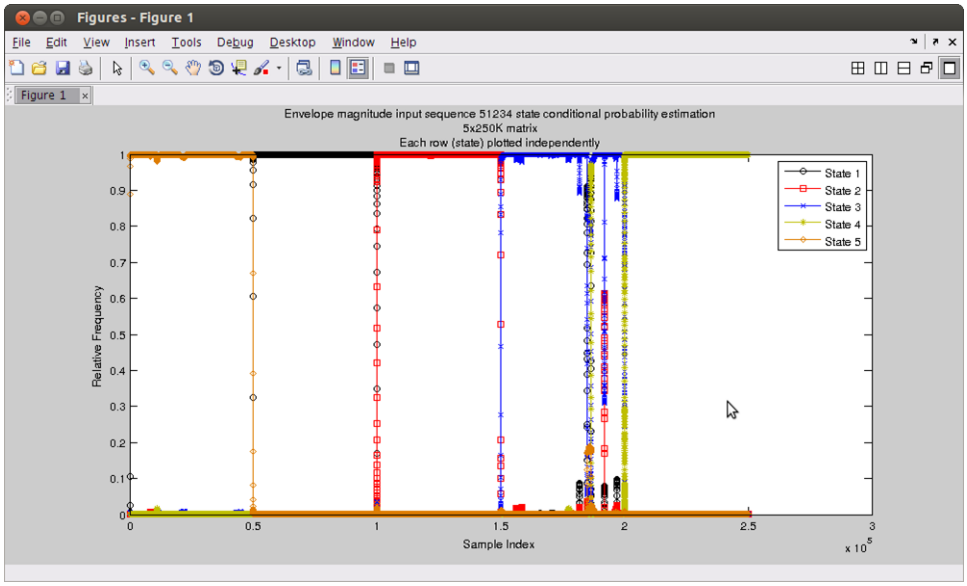

Figure A.96: CEM Sequence Recognition

partial responses within each state and false detections within other states reducing accuracy and contributing to Type I and Type II errors.

Complex Envelope Magnitude Figure A.96 illustrates the detection of each state in the CEM sequence. Note that this HMM recognized the first 50K samples as state 5, the next 50K samples as state1, etc. Note that there are partial responses within each state and false detections within other states reducing accuracy and contributing to Type I and Type II errors.

Complex Envelope Phase Figure A.97 illustrates the detection of each state in the CEP sequence. Note that this HMM recognized the first 50K samples as state 5, the next 50K samples as state1, etc. Note that there are partial responses within each state and false detections within other states reducing accuracy and contributing to Type I and Type II errors.

Tc Magnitude Figure A.98 illustrates the detection of each state in the TcM sequence. Note that this HMM recognized a portion of the first 50K samples as state 5, but was not effective at discriminating between state 5 and the other states. This HMM performed poorly for the other states. Note that there are partial responses within each state and false detections within other

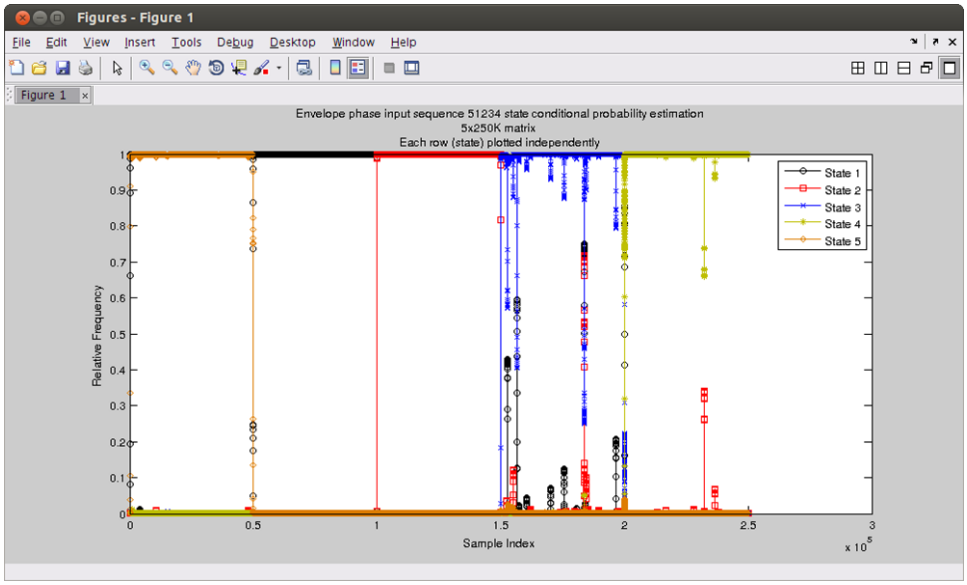

Figure A.97: CEP Sequence Recognition

states reducing accuracy and contributing to Type I and Type II errors.

Tc Phase Figure A.99 illustrates the detection of each state in the TcP sequence. Note that this HMM recognized the first 50K samples as state 5, the next 50K samples as state1, etc. Note that there are partial responses within each state and false detections within other states reducing accuracy and contributing to Type I and Type II errors.

Doppler Spread Magnitude Figure A.100 illustrates the detection of each state in the DPM sequence. Note that this HMM did not recognize the first 50K samples as state 5, and also poorly at discriminating between any of the states.

Doppler Spread Phase Figure A.101 illustrates the detection of each state in the DPP sequence. Note that this HMM failed to recognize the first 50K samples as state 5, and performed poorly at discriminating among any of the states.

BWc Magnitude Figure A.102 illustrates the detection of each state in the BWM sequence. Note that this HMM recognized a portion of the first 50K samples as state 5, but did recognize a large

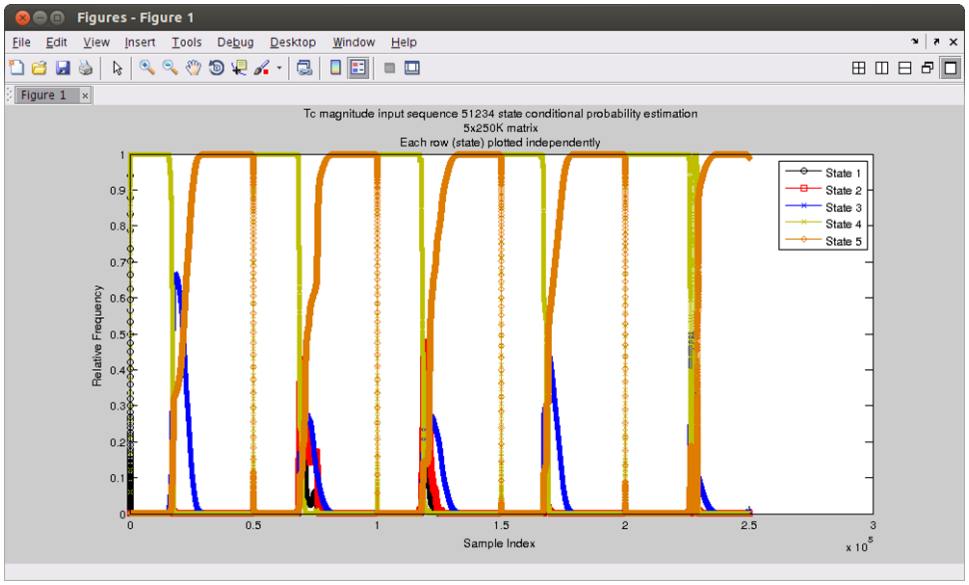

Figure A.98: TcM Sequence Recognition

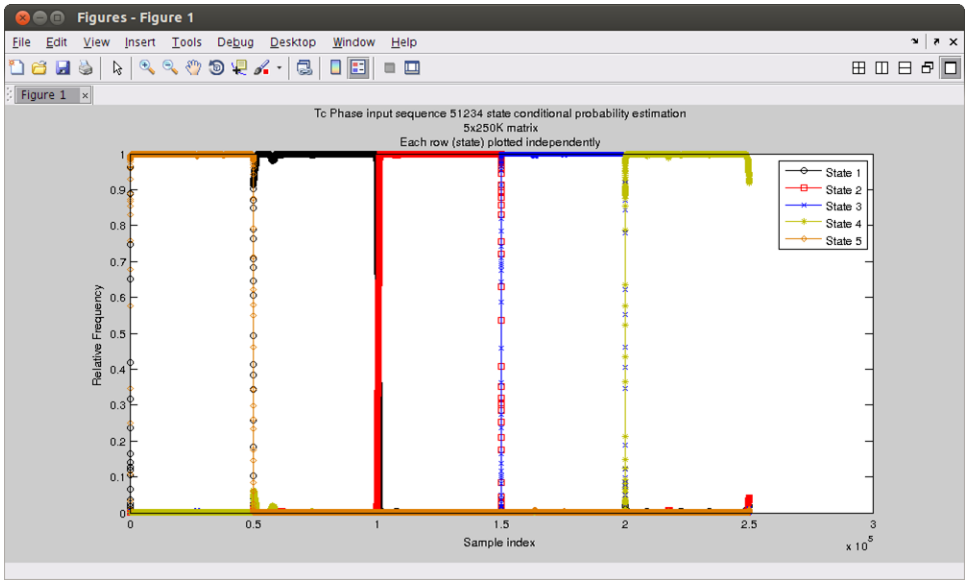

Figure A.99: TcP Sequence Recognition

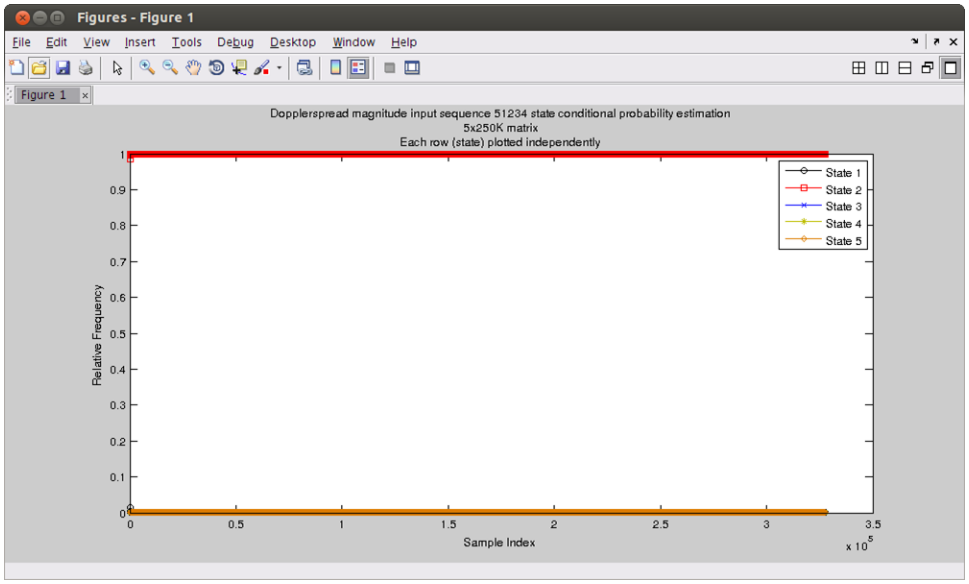

Figure A.100: DPM Sequence Recognition

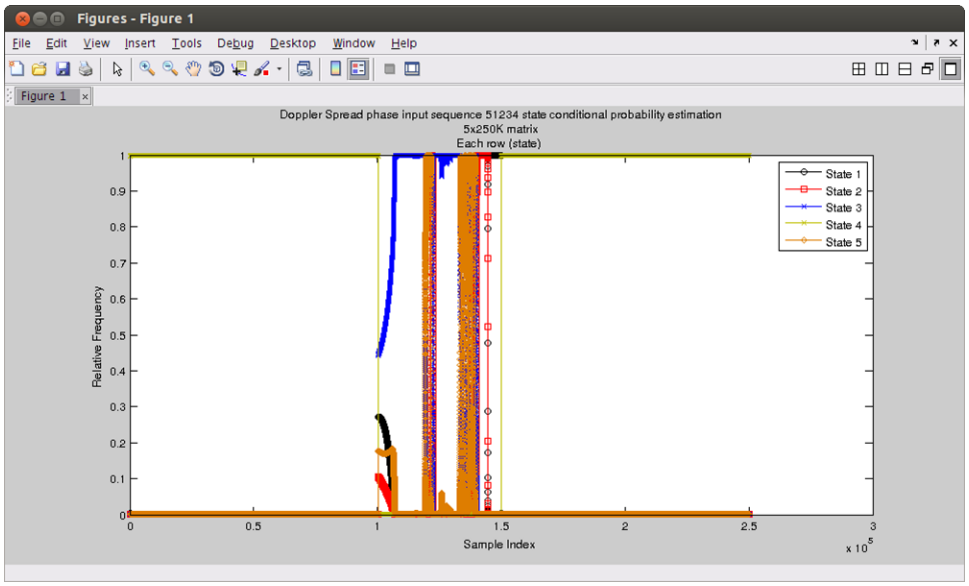

Figure A.101: DPP Sequence Recognition

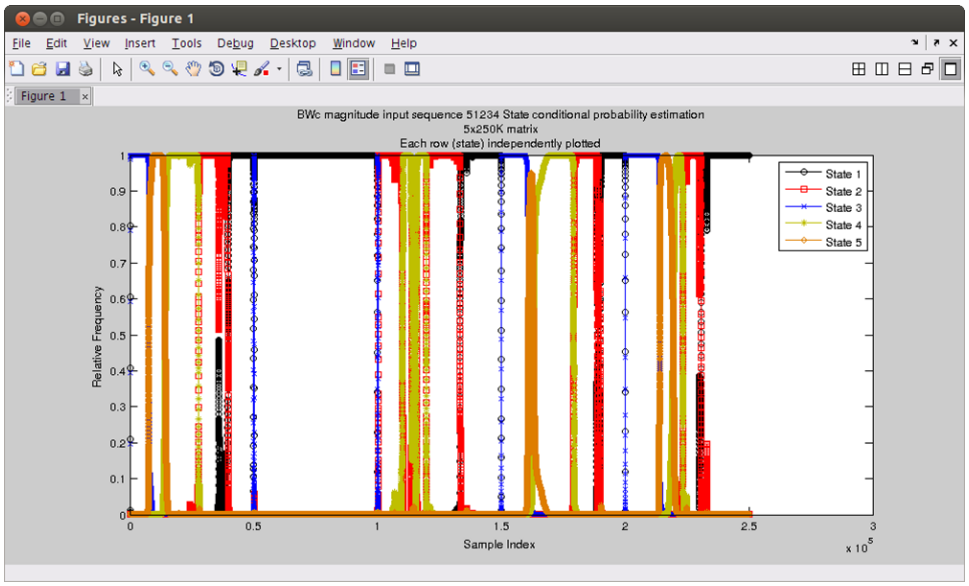

Figure A.102: BWM Sequence Recognition

portion of the next 50K samples as state 1. It did not discriminate between the remaining states.

BWc Phase Figure A.103 illustrates the detection of each state in the BWP sequence. Note that this HMM recognized the first 50K samples as state 5, the next 50K samples as state1, etc. Note that there are partial responses within each state and false detections within other states reducing accuracy and contributing to Type I and Type II errors.

Delay Spread Magnitude Figure A.104 illustrates the detection of each state in the DSM sequence. Note that this HMM failed to recognize the first 50K samples as state 5, and performed poorly at discriminating between all the states.

Delay Spread Phase Figure A.105 illustrates the detection of each state in the delay spread sequence. Note that this HMM failed to recognize the first 50K samples as state 5, and was not effective at discriminating between all the states.

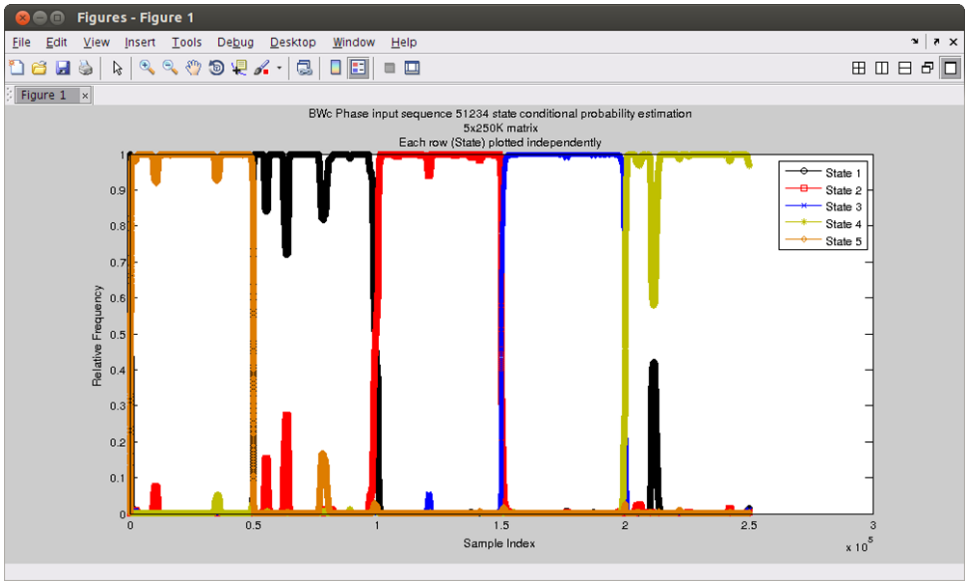

Figure A.103: BWP Sequence Recognition

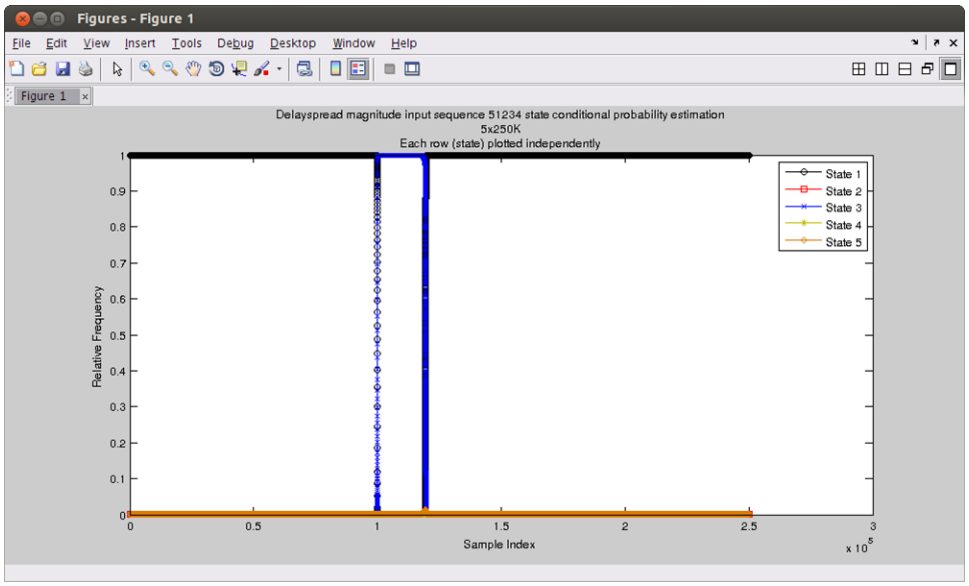

Figure A.104: DSM Sequence Recognition

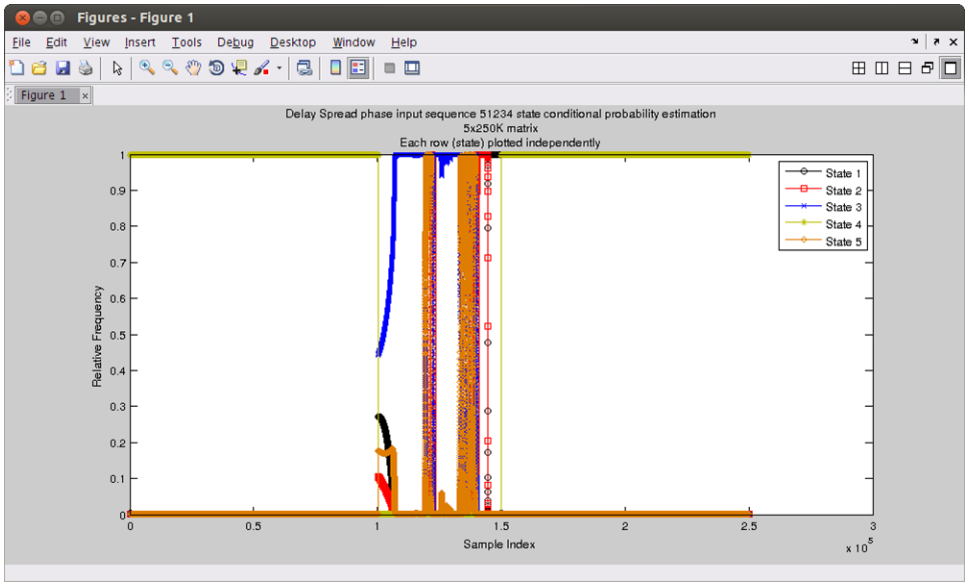

Figure A.105: DSP Sequence Recognition

A.11.5 Extracted Feature State Likelihood vs Timeblock Estimates

This section defines the results of extracting state probabilities from each feature HMM output. Each feature HMM estimates the likelihood that its input matches the training sequence and provides 5 conditional probability sequences which are accumulated and normalized to form an estimate of the feature state probability for each timeblock. These values are displayed to provide the likelihood that the input sequence agrees with the training sequence utilized to train the HMM.

State Sequence 12345

Figure A.106 displays the liklihood from the CEM HMM; the CSM state probabilities are shown in each row while each timeblock is shown in each column. Note the state sequence 12345 was recognized with an estimated likelihood greater than 99% along the diagonal of the matrix while all other states were found to be not likely.

Figure A.107 displays the likelihoods from the CEP HMM; the CSM state likelihoods are shown in each row while each timeblock is shown in each column. Note the state sequence 12345 was recognized with an estimated likelihood greater than 99% along the diagonal of the matrix while

	1	2	3	4	5
1	0.9999	4.0213e-06	0.0017	2.2114e-07	7.8687e-07
2	9.2890e-05	1.0000	0.0010	1.4709e-06	8.0427e-06
3	8.2162e-06	2.0386e-05	0.9869	2.4116e-04	0.0010
4	4.8012e-07	3.2256e-06	0.0041	0.9998	4.9035e-04
5	7.0112e-06	5.4838e-06	0.0063	6.6895e-06	0.9985

Figure A.106: State Sequence 12345 CEM State Likelihood Estimates vs. Timeblocks

	1	2	3	4	5
1	1.0000	6.0062e-05	0.0014	1.2871e-06	8.3011e-06
2	1.9123e-10	0.9999	5.0489e-04	1.2675e-04	5.6682e-06
3	3.5665e-09	2.0880e-07	0.9955	6.4845e-06	3.7550e-04
4	7.4246e-09	1.4438e-07	0.0015	0.9999	3.6490e-04
5	3.3816e-09	5.5089e-08	0.0012	7.5531e-06	0.9992

Figure A.107: State Sequence 12345 CEP State Likelihood Estimates vs. Timeblocks

all other states were found to be not likely.

Figure A.108 displays the likelihoods from the TcM HMM; the CSM state likelihoods are shown in each row while each timeblock is shown in each column. Note the state sequence 12345 was not recognized along the diagonal of the matrix while all other states were found to be nearly equally likely.

Figure A.109 displays the likelihoods from the TcP HMM; the CSM state likelihoods are shown in each row while each timeblock is shown in each column. Note the state sequence 12345 was estimated with greater than 99% likelihood along the diagonal of the matrix while all other states were found to be not likely.

Figure A.110 displays the likelihoods from the Doppler Spread magnitude HMM; the CSM state likelihoods are shown in each row while each timeblock is shown in each column. Note while State 1 was recognized in Timeblock 1, the state sequence 12345 was not recognized along the diagonal

	1	2	3	4	5
1	0.0117	0.0112	3.6131e-04	0.0013	1.4006e-04
2	0.0369	0.0310	8.4986e-04	0.0025	2.4291e-04
3	0.0343	0.0398	0.0488	0.0223	0.0798
4	0.3734	0.3664	0.3583	0.5608	0.3429
5	0.5438	0.5517	0.5917	0.4132	0.5769

Figure A.108: State Sequence 12345 TcM State Likelihood Estimates vs. Timeblocks

	1	2	3	4	5
1	0.9983	0.0074	1.8807e-06	5.8036e-04	1.0275e-06
2	8.4871e-04	0.9924	4.2411e-05	2.0890e-04	2.4317e-06
3	1.7446e-07	7.0082e-05	0.9995	5.5596e-05	4.6715e-04
4	8.5606e-04	1.3357e-04	6.0671e-05	0.9990	3.7625e-05
5	1.7604e-07	5.5704e-07	3.4704e-04	1.8441e-04	0.9995

Figure A.109: State Sequence 12345 TcP State Likelihood Estimates vs. Timeblocks

	1	2	3	4	5
1	1.0000	0.3029	0	0	0
2	4.7688e-20	0.6971	0.6292	6.1908e-24	1.1375e-79
3	0	0	0.3229	0.5272	0.2458
4	0	0	0.0435	0.3249	0.3390
5	0	0	0.0043	0.1479	0.4151

Figure A.110: State Sequence 12345 DPM State Likelihood Estimates vs. Timeblocks

of the matrix while all other states were found to be equally likely.

Figure A.111 displays the likelihoods from the DPP HMM; the CSM state likelihoods are shown in each row while each timeblock is shown in each column. Note while State 1 was recognized in Timeblock 1, the state sequence 12345 was not recognized along the diagonal of the matrix while all other states were found to be equally likely.

Figure A.112 displays the likelihoods from the BWM HMM; the CSM state likelihoods are shown in each row while each timeblock is shown in each column. Note while State 1 was recognized in Timeblock 1, the state sequence 12345 was not recognized along the diagonal of the matrix while all other states were found to be equally likely.

Figure A.113 displays the likelihoods from the BWP HMM; the CSM state likelihoods are shown in each row while each timeblock is shown in each column. Note the state sequence 12345 was recognized along the diagonal of the matrix while all other states were found to be not likely.

	1	2	3	4	5
1	0.9963	0.4075	0.1075	0.0017	0.1421
2	4.5793e-08	0.3119	0.3157	2.4982e-06	3.2219e-05
3	0.0031	1.8791e-04	0.3974	0.9871	0.0480
4	3.8635e-05	0.0957	0.0981	1.8042e-04	0.6760
5	6.1722e-04	0.1847	0.0813	0.0111	0.1339

Figure A.111: State Sequence 12345 DPP State Likelihood Estimates vs. Timeblocks

	1	2	3	4	5
1	0.9964	0.3304	0.2202	0.3890	0.2110
2	9.5289e-05	0.4969	0.1961	0.1443	0.2366
3	0.0035	0.0032	0.2208	0.2793	0.1558
4	1.1018e-05	0.1692	0.3152	0.0806	0.2661
5	8.5673e-06	3.3614e-04	0.0478	0.1068	0.1304

Figure A.112: State Sequence 12345 BWM State Likelihood Estimates vs. Timeblocks

	1	2	3	4	5
1	0.9544	0.0039	2.9692e-04	0.0193	9.6919e-04
2	0.0337	0.9928	0.0062	0.0018	0.0034
3	3.1672e-04	0.0023	0.9886	0.0037	5.1815e-04
4	0.0015	4.3023e-04	0.0040	0.9728	0.0041
5	0.0101	5.2223e-04	8.9848e-04	0.0024	0.9910

Figure A.113: State Sequence 12345 BWP State Likelihood Estimates vs. Timeblocks

Figure A.114 displays the likelihoods from the DSM HMM; the CSM state likelihoods are shown in each row while each timeblock is shown in each column. Note the state sequence 12345 was not recognized along the diagonal of the matrix while all other states were found to be equally likely.

Figure A.115 displays the likelihoods from the DSP HMM; the CSM state likelihoods are shown in each row while each timeblock is shown in each column. Note the state sequence 12345 was not recognized along the diagonal of the matrix while all other states were found to be equally likely.

State Sequence 23451

Figure A.116 displays the liklihood from the CEM HMM; the CSM state likelihoods are shown in each row while each timeblock is shown in each column. Note the state sequence 23451 was recognized with an estimated likelihood greater than 98% in each column while all other states were found to be not likely.

	1	2	3	4	5
1	0.7662	0.7147	0.6960	0.6985	0.6924
2	4.6239e-05	6.5290e-05	1.5565e-05	7.6081e-05	2.5439e-05
3	0.2334	0.2848	0.3036	0.3007	0.3070
4	2.3050e-05	2.0952e-05	9.7606e-06	2.4008e-05	1.2479e-05
5	3.8116e-04	3.6476e-04	3.4561e-04	6.7052e-04	5.5347e-04

Figure A.114: State Sequence 12345 DSM State Likelihood Estimates vs. Timeblocks

	1	2	3	4	5
1	0.1300	0.0325	0.0305	1.1073e-09	0.0305
2	0.1027	0.1586	0.1169	6.0041e-05	0.1249
3	0.6061	0.6258	0.6613	5.1697e-10	0.6431
4	0.0048	0.0050	0.0050	0.9999	0.0050
5	0.1564	0.1782	0.1863	8.7631e-09	0.1965

Figure A.115: State Sequence 12345 DSP State Probablity Estimates vs. Timeblocks

	1	2	3	4	5
1	1.2278e-06	0.0017	2.2114e-07	7.8688e-07	0.9998
2	0.9999	9.8925e-04	1.4708e-06	8.0427e-06	8.0138e-07
3	3.3631e-05	0.9869	2.2943e-04	0.0010	1.3106e-06
4	5.1416e-06	0.0041	0.9998	4.7093e-04	4.0904e-08
5	1.2176e-05	0.0063	7.1979e-06	0.9985	1.8848e-04

Figure A.116: State Sequence 23451 CEM State Likelihood Estimates vs. Timeblocks

Figure A.117 displays the likelihoods from the CEP HMM; the CSM state likelihoods are shown in each row while each timeblock is shown in each column. Note the state sequence 23451 was recognized with an estimated likelihood greater than 99% in each column of the matrix while all other states were found to be not likely.

Figure A.118 displays the likelihoods from the TcM HMM; the CSM state likelihoods are shown in each row while each timeblock is shown in each column. Note the state sequence 23451 was not recognized in the columns of the matrix while all other states were found to be nearly equally likely.

Figure A.119 displays the likelihoods from the TcP HMM; the CSM state likelihoods are shown in each row while each timeblock is shown in each column. Note the state sequence 23451 was recognized in the columns of the matrix while all other states were found to be not likely.

	1	2	3	4	5
1	4.0085e-05	0.0014	1.2871e-06	8.3011e-06	0.9999
2	1.0000	4.8548e-04	1.2675e-04	5.6682e-06	1.3388e-09
3	7.8884e-07	0.9955	5.7128e-06	3.7538e-04	2.0381e-07
4	1.1731e-07	0.0015	0.9999	3.4630e-04	1.9496e-08
5	5.6318e-08	0.0012	8.8024e-06	0.9993	1.2598e-04

Figure A.117: State Sequence 23451 CEP State Likelihood Estimates vs. Timeblocks

	1	2	3	4	5
1	0.0112	3.6133e-...	0.0013	1.4263e-...	0.0113
2	0.0310	8.4988e-...	0.0025	2.4495e-...	0.0369
3	0.0398	0.0488	0.0223	0.0798	0.0343
4	0.3663	0.3583	0.5608	0.3430	0.3735
5	0.5517	0.5917	0.4132	0.5768	0.5441

Figure A.118: State Sequence 23451 TcM State Likelihood Estimates vs. Timeblocks

	1	2	3	4	5
1	0.0100	2.1816e-06	5.8012e-04	9.9501e-05	0.9979
2	0.9898	3.6069e-05	2.0901e-04	3.5269e-06	3.1417e-04
3	8.3591e-05	0.9995	4.8793e-05	4.7118e-04	3.4693e-07
4	1.3238e-04	7.3336e-05	0.9990	3.9579e-05	0.0018
5	6.3093e-07	3.4700e-04	1.9965e-04	0.9994	1.2143e-05

Figure A.119: State Sequence 23451 TcP State Likelihood Estimates vs. Timeblocks

Figure A.120 displays the likelihoods from the Doppler Spread magnitude HMM; the CSM state likelihoods are shown in each row while each timeblock is shown in each column. Note while State 1 was estimated in Timeblock 1, it was not discrimated from the other states in timeblocks 2-5. Additionally, the state sequence 23451 was not recognized in the colums of the matrix while all other states were found to be equally likely.

Figure A.121 displays the likelihoods from the DPP HMM; the CSM state likelihoods are shown in each row while each timeblock is shown in each column. Note that state 4 was estimted as most likely in all timeblocks except timeblock 4. The state sequence 23451 was not recognized in the columns of the matrix while all other states were found to be equally likely.

Figure A.122 displays the likelihoods from the BWM HMM; the CSM state likelihoods are shown in each row while each timeblock is shown in each column. Note the state sequence 23451 was

	1	2	3	4	5
1	3.9741e-06	8.4843e-10	6.0747e-10	1.7566e-09	7.8249e-10
2	1.0000	1.0000	1.0000	1.0000	1.0000
3	9.5970e-10	8.4843e-10	6.0747e-10	1.7566e-09	7.8249e-10
4	9.5970e-10	8.4843e-10	6.0747e-10	1.7566e-09	7.8249e-10
5	9.5968e-10	8.4842e-10	6.0746e-10	1.7566e-09	7.8248e-10

Figure A.120: State Sequence 23451 DPM State Likelihood Estimates vs. Timeblocks

	1	2	3	4	5
1	0.0039	1.7388e-05	0.1005	0.0148	8.6321e-05
2	4.9948e-06	5.6680e-05	5.0230e-05	0.4070	3.9008e-06
3	0.0161	2.1071e-05	0.0289	0.0029	6.4148e-05
4	0.9777	0.9999	0.7906	0.4172	0.9998
5	0.0023	2.4548e-05	0.0801	0.1581	4.8463e-05

Figure A.121: State Sequence 23451 DPP State Likelihood Estimates vs. Timeblocks

	1	2	3	4	5
1	0.3304	0.2202	0.3890	0.2110	0.9964
2	0.4969	0.1961	0.1443	0.2366	9.5288e-05
3	0.0032	0.2208	0.2793	0.1558	0.0035
4	0.1692	0.3152	0.0806	0.2661	1.1017e-05
5	3.3613e-04	0.0478	0.1068	0.1304	8.5652e-06

Figure A.122: State Sequence 23451 BWM State Likelihood Estimates vs. Timeblocks

not estimated in the columns of the matrix while all other states were found to be equally likely.

Figure A.123 displays the likelihoods from the BWP HMM; the CSM state likelihoods are shown in each row while each timeblock is shown in each column. Note the state sequence 23451 was recognized along the diagonal of the matrix while all other states were found to be not likely.

Figure A.124 displays the likelihoods from the DSM HMM; the CSM state likelihoods are shown in each row while each timeblock is shown in each column. Note the state sequence 23451 was not recognized along the diagonal of the matrix while all other states were found to be equally likely.

Figure A.125 displays the likelihoods from the DSP HMM; the CSM state likelihoods are shown in each row while each timeblock is shown in each column. Note that state 3 was estimated as most likely in timeblocks 1-3 and state 4 in timeblock 4. The state sequence 23451 was not recognized along the diagonal of the matrix while all other states were found to be equally likely.

	1	2	3	4	5
1	0.0095	2.9690e-04	0.0193	0.0030	0.9628
2	0.9873	0.0062	0.0018	0.0034	0.0201
3	0.0023	0.9886	0.0037	5.1597e-04	6.8287e-04
4	4.2670e-04	0.0040	0.9728	0.0040	0.0041
5	4.5361e-04	8.9901e-04	0.0024	0.9891	0.0123

Figure A.123: State Sequence 23451 BWP State Likelihood Estimates vs. Timeblocks

	1	2	3	4	5
1	0.7662	0.7147	0.6960	0.6985	0.6924
2	4.6239e-05	6.5290e-05	1.5565e-05	7.6081e-05	2.5439e-05
3	0.2334	0.2848	0.3036	0.3007	0.3070
4	2.3050e-05	2.0952e-05	9.7606e-06	2.4008e-05	1.2479e-05
5	3.8116e-04	3.6476e-04	3.4561e-04	6.7052e-04	5.5347e-04

Figure A.124: State Sequence 23451 DSM State Likelihood Estimates vs. Timeblocks

	1	2	3	4	5
1	0.1300	0.0325	0.0305	1.1073e-09	0.0305
2	0.1027	0.1586	0.1169	6.0041e-05	0.1249
3	0.6061	0.6258	0.6613	5.1697e-10	0.6431
4	0.0048	0.0050	0.0050	0.9999	0.0050
5	0.1564	0.1782	0.1863	8.7631e-09	0.1965

Figure A.125: State Sequence 23451 DSP State Probablity Estimates vs. Timeblocks

State Sequence 34512

Figure A.126 displays the liklihood from the CEM HMM; the CSM state likelihoods are shown in each row while each timeblock is shown in each column. Note the state sequence 34512 was recognized with an estimated likelihood greater than 98% in each column while all other states were found to be not likely.

Figure A.127 displays the likelihoods from the CEP HMM; the CSM state likelihoods are shown in each row while each timeblock is shown in each column. Note the state sequence 34512 was recognized with an estimated likelihood greater than 99% in each column of the matrix while all other states were found to be not likely.

Figure A.128 displays the likelihoods from the TcM HMM; the CSM state likelihoods are shown in each row while each timeblock is shown in each column. Note that state 5 recognized as most

	1	2	3	4	5
1	0.0017	2.2113e-07	7.8687e-07	0.9998	3.1926e-05
2	9.6539e-04	1.4707e-06	8.0427e-06	6.1376e-05	1.0000
3	0.9869	2.1844e-04	0.0010	1.2152e-06	6.7936e-06
4	0.0041	0.9998	4.5171e-04	4.7364e-08	3.2565e-06
5	0.0063	7.8574e-06	0.9985	1.6865e-04	5.5801e-06

Figure A.126: State Sequence 34512 CEM State Likelihood Estimates vs. Timeblocks

	1	2	3	4	5
1	0.0014	1.2872e-06	8.3060e-06	0.9999	1.2006e-04
2	4.6908e-04	1.2675e-04	5.6682e-06	1.3219e-09	0.9999
3	0.9955	5.0636e-06	3.7540e-04	1.7323e-07	7.3058e-08
4	0.0015	0.9999	3.2793e-04	1.9373e-08	1.4766e-07
5	0.0012	1.0306e-05	0.9993	1.0601e-04	5.4052e-08

Figure A.127: State Sequence 34512 CEP State Likelihood Estimates vs. Timeblocks

	1	2	3	4	5
1	5.8069e-04	0.0013	1.4265e-04	0.0113	0.0112
2	8.4979e-04	0.0025	2.4496e-04	0.0369	0.0310
3	0.0488	0.0223	0.0798	0.0343	0.0398
4	0.3581	0.5608	0.3430	0.3737	0.3662
5	0.5917	0.4132	0.5768	0.5439	0.5519

Figure A.128: State Sequence 34512 TcM State Likelihood Estimates vs. Timeblocks

likely in all timeblocks and that the state sequence 34512 was not recognized in the columns of the matrix while all other states were found to be nearly equally likely.

Figure A.129 displays the likelihoods from the TcP HMM; the CSM state likelihoods are shown in each row while each timeblock is shown in each column. Note the state sequence 34512 was estimated with greater than 99% likelihood in the columns of the matrix while all other states were found to be not likely.

Figure A.130 displays the likelihoods from the DPM HMM; the CSM state likelihoods are shown in each row while each timeblock is shown in each column. Note that state 2 was incorrectly estimated as most likely in all timeblocks . Additionally, the state sequence 34512 was not recognized in the columns of the matrix while all other states were found to be equally likely.

	1	2	3	4	5
1	9.2471e-05	5.7981e-04	1.1470e-04	0.9973	0.0074
2	8.4321e-07	2.0910e-04	3.5468e-06	9.2128e-04	0.9925
3	0.9995	4.5118e-05	4.7111e-04	3.0179e-07	3.6035e-07
4	8.8961e-05	0.9990	3.6659e-05	0.0017	1.3269e-04
5	3.4555e-04	2.1536e-04	0.9994	8.6509e-06	3.9787e-07

Figure A.129: State Sequence 34512 TcP State Likelihood Estimates vs. Timeblocks

	1	2	3	4	5
1	7.7200e-05	1.1621e-09	1.2177e-09	7.8828e-10	7.8650e-10
2	0.9999	1.0000	1.0000	1.0000	1.0000
3	5.2045e-09	1.1621e-09	1.2177e-09	7.8828e-10	7.8650e-10
4	5.2045e-09	1.1621e-09	1.2177e-09	7.8828e-10	7.8650e-10
5	5.2044e-09	1.1620e-09	1.2176e-09	7.8827e-10	7.8649e-10

Figure A.130: State Sequence 34512 DPM State Likelihood Estimates vs. Timeblocks

	1	2	3	4	5
1	9.7660e-08	1.9627e-12	1.9627e-12	1.9627e-12	0.1312
2	4.0226e-12	2.0113e-12	2.0113e-12	2.0113e-12	0.1248
3	4.0223e-12	2.0112e-12	2.0112e-12	2.0112e-12	0.5878
4	1.0000	1.0000	1.0000	1.0000	0.0046
5	3.9568e-12	1.9784e-12	1.9784e-12	1.9784e-12	0.1515

Figure A.131: State Sequence 34512 DPP State Likelihood Estimates vs. Timeblocks

Figure A.131 displays the likelihoods from the DPP HMM; the CSM state likelihoods are shown in each row while each timeblock is shown in each column. Note that state 4 was incorrectly estimated in all timeblocks. The state sequence 34512 was not recognized in the columns of the matrix while all other states were found to be equally likely.

Figure A.132 displays the likelihoods from the BWM HMM; the CSM state likelihoods are shown in each row while each timeblock is shown in each column. Note while State 1 was correclty estimated in Timeblock 4, the state sequence 34512 was not recognized along the diagonal of the matrix while all other states were found to be equally likely.

Figure A.133 displays the likelihoods from the BWP HMM; the CSM state likelihoods are shown in each row while each timeblock is shown in each column. Note the state sequence 34512 was estimated with greater than 95% likelihood along the columns of the matrix while all other states

	1	2	3	4	5
1	0.2202	0.3890	0.2110	0.9964	0.3304
2	0.1961	0.1443	0.2366	9.5296e-05	0.4969
3	0.2207	0.2793	0.1558	0.0035	0.0032
4	0.3152	0.0806	0.2661	1.1020e-05	0.1692
5	0.0478	0.1068	0.1304	8.5681e-06	3.3614e-04

Figure A.132: State Sequence 34512 BWM State Likelihood Estimates vs. Timeblocks

	1	2	3	4	5
1	0.0042	0.0193	0.0030	0.9543	0.0039
2	5.0085e-04	0.0018	0.0034	0.0337	0.9933
3	0.9903	0.0037	5.1575e-04	3.1734e-04	0.0018
4	0.0040	0.9728	0.0040	0.0015	4.2702e-04
5	9.7320e-04	0.0024	0.9891	0.0102	5.1358e-04

Figure A.133: State Sequence 34512 BWP State Likelihood Estimates vs. Timeblocks

	1	2	3	4	5
1	9.7660e-08	1.9627e-12	1.9627e-12	9.6777e-08	0.1445
2	4.0226e-12	2.0113e-12	2.0113e-12	2.0134e-10	0.1158
3	4.0223e-12	2.0112e-12	2.0112e-12	1.0137e-10	0.0842
4	1.0000	1.0000	1.0000	1.0000	0.6356
5	3.9568e-12	1.9784e-12	1.9784e-12	5.4100e-11	0.0199

Figure A.134: State Sequence 34512 DSM State Likelihood Estimates vs. Timeblocks

were found to be not likely.

Figure A.134 displays the likelihoods from the DSM HMM; the CSM state likelihoods are shown in each row while each timeblock is shown in each column. Note that state 4 was incorrectly estimated to be the most likely state in all timeblocks. The state sequence 34512 was not recognized along the diagonal of the matrix while all other states were found to be equally likely.

Figure A.135 displays the likelihoods from the DSP HMM; the CSM state likelihoods are shown in each row while each timeblock is shown in each column. Note that state 4 was estimated as most likely in all timeblocks. The state sequence 34512 was not recognized along the diagonal of the matrix while all other states were found to be equally likely.

	1	2	3	4	5
1	9.7660e-08	1.9627e-12	1.9627e-12	1.9627e-12	0.1312
2	4.0226e-12	2.0113e-12	2.0113e-12	2.0113e-12	0.1248
3	4.0223e-12	2.0112e-12	2.0112e-12	2.0112e-12	0.5878
4	1.0000	1.0000	1.0000	1.0000	0.0046
5	3.9568e-12	1.9784e-12	1.9784e-12	1.9784e-12	0.1515

Figure A.135: State Sequence 34512 DSP State Probablity Estimates vs. Timeblocks

	1	2	3	4	5
1	4.1852e-06	7.8686e-07	0.9998	2.0447e-05	0.0017
2	1.4600e-06	8.0426e-06	6.9805e-05	1.0000	0.0010
3	7.7036e-07	0.0010	1.1276e-06	1.5266e-05	0.9871
4	1.0000	4.3263e-04	5.5735e-08	3.2618e-06	0.0039
5	6.7969e-06	0.9986	1.4883e-04	5.6436e-06	0.0063

Figure A.136: State Sequence 45123 CEM State Likelihood Estimates vs. Timeblocks

	1	2	3	4	5
1	1.8637e-06	9.2829e-06	0.9999	1.0006e-04	0.0012
2	1.2681e-04	5.6682e-06	1.2883e-09	0.9999	5.4428e-04
3	1.4448e-06	3.7541e-04	1.4380e-07	7.8374e-08	0.9968
4	0.9999	3.0984e-04	1.9244e-08	1.4732e-07	8.3230e-05
5	1.1399e-05	0.9993	8.7022e-05	5.4061e-08	0.0013

Figure A.137: State Sequence 45123 CEP State Likelihood Estimates vs. Timeblocks

State Sequence 45123

Figure A.136 displays the liklihood from the CEM HMM; the CSM state likelihoods are shown in each row while each timeblock is shown in each column. Note the state sequence 45123 was recognized with an estimated likelihood greater than 98% in each column while all other states were found to be not likely.

Figure A.137 displays the likelihoods from the CEP HMM; the CSM state likelihoods are shown in each row while each timeblock is shown in each column. Note the state sequence 45123 was recognized with an estimated likelihood greater than 99% in each column of the matrix while all other states were found to be not likely.

Figure A.138 displays the likelihoods from the TcM HMM; the CSM state likelihoods are shown in each row while each timeblock is shown in each column. Note that state 5 was incorrectly estimated as most likely in all timeblocks except timeblock 1 and that the state sequence 45123 was not recognized in the columns of the matrix while all other states were found to be nearly equally likely.

Figure A.139 displays the likelihoods from the TcP HMM; the CSM state likelihoods are shown in each row while each timeblock is shown in each column. Note the state sequence 45123 was

	1	2	3	4	5
1	0.0016	1.4266e-04	0.0113	0.0112	3.5924e-04
2	0.0025	2.4497e-04	0.0369	0.0310	8.4827e-04
3	0.0223	0.0798	0.0343	0.0398	0.0488
4	0.5605	0.3430	0.3737	0.3664	0.3581
5	0.4131	0.5768	0.5439	0.5517	0.5918

Figure A.138: State Sequence 45123 TcM State Likelihood Estimates vs. Timeblocks

	1	2	3	4	5
1	0.0057	1.3043e-04	0.9973	0.0074	4.4486e-07
2	2.0808e-04	3.5752e-06	9.2639e-04	0.9924	5.7295e-05
3	5.2986e-06	4.7103e-04	2.6485e-07	4.5460e-05	0.9996
4	0.9939	3.3964e-05	0.0017	1.3355e-04	5.3913e-07
5	2.3130e-04	0.9994	5.7294e-06	4.4415e-07	3.4801e-04

Figure A.139: State Sequence 45123 TcP State Likelihood Estimates vs. Timeblocks

estimated wiht greater that 99% likelihood in the columns of the matrix while all other states were found to be not likely.

Figure A.140 displays the likelihoods from the DPM HMM; the CSM state likelihoods are shown in each row while each timeblock is shown in each column. Note that state 2 was incorrectly estimated as most likely in all timeblocks . Additionally, the state sequence 45123 was not recognized in the colums of the matrix while all other states were found to be equally likely.

Figure A.141 displays the likelihoods from the DPP HMM; the CSM state likelihoods are shown in each row while each timeblock is shown in each column. Note that state 4 was incorrectly estimated as most likely in all timeblocks except timeblock 1. The state sequence 45123 was not recognized in the columns of the matrix while all other states were found to be equally likely.

	1	2	3	4	5
1	2.2842e-06	6.8614e-10	7.9753e-10	7.9972e-10	7.6816e-10
2	1.0000	1.0000	1.0000	1.0000	1.0000
3	1.7910e-09	6.8614e-10	7.9753e-10	7.9972e-10	7.6816e-10
4	1.7910e-09	6.8614e-10	7.9753e-10	7.9972e-10	7.6816e-10
5	1.7909e-09	6.8613e-10	7.9752e-10	7.9971e-10	7.6815e-10

Figure A.140: State Sequence 45123 DPM State Likelihood Estimates vs. Timeblocks

	1	2	3	4	5
1	0.1029	0.0147	3.0163e-05	1.8143e-05	0.0022
2	0.4070	1.0741e-06	7.7397e-05	3.1598e-06	5.2728e-06
3	0.0290	0.0027	1.6533e-05	1.8529e-05	0.0161
4	0.3808	0.8245	0.9999	0.9999	0.9794
5	0.0802	0.1580	1.3930e-05	1.3867e-05	0.0023

Figure A.141: State Sequence 45123 DPP State Likelihood Estimates vs. Timeblocks

	1	2	3	4	5
1	0.3890	0.2110	0.9964	0.3304	0.2202
2	0.1443	0.2366	9.5296e-05	0.4969	0.1961
3	0.2792	0.1558	0.0035	0.0032	0.2208
4	0.0806	0.2661	1.1020e-05	0.1692	0.3152
5	0.1068	0.1304	8.5684e-06	3.3614e-04	0.0478

Figure A.142: State Sequence 45123 BWM State Likelihood Estimates vs. Timeblocks

Figure A.142 displays the likelihoods from the BWM HMM; the CSM state likelihoods are shown in each row while each timeblock is shown in each column. Note while State 1 was correctly estimated in Timeblock 3, the state sequence 45123 was not recognized along the diagonal of the matrix while all other states were found to be equally likely.

Figure A.143 displays the likelihoods from the BWP HMM; the CSM state likelihoods are shown in each row while each timeblock is shown in each column. Note the state sequence 45123 was estimated with greater than 95% likelihood along the columns of the matrix while all other states were found to be not likely.

Figure A.144 displays the likelihoods from the DSM HMM; the CSM state likelihoods are shown in each row while each timeblock is shown in each column. Note that state 1 was incorrectly estimated to be the most likely state in all timeblocks. The state sequence 45123 was not recognized

	1	2	3	4	5
1	0.0242	0.0030	0.9543	0.0039	2.9612e-04
2	0.0018	0.0034	0.0337	0.9928	0.0062
3	5.4002e-04	5.1553e-04	3.1736e-04	0.0023	0.9922
4	0.9712	0.0040	0.0015	4.3038e-04	5.1579e-04
5	0.0023	0.9891	0.0102	5.2257e-04	8.1920e-04

Figure A.143: State Sequence 45123 BWP State Likelihood Estimates vs. Timeblocks

	1	2	3	4	5
1	1.0000	1.0000	0.9998	0.6125	1.0000
2	1.3198e-07	1.3203e-07	2.6553e-07	2.3707e-05	2.5679e-07
3	6.6508e-08	6.6525e-08	2.1839e-04	0.3873	1.2800e-07
4	9.9400e-08	9.9430e-08	2.0001e-07	1.2324e-05	1.9261e-07
5	7.9435e-08	7.9456e-08	1.6288e-07	2.3764e-04	1.5336e-07

Figure A.144: State Sequence 45123 DSM State Likelihood Estimates vs. Timeblocks

	1	2	3	4	5
1	9.7660e-08	1.9627e-12	1.9627e-12	0.1312	2.0054e-05
2	4.0226e-12	2.0113e-12	2.0113e-12	0.1248	4.9020e-12
3	4.0223e-12	2.0112e-12	2.0112e-12	0.5878	4.9016e-12
4	1.0000	1.0000	1.0000	0.0046	1.0000
5	3.9568e-12	1.9784e-12	1.9784e-12	0.1515	4.8357e-12

Figure A.145: State Sequence 45123 DSP State Probablity Estimates vs. Timeblocks

along the diagonal of the matrix while all other states were found to be equally likely.

Figure A.145 displays the likelihoods from the DSP HMM; the CSM state likelihoods are shown in each row while each timeblock is shown in each column. Note that state 4 was estimated as most likely in all timeblocks except timeblock 4. The state sequence 45123 was not recognized along the diagonal of the matrix while all other states were found to be equally likely.

State Sequence 51234

Figure A.146 displays the liklihood from the CEM HMM; the CSM state likelihoods are shown in each row while each timeblock is shown in each column. Note the state sequence 51234 was recognized with an estimated likelihood greater than 98% in each column while all other states were found to be not likely.

Figure A.147 displays the likelihoods from the CEP HMM; the CSM state likelihoods are shown in each row while each timeblock is shown in each column. Note the state sequence 51234 was recognized with an estimated likelihood greater than 99% in each column of the matrix while all other states were found to be not likely.

	1	2	3	4	5
1	3.6496e-06	0.9998	1.0996e-05	0.0017	2.2107e-07
2	8.0351e-06	8.0168e-05	1.0000	0.0010	1.4713e-06
3	0.0010	1.0822e-06	1.7254e-05	0.9869	2.5363e-04
4	4.6825e-05	6.9957e-08	3.2489e-06	0.0041	0.9997
5	0.9989	1.2904e-04	5.5932e-06	0.0063	3.0570e-06

Figure A.146: State Sequence 51234 CEM State Likelihood Estimates vs. Timeblocks

	1	2	3	4	5
1	1.4800e-04	0.9999	8.0059e-05	0.0014	1.2869e-06
2	5.6597e-06	1.2881e-09	0.9999	5.2478e-04	1.2675e-04
3	3.8166e-04	1.1804e-07	9.7443e-08	0.9955	7.2714e-06
4	3.6863e-05	1.8908e-08	1.4650e-07	0.0014	0.9999
5	0.9994	7.0569e-05	5.4150e-08	0.0012	2.7786e-06

Figure A.147: State Sequence 51234 CEP State Likelihood Estimates vs. Timeblocks

Figure A.148 displays the likelihoods from the TcM HMM; the CSM state likelihoods are shown in each row while each timeblock is shown in each column. Note that state 5 was incorrectly estimated as most likely in all timeblocks except timeblock 5 and that the state sequence 51234 was not recognized in the columns of the matrix while all other states were found to be nearly equally likely.

Figure A.149 displays the likelihoods from the TcP HMM; the CSM state likelihoods are shown in each row while each timeblock is shown in each column. Note the state sequence 51234 was recognized with greater than 99% likelihood in the columns of the matrix while all other states were found to be not likely.

Figure A.150 displays the likelihoods from the DPM HMM; the CSM state likelihoods are shown in each row while each timeblock is shown in each column. Note that state 2 was incorrectly esti-

	1	2	3	4	5
1	4.9939e-04	0.0113	0.0112	3.6130e-04	0.0013
2	2.4458e-04	0.0369	0.0310	8.4985e-04	0.0025
3	0.0798	0.0343	0.0398	0.0488	0.0223
4	0.3428	0.3737	0.3664	0.3583	0.5606
5	0.5766	0.5439	0.5517	0.5917	0.4133

Figure A.148: State Sequence 51234 TcM State Likelihood Estimates vs. Timeblocks

	1	2	3	4	5
1	2.6830e-04	0.9973	0.0074	1.6070e-06	6.7734e-04
2	2.3950e-06	9.3150e-04	0.9924	4.9366e-05	3.1233e-04
3	4.7447e-04	2.4278e-07	5.7198e-05	0.9996	6.4942e-05
4	9.8591e-06	0.0017	1.3356e-04	4.9157e-05	0.9989
5	0.9992	4.0552e-06	4.9867e-07	3.4708e-04	7.3440e-06

Figure A.149: State Sequence 51234 TcP State Likelihood Estimates vs. Timeblocks

	1	2	3	4	5
1	4.4384e-07	8.0375e-10	7.9294e-10	8.0533e-10	7.9353e-10
2	1.0000	1.0000	1.0000	1.0000	1.0000
3	8.0050e-10	8.0375e-10	7.9294e-10	8.0533e-10	7.9353e-10
4	8.0050e-10	8.0375e-10	7.9294e-10	8.0533e-10	7.9353e-10
5	8.0049e-10	8.0373e-10	7.9293e-10	8.0531e-10	7.9351e-10

Figure A.150: State Sequence 51234 DPM State Likelihood Estimates vs. Timeblocks

mated as most likely in all timeblocks . Additionally, the state sequence 51234 was not recognized in the colums of the matrix while all other states were found to be equally likely.

Figure A.151 displays the likelihoods from the DPP HMM; the CSM state likelihoods are shown in each row while each timeblock is shown in each column. Note that state 4 was incorrectly estimated as most likely in all timeblocks except timeblock 1. The state sequence 51234 was not recognized in the columns of the matrix while all other states were found to be equally likely.

Figure A.152 displays the likelihoods from the BWM HMM; the CSM state likelihoods are shown in each row while each timeblock is shown in each column. Note while State 1 was correctly estimated in Timeblock 2, the state sequence 51234 was not recognized along the diagonal of the matrix while all other states were found to be equally likely.

	1	2	3	4	5
1	9.7660e-08	1.9627e-12	0.1312	2.0054e-05	1.9722e-12
2	4.0226e-12	2.0113e-12	0.1248	4.8920e-12	2.0213e-12
3	4.0223e-12	2.0112e-12	0.5878	4.8916e-12	2.0212e-12
4	1.0000	1.0000	0.0046	1.0000	1.0000
5	3.9568e-12	1.9784e-12	0.1515	4.8260e-12	1.9881e-12

Figure A.151: State Sequence 51234 DPP State Likelihood Estimates vs. Timeblocks

	1	2	3	4	5
1	0.0090	0.9542	0.0039	2.9694e-04	0.0190
2	0.0034	0.0337	0.9928	0.0062	0.0017
3	4.6779e-04	3.1739e-04	0.0023	0.9886	0.0036
4	0.0026	0.0015	4.3031e-04	0.0040	0.9747
5	0.9846	0.0102	5.2240e-04	8.9795e-04	9.4656e-04

Figure A.152: State Sequence 51234 BWM State Likelihood Estimates vs. Timeblocks

	1	2	3	4	5
1	0.0090	0.9542	0.0039	2.9694e-04	0.0190
2	0.0034	0.0337	0.9928	0.0062	0.0017
3	4.6779e-04	3.1739e-04	0.0023	0.9886	0.0036
4	0.0026	0.0015	4.3031e-04	0.0040	0.9747
5	0.9846	0.0102	5.2240e-04	8.9795e-04	9.4656e-04

Figure A.153: State Sequence 51234 BWP State Likelihood Estimates vs. Timeblocks

Figure A.153 displays the likelihoods from the BWP HMM; the CSM state likelihoods are shown in each row while each timeblock is shown in each column. Note the state sequence 51234 was estimated with greater than 95% likelihood along the columns of the matrix while all other states were found to be not likely.

Figure A.154 displays the likelihoods from the DSM HMM; the CSM state likelihoods are shown in each row while each timeblock is shown in each column. Note that state 1 was incorrectly estimated to be the most likely state in all timeblocks. The state sequence 51234 was not recognized along the diagonal of the matrix while all other states were found to be equally likely.

Figure A.155displays the likelihoods from the DSP HMM; the CSM state likelihoods are shown in each row while each timeblock is shown in each column. Note that state 4 was estimated as most likely in all timeblocks except timeblock 3. The state sequence 51234 was not recognized along

	1	2	3	4	5
1	1.0000	0.9998	0.6125	1.0000	1.0000
2	1.3198e-07	2.6553e-07	2.3707e-05	1.3203e-07	2.5679e-07
3	6.6508e-08	2.1839e-04	0.3873	6.6525e-08	1.2800e-07
4	9.9400e-08	2.0001e-07	1.2324e-05	9.9430e-08	1.9261e-07
5	7.9435e-08	1.6288e-07	2.3764e-04	7.9456e-08	1.5336e-07

Figure A.154: State Sequence 51234 DSM State Likelihood Estimates vs. Timeblocks

	1	2	3	4	5
1	9.7660e-08	1.9627e-12	0.1312	2.0054e-05	1.9722e-12
2	4.0226e-12	2.0113e-12	0.1248	4.8920e-12	2.0213e-12
3	4.0223e-12	2.0112e-12	0.5878	4.8916e-12	2.0212e-12
4	1.0000	1.0000	0.0046	1.0000	1.0000
5	3.9568e-12	1.9784e-12	0.1515	4.8260e-12	1.9881e-12

Figure A.155: State Sequence 51234 DSP State Probablity Estimates vs. Timeblocks

Table A.3: Feature Definitions

Feature	Abreviation
Complex Envelope Magnitude	CEM
Complex Envelope Phase	CEP
Coherence Time Magnitude	TcM
Coherence Time Phase	TcP
Doppler Spread Magnitude	DPM
Doppler Spread Phase	DPP
Coherence Bandwidth Magnitude	BWM
Coherence Bandwidth Phase	BWP
Delay Spread Magnitude	DSM
Delay Spread Phase	DSP

the diagonal of the matrix while all other states were found to be equally likely.

A.11.6 CSR Feature State Estimates

This section provides graphs of feature hard decisions vs. timeblocks. Each feature is defined in Table A.3. These features were extracted and aggregated from each of the feature state HMM outputs to formulate the diagrams in this section.

State Sequence 12345

Each of the feature recognition HMM state hard decisions for the input state sequence 12345 from the previous section were combined as shown in Figure A.156. Row 1correspondes to the first row of Table A.3 (CEM) while row 10 corresponds to row 10 (DSP). Each of the columns correspond to timeblock 1 to 5 consecutively. This information highlights the detection performance differences between each feature recognition HMM in each of the timeblocks. Note that the CEM,CEP, Tc

	1	2	3	4	5
1	1	2	3	4	5
2	1	2	3	4	5
3	0	0	0	0	0
4	1	2	3	4	5
5	1	0	0	0	0
6	1	0	0	3	0
7	1	0	0	0	0
8	1	2	3	4	5
9	0	0	0	0	0
10	0	0	0	4	0

Figure A.156: State Sequence 12345 CSR Combined Feature State Decisions vs. Timeblocks

phase, and BWc phase tracked CSM states effectively while the remaining features did poorly. Additionally, Figure A.157shows the same data as a surface plot, where the features that tracked the input state sequence can be clearly identified.

State Sequence 23451

Each of the feature recognition HMM state hard decisions for the input state sequence 23451 from the previous section were combined as shown in Figure A.158. Row 1 is mapped to first row of Table A.3 (CEM) while row 10 is mapped to row 10 (DSP). Each of the columns correspond to timeblock 1 to 5 consecutively. This information highlights the detection performance differences between each feature recognition HMM in each of the timeblocks. Note that the CEM,CEP, Tc phase, and BWc phase tracked CSM states effectively while the remaining features did poorly. Additionally, Figure A.159shows the same data as a surface plot, where the features that tracked the input state sequence can be clearly identified.

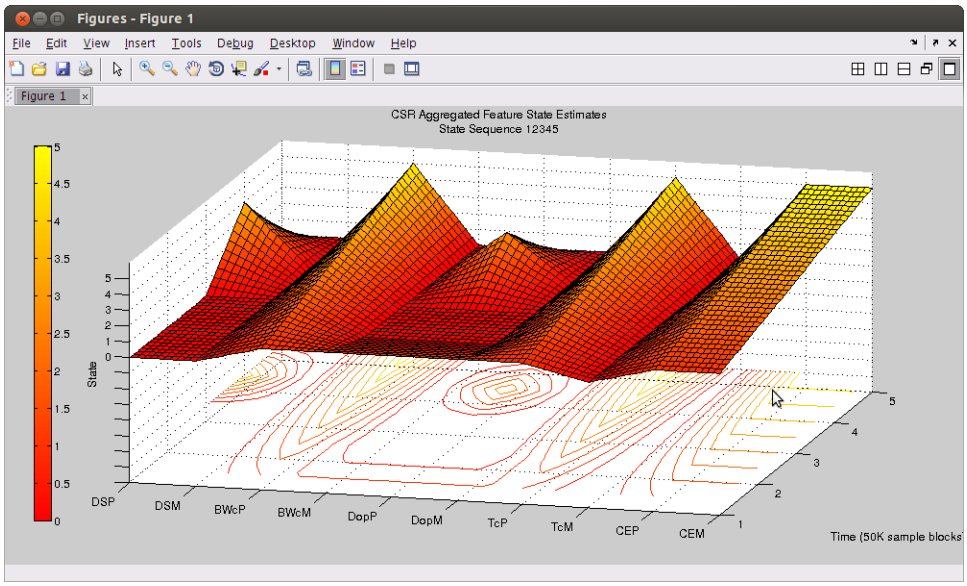

Figure A.157: State Sequence 12345 Feature State Decisions vs. Timeblocks

	1	2	3	4	5
1	2	3	4	5	1
2	2	3	4	5	1
3	0.1000	0	0	0	0
4	2	3	4	5	1
5	2	2	2	2	2
6	4	4	0	0	4
7	0.1000	0	0	0	1
8	2	3	4	5	1
9	0.1000	1	1	1	1
10	0.1000	4	4	4	4

Figure A.158: State Sequence 23451 CSR Combined Feature State Decisions vs. Timeblocks

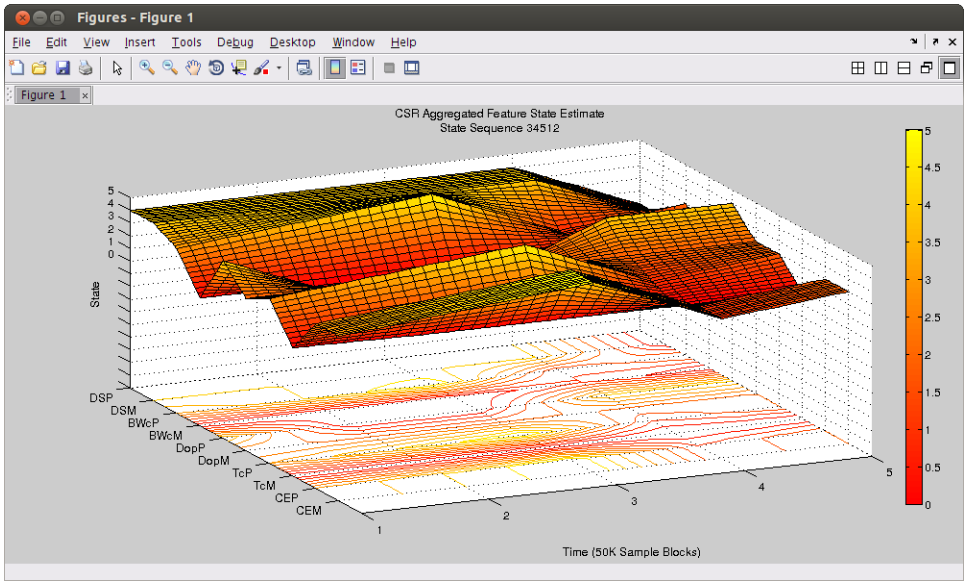

Figure A.159: State Sequence 23451 Feature State Decisions vs. Timeblocks

State Sequence 34512

Each of the feature recognition HMM state hard decisions for the input state sequence 34512 from the previous section were combined as shown in Figure A.160. Row 1 corresponds to first row of Table A.3 (CEM) while row 10 corresponds to row 10 (DSP). Each of the columns correspond to timeblock 1 to 5 consecutively. This information highlights the detection performance differences between each feature recognition HMM in each of the timeblocks. Note that the CEM,CEP, Tc phase, and BWc phase tracked CSM states effectively while the remaining features did poorly.

Additionally, Figure A.161shows the same data as a surface plot, where the features that tracked the input state sequence can be clearly identified.

State Sequence 45123

Each of the feature recognition HMM state hard decisions for the input state sequence 34512 from the previous section were combined as shown in Figure A.162. Row 1 corresponds to first row of Table A.3 (CEM) while row 10 corresponds to row 10 (DSP). Each of the columns correspond to timeblock 1 to 5 consecutively. This information highlights the detection performance differences

	1	2	3	4	5
1	3	4	5	1	2
2	3	4	5	1	2
3	0.1000	0	0	0	0
4	3	4	5	1	2
5	2	2	2	2	2
6	4	0	0	4	4
7	0.1000	0	0	1	0
8	3	4	5	1	2
9	4	4	4	4	0
10	4	4	4	4	0

Figure A.160: State Sequence 34512 CSR Combined Feature State Decisions vs. Timeblocks

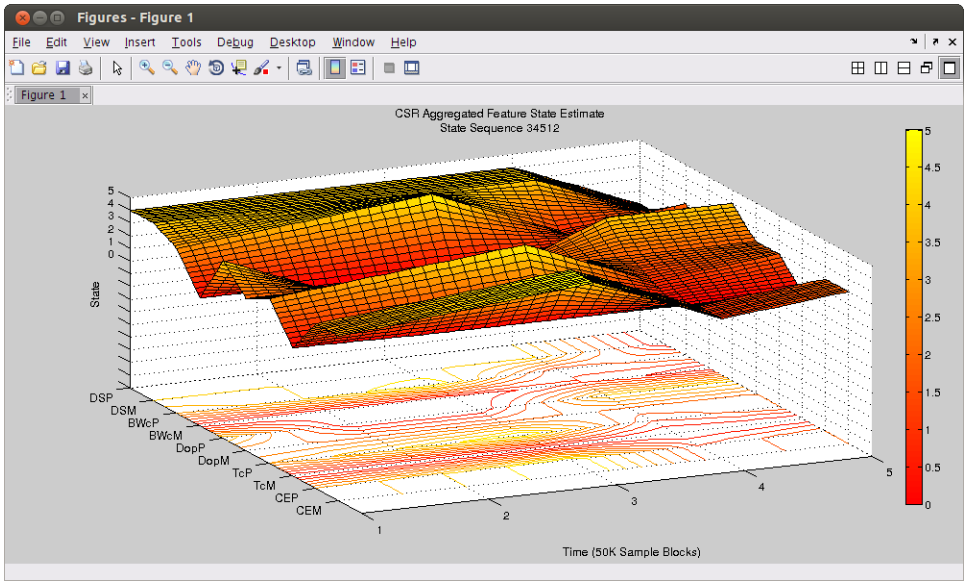

Figure A.161: State Sequence 34512 Feature State Decisions vs. Timeblocks

	1	2	3	4	5
1	4	5	1	2	3
2	4	5	1	2	3
3	0.1000	0	0	0	0
4	4	5	1	2	3
5	2	2	2	2	2
6	0.1000	0	4	4	4
7	0.1000	0	1	0	0
8	4	5	1	2	3
9	1	1	1	0	1
10	4	4	4	0	4

Figure A.162: State Sequence 45123 CSR Combined Feature State Decisions vs. Timeblocks

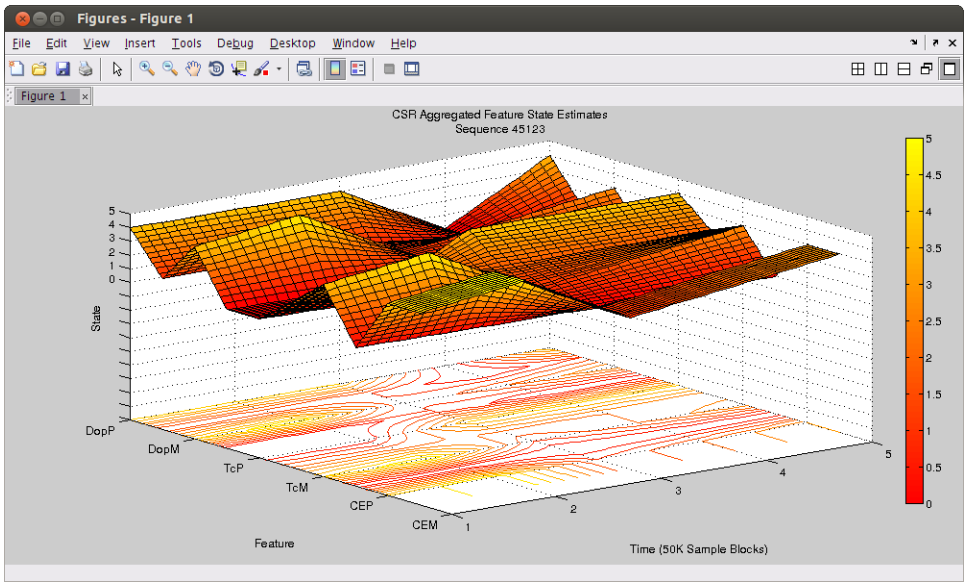

Figure A.163: State Sequence 45123 Feature State Decisions vs. Timeblocks

between each feature recognition HMM in each of the timeblocks. Note that the CEM,CEP, Tc phase, and BWc phase tracked CSM states effectively while the remaining features did poorly. Additionally, Figure A.163shows the same data as a surface plot, where the features that tracked the input state sequence can be clearly identified.

	1	2	3	4	5
1	5	1	2	3	4
2	5	1	2	3	4
3	0.1000	0	0	0	0
4	5	1	2	3	4
5	2	2	2	2	2
6	4	4	0	4	4
7	0.1000	1	0	0	0
8	5	1	2	3	4
9	1	1	0	1	1
10	4	4	0	4	4

Figure A.164: State Sequence 51234 CSR Combined Feature State Decisions vs. Timeblocks

State Sequene 51234

Each of the feature recognition HMM state hard decisions for the input state sequence 51234 from the previous section were combined as shown in Figure A.164. Row 1 corresponds to first row of Table A.3 (CEM) while row 10 corresponds to row 10 (DSP). Each of the columns correspond to timeblock 1 to 5 consecutively. This information highlights the detection performance differences between each feature recognition HMM in each of the timeblocks. Note that the CEM,CEP, Tc phase, and BWc phase tracked CSM states effectively while the remaining features did poorly.

Additionally, Figure A.165 shows the same data as a surface plot, where the features that tracked the input state sequence can be clearly identified.

A.11.7 CSR Output State Estimation

State Sequence 12345

Figure A.166 shows the timeblock 1 hard decision frequency distribution that were produced from the FSE for the input state sequence 12345.

Figure A.167 shows the timeblock 2 hard decision frequency distribution that were produced from the FSE for the input state sequence 12345.

Figure A.168 shows the timeblock 3 hard decision frequency distribution that were produced from

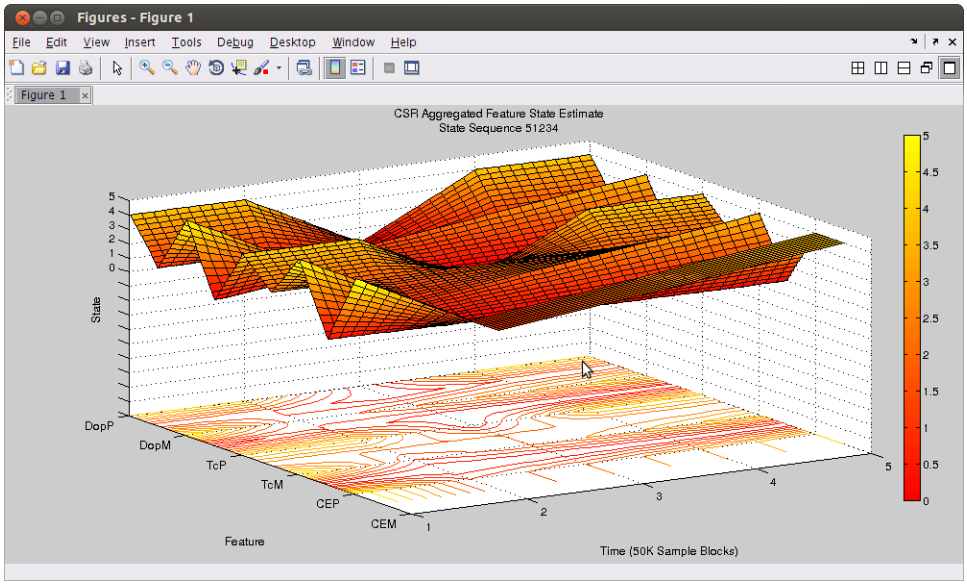

Figure A.165: State Sequence 51234 Feature State Decisions vs. Timeblocks

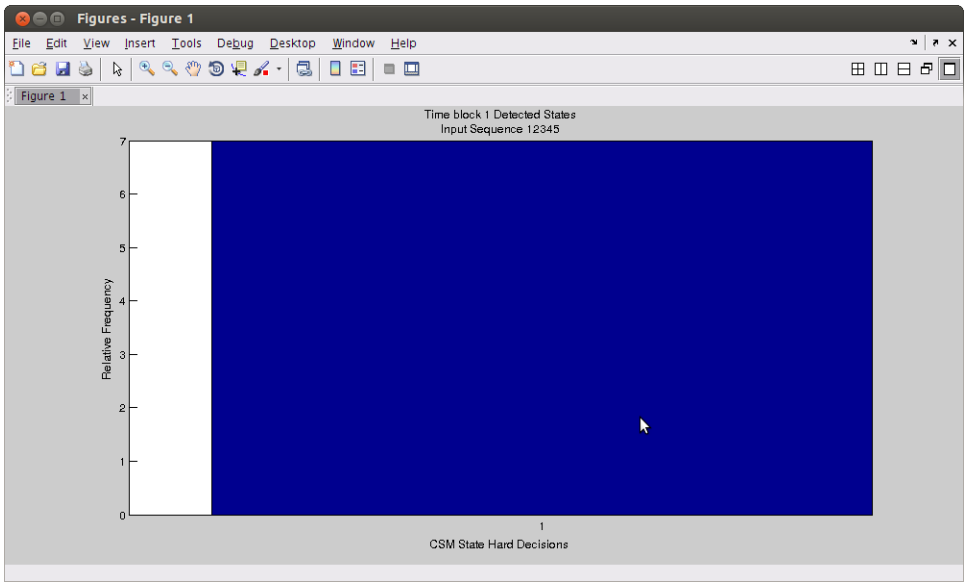

Figure A.166: Timeblock 1 State Frequency Distribution for State Sequence 12345

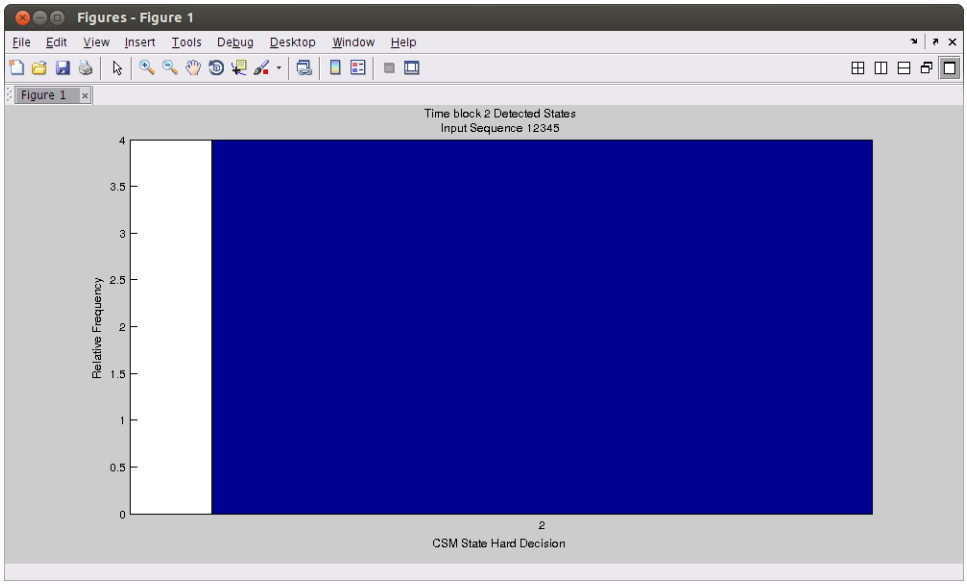

Figure A.167: Timeblock 2 State Frequency Distribution for State Sequence 12345

the FSE for the input state sequence 12345.

Figure A.169 shows the timeblock 4 hard decision frequency distribution that were produced from the FSE for the input state sequence 12345.

Figure A.170 shows the timeblock 5 hard decision frequency distribution that were produced from the FSE for the input state sequence 12345.

Figure A.171 shows the CSR algorithm output CSM CSE sequence that are the result of selecting the maximum of the hard decision frequency distribution for each time block and the input state sequence 12345.

State Sequence 23451

Figure A.172 shows the timeblock 1 hard decision frequency distribution that were produced from the FSE for the input state sequence 12345.

Figure A.173 shows the timeblock 2 hard decision frequency distribution that were produced from the FSE for the input state sequence 23451.

Figure A.174 shows the timeblock 3 hard decision frequency distribution that were produced from

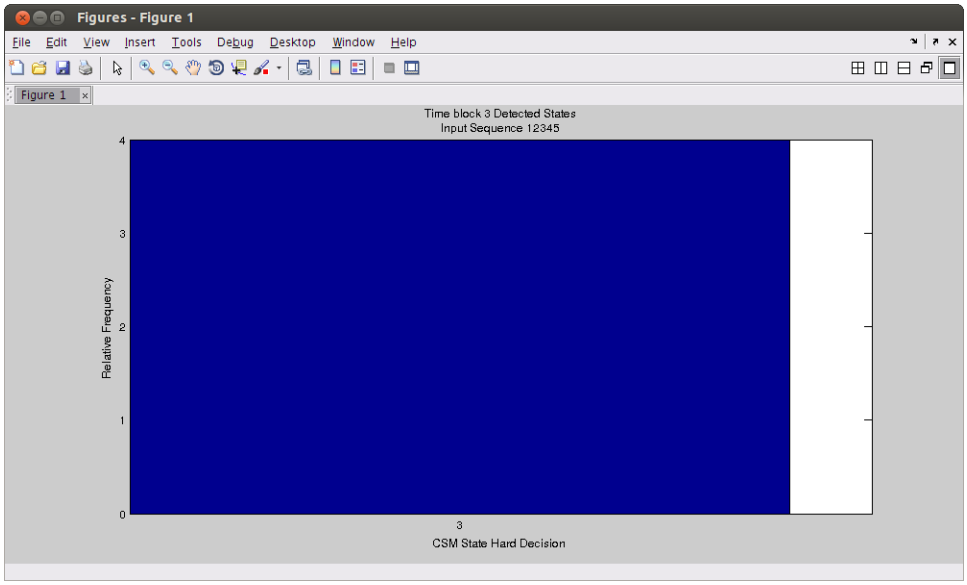

Figure A.168: Timeblock 3 State Frequency Distribution for State Sequence 12345

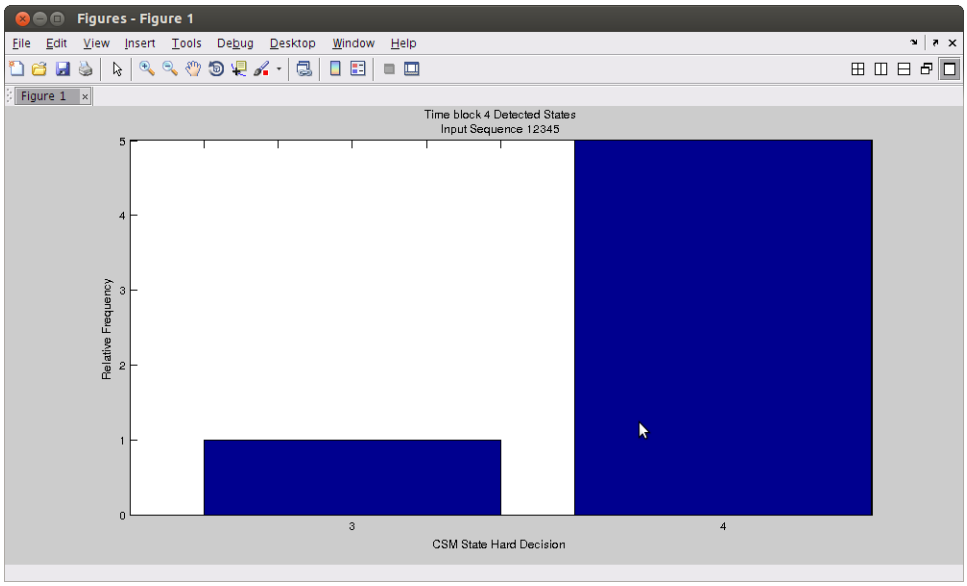

Figure A.169: Timeblock 4 State Frequency Distribution for State Sequence 12345

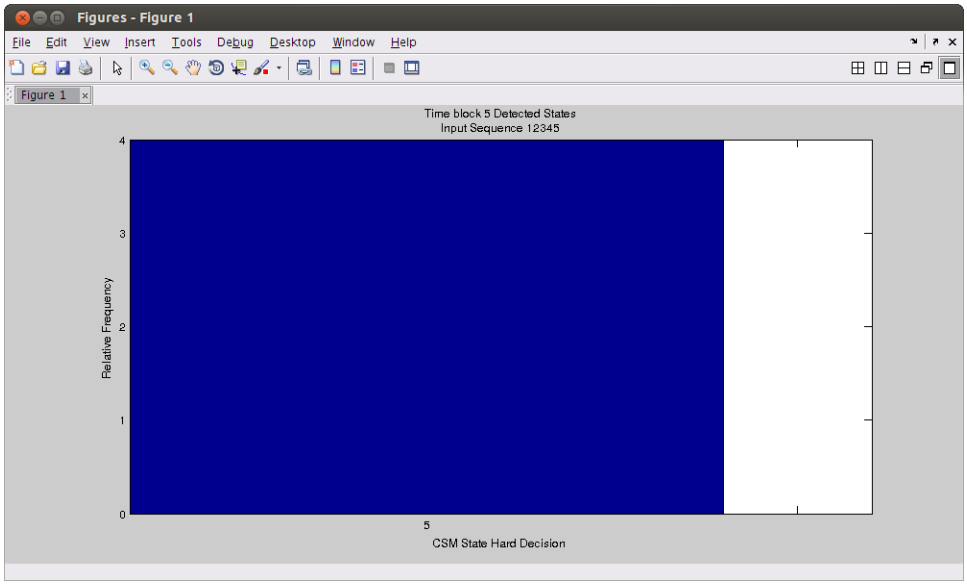

Figure A.170: Timeblock 5 State Frequency Distribution for State Sequence 12345

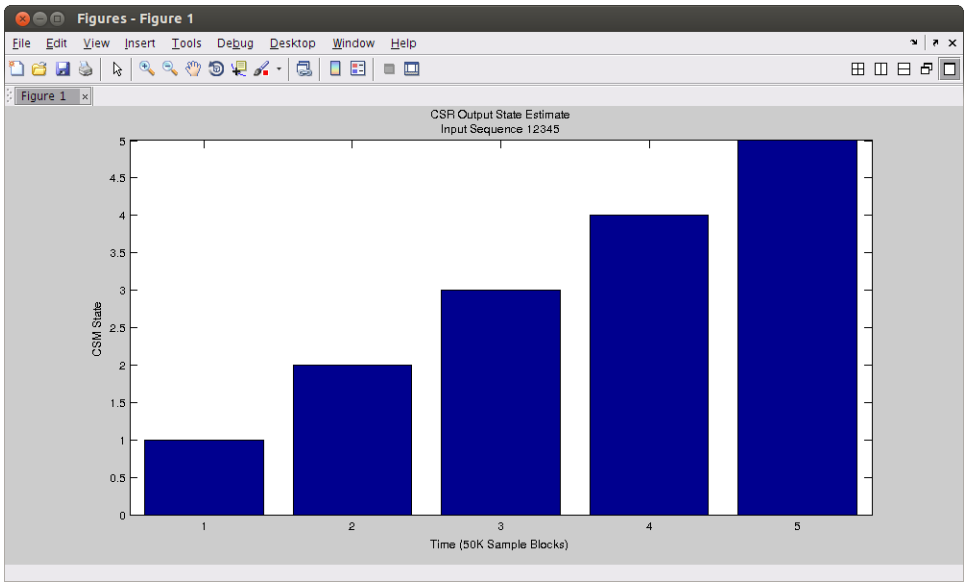

Figure A.171: CSR Output State Estimates for State Sequences 12345

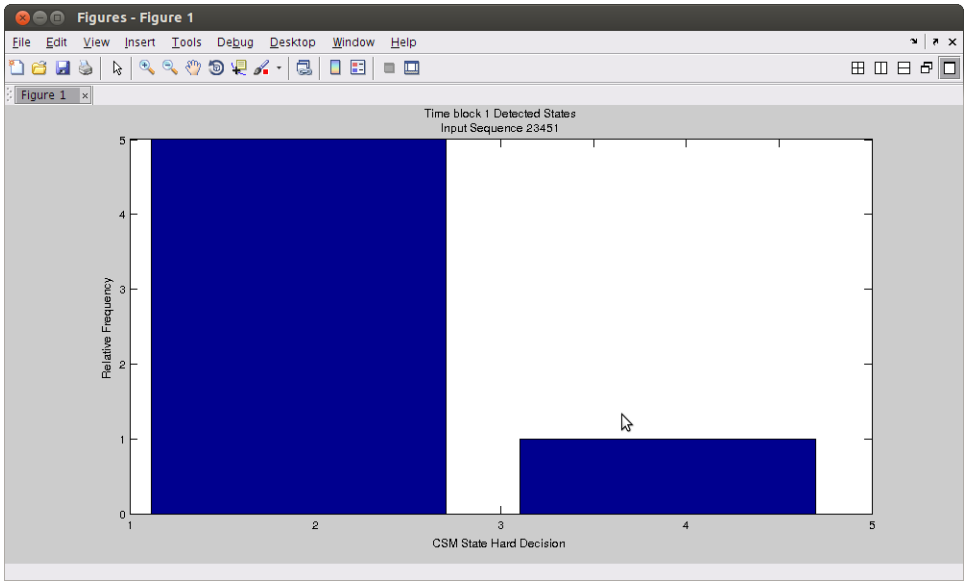

Figure A.172: Timeblock 1 State Frequency Distribution for State Sequence 23451

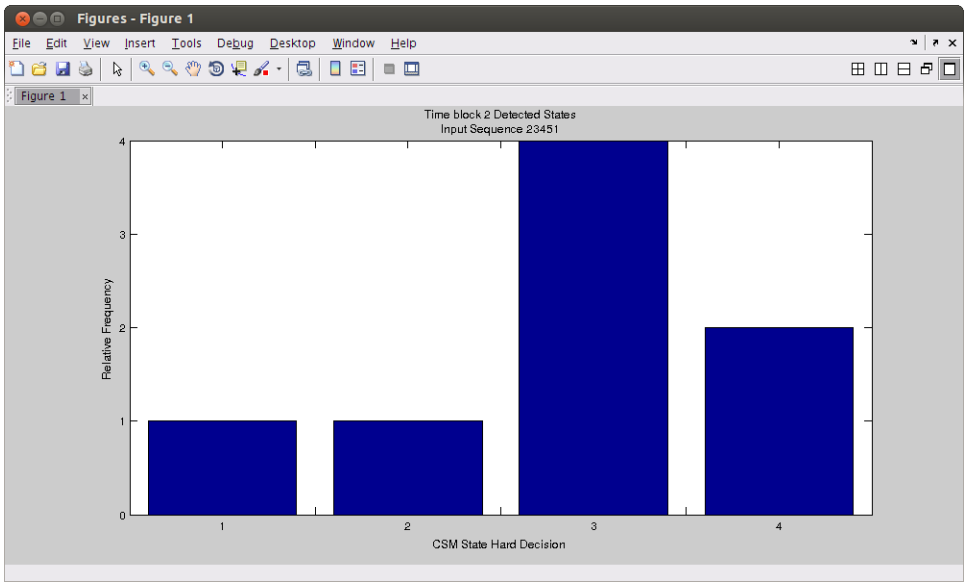

Figure A.173: Timeblock 2 State Frequency Distribution for State Sequence 23451

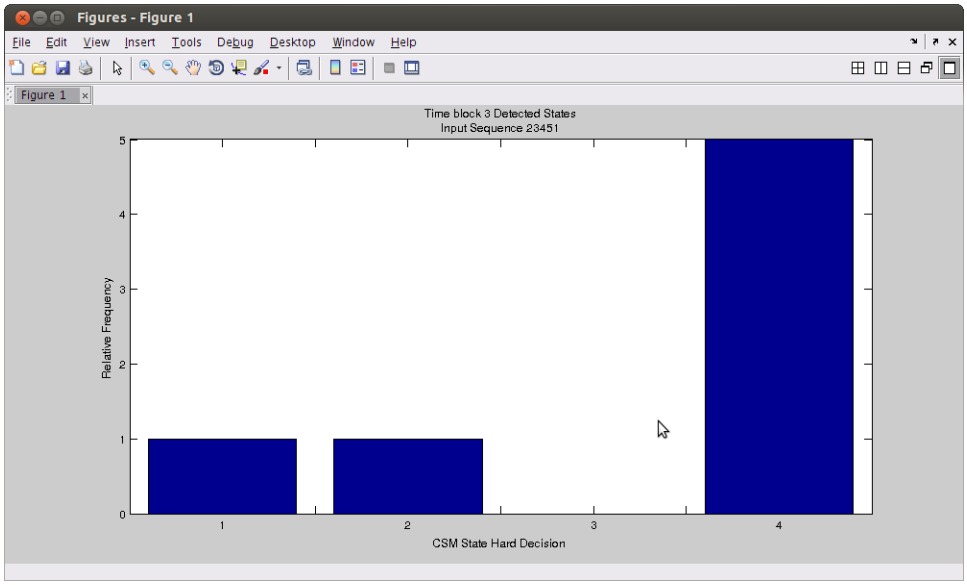

Figure A.174: Timeblock 3 State Frequency Distribution for State Sequence 23451

the FSE for the input state sequence 23451.

Figure A.175 shows the timeblock 4 hard decision frequency distribution that were produced from the FSE for the input state sequence 12345.

Figure A.176 shows the timeblock 5 hard decision frequency distribution that were produced from the FSE for input sequence 23451.

Figure A.177 shows the CSR algorithm output CSM CSE sequence that are the result of selecting the maximum of the hard decision frequency distribution for each time block and the input state sequence 23451.

State Sequence 34512

Figure A.178 shows the timeblock 1 hard decision frequency distribution that were produced from the FSE for the input state sequence 34521.

Figure A.179 shows the timeblock 2 hard decision frequency distribution that were produced from the FSE for the input state sequence 34512.

Figure A.180 shows the timeblock 3 hard decision frequency distribution that were produced from

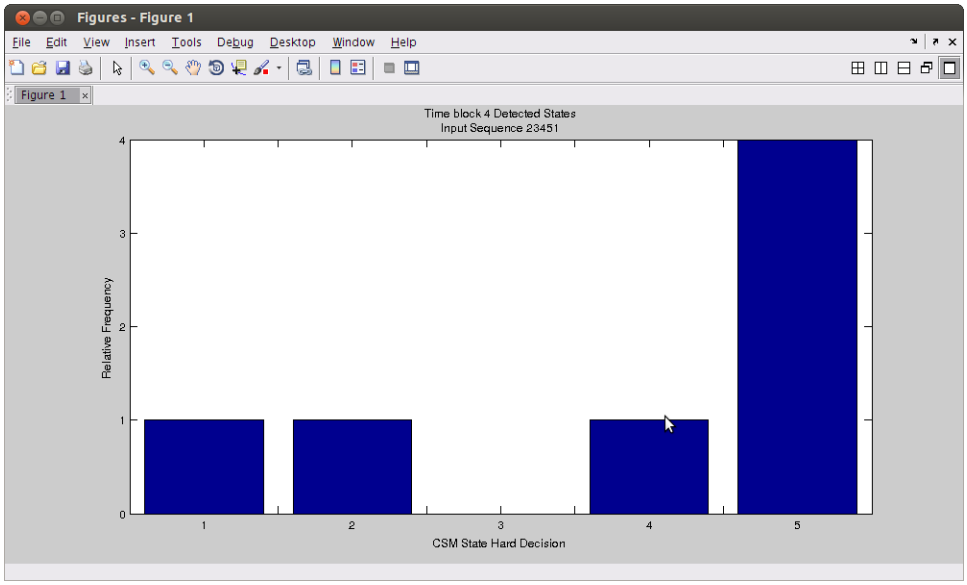

Figure A.175: Timeblock 4 State Frequency Distribution for State Sequence 23451

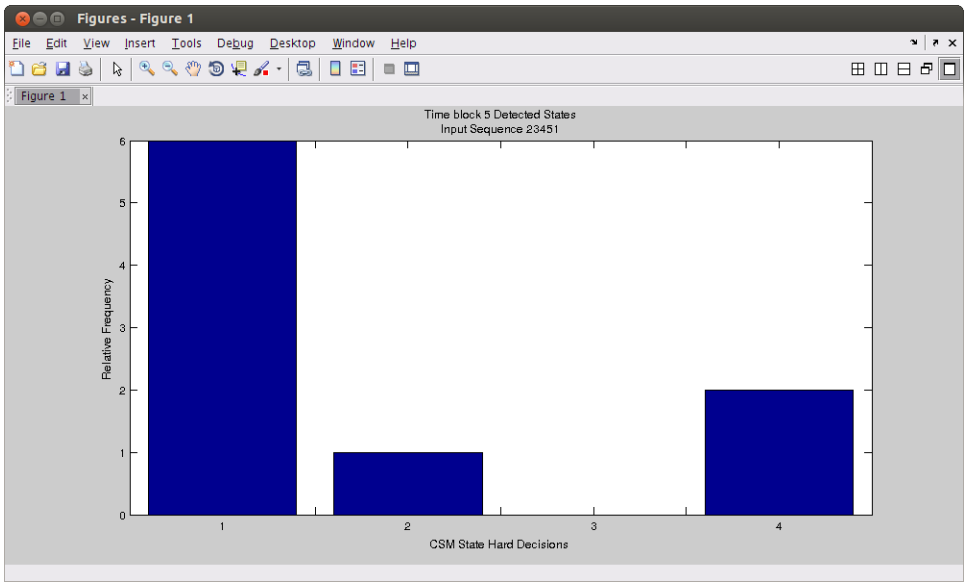

Figure A.176: Timeblock 5 State Frequency Distribution for State Sequence 23451

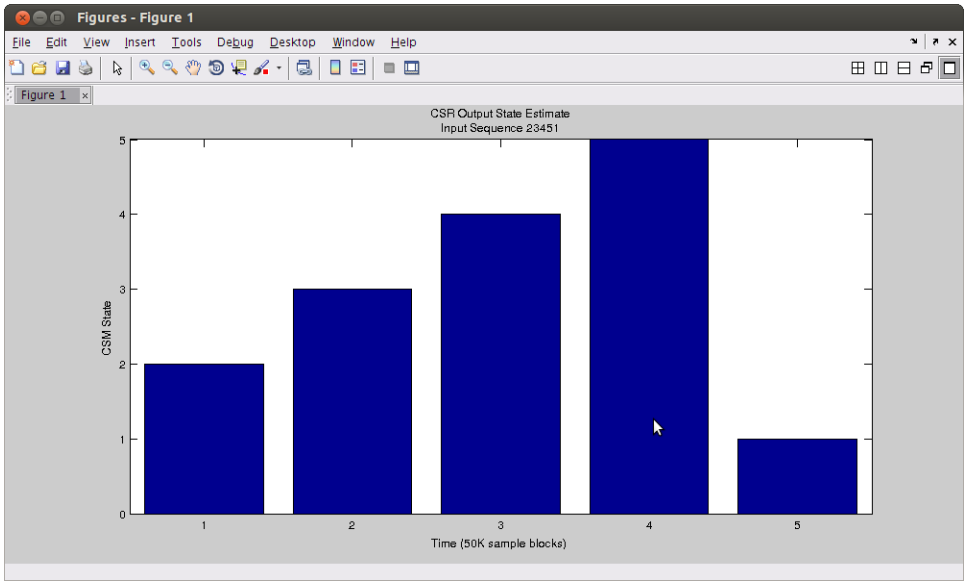

Figure A.177: CSR Output State Estimates for State Sequences 23451

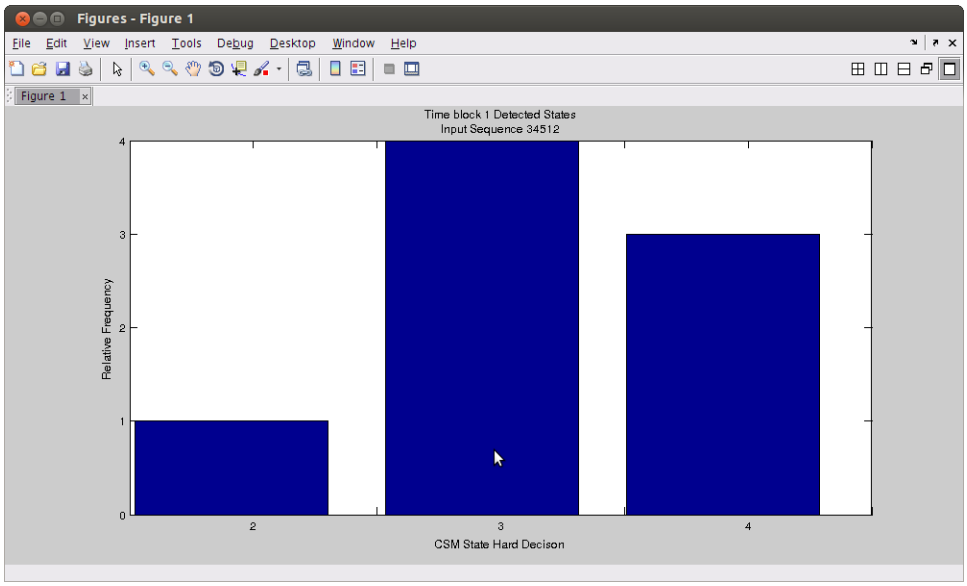

Figure A.178: Timeblock 1 State Frequency Distribution for State Sequence 34512

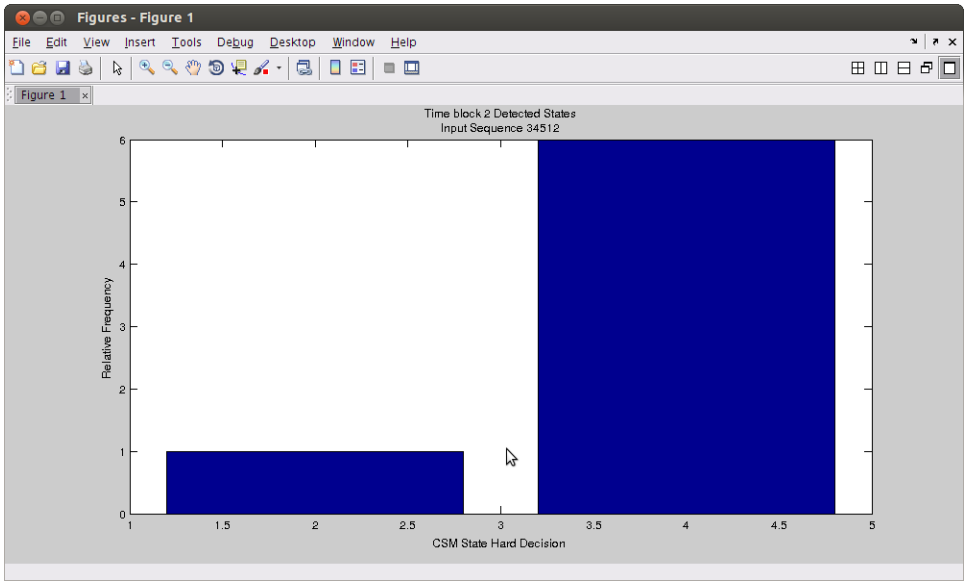

Figure A.179: Timeblock 2 State Frequency Distribution for State Sequence 34512

the FSE for the input state sequence 34512.

Figure A.181 shows the timeblock 4 hard decision frequency distribution that were produced from the FSE for the input state sequence 34512.

Figure A.182 shows the timeblock 5 hard decision frequency distribution that were produced from the FSE for input sequence 34512.

Figure A.183 shows the CSR algorithm output CSM CSE sequence that are the result of selecting the maximum of the hard decision frequency distribution for each time block and the input state sequence 34512.

State Sequence 45123

Figure A.184 shows the timeblock 1 hard decision frequency distribution that were produced from the FSE for the input state sequence 45123.

Figure A.185 shows the timeblock 2 hard decision frequency distribution that were produced from the FSE for the input state sequence 45123.

Figure A.186 shows the timeblock 3 hard decision frequency distribution that were produced from

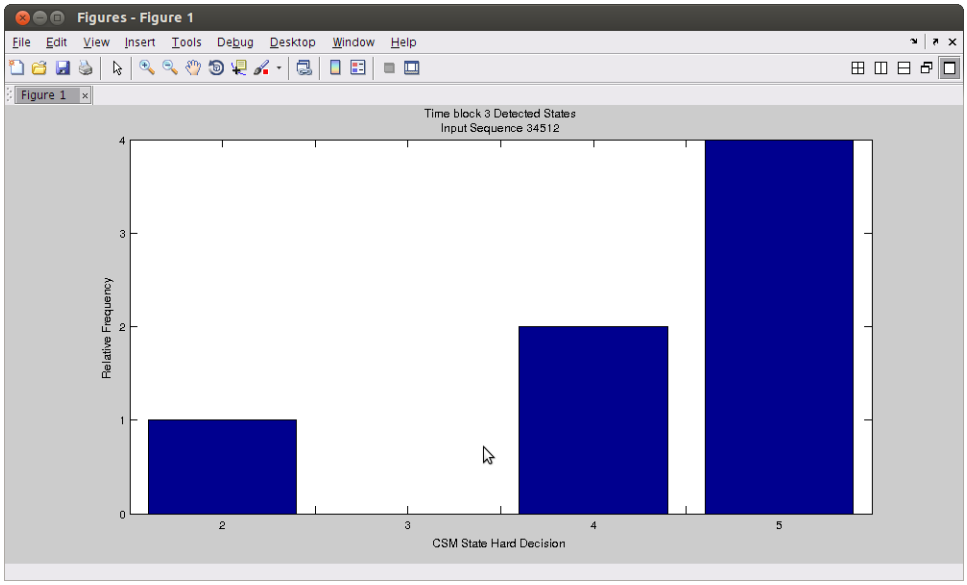

Figure A.180: Timeblock 3 State Frequency Distribution for State Sequence 34512

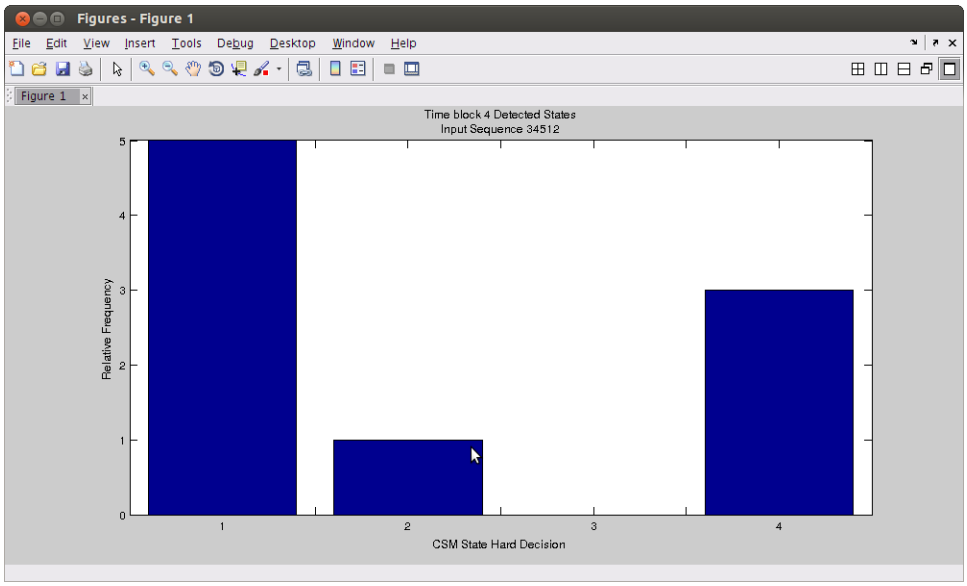

Figure A.181: Timeblock 4 State Frequency Distribution for State Sequence 34512

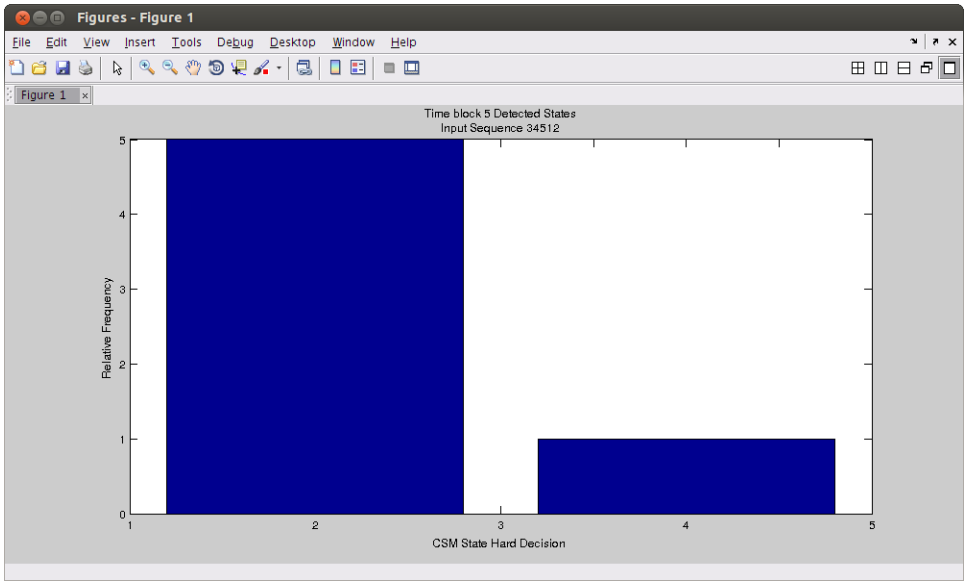

Figure A.182: Timeblock 5 State Frequency Distribution for State Sequence 34512

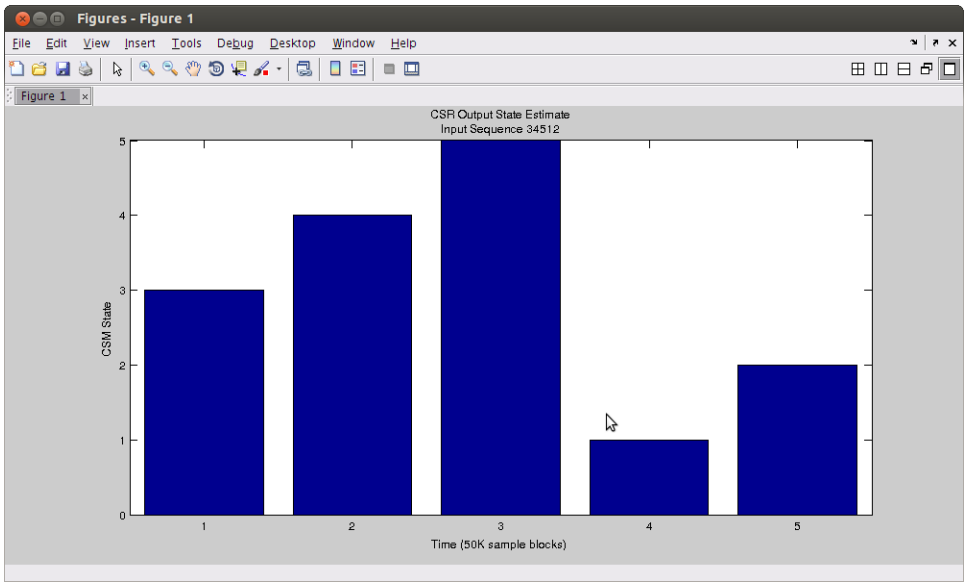

Figure A.183: CSR Output State Estimates for State Sequences 34512

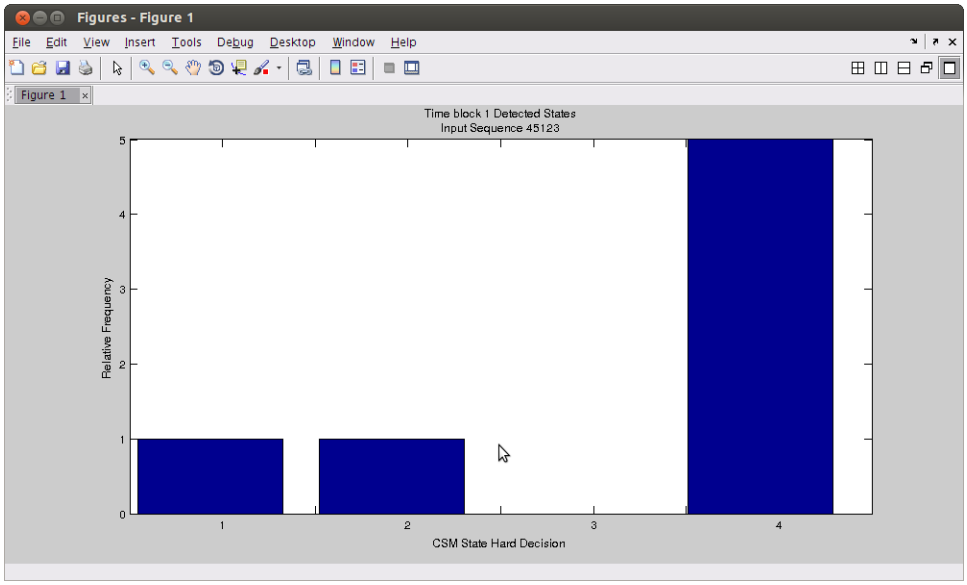

Figure A.184: Timeblock 1 State Frequency Distribution for State Sequence 45123

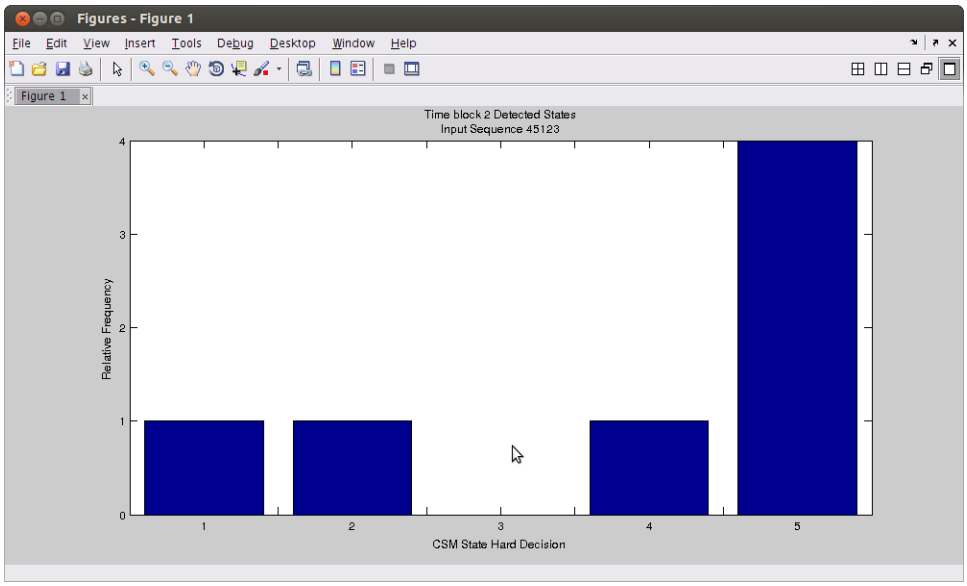

Figure A.185: Timeblock 2 State Frequency Distribution for State Sequence 45123

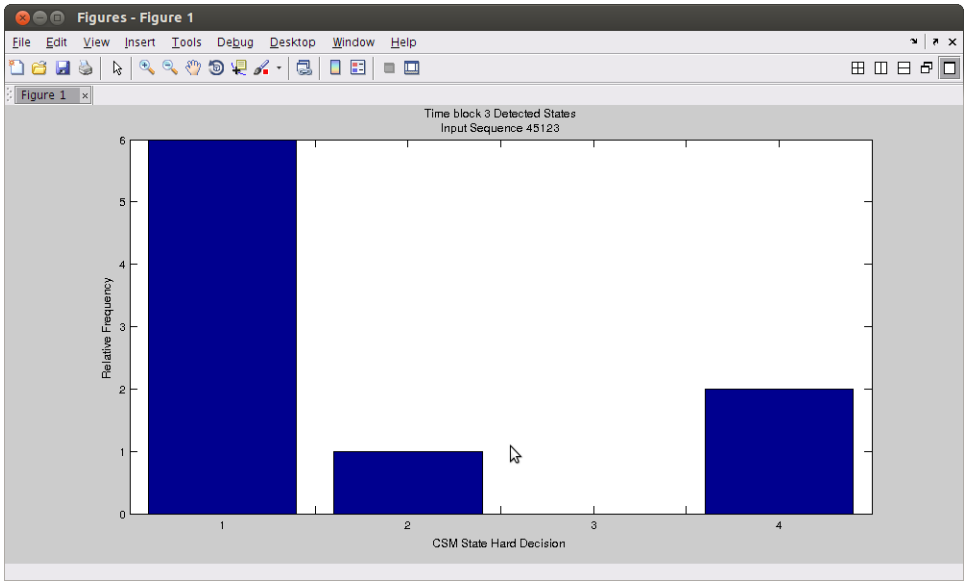

Figure A.186: Timeblock 3 State Frequency Distribution for State Sequence 45123

the FSE for the input state sequence 45123.

Figure A.187 shows the timeblock 4 hard decision frequency distribution that were produced from the FSE for the input state sequence 45123.

Figure A.188 shows the timeblock 5 hard decision frequency distribution that were produced from the FSE for input sequence 45123.

Figure A.189 shows the CSR algorithm output CSM CSE sequence that are the result of selecting the maximum of the hard decision frequency distribution for each time block and the input state sequence 45123.

State Sequene 51234

Figure A.190 shows the timeblock 1 hard decision frequency distribution that were produced from the FSE for the input state sequence 51234.

Figure A.191 shows the timeblock 2 hard decision frequency distribution that were produced from the FSE for the input state sequence 51234.

Figure A.192 shows the timeblock 3 hard decision frequency distribution that were produced from

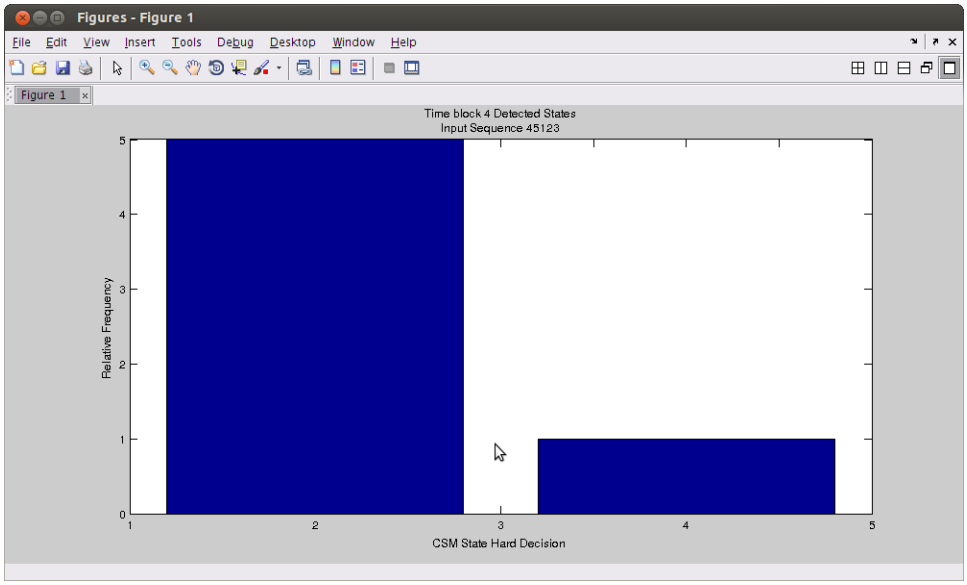

Figure A.187: Timeblock 4 State Frequency Distribution for State Sequence 45123

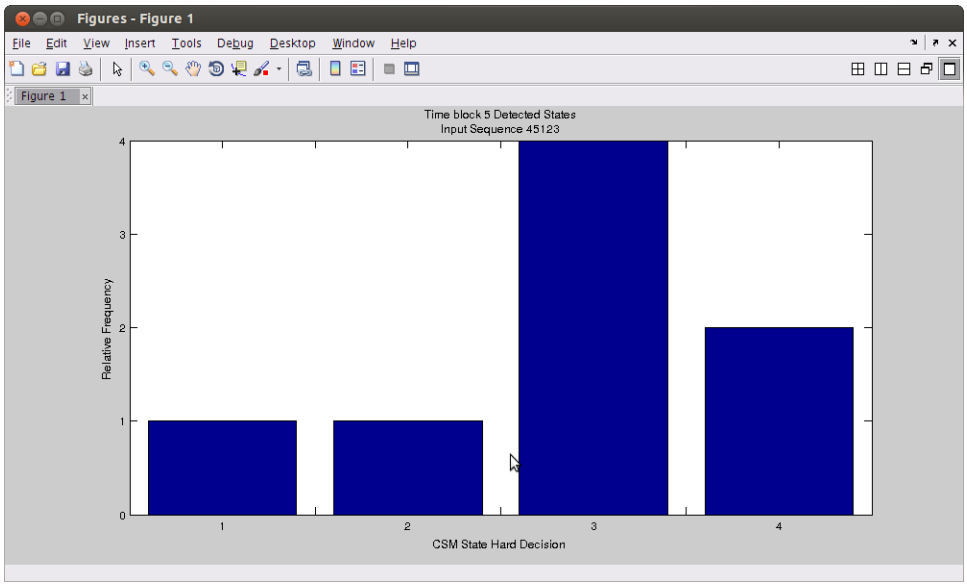

Figure A.188: Timeblock 5 State Frequency Distribution for State Sequence 45123

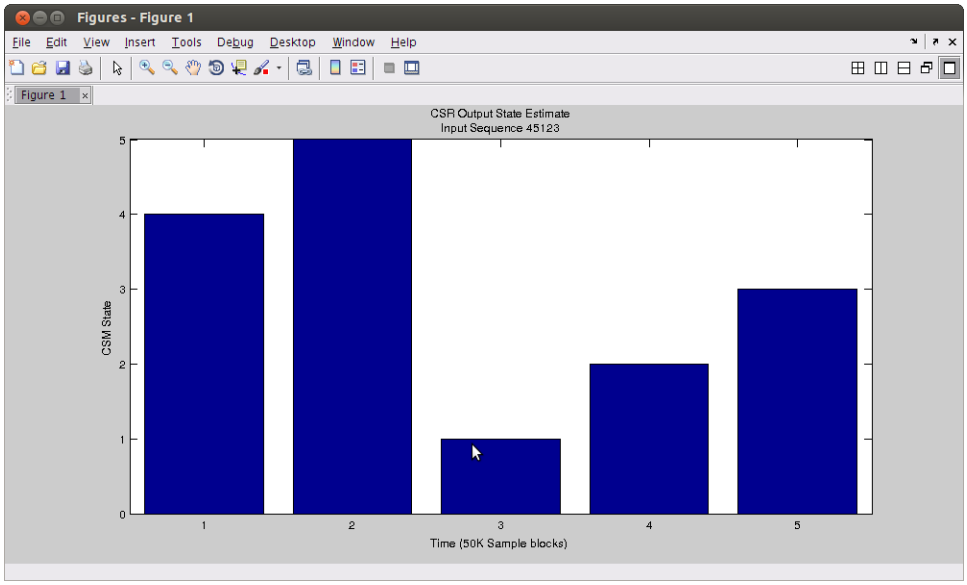

Figure A.189: CSR Output State Estimates for State Sequences 45123

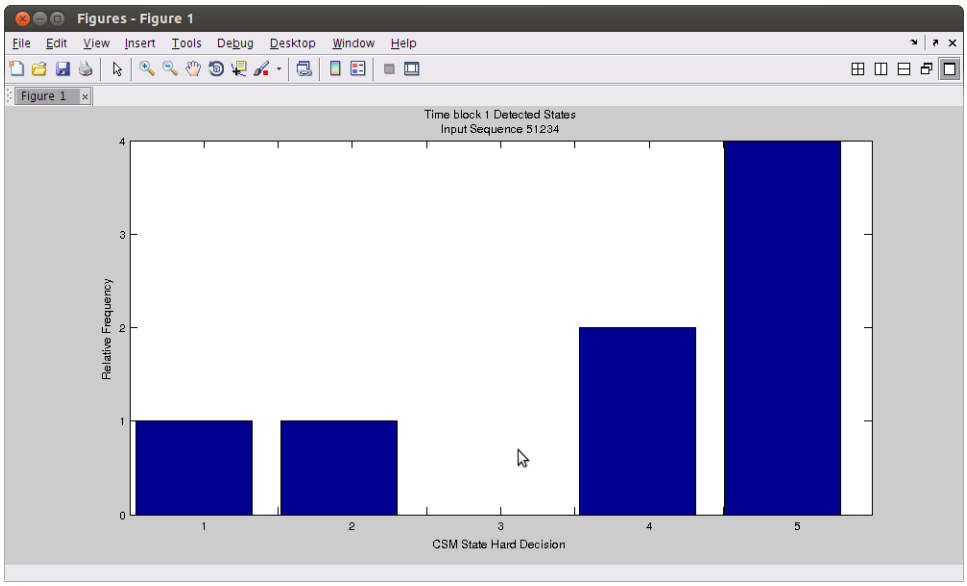

Figure A.190: Timeblock 1 State Frequency Distribution for State Sequence 51234

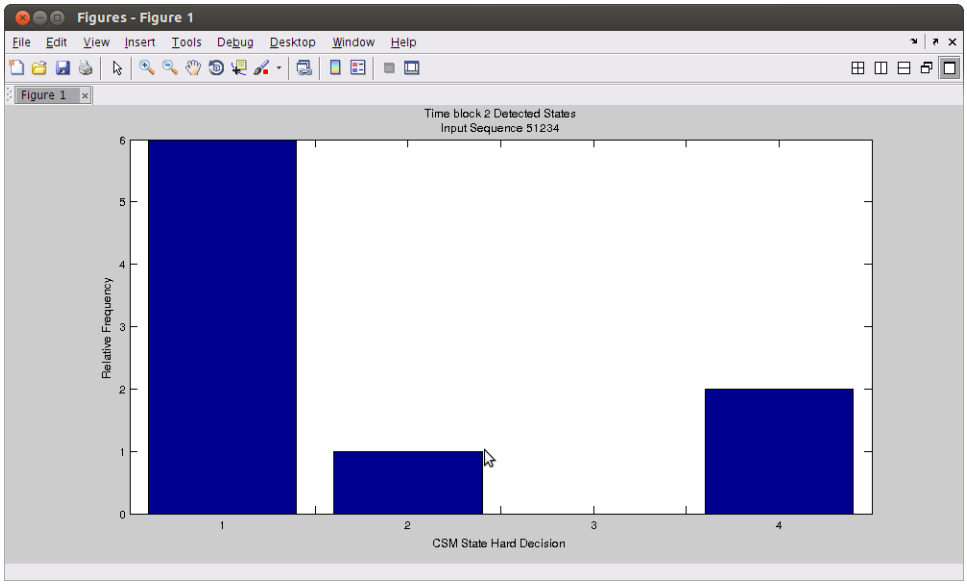

Figure A.191: Timeblock 2 State Frequency Distribution for State Sequence 51234

the FSE for the input state sequence 51234.

Figure A.193 shows the timeblock 4 hard decision frequency distribution that were produced from the FSE for the input state sequence 51234.

Figure A.194 shows the timeblock 5 hard decision frequency distribution that were produced from the FSE for input sequence 51234.

Figure A.195 shows the CSR algorithm output CSM CSE sequence that are the result of selecting the maximum of the hard decision frequency distribution for each time block and the input state sequence 51234.

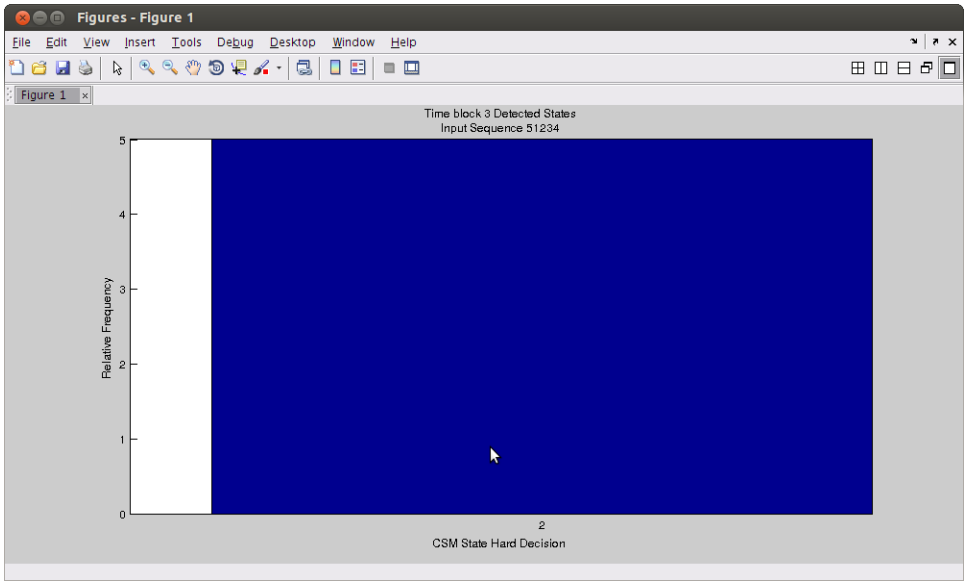

Figure A.192: Timeblock 3 State Frequency Distribution for State Sequence 51234

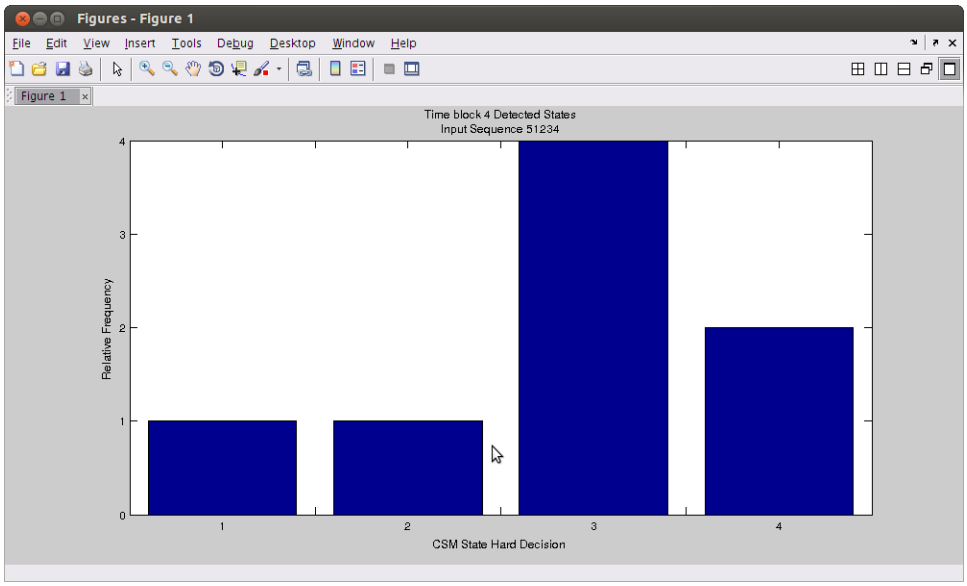

Figure A.193: Timeblock 4 State Frequency Distribution for State Sequence 51234

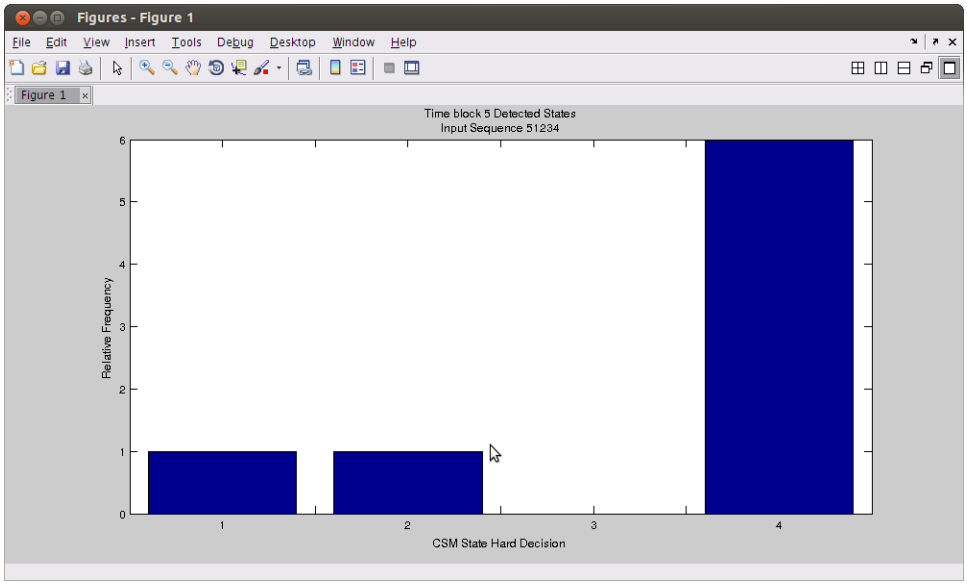

Figure A.194: Timeblock 5 State Frequency Distribution for State Sequence 51234

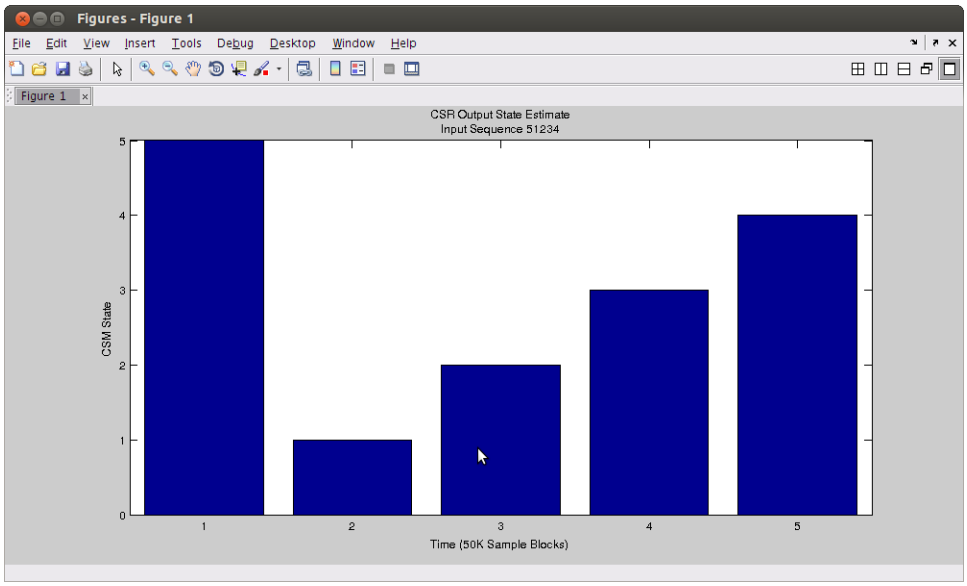

Figure A.195: CSR Output State Estimates for State Sequences 51234